LIBRARY
Te Tumu Herenga
THE UNIVERSITY OF AUCKLAND

RESEARCHSPACE@AUCKLAND

http://researchspace.auckland.ac.nz

***ResearchSpace@Auckland***

**Copyright Statement**

The digital copy of this thesis is protected by the Copyright Act 1994 (New Zealand).

This thesis may be consulted by you, provided you comply with the provisions of the Act and the following conditions of use:

- Any use you make of these documents or images must be for research or private study purposes only, and you may not make them available to any other person.
- Authors control the copyright of their thesis. You will recognise the author's right to be identified as the author of this thesis, and due acknowledgement will be made to the author where appropriate.
- You will obtain the author's permission before publishing any material from their thesis.

To request permissions please use the Feedback form on our webpage. http://researchspace.auckland.ac.nz/feedback

**General copyright and disclaimer**

In addition to the above conditions, authors give their consent for the digital copy of their work to be used subject to the conditions specified on the Library Thesis Consent Form.

# SELECTED RESONANT CONVERTERS FOR IPT POWER SUPPLIES

●

**Aiguo Patrick Hu**

# SELECTED RESONANT CONVERTERS FOR IPT POWER SUPPLIES

*By*

**Aiguo Patrick Hu**

A thesis submitted in partial fulfilment of the requirements
for the degree of
Doctor of Philosophy in Engineering

Department of Electrical and Electronic Engineering
The University of Auckland

New Zealand

October 2001

InductEV, Inc.
Exhibit 1020
Page 004

*To my loving*

*wife Fiona and daughter Alice*

# Abstract

For more than a century it has been known that signals and power can be transferred electromagnetically. This knowledge has motivated substantial research and development into wireless signal transmission which today is competitive with traditional conductive cabling systems. Power transfer across air gaps, however, has seen more modest development and has tended to be restricted to electric machines that have tight magnetic couplings. It is only very recently that a novel technique termed IPT (Inductive Power Transfer) has made power delivery to movable objects across large air gaps a practical reality.

A typical IPT system comprises a primary power converter supplying high frequency alternating current to a conductive track loop with multiple secondary power pick-up circuits loosely coupled to it. IPT employs modern power conversion, control, and magnetic coupling techniques to achieve clean and reliable power transfer without direct electrical contact. Many practical applications have been found for IPT in materials handing, lighting, and transportation systems. One of the major constraints, however, is the primary power supply, particularly at high power levels and when power transfer over large distances is required.

In this thesis selected resonant converters suitable for IPT power supplies are investigated using mathematical analysis, computer simulations and practical experiments. The basic characteristics and underlying principles of the converters are studied in order to determine their dynamic performance and power transfer capability. Special attention is given to improving existing IPT power supplies while investigating new power converters in order to achieve high efficiency and reliable operation at reduced cost.

The current-fed parallel resonant converter power supply has been the basis of most commercial applications to date. It has a high efficiency and produces good voltage and current waveforms. However, both the track length that it can drive and the power level it can operate at are limited and the system may vary in frequency if the track resonant circuit and the pick-up load are not carefully designed. As a result, this supply, in its simple form, is only suitable for short track lengths and low power applications. The voltage-fed series



InductEV, Inc.
Exhibit 1020
Page 008

quasi-resonant converter power supply controls the frequency directly and is capable of driving longer track lengths as a result of series compensation employed in the track loop. However, its voltage and current waveforms contain more harmonics, and while high efficiency may be achieved with soft switching, the condition is very dependent on the track compensation and is difficult to meet during start-up and shut down transients. In consequence, this supply is suitable for medium track lengths and medium power level applications.

Improved current-fed and voltage-fed IPT power supplies are proposed in this thesis. They have the most preferred track current properties, including constant magnitude and nearly pure sine wave characteristics. Despite the circuit complexity and high system cost involved, these supplies are ideally suitable for long track lengths and high power applications.

A novel converter based on free oscillation and energy injection control is also presented and shown to be capable of achieving high frequency AC power generation at very low switching frequencies while reducing the system cost. As such it is appealing for long track length, high track current, high frequency, and low voltage source applications. Finally, a very simple converter based on self-sustained oscillation without an external controller is demonstrated at low operating voltages, and a cost-effective option to overcome the start-up problems exhibited by most IPT power supplies at high voltages is shown with excellent dynamic zero voltage switching performance.



InductEV, Inc.
Exhibit 1020
Page 009

# Acknowledgments

There are many people whom I am indebted to during my Ph.D study in the past four years. They have helped me in numerous ways that have enabled this thesis to come into being.

First and foremost, I wish to thank my supervisor Prof. John T Boys for introducing me into the field of IPT (Inductive Power Transfer) and giving me valuable guidance throughout the course of my study. His deep insights and positive manner have always been helpful and encouraging.

Next, special thanks should go to Dr. Grant Covic for his numerous helps, particularly for his patience in reading my draft writings. I would also like to thank Dr. Andrew Green, Dr. Oscar Stielau, and Dr. Udaya Madawala who inspired me a lot in the field of power electronics and IPT. Their advice and assistance are highly appreciated. The friendly academic discussions in the Power Electronics Research Group have made my study very productive and interesting.

Thirdly, I would like to express my gratitude to the University of Auckland for bestowing me with a Ph.D Scholarship and offering a lectureship position so that I can continue my research interest in the field of power and control. Thanks to Wampfler AG, Germany, through the Auckland Uniservices Ltd, for offering me an industrial scholarship as well as technical and experimental assistance. Thanks also go to the Asia 2000 Foundation for the scholarship which made my four months study visit to the Power Electronic Research Centre of the National University of Singapore possible. I would like to express my special gratitude to Associate Prof. Ramesh Oruganti for his advice and assistance during my stay there.

In addition, I wish to thank Mr. Aaron Taylor, Mr. Evans Leung, and Mr. Howard Lu for their laboratory assistance, and thank Dr. Yanzhen Wu for proofreading the thesis draft. Also, I can never forget my schoolmates and friends including Mr. Brian Mitchell, Mr. Jason James, Mr. Scott Liang, Mr. Ian Brownlie, Mr. Yongsheng Wang, Mr. Zhusheng Sing Chen, Mr. Lijun Yu, Mr. Zhen Li, Mr. Lei Ming, Mr. Peter Liu, Ms. Julia Wu, Ms. Jie Wang, and Mr. Edward Xu for their company, friendship, and various help.



InductEV, Inc.
Exhibit 1020
Page 010

Last but not least, I would like to take this limited space to express my gratitude to my Mum and Dad, brothers and sisters for their consistent help and moral support. Sincere gratitude goes to my loving wife and daughter for their deep understanding and full support in the journey of my academic career.

Patrick Aiguo Hu

1 October 2001 Auckland



InductEV, Inc.
Exhibit 1020
Page 011

# Table of Contents

*Abstract* ..... *i*
*Acknowledgments* ..... *iii*
*Table of Contents* ..... *v*
*Nomenclature* ..... *ix*
*List of Figures* ..... *xii*
*List of Tables* ..... *xvi*

*Chapter 1: Introduction* ..... *1*
**1.1 A Perspective of Contactless Power Transfer** ..... **1**
**1.2 Introduction to IPT Power Supplies** ..... **4**
1.2.1 Basic Structure and Operating Principle ..... 5
1.2.2 General Features ..... 6
1.2.3 Suitable Applications ..... 7
**1.3 Advances and Challenges of IPT** ..... **7**
1.3.1 Historical Achievements ..... 7
1.3.2 Present Challenges ..... 10
**1.4 Scope of the Thesis** ..... **12**
**1.5 References** ..... **13**

*Chapter 2: An Overview of IPT Power Supply Technologies* ..... *17*
**2.1 Introduction** ..... **17**
**2.2 The Track Coil and Its Tuning Circuits** ..... **18**
2.2.1 Track Layout ..... 18
2.2.2 Track Tuning Circuits ..... 19
**2.3 Power Electronic Converters for IPT Track Power Supplies** ..... **21**
2.3.1 Basic Power Conversion Formats ..... 21
2.3.2 PWM Hard Switching and Resonant Soft Switching Converters ..... 22
2.3.3 Voltage-Fed and Current-fed Converters ..... 24
2.3.4 Switching Devices ..... 26
**2.4 Power Transfer Control and Conditioning** ..... **28**
2.4.1 Coupling Coefficient and Coupling Factor ..... 28
2.4.2 Pick-up Tuning and Power Transfer Capacities ..... 31



InductEV, Inc.
Exhibit 1020
Page 012

2.4.3 Power Transfer Control ..... 35
**2.5 Track Current Control and Stability ..... 37**
2.5.1 General Requirements for Track Power Supplies ..... 37
2.5.2 Basic Track Current Control Strategies ..... 39
2.5.3 Pick-up Load Modelling ..... 41
2.5.4 Power Blocking and System Stability Concerns ..... 43
**2.6 Summary ..... 45**
**2.7 References ..... 45**

***Chapter 3: Current-fed Parallel Resonant Converter Power Supplies ..... 48***
**3.1 Fundamentals of Current-fed Parallel Resonant Converters ..... 48**
3.1.1 Basic Inverting Network Topologies ..... 48
3.1.2 Switching Constraints ..... 50
3.1.3 DC to AC Voltage Balance Analysis ..... 53
3.1.4 Fixed Frequency and Variable Frequency Operation ..... 55
**3.2 ZVS Frequency Analysis ..... 56**
3.2.1 Identification of Various Resonant Frequencies ..... 56
3.2.2 ZVS Frequency Analysis and Computation ..... 60
3.2.3 Analysis Results and Discussion ..... 66
**3.3 Frequency Stability Analysis and Stability Enhancing Methods ..... 68**
3.3.1 A General Scenario of the Frequency Stability Problem ..... 68
3.3.2 Series Tuned Track and Pick-ups ..... 69
3.3.3 Other Tuning Circuits ..... 77
3.3.4 Frequency Stability Enhancing Methods ..... 79
**3.4 Improved Power Supply with Dynamic ZVS Start-up ..... 84**
3.4.1 Zero Voltage Crossing Problems at Start-up ..... 84
3.4.2 Initially Forced DC Current Solution ..... 87
3.4.3 Zero Voltage Crossing Conditions ..... 88
3.4.4 Simulation and Experimental Results ..... 89
**3.5 Summary ..... 92**
**3.6 References ..... 93**

***Chapter 4: Improved Current-fed CLC Parallel-Series Resonant Converter Power Supplies ..... 95***
**4.1 Introduction ..... 95**
**4.2 Constitution and Operating Principles ..... 96**
4.2.1 Basic Structure of the Proposed Power Supply ..... 96



InductEV, Inc.
Exhibit 1020
Page 013

4.2.2 Significant Property Improvements ..... 98
**4.3 G3 Power Supply Design Methodology ..... 104**
4.3.1 Design Concepts and Practical Considerations ..... 104
4.3.2 Basic Design Procedure and Equations ..... 105
**4.4 Analysis of the Resonant Track Network ..... 108**
4.4.1 Poles and Zeroes of the Admittance Transfer Function ..... 108
4.4.2 Sensitivity Analysis ..... 112
**4.5 System Dynamic Simulations ..... 121**
4.5.1 A Typical Current-fed G3 IPT System ..... 121
4.5.2 Simulation Results and Discussion ..... 124
**4.6 Summary ..... 128**
**4.7 References ..... 129**

***Chapter 5: Voltage-fed Resonant Converter Power Supplies ..... 131***
**5.1 Introduction ..... 131**
**5.2 Voltage-fed Series Resonant Converter Power Supplies ..... 132**
5.2.1 Elements and Structure of the Converter ..... 132
5.2.2 Phase Shift Regulation of the Track Current ..... 132
5.2.3 Soft Switching Operation Analysis ..... 135
**5.3 Improved Series-Parallel Resonant Converter Power Supplies ..... 140**
5.3.1 Dual Circuit Transformation from CLC Network to LCL Network ..... 140
5.3.2 Zero Current Switching Operation ..... 142
5.3.3 Duty Cycle Track Current Regulation and Soft switching Operation ..... 143
**5.4 Simulation/Experimental Results and Discussion ..... 144**
5.4.1 Basic voltage-fed series resonant converter power supply ..... 144
5.4.2 Discussion on the voltage-fed G3 power supply ..... 147
**5.5 Summary ..... 149**
**5.6 References ..... 150**

***Chapter 6: Mathematical Modelling of a Current-fed IPT System ..... 152***
**6.1 Introduction ..... 152**
**6.2 Basics of GSSA Modelling ..... 153**
**6.3 Non-linear Description of a Current-fed G3 Supply ..... 156**
6.3.1 Circuit Representation with Controlled Sources ..... 156
6.3.2 Nonlinear Differential State Space Equations ..... 157
**6.4 GSSA Linear Modelling and Analysis ..... 158**
6.4.1 Continuous Linear Model ..... 158



InductEV, Inc.
Exhibit 1020
Page 014

6.4.2 Discrete Linear Model ..... 160
6.4.3 Steady State and Dynamic Analysis Using the Linear Models ..... 161
**6.5 Summary ..... 166**
**6.6 References ..... 167**

***Chapter 7: Innovative Resonant Converters and Practical Implementation ..... 169***
**7.1 Introduction ..... 169**
**7.2 High Frequency Power Generation with Energy Injection Control ..... 170**
7.2.1 Basic Concept of Free Oscillation and Energy Injection Control ..... 170
7.2.2 Proposal and Analysis of a Simple DC-AC Converter ..... 170
7.2.3 Experimental Results ..... 174
7.2.4 Investigation of a Direct AC-AC Converter ..... 174
**7.3 Self-sustained Operations without External Controllers ..... 177**
7.3.1 Structure of the Proposed Converter ..... 177
7.3.2 Self-sustained Operation Analysis ..... 179
7.3.3 Experimental Results and Discussion ..... 181
**7.4 Implementation of Self-sustained Converters for High Power Applications ... 177**
7.4.1 Gate Drive Problems of the Self-sustained Converter at High Voltage Levels ..... 179
7.4.2 Practical IPT Power Supplies Using PLL and ZVD Techniques ..... 181
**7.5 Summary ..... 189**
**7.6 References ..... 190**

***Chapter 8: Conclusions and Suggestions for Future Work ..... 191***
**8.1 General Conclusions ..... 191**
**8.2 Comparison of Different IPT Power Supplies ..... 201**
**8.3 Contributions of This Thesis Work ..... 201**
**8.4 Suggestions for Future Work ..... 202**
**8.5 References ..... 206**

***Appendices ..... 208***
**A. Derivation of the Maximum Pick-up Loading Condition ..... 208**
**B. System Data of a Current-fed Full-bridge G3 IPT Power Supply ..... 210**
**C. PSpice Schematic Set-up for System Dynamic Simulation ..... 212**

***Bibliographies ..... 213***



InductEV, Inc.
Exhibit 1020
Page 015

# Nomenclature

**Acronyms**

| | | |
|---|---|---|
| AC | - | Alternating current |
| AGV | - | Automatic guided vehicle |
| CLC | - | Capacitor-inductor–capacitor connection |
| CPT | - | Capacitive power transfer |
| DC | - | Direct current |
| EMC | - | Electro-magnetic compatibility |
| emf | - | Electro-motive force |
| EMI | - | Electro-magnetic interference |
| EMS | - | Electro-magnetic susceptibility |
| ESR | - | Equivalent series resistance |
| EV's | - | Electric vehicles |
| G1 | - | Generation one (current-fed parallel resonant) IPT power supply |
| G2 | - | Generation two (voltage-fed series resonant) IPT power supply |
| G3 | - | Generation three (voltage-fed or current-fed) IPT power supplies |
| GSSA | - | Generalised state space averaging |
| GTO | - | Gate turn off thyristor |
| ICPT | - | Inductively coupled power transfer |
| IEGT | - | Injection enhanced gate transistor |
| IGBT | - | Insulated gate bipolar transistor |
| IGCT | - | Integrated gate commutated thyristor |
| IPT | - | Inductive power transfer |
| LCL | - | Inductor–capacitor-capacitor connection |
| mmf | - | Magneto-motive force |
| MOSFET | - | Metal oxide silicon field effect transistor |
| ms | - | Milliseconds |
| PI | - | Proportional and integral control |
| PLL | - | Phase locked loop |
| PWM | - | Pulse width modulation |
| Q | - | Quality factor |
| RFI | - | Radio frequency interference |



InductEV, Inc.
Exhibit 1020
Page 016

| | | |
|---|---|---|
| rms | - | Root mean square |
| s | - | Seconds |
| SCR | - | Silicon controlled rectifier |
| SPICE | - | Simulation program with integrated circuit emphasis |
| ZVD | - | Zero voltage detection |
| ZCS | - | Zero current switching |
| ZVS | - | Zero voltage switching |

**Symbols**

| | | |
|---|---|---|
| $3\phi$ | - | Three phase |
| $\varepsilon$ | - | Truncation error |
| C | - | Capacitor (Farads) |
| E | - | Electro-motive force (Voltages) |
| f | - | Frequency (Hz) |
| $f_0$ | - | Undamped natural frequency (Hz) |
| $f_r$ | - | Zero phase angle resonant frequency (Hz) |
| $f_f$ | - | Natural (free ringing) frequency (Hz) |
| $f_{vc_m}$ | - | Maximum capacitor voltage frequency (Hz) |
| $f_{iL_m}$ | - | Maximum inductor current frequency (Hz) |
| $f_{zvs}$ | - | Zero voltage switching frequency (Hz) |
| $\omega$ | - | Angular frequency (radians/s) |
| i | - | Instantaneous current (Amperes) |
| I | - | Current magnitude (Amperes) |
| j | - | Complex operator ( $\sqrt{-1}$ ) |
| k | - | Magnetic coupling coefficient |
| $k_f$ | - | Magnetic coupling factor |
| L | - | Self inductance (Henrys) |
| M | - | Mutual inductance (Henrys) |
| R | - | Resistance ($\Omega$) |
| v | - | Instantaneous voltage (Volts) |
| V | - | Voltage magnitude (Volts) |
| N | - | The number of the pick-ups |
| T | - | Time constant (seconds) |
| s | - | Laplace transformation variable |



InductEV, Inc.
Exhibit 1020
Page 017

| | | |
|---|---|---|
| $z$ | - | Damping factor |
| $\phi$ | - | Phase angle |
| t | - | time (seconds) |

**Algebraic Notations**

| | | |
|---|---|---|
| $\underline{\Phi}$, $\underline{\Gamma}$ | - | Control and input matrices of a discrete state space equation |
| $\|\langle x\rangle_1\|$ | - | The norm of $\langle x\rangle_1$ |
| $\langle x\rangle_0$ | - | DC component of Fourier complex coefficient |
| $\langle x\rangle_1$, $\langle x\rangle_{-1}$ | - | The first order Fourier complex coefficients |
| $\underline{A}$, $\underline{B}$ | - | Control and input matrices of a continuous state space equation |
| $\underline{A}^{-1}$ | - | Inverse of $\underline{A}$ |
| d/dt | - | Differential operator |
| $\underline{I}$ | - | Identity square matrix |
| Im | - | Imaginary part of a complex expression |
| Re | - | Real part of a complex expression |

**Subscripts**

| | | |
|---|---|---|
| ac | - | AC value |
| d(c) | - | DC value |
| lk | - | Leakage |
| m | - | Maximum value |
| oc | - | Open circuit |
| p | - | Primary track |
| r | - | Referred back from the pick-up to the primary track |
| s | - | Secondary pick-ups |
| sc | - | Short circuit |
| sp | - | Phase splitting transformer |
| ss | - | Steady state |

**Superscripts**

| | | |
|---|---|---|
| ^ | - | Peak value |
| n | - | Nth order power |



InductEV, Inc.
Exhibit 1020
Page 018

# List of Figures

Fig. 1-1: Basic structure of a typical IPT system ..... 5
Fig. 1-2: IPT powered monorail trolleys for materials handling applications ..... 8
Fig. 1-3: Typical applications of IPT in electric vehicles ..... 9

Fig. 2-1: IPT coupling between the track loop and the pick-up ..... 17
Fig. 2-2: Track layout ..... 18
Fig. 2-3: Track tuning methods ..... 20
Fig. 2-4: Typical AC-DC-AC configuration for IPT power supplies ..... 22
Fig. 2-5: Full bridge and half bridge voltage-fed inverters ..... 24
Fig. 2-6: Full bridge and push pull current-fed inverters ..... 25
Fig. 2-7: Combined bi-directional fully controlled power switches ..... 28
Fig. 2-8: Open circuit voltage and short circuit current of the pick-up coil ..... 29
Fig. 2-9: Typical coupling configurations between the track coil and the pick-up ..... 31
Fig. 2-10: Equivalent circuits of the pick-up coil ..... 31
Fig. 2-11: Series tuned pick-up ..... 32
Fig. 2-12: Parallel tuned pick-up ..... 32
Fig. 2-13: Pick-up voltage and current characteristics ..... 33
Fig. 2-14: Composite compensation of the pick-up ..... 34
Fig. 2-15: Power flow control methods ..... 35
Fig. 2-16: Pick-up power flow control with a shorting switch ..... 36
Fig. 2-17: Dual coil power flow control ..... 37
Fig. 2-18: Load modelling of n parallel tuned pick-ups ..... 42
Fig. 2-19: Equivalent circuit of n parallel tuned pick-ups ..... 42

Fig. 3-1: Full bridge current-fed parallel resonant converters ..... 48
Fig. 3-2: Push-pull current-fed parallel resonant converters ..... 49
Fig. 3-3: Equivalent circuits of a phase splitting transformer ..... 50
Fig. 3-4: Typical voltage and current waveforms without series blocking diodes ..... 52
Fig. 3-5: AC and DC voltage balance of current-fed resonant converter at ZVS condition ..... 53
Fig. 3-6: A push pull current-fed resonant converter ..... 56



InductEV, Inc.
Exhibit 1020
Page 019

Fig. 3-7: Various resonant frequencies of a series-loaded parallel-resonant tank ..... 57
Fig. 3-8: The effect of the third harmonics on the shift of the zero voltage crossing..... 61
Fig. 3-9: Step current injection model..... 62
Fig. 3-10: Complete voltage and current waveforms..... 63
Fig. 3-11: Iterative numerical analysis..... 65
Fig. 3-12: ZVS frequency results..... 66
Fig. 3-13: Resonant frequencies versus Q..... 67
Fig. 3-14: Variable frequency operation system..... 69
Fig. 3-15: Input impedance of series tuned track and pick-up circuit..... 69
Fig. 3-16: Variation of zero phase angle frequency crossings (k=0.1) ..... 73
Fig. 3-17: Zero phase angle frequency shift for series-tuned circuits (k=0.1)..... 75
Fig. 3-18: Approximation of a practical pick-up circuit ..... 77
Fig. 3-19: Approximation of a practical parallel track tuning circuit ..... 78
Fig. 3-20: Zero phase angle frequency shift for practical parallel-tuned circuits (k=0.1) ..... 79
Fig. 3-21: Increasing the maximum loading by increasing the nominal frequency..... 80
Fig. 3-22: Adding bias network to increase the system frequency stability..... 82
Fig. 3-23: Dynamic parameter tuning methods..... 83
Fig. 3-24: Equivalent circuit and ramp current input model..... 84
Fig. 3-25: Voltage and current waveforms after the first switch is on..... 86
Fig. 3-26: Zero voltage crossing analysis during start-up ..... 89
Fig. 3-27: PSpice simulation results of ZVS start-up..... 90
Fig. 3-28: Experimental voltage and current waveforms..... 92

Fig. 4-1: Proposed CLC parallel-series resonant converter ..... 96
Fig. 4-2: Current-fed G3 Track Network..... 99
Fig. 4-3: Frequency response of the input admittance ..... 100
Fig. 4-4: Unity power factor input transformation..... 100
Fig. 4-5: Constant track current transformation..... 101
Fig. 4-6: The frequency response of the trans-conductance $G(j\omega)=I_t(j\omega)/V_{ac}(j\omega)$ ..... 102
Fig. 4-7: Improved frequency stability of the G3 supply..... 103
Fig. 4-8: Zeroes and poles location of a current-fed G3 track network ..... 111
Fig. 4-9: Tuned track network for sensitivity analysis..... 112
Fig. 4-10: Monte Carlo analysis of the track current and input current phase (Tolerance: ±2%).... 117
Fig. 4-11: Frequency shifts caused by a 1% increase of the circuit components..... 118



InductEV, Inc.
Exhibit 1020
Page 020

Fig. 4-12: Worst case frequency shift AC sweep compared with the nominal situation..... 120
Fig. 4-13: Monte Carlo analysis of the zero phase angle frequency shift of the CLC track network ..... 121
Fig. 4-14: Schematic diagram of a current-fed G3 IPT system (zero bias) ..... 122
Fig. 4-15: Variable frequency control based on voltage errors ..... 124
Fig. 4-16: Load increase transient response..... 126
Fig. 4-17: Load decrease transient response ..... 127

Fig. 5-1: A typical voltage-fed series resonant converter power supply (G2)..... 132
Fig. 5-2: Phase shift control..... 133
Fig. 5-3: Closed loop track current regulation..... 134
Fig. 5-4: Soft switched waveforms of a voltage-fed series resonant converter ..... 136
Fig. 5-5: The soft switching process of a voltage-fed converter..... 137
Fig. 5-6: Equivalent circuit of capacitor charging and discharging during dead time..... 139
Fig. 5-7: Dual transformation from current-fed CLC network to voltage-fed LCL network ..... 140
Fig. 5-8: Constant track current and unity power factor properties of the LCL network ..... 141
Fig. 5-9: Improved voltage-fed series-parallel resonant converter (G3) ..... 142
Fig. 5-10: Simulated switching waveforms of a G2 power supply..... 145
Fig. 5-11: Gate signal and switching waveforms of one of the switches ..... 146
Fig. 5-12: Measured voltage and current waveforms of a practical G2 power supply..... 147
Fig. 5-13: Voltage-fed LCL resonant converter running at nominal frequency..... 148
Fig. 5-14: Detuned ZCS operation of a voltage-fed LCL resonant converter ..... 149

Fig. 6-1: Illustration of the GSSA (Generalised State Space Averaging) modelling method ..... 154
Fig. 6-2: Equivalent circuit of a current-fed G3 IPT power supply..... 156
Fig. 6-3: Load increase transient response obtained from GSSA model and PSpice simulation.... 164
Fig. 6-4: Load transient response from the discrete GSSA linear models using different sampling times ..... 166

Fig. 7-1: A simple inverter based on free oscillation and energy injection control..... 171
Fig. 7-2: Transient response of a DC-AC converter based on direct energy injection control..... 173
Fig. 7-3: Simulation and experimental results of a DC-AC converter based on energy injection control..... 175
Fig. 7-4: A direct AC-AC power converter ..... 176
Fig. 7-5: Injection and track current waveforms of the direct AC-AC converter..... 177



InductEV, Inc.
Exhibit 1020
Page 021

Fig. 7-6: Proposed DC-AC converter without external controllers ..... 178
Fig. 7-7: Typical simulated waveforms of the proposed converter..... 180
Fig. 7-8: Experimental result of the proposed converter..... 181
Fig. 7-9: Passive gate drive circuits for the self-sustained resonant converter..... 184
Fig. 7-10: PLL gate drive technique..... 185
Fig. 7-11: Direct ZVD gate drive technique ..... 186
Fig. 7-12: Steady state waveforms of an IPT power supply using direct ZVD ..... 187
Fig. 7-13: Steady state waveforms of an IPT power supply using PLL..... 187
Fig. 7-14: Start-up waveforms of a practical IPT power supply using direct ZVD..... 188



InductEV, Inc.
Exhibit 1020
Page 022

# List of Tables

Table 1-1: Electric power transfer options ..... 3

Table 2-1: Comparison of semiconductor power switching devices ..... 27
Table 2-2: The output properties of the different pick-up compensations ..... 32

Table 3-1: Comparison of different resonant frequencies ..... 68
Table 3-2: Converter data for the ZVS dynamic start-up ..... 91

Table 4-1: Poles and zeroes of a practical parallel-series tuned track network ..... 110
Table 4-2: Nominal values of the tuned track network ..... 112
Table 4-3: Sensitivity and worst case analysis results of parallel-series tuned track at 15kHz ..... 115
Table 4-4: Sensitivity and worst-case analysis result of the frequency shift ..... 118

Table 5-1: Converter data of a voltage-fed parallel resonant IPT power supply ..... 145
Table 5-2: Parameter modifications for the improved voltage-fed G3 power supply ..... 148

Table 6-1: Steady state results based on the linear GSSA models ..... 162

Table 8-1: Comparison of IPT power supplies based on different resonant converters ..... 201



InductEV, Inc.
Exhibit 1020
Page 023

## Chapter 1

# Introduction

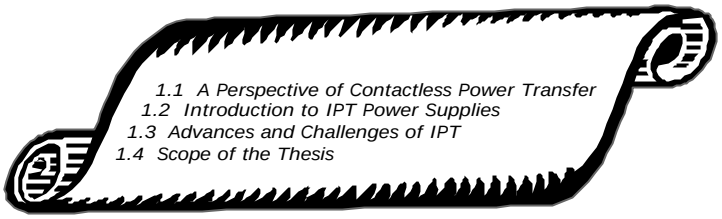


## 1.1 A Perspective of Contactless Power Transfer

Power and signals are two of the most important aspects of modern electrical and electronic engineering. They coexist in an electric system: every signal relies on some power to exist and all power carries some information in it. Nevertheless, power and signals have different aspects of focus when considered individually: the former puts emphasis on the driving force or energy required to operate the system; while the latter puts emphasis on the information with regard to system status and control commands. Without signals, the workings of a system would be unknown and could not be controlled as desired, whereas without power, a system would be completely dead with no operation possible.

It has been known for more than a century that signals and power can be transferred from one place to another in electromagnetic forms. This usually occurs by conduction via a closed circuit with direct cabling connections. Alternatively, it is possible to transfer power and signals through electromagnetic coupling without direct electrical contact. It is well known that traditional radio and TV systems transmit signals in the open air over a long distance. Now, competing with the traditional cabling systems, wireless communication techniques such as mobile phones and wireless Internet connections are becoming very popular. As for power transfer, magnetic couplings are widely used in traditional transformers and electrical machines. However, for a long time it was considered impractical, if not impossible, to transfer high levels of power across large air gaps, not to mention long distance power transfer in the open air. In this sense, the development of power



InductEV, Inc.
Exhibit 1020
Page 024

transfer is lagging far behind that of signal transfer. The main reason for this is that the practical constraints and design considerations for a power transfer system are quite different from those of a signal transfer system. Consider the design of a signal transfer system such as for radio, a transmission power loss of more than one hundred decibels may be acceptable as long as the information carried on the signal can be received by the receiver [1]. Yet, a loss of 3dB is considered too high for a power transfer system since it corresponds to a fifty-percent power loss. Moreover, a radio system may have a quality factor Q as high as 100 for its resonant tuning circuits; whereas in a power system the quality factor Q should be designed to be as small as possible to reduce the system cost, size, and power losses. Too large a Q can also make the circuit tuning very tedious and cause over sensitivity problems in the power flow with respect to parameter variations. Normally, the quality factor in power transmission systems should therefore be designed to be smaller than 10. All these reasons make contactless power transfer a formidable task to fulfil.

With the development of power semiconductor switching devices and power conversion techniques, a novel technique termed IPT (Inductive Power Transfer) has made power transfer across a large air gap practical [2]. An IPT power supply distribution system can be regarded as somewhere between a tightly coupled transformer in power systems and the transmitter and receiver configuration in radio systems. The key issue involved in this novel technique is the power conversion from a low frequency system such as a DC or 50/60Hz mains power supply to a much higher frequency system with a frequency of about 10-100kHz [*]. This power conversion makes power flow across an air gap feasible in practice. Thus, power electronics is the enabling technology of IPT.

From a more general point of view, there are other ways to achieve contactless power transfer. Table 1-1 outlines possible options for electric power transfer in electromagnetic forms. In addition to conventional systems with direct electrical contact, contactless power transfer can, theoretically, be obtained inductively, capacitively, or via electromagnetic waves – particularly microwaves.

Conductive power transfer is based on a closed circuit that allows for direct power flow along the conductors. The closed circuit is normally formed with hard wiring connections. However, when power delivery to a movable object, such as a monorail trolley is required, it is very inconvenient since either a fixed connection with a trailing cable or a moving contact connection has to be used. In this situation, contactless power transfer without direct electrical contact is preferable.

[*] In radio systems, 10kHz–100kHZ fall into VLF (Very Low Frequency) band. However, in comparison to 50/60HZ in power systems, they are very high frequencies. For this reason, they are also referred to as medium frequencies in applications such as induction heating.



InductEV, Inc.
Exhibit 1020
Page 025

**Table 1-1: Electric power transfer options**

| | **Direct Contact** | **Contactless** | | | | |
|---|---|---|---|---|---|---|
| ***Features*** | **Conductive** | **Inductive** | | **Capacitive** | | **Wave** |
| ***Types*** | Hard wiring, moving contact | Closely Coupled | Loosely Coupled | Closely Coupled | Loosely Coupled | Electromag-netic waves |
| ***Basic Theories*** | Electric circuit, Electric arc & contact theories | Magnetic Circuit, AC circuit theories | Distributed magnetic field, Power electronics | Confined electric field, AC circuit | Distributed electric field, Power electronics | Wave propagation |
| ***Typical Techniques*** | Cables and contacts | Transformers | IPT | Capacitors | CPT | Wave guides, Parabolic antennas, etc. |
| **Illustration** | 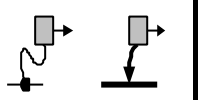 | 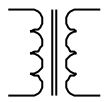 | 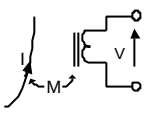 | 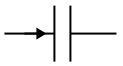 | | |

As shown in table 1-1, contactless power transfer can be achieved inductively or capacitively depending on whether it is via magnetic field coupling or electric field coupling. The tightly coupled versions - traditional transformers and capacitors are nothing new. Theoretically they can transfer power without direct electrical contacts, but practically, they are not suitable for delivering power to moving objects since the magnetic or electric field in these components have to be confined within iron cores or electrolytic media. An exception to this is the electric machines, especially the linear motors that allow more freedom of mechanical movement. However, the power efficiency and power factor of a linear motor are very low, and its expanded “stator” are very costly, therefore it is only suitable for transferring power over a very short distance, eg., within a machine tool.

It is well known that the power transfer from the primary to secondary of a transformer is nearly impossible at low frequencies such as 50Hz or 60Hz if its coils are separated far apart without maintaining a tight magnetic coupling. However, as mentioned before, if the operating frequency is increased to a very high value, then the fast changing rate of the magnetic field will cause a much stronger induction effect between the two coils. Thus, power jumping across the air gap becomes feasible in a practical sense. This leads to the basic concept of IPT.

Theoretically another way of supplying contactless power to movable objects is via CPT (Capacitive Power Transfer) which is analogous to IPT. Here the two plates of a capacitor can be



InductEV, Inc.
Exhibit 1020
Page 026

set apart, forming a large air gap for the power to jump across. One of the capacitor plates is mechanically free to move so that power can be transferred from a static frame to movable objects by combining two or more of such capacitors in a circuit. Unlike an IPT system where a distributed magnetic field offers a power flow channel, in a CPT system a distributed electric field serves as a power flow passage. Consequently, the voltage, instead of the current as in an IPT system, would be of the greatest importance to a CPT power supply. It is interesting to note that like an IPT system, a high frequency is also beneficial to the power flow via the air gap of a split "capacitor". Therefore, high frequency power conversion may also be a major issue, with power electronics being the enabling technology. It should be noted that CPT is simply a new concept proposed here to serve as a counterpart to IPT. CPT has problems with high electric field intensity exceeding 30kV/cm in air and very low permittivity $\varepsilon_0$ ($8.854\times10^{-12}$) compared with the permeability $\mu_0$ ($4\pi\times10^{-7}$) which makes it $10^5$ times more difficult! Moreover, materials with relative permeability greater than 100,000 also contribute to the fact that inductive power transfer is more practical than capacitive. Therefore, the engineering feasibility of CPT and its possible application need further investigation beyond the scope of this thesis.

As in wireless signal communications, contactless power transfer can also be achieved via electromagnetic waves. However, unlike the transfer of signals, transferring a large amount of power over a long distance in the open air using traditional wave guides or parabolic antennas can be very difficult for normal use due to the complexities involved in the power flow control.

This thesis is about IPT power supplies which are the most feasible contactless power supplies using modern power converter techniques.

## 1.2 Introduction to IPT Power Supplies

Since IPT is a relatively new technology, until now, there has been no standard definition for it. Sometimes it has also been referred to as ICPT (Inductively Coupled Power Transfer). As this name implies, it is a power transfer system based on magnetic coupling. In this thesis the term IPT normally refers to a loosely coupled system designed for delivering power to movable objects. Traditional closely coupled transformers and induction machines are not covered in this term. Regarding the areas covered, IPT is a synergy of disciplines covering a large range of technical expertise (including modern power electronics, control, and electromagnetism), which requires proper power conversion, power flow control & conditioning, and magnetic coupling.



InductEV, Inc.
Exhibit 1020
Page 027

In short, IPT can be described as a loosely coupled power supply system using modern *power conversion*, *control*, and *magnetic coupling* techniques to achieve contactless power transfer from a static frame to movable objects.

### *1.2.1 Basic Structure and Operating Principle*

Fig. 1-1 shows the basic structure of a typical IPT system. It can be seen that an IPT system comprises two electrically isolated parts. The first part consists of a power converter and a primary conductive path which can be an elongated "track" or lumped "coil". The main function of the power converter is to supply a constant high frequency AC current (normally a 10-100kHz current with a sinusoidal waveform) along the track loop; this part is therefore often referred to as the track power supply. The second part consists of a pick-up coil and a power conditioner. Due to the mutual magnetic coupling between the primary track loop and the secondary pick-up coil, an inductive electromotive force is induced in the pick-up coil which forms a voltage source for the secondary power supply. Since the magnetic coupling is loose, ie. Low, compared to normal transformers, the induced voltage source is usually unsuitable to be used by the equipment directly. As such, a power conditioner is required to regulate the power into the form required by the load, such as a motor controller or a lamp.

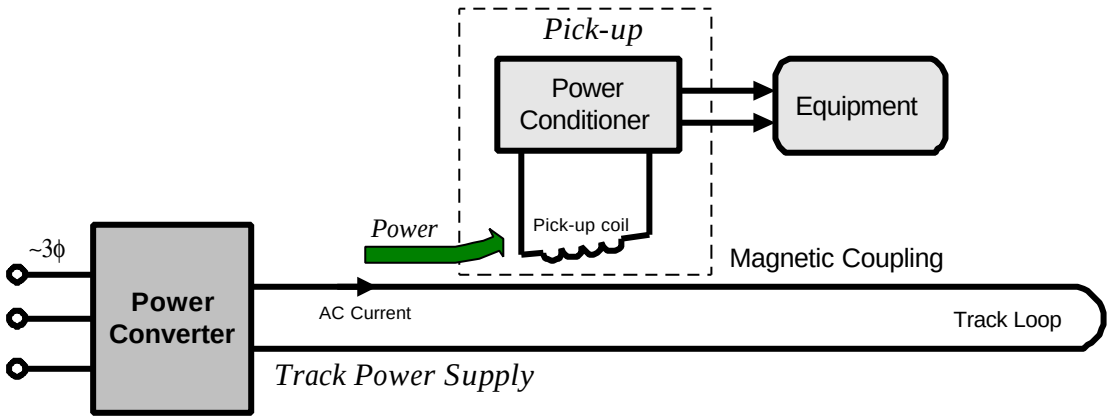


**Fig. 1-1: Basic structure of a typical IPT system**

It can be seen that a high quality track current generated by the power converter is essential for proper operation of the whole IPT system. This current affects the performance of all other parts of the system (such as the magnetic coupling and the pick-up conditioning), and hence the general power flow from the static power supply to the pick-up coil. In fact, the track power supply accounts for the majority of the system cost. Normally, in order to make full use of the track power supply, multiple pick-ups are attached to a single track loop.



InductEV, Inc.
Exhibit 1020
Page 028

### 1.2.2 General Features

When compared with the conventional power supplies, an IPT system has the following features:

***Freedom of mechanical movement***. Because of the loose coupling between the primary and secondary of an IPT system, the pick-up can move along the track loop while allowing for some lateral displacement from the track centre. This is one of the most outstanding characteristics of IPT and differentiates it from traditional transformers. This freedom makes it possible to deliver power to movable equipment without direct electrical contact.

***Safe operation.*** In direct contrast to the conventional sliding contact power supplies (such as conductor bars in monorail trolleys), there is no direct electrical contact in the path of the power flow, so it is spark free. In addition, there are no open live wires, thus the possibility of accidental electric shock is eliminated. Moreover, IPT supplies enhance the insulation between the primary and the secondary sides, further improving the safety level to personnel and devices.

***Environmentally friendly.*** Because IPT has two independently enclosed parts, its operation is not affected by dirt, dust, water, or chemicals. Therefore, it can work in very harsh environments. Furthermore, it does not generate carbon residues, as is the case with traditional sliding contact systems using carbon brushes, and has no harmful effects on surroundings. Apart from magnetic and metal components, IPT appears inert to other materials when practical power transfer levels are considered. However, one serious concern that has been raised about the application of IPT, is whether it has any significant magnetic effect on human beings such as on-site workers. Studies carried out by the Power Electronics Research Group and the Medical School of the University of Auckland show that Very Low Frequency (VLF) electromagnetic fields, such as those at 10kHz, have no observable negative biological effects [3]. A possible explanation for this is that VLFs are far above any naturally occurring frequencies in the human body, at the same time, they are normally not high enough to possess sufficient power density to “heat” body cells as radio frequencies may do.

***Reliable and robust.*** There is no direct friction in an IPT system so that mechanical wear & tear, and electrical erosion are eliminated. In addition, chemical erosion of the conductors is essentially non existent because the electrical components can be completely enclosed. Consequently, the system is very reliable and robust, requiring almost no maintenance.



InductEV, Inc.
Exhibit 1020
Page 029

### 1.2.3 Suitable Applications

Based on its characteristics, IPT would be suitable for the following types of applications:

***Powering movable objects.*** IPT is particularly good for delivering power to movable objects such as monorail trolleys, AGVs (Automatic Guided Vehicles), moving parts within machine tools, etc. In these situations the relative movement may be a basic operational requirement, or simply designed for easy engineering implementation. There is no doubt that conductive cabling systems will continue to dominate in power supplies for static electric loads. However, IPT does offer a very good substitute for powering movable objects such as a monorail trolley, or an electric bus.

***Meeting special safety requirements.*** In some hazardous places such as in painting workshops and underground coalmines, IPT is very desirable as the potential dangers of fire and explosion from mechanical friction or electric spark are eliminated.

***Operating in harsh environments.*** IPT is suitable for supplying power in harsh environments where the conventional power supplies have great difficulties. These include under water, in the rain, under snow, and other harsh environments where dirt, dust, and chemicals may exist.

***Keeping reliable operation with minimised maintenance.*** If maintenance is to be minimised without compromising long life and reliable operation, IPT is a good option. For example, IPT can be used for contactless battery charging, or even better, to drive an EV (Electric Vehicle) on-line without using any batteries. Consequently, regular maintenance such as changing the battery electrolytes and cleaning the contact parts can be reduced or eliminated.

## 1.3 Advances and Challenges of IPT

### 1.3.1 Historical Achievements

The concept of loosely coupled inductive power transfer is not new. It has been investigated by several researchers since the early 1980s [4]. However, it is the development of power electronics, particularly the rapid advances in semiconductor power switches, that make IPT practically viable.

The pioneering research work which really put IPT into industrial practice was undertaken by the Power Electronics Research Group of the University of Auckland in early 1990s. Following the success of a prototype IPT system rated at 180W at the University of Auckland, the first significant commercial application of IPT was found in Daifuku Ltd of Osaka, Japan [5]. Daifuku, being one of



InductEV, Inc.
Exhibit 1020
Page 030

the world's largest materials handling system manufacturers, has been using IPT in its "Ramrun" electrified overhead monorail systems and AGVs.

"Ramrun" powered by IPT is widely used in manufacturing, storage and retrieval systems. Its advantages are obvious in "clean rooms" where semiconductors are made. It is also very popular in the car assembly industry because of its safe and reliable operation at a comparatively low cost. Fig. 1-2 shows two typical IPT powered trolleys for such materials handling applications. Here the two track conductors carry a current of 60A at a frequency of 10kHz. The pick-up system takes power from the track to drive a cage induction motor which can transport loads of 200 kg at a speed up to two metres per second. Practically, the track is powered in 100m section lengths, and can be driven with up to 10 trolleys running along it. Each trolley can receive up to 750W of power from the track [6-7].

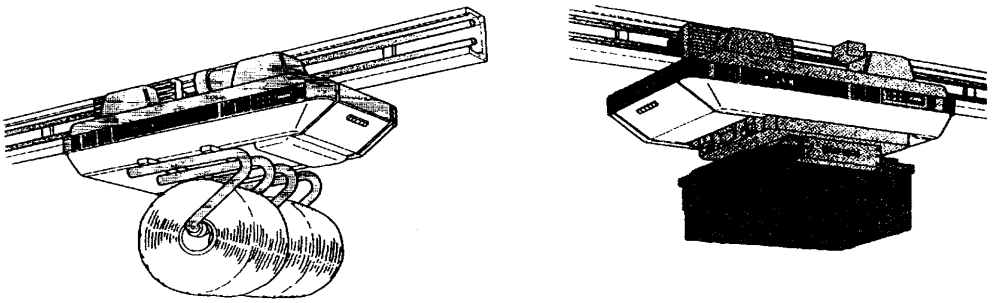

**Fig. 1-2: IPT powered monorail trolleys for materials handling applications**

An AGV is a cost-effective way of transporting low amounts of materials over a short distance. Compared with traditional battery powered AGVs, IPT powered AGVs have much less maintenance requirement and have a much longer life span due to the contactless battery charging or battery free operation. The AGV developed in Daifuku has a 3kW pick-up which is positioned 30mm above the track and allows ±30mm lateral off-centre movement without significant power reduction. It is interesting to note that AGVs are normally guided by a magnetic trip. In the case of IPT powered AGVs, in addition to power, the track can provide guiding information for the movement of AGV, so that self auto-steering is possible [8]. In addition, communications along the track and pick-up channels can be implemented for measurement and control purposes [9-11].

In 1994, a prototype IPT supply for an electric car was successfully developed for Walt Disney Imagineering (WDI) Ltd, which is an engineering branch of the Disney Empire. The application intended to use IPT to power small two-seater cars which travel around an 800m track in their "Autopia" attraction. The prototype track power supply was rated at 15 kW with a track length of 200m. Apart from the electric pick-ups, the vehicle also has batteries on it to supply the peak power.



InductEV, Inc.
Exhibit 1020
Page 031

Therefore, the system ran in partial on-line mode. During on-line operation, the pick-up is 65mm above the track and a ±300mm lateral displacement is allowed. Unfortunately, while successful, budget constraints halted the construction of this project.

A very novel project on IPT lighting, called IPT road studs (cats' eyes), was implemented in 1997 [12-13]. A 2 kW, 20A/20kHz, power converter was connected to a long closed track loop cable which was buried under the road. The road studs have small pick-up coils in them and the power picked up from underground is conditioned to light LEDs (Light Emitting Diodes), which divide the road lanes very clearly in dark, rain, or snow conditions. This project was successfully completed and an application can be seen in a tunnel in the suburb of Wellington, New Zealand.

Wampfler AG, Germany, in association with Auckland Uniservices Ltd and the Department of Electrical and Electronics at the University of Auckland, has successfully implemented a world first IPT project for people mover applications in 1997. In this project, a high power IPT electric power charger is used to inductively charge the batteries in an Electric Vehicle rated at 30 kW [14-15]. A charging coil carrying a current of 80A at 13kHz is buried underground and connected to a power converter. There are in total, ten pick-ups on each vehicle and each set of three batteries are charged at a current of up to 250 A! At such a fast charging speed, as illustrated in Fig. 1-3 (a), the batteries can be replenished in 2-3 minutes during its stay at a station where the passengers get on and off the vehicle. The vehicle is now in operation in a thermal park in Rotorua, New Zealand, where the environment is very harsh because of the existence of sulphur acid, dust and vapours from the geyser and boiling mud pools. During this same period, Wampfler AG developed a prototype electric train rated at 100 kW as shown in Fig. 1-3 (b). The train receives power inductively from the cables attached along a 400-metre track so that no on-board batteries are required [16].

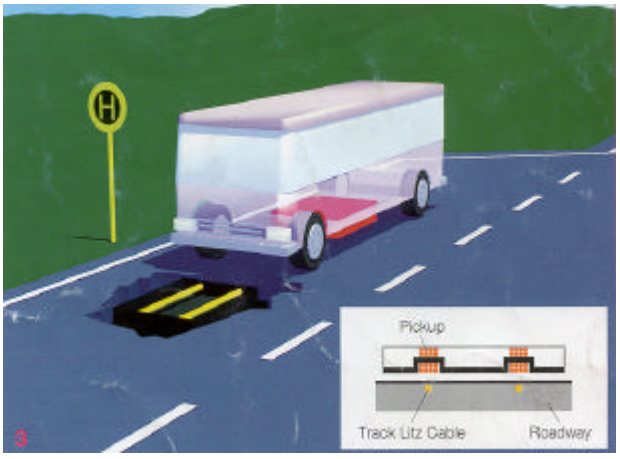


(a) Illustration of an inductively charged electric bus

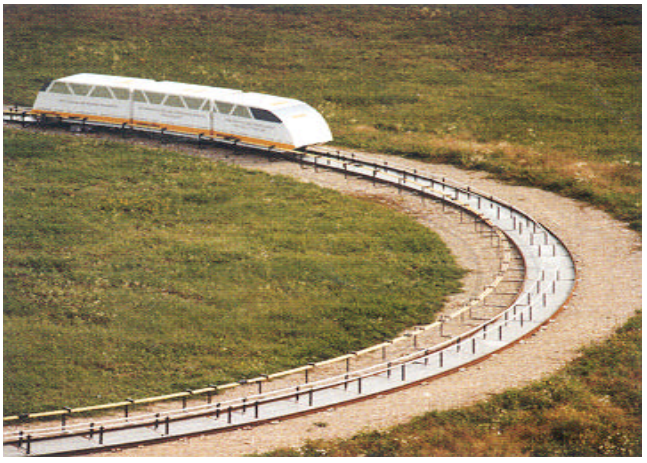

(b) A 100 kW prototype electric train

**Fig. 1-3: Typical applications of IPT in electric vehicles**



InductEV, Inc.
Exhibit 1020
Page 032

Apart from the projects mentioned above, other special applications of IPT have also been investigated. There are many publications on inductive battery chargers for electric vehicles [9,17-26]. Research work has also been reported on various areas such as aircraft entertainment systems [27], cordless power stations [28], machine tools [29], robot manipulators [10,30], coalmine power supplies [31], and underwater power plugs [32], although their practical applications have not yet been seen.

A very interesting medical application of inductive power transfer has been carried out by Djemouai of Montreal University of Canada [33]. Contactless battery charging techniques similar to those used in IPT have been employed to replenish the cells of implanted human organs from outside the skin. The power level reported is about 50mW and the operating frequency is as high as 20MHz. Obviously, the supply at such a low power level and high frequency is not suitable for normal IPT industrial applications.

### *1.3.2 Present Challenges*

Like most other new techniques, the development of IPT systems involve many challenges, including the theoretical development, technical implementation, and studies as to its social & economic effects.

As IPT mainly relies on power conversion and control techniques, its theoretical development is closely related to the field of Power Electronics. Power Electronics itself is a relatively new inter-disciplinary subject which covers a large area including electronics, control and communications. Among many involved theoretical aspects, the analysis and modelling of switch mode nonlinear circuits are of the main concern. Like most other power electronic applications, the further development of IPT depends largely on some fundamental advances in switch mode nonlinear theories. Moreover, the loose magnetic coupling between the primary track and the secondary pick-up coils of an IPT power supply is more difficult to analyse than a traditional closely coupled transformer. This further increases the circuit complexity so that proper compensation and control have to be taken into consideration in the design of an IPT system [15,34].

In addition to the theoretical problems, there are many existing technical limitations in the design of an IPT system. For example, apart from the passive components, the maximum voltage and current ratings combined with the switching speed of the semiconductor power devices are major constraints. The most suitable switching devices for IPT applications seem to be IGBTs (Insulated



InductEV, Inc.
Exhibit 1020
Page 033

Gate Bipolar Transistors) with commercial products up to the power level of 3kV/2kA, and a switching frequency up to 80kHz. The VA ratings of thyristors are much higher but their switching speed is too slow, whereas power MOSFETs (Metal Oxide Silicon Field Effect Transistors) can switch at a speed up to 1 MHz, but their voltage levels are too low for high power IPT applications.

The final aspect is related to economic and social concerns. Minimising the installation and operating cost is a main concern of a system design. Although the price of semiconductors has been dropping over the last two decades, the installation cost of an IPT system is still much higher than conventional power supplies. In addition, the maximum efficiency of an IPT system is about 85% at a rated load, compared with 98% for a typical power transformer. As a power supply system, this is not competitive. Moreover, although IPT is both safe and environmentally benign, its EMI (Electromagnetic Interference) needs to be considered carefully in the practical system design.

The three aspects mentioned above are closely related in a practical system design and implementation. Economic and social needs are the direct driving force of any engineering project but the real development depends on the available technical conditions and theoretical status. Regarding IPT, although many practical achievements have been obtained to date, technological advancement is still needed in the following aspects:

1) **The power level**. The maximum power level can be transferred via IPT is now about 300 kW. This level is low in comparison to normal power system supplies. It is not high enough to meet some heavy industry applications as well as public transportation systems such as large railway trains used for mass transportation.

2) **The track length**. The maximum track length of IPT now is in the range of several kms at low power levels. At 200kW, practical lengths of around 400m have been achieved [16]. This is clearly not enough for long distance power transfer applications, such as public transportation vehicles.

3) **System stability control**. It is always important to have a stable system in practical applications. At present some variable frequency controlled IPT power supplies can become unstable if not designed properly [35].

4) **EMC concerns**. Minimising the conducted EMI (Electromagnetic Interference) to the mains power supply and radiated EMI to surroundings is a challenging task. Having a high quality



InductEV, Inc.
Exhibit 1020
Page 034

track current with minimal harmonic distortion is particularly important for an IPT system, as the track is normally large and can not be enclosed in a box.

5) **Cost, efficiency and reliability.** To minimise cost and achieve high efficiency without compromising the system reliability is a general requirement for an engineering design. This is especially challenging for IPT for the reasons mentioned before.

In a practical design it is normally impossible to meet all the requirements to their best conditions at the same time, therefore trade-offs are inevitable and an optimisation is only possible under certain conditions related to a specific application. Nevertheless, having a deep understanding of the system properties and being able to determine the most important issues involved are crucial for a good system design. The limiting factors for IPT listed above are for the whole IPT system, however, the track power supply is of the most important concern as it largely determines the overall performance of an IPT system.

## 1.4 Scope of the Thesis

This thesis is a basic study on selected resonant converters for IPT applications aiming at improving the overall performance of IPT power supplies. Particular interest is to investigate various converter topologies and control methods in order to increase the power delivery level, improve the efficiency, as well as reduce the system cost. Although the whole system, including the secondary power pick-ups, is covered in the thesis, special attention is paid to high frequency track power supplies.

The following chapters of the thesis are arranged as follows.

Chapter 2 is a general overview on the technologies involved in IPT power supplies. It covers the fundamental parts of an IPT system and the major design techniques, including the track tuning, voltage-fed and current-fed inverting network topologies, pick-up tuning, power transfer control, and track current control.

In Chapter 3, the basic properties of the current-fed parallel resonant converters are studied. Various resonant frequencies are identified and ZVS (Zero Voltage Switching) frequency is analysed. In addition, the maximum loading condition as well as the frequency shift range are derived, and several frequency stability enhancing methods are proposed. Moreover, an improved current-fed resonant converter with dynamic ZVS start-up properties is proposed and implemented.



InductEV, Inc.
Exhibit 1020
Page 035

Chapter 4 proposes an improved current-fed parallel-series resonant converter which uses a CLC (Capacitor-Inductor-Capacitor connection) π trans-conductance network to improve the track current properties. It covers a basic property study and sensitivity analysis of a resonant track network. The simulation on the whole system, including the pick-ups, is undertaken to investigate the system dynamic properties.

Chapter 5 deals with the voltage-fed resonant converters. The phase shift control and soft switching operation of a normal voltage-fed series resonant converter are analysed first. Then an improved voltage-fed LCL (Inductor-Capacitor-Inductor connection) series-parallel resonant converter is discussed as a dual circuit of the current-fed parallel-series resonant converter.

Chapter 6 describes the mathematical modelling of a complete IPT system based on an improved current-fed CLC resonant converter using GSSA (Generalised State Space Averaging) techniques. The pick-ups and their tuning are included in this modelling.

Chapter 7 proposed two novel ways of generating high frequency AC currents. The first is concerned with a conceptually new method based on free oscillation and energy injection control. A simple example of a DC-AC converter is simulated and experimentally verified. A potential direct AC-AC converter is also proposed and its EMI (Electro-magnetic Interference) issue is discussed. A second approach using a current-fed converter based on self-sustained oscillation without an external controller is presented and its modified versions using PLL (Phase Locked Loop) and direct ZVD (Zero Voltage Detection) techniques are implemented for practical high power IPT applications.

Finally, Chapter 8 summarises the conclusions reached in this thesis. The major advantages and disadvantages of different resonant converters for IPT power supplies are compared. The contributions of the thesis are outlined and directions for future work are suggested.

## 1.5 References

[1] Terman, F. E.: *Radio Engineering*, McGraw Hill, Inc., 3rd edition, 1947.

[2] Boys, J. T. and Green, A. W.: “Inductively coupled power transmission – concept, design and application”, *IPENZ Transactions*, No.22, (1) EMCH, pp.1-9, 1995.



InductEV, Inc.
Exhibit 1020
Page 036

[3] Elliott, G.: "An investigation into the biological effects of 10 kHz (VLF) electromagnetic fields", *G. T. Murray Memorial Prize, IPENZ NZ,* ISBN-099460-06-9, pp.GAJE 1-10, 1994.

[4] Lukacs, J., Kiss, M., Nagy, I., Gonter, G., Hadik, R., Kaszap, K., and Tarsoly, A.: "Transmission of high frequency energy over long distances", *Proceedings of the Fourth Power Electronics Conference*, Budapest, 1981.

[5] Green, A. W. and Boys, J. T.: "An inductively coupled high frequency power system for material handling applications", *International Power Electronics Conference*, IPEC'93, Singapore, (2), pp.821-826, 1993.

[6] Chung, G.: *An intelligent controller for Inductive power systems - a modular design methodology*, ME thesis, Electrical and Electronic Department, the University of Auckland, November 1995.

[7] Green, A. W. and Boys, J. T.: "10kHz Inductively coupled power transfer – concept and control", *IEE Power Electronics and Variable Speed Drives Conference*, PEVD, Pub.399, pp.694-699, 1994.

[8] Dunlop, G. R, Jufer, M. and Perrottet, M.: "A phase sensitive guidance system for an inductively powered automatic guided vehicle", *Proceedings of 8th International Conference on Advanced Robotics*, ICAR'97, pp.181-186, 1997.

[9] Esser, A. "Contactless charging and communication system for electric vehicles" *IEEE Industry Applications Society Annual Meeting,* Conference Record, 1993.

[10] Kawamura, A., Ishioka, K. and Hirai, J.: "Wireless transmission of power and information through one high-frequency resonant AC link inverter for robot manipulator applications", *IEEE Transactions on Industry Applications*, Vol.32, No.3, May-June 1996.

[11] Zierhofer, C. M.: "A class-E tuned power oscillator for inductive transmission of digital data and power", *Proceedings of Sixth Mediterranean Electrotechnical Conference*, 1991.

[12] Boys, J. T. and Green, A.W.: "Intelligent road-studs – lighting the paths of the future", *IPENZ Transactions*, No.24, (1) EMCH, pp.33-40, 1997.

[13] Gurr, W: "Hardings road studs: 2kW series tuned IPT power supply", *Research Report of Auckland Uniservices Ltd, the University of Auckland*, 1997.

[14] Stielau, O. H., Boys, J.T., Covic, G. A. and Elliot, G. "Battery charging using loosely coupled inductive power transfer." *Eighth European Conference on Power Electronics and Applications*, EPC'99, September 1999.



InductEV, Inc.
Exhibit 1020
Page 037

[15] Covic, G. A, Elliott, G, Stielau, O. H. and Green, R. M.: "The design of contact-less energy transfer system for a people mover system", *Proceedings of International conference on power system technology*, Perth, Australia, pp79-84, December 2000.

[16] Hu, A., and Boys, J.: "Series-parallel resonant converters, Stage I: Current-fed, single ended, series-parallel converter simulation", *Research Report of Auckland Uniservices Ltd* for Wampfler AG, Germany, and Daifuku Ltd, Japan, 52 pages, June 1998.

[17] Hirai, J., Kim, T. W. and Kawamura, A.: "Study on intelligent battery charging using inductive transmission of power and information", *IEEE Transactions on Power Electronics*, Vol.15, No.2, March 2000.

[18] Juby L., Green, A. and Collinson, A.: "The design of a non-contact charging system for electric vehicles", *European Power Electronics Conference*, pp.573-576, 1997.

[19] Laouamer, R., Brunello, M, Ferrieux, J. P., Normand, O. and Buchheit, N.: "A multi-resonant converter for non-contact charging with electromagnetic coupling." *23rd International Conference on Industrial Electronics, Control and Instrumentation*, IECON97, Vol 2, pp.792-797, 1997.

[20] Abe, H., Sakamoto, H. and Harada, K.: "A non-contact charger using a resonant converter with parallel capacitor of the secondary coil", *IEEE Transactions on Industry Applications*, Vol. 36, No.2, March/April 2000.

[21] Hayes, J. G., Hall, J. T., Egan, M.G. and Murphy, J. M. D.: "Full-bridge, series resonant converter supplying the SAE J-1773 electric vehicle inductive charging interface", *IEEE Power Electronics Specialists Conference*, PESC'96, 29, pp.1913-1918, 1996.

[22] Hirai, J., Kim, T. W. and Kawamura, A.: "Study on intelligent battery charging using inductive transmission of power and information", *IEEE Transactions on Power Electronics*, Vol.15, No.2, March 2000.

[23] Klontz, K. W., Esser, A., Bacon, R. R., Divan, D. M., Novotny, D. W. and Lorenz, R. D.: "An electric vehicle charging system with 'universal' inductive interface", *Record of the Power Conversion Conference*, Yokohama, 1993.

[24] Kutkut, N. H., Divan, D. M., Novotny, D. W. and Marion, R. H.: "Design considerations and topology selection for a 120-kW IGBT converter for EV fast charging", *IEEE Transactions on Power Electronics*, Vol. 13, No. 1, January 1998.

[25] Sakamoto, H., Harada, K., Washimiya, S., Takehara, K., Matsuo, Y. and Nakao, F.: "Large air-gap coupler for inductive charger", *IEEE Transactions on Magnetics*, Vol.35, No.5, Part 2, September 1999.



InductEV, Inc.
Exhibit 1020
Page 038

[26] Severns, R., Yeow, E., Woody, G., Hall, J. and Hayes, J.: "An ultra-compact transformer for a 100w to 120kW inductive coupler for electric vehicle battery charging", *Proceedings of 11th Annual Applied Power Electronics Conference and Exposition*, APEC '96, Vol.1, pp.32-38, 1996.

[27] Kelley, A. W. and Owens, W.R.: "Connectorless power supply for an aircraft-passenger entertainment system", *IEEE Transactions on Power Electronics*, PE-4, (3), pp.348-354, 1989.

[28] Murakami, J., Sato, F., Watanabe, T., Matsuki, H., Kikuchi, S., Harakawa, K. and Satoh, T.: "Consideration on cordless power station - contactless power transmission system", *IEEE Transactions on Magnetics*, Vol.32, No. 5, Part 2, September, 1996.

[29] Hiraga, Y., Hirai, J., Kaku, Y., Nitta, Y., Kawamura, A. and Ishioka, K.: "Decentralised control of machines with the use of inductive transmission of power and signal", *Conference Record of the 1994 IEEE Industry Applications Society Annual Meeting*, Vol.2, pp.875-881, 1994.

[30] Esser, A. and Skudelny, H. C.: "A new approach to power supplies for robots", *IEEE Transactions on Industry Applications*, Vol.27, No.5, September-October 1991.

[31] Klontz, K.W., Divan, D. M., Novotny, D.W. and Lorenz, R.D. "Contactless power delivery system for mining applications", *IEEE Trans. Ind. Appl.*, IA-30, (1), pp.27-35, 1995.

[32] Heeres, B. J., Novotny, D. W., Divan, D. M. and Lorenz, R. D.: "Contactless underwater power delivery", *25th Annual IEEE Power Electronics Specialists Conference*, PESC '94 Record, Vol.1, pp.418-423, 1994.

[33] Djemouai, A.: "Prosthetic power supplies", *Wiley Encyclopedia of Electrical and Electronics Engineering Online*, John Wiley & Sons, Inc., December, 1999.

[34] Stielau, O. H. and Covic, G. A.: "Design of loosely coupled inductive power transfer systems," *IEEE-PES/IEE/CSEE International Conference on Power System Technology*, POWERCON 2000, December 2000.

[35] Boys, J. T., Covic, G. A. and Green, A. W.: "Stability and control of inductively coupled power transfer systems," *IEE Proceedings of Electric Power Applications*, Vol. 147, No.1, pp.37-43, January 2000.



InductEV, Inc.
Exhibit 1020
Page 039

## Chapter 2

# An Overview of IPT Power Supply Technologies

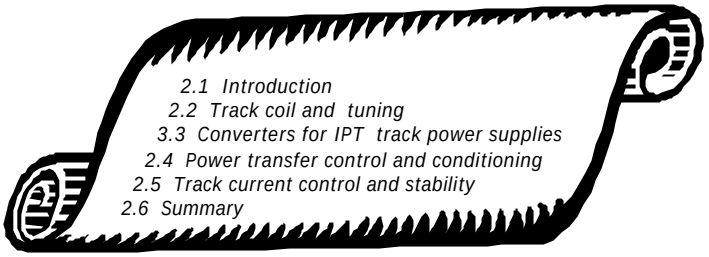


## 2.1 Introduction

The main objective of an IPT system is to transfer a large amount of power from a static track loop to some galvanically isolated "pick-up" circuits over a large air gap. The air gap gives much freedom to the mechanical movement of secondary power "pick-ups" but makes IPT a very loosely coupled system. In a practical situation the track "wire" may be very long while the magnetic "pick-up" coils may be quite short so that the actual coupling coefficient is typically 1% or less, compared with about 95-98% for transformers and 92% for induction motors [1]. To transfer power from the primary track loop to the secondary pick-up coil across an air gap, a high frequency alternating magnetic field linking the primary and the secondary as illustrated in the dotted line in Fig. 2-1 is required. Therefore, a power converter is necessary to generate a high frequency AC current along the track loop. Because the induced voltage in a pick-up coil is normally unsuitable to be used directly, a power conditioner is usually needed to maximise the power transfer capacity and regulate the pick-up voltage or current to meet the load requirement.

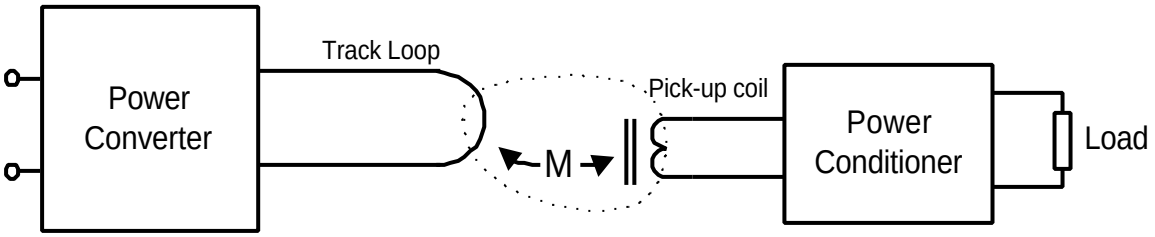


**Fig. 2-1: IPT coupling between the track loop and the pick-up**



InductEV, Inc.
Exhibit 1020
Page 040

Although other options exist, having a constant track current along the primary track coil is preferable in most cases to simplify the system design, especially when multiple pick-up loads are to be powered. In this sense, an IPT track power supply can be regarded as a high frequency AC current generator. Thus, the coupling of an IPT system appears to be more akin to a current transformer than a voltage transformer. It is however, the characteristics of an expanded track loop, a larger air gap, and high frequency power conditioning that differentiate an IPT power supply from a normal power transformer and ultimately determine its performance.

This chapter outlines the main technologies involved in IPT power supplies, including the track layout and tuning, power converting network topologies, mutual magnetic coupling, pick-up tuning, power flow control, as well as track current control. This overview is mainly based on published projects and papers, but the author's judgement and opinions are used here to set up a basic framework of IPT, so that the major problems and technical options can be covered and considered in a general picture. As IPT is a relatively new inter-disciplinary area, the general overview undertaken in this chapter is not only necessary for the rest of this thesis, but also can be used as a reference for future research work.

## 2.2 The Track Coil and Its Tuning Circuits

### *2.2.1 Track Layout*

According to different applications, the track coil of an IPT system can be laid out using extended parallel cables, partially parallel cables, or a lumped coil as shown in Fig. 2-2 (a)-(c) respectively.

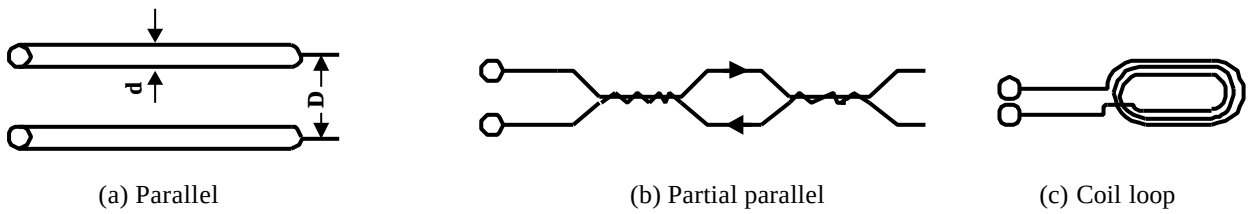


(a) Parallel (b) Partial parallel (c) Coil loop

**Fig. 2-2: Track layout**

Parallel cables can be set up overhead, buried underground, or attached along a rail. Their applications include monorail trolleys, AGVs (Automatic Guided Vehicles), and roadway vehicles [2]. The equivalent inductance per meter of parallel cables shown in Fig. 2-2 (a) can be expressed with the following equation [3]:



InductEV, Inc.
Exhibit 1020
Page 041

$$L = \frac{m}{p}\left[\frac{1}{4} + \ln\left(\frac{2D}{d}\right)\right] \quad (H/m) \qquad (2\text{-}1)$$

where μ is the permeability, d is the diameter of the cable, and D is the spacing distance between the conductors. Normally it is too costly to lay magnetic permeable materials along the track, therefore $m \approx m_0 = 4p \times 10^{-7}$ H/m.

In some applications such as lighting roadway studs (cats' eyes) [4], the pick-up loads are distributed at certain locations rather than moving along the whole track length. In this situation, as illustrated in Fig. 2-2 (b), the unused parts of the track wire are twisted together, thus essentially cancelling its magnetic effects on the cable surroundings along the majority of the track length. The total inductance of the track is thereby reduced since the twisted parts of the wire have almost zero inductance. This allows the generation of higher currents along a particular track length for a given power supply voltage.

In applications where only local IPT power transfer is required, such as an IPT electric battery charger [5-6], a lumped coil instead of an extended track can be used as illustrated in Fig. 2-2 (c).

Because of skin effects and proximity effects, at high frequencies, the ESR (Equivalent Series Resistance) of the track conductors are usually much higher than at DC. This may result in high conduction losses and thus poor power efficiency. To mitigate this problem, multiple strand individually insulated wires (Litz wires) may be used [1-3].

### *2.2.2 Track Tuning Circuits*

Although it is possible to drive an IPT track coil directly, there are several advantageous reasons for tuning a track with additional reactive components such as capacitors and inductors.

The first reason is for the compensation of the track inductance. This is because for a long track, or a coil with a large number of turns, the track inductance can be very large, up to several hundreds of micro-henries. At high frequencies, the inductance of the track may be too large for the power supply to drive given the limited voltage ratings of the available semiconductors. In other words, the track length cannot be too long if a certain track current level is required. In practice, the track inductance is typically about one micro-Henry per meter. If the track driving voltage available from the power converter is 1000V rms, then to get a track current of 100A rms at 15kHz, the maximum



InductEV, Inc.
Exhibit 1020
Page 042

length that can be driven is only about 106m. It is clear that in this situation having a series tuning capacitor $C_p$ as shown in Fig. 2-3 (a) can compensate for the track inductance, and accordingly increase the track length that can be handled.

Another important reason for track tuning is to construct resonant tanks for resonant converters. As will be discussed later, resonant converters are often desirable and suit IPT applications. Resonant circuits (also known as resonant tanks or resonant networks) enable "soft-switched" operation of the semiconductor switches which reduces switch losses and EMI (Electro-magnetic Interference). However, at least one inductor and capacitor pair has to be designed for electrical oscillations in a resonant circuit for this purpose. For IPT, the track inductor is already available as a necessary part of the IPT system. It can be tuned in series, or parallel, or in a composite form as shown in Fig. 2-3 (a)-(c). In fact, a resonant tank is a very important part of most resonant converters. Different track tuning configurations may result in different types of resonant power supplies with quite different properties in aspects such as reactive power flow, power factor, track current sensitivity, stability, and efficiency. Dynamic track tuning using mechanical movement, magnetic amplifiers, or switch mode control methods is all possible to vary the tuning capacitors and inductors. However, normally it is very expensive to change the values of these reactive components at high power levels.

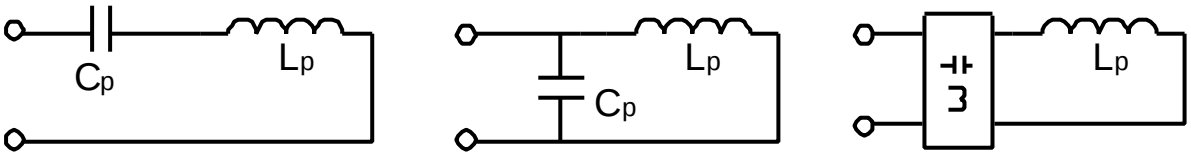


(a) Series tuning (b) Parallel tuning (c) Composite tuning

**Fig. 2-3: Track tuning methods**

In some cases, track tuning is undertaken for harmonic filtering purposes. It can improve the current and voltage waveforms, particularly the current waveforms of an exposed track loop, so that the radiated EMI can be reduced. In addition, it can also effectively prevent the harmonic propagation in the circuit due to its filtering function, therefore the conducted EMI as well as the EMS (Electro-magnetic Susceptibility) can be improved.

For the reasons mentioned above, the tuning circuit between the track and the switching network is often called a compensation circuit, a resonant circuit/tank, or an EMC (Electromagnetic Compatibility) filter, depending on which aspect is emphasised.



InductEV, Inc.
Exhibit 1020
Page 043

## 2.3 Power Electronic Converters for IPT Track Power Supplies

### *2.3.1 Basic Power Conversion Formats*

There are two basic approaches to obtaining a high frequency track current output using IPT power supplies: one is via a linear amplifier and the other is to use a switch mode power converter. In the former case, the semiconductor devices operate in a linear region where power loss is high [7]. Therefore, this approach is only practical for low power applications where power efficiency is perhaps not so important but high quality output waveforms are of great significance. For medium to large power supply IPT applications, power efficiency is of the major concern. As such, switch mode power converters are dominant.

The input power source to a switch mode IPT power converter can be either AC or DC. Thus in principle, power converters for IPT can use either a direct AC-AC converter, a DC-AC converter/inverter, or a two stage AC-DC-AC converter, as long as they can generate the required high frequency AC current along the track loop. However, existing AC-AC converters, including the phase controlled AC voltage regulators, PWM controlled AC choppers, cycloconverters and their variations - matrix converters, are unable to generate very high frequency AC outputs compared to its input source [8]. Therefore, they are not suitable for IPT applications. A new concept AC-AC converter based on energy injection control and free oscillation is proposed in Chapter 7 of this thesis, but further study on its conducted EMI is necessary. To date the most common option for IPT track power supplies is the DC-AC power converter/inverter. The DC power input to the inverter may be sourced either from batteries or a regulated DC power supply. However, in high power industrial applications, AC-DC rectifiers converting the mains power supply to a DC voltage source are most commonly used. With more stringent requirements in EMC and power quality, extensive research is being carried out on harmonic and power factor control of rectifiers, particularly in the area of reversible rectifiers [9]. To improve the power efficiency, attention is also being paid to the use of synchronous rectifiers in which active switches such as MOSFETs with low on-state resistances are used to replace traditional rectifier diodes [8]. Nevertheless, being simple, reliable and cheap, normal diode rectifiers (as shown in Fig. 2-4) are still being widely used in practical applications. LC passive harmonics filters are normally added at the front end of the rectifier to mitigate the harmonic problem. Alternatively, active filters and PFCs (Power Factor Controllers) can be used [10], even though they are still very expensive for most applications. Other power conditioning techniques such as harmonic injection approaches have also



InductEV, Inc.
Exhibit 1020
Page 044

been proposed to improve the input current waveforms so that "harmonic pollution" of the mains power supply can be minimised [11].

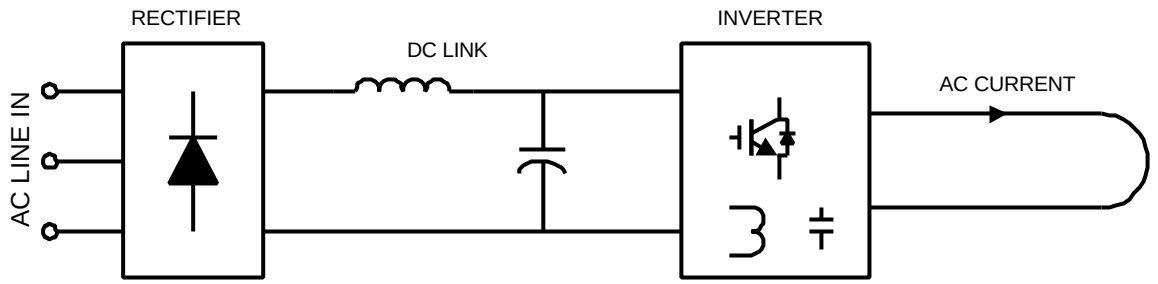


**Fig. 2-4: Typical AC-DC-AC configuration for IPT power supplies**

### *2.3.2 PWM Hard Switching and Resonant Soft Switching Converters*

PWM (Pulse Width Modulation), promoted by the development of fully controlled semiconductor switching devices, is a very popular technique employed in modern power electronics. Compared to the traditional phase controlled converters using semi-controllable switching devices such as SCRs (Silicon Controlled Rectifiers, also called thyristors), PWM switching techniques have led to higher quality power conversion and control. Moreover, PWM switching generates less low frequency harmonic components, making the EMC filters smaller and easier to design. However, normal PWM is characterised by hard switching operations, which means that the "on" and "off" transitions of the switching devices occur at non-zero voltage or zero current instants. Consequently, switching losses are high and the power efficiency is poor. This limits the switching frequency and thereby the minimisation of the converter size. Normally additional soft switching capacitors have to be designed in these converters to shift the dynamic voltage and current waveforms apart to reduce the switching losses and ensure the switches are within their safe operation area. Another drawback of traditional PWM control is that it generates square waveforms causing high dv/dt or di/dt and large harmonics, which not only increases the stress on the switches, but also causes larger EMI.

To overcome the problems mentioned above, i.e., to minimise switching losses and EMI, soft switching techniques have achieved considerable interest over the past decade. The basic idea here is to control the transitions of the switches to occur at zero voltage or zero current points - ZVS (Zero Voltage Switching) and ZCS (Zero Current Switching) respectively - so that the switching losses are essentially eliminated. In general, full or quasi resonance soft switching of a power switch occurs at one or more of the following four conditions.



InductEV, Inc.
Exhibit 1020
Page 045

Switching on and off at zero voltage points of a parallel capacitor. As the capacitor voltage cannot change instantaneously, and the time for the switches to turn on and turn off is relatively short, ZVS can be approximately achieved.

For the similar reason as 1), switching on and off can occur at zero current points of a series inductor due to the slow rate of change of current (di/dt) at that point. Consequently, approximate ZCS can be achieved.

Switching on and off at zero voltage when a parallel diode is conducting. The anti-parallel body diodes of many power switches, such as those of MOSFETs and IGBTs, are often used for this purpose.

Switching on and off at intervals of a discontinuous current mode. As the circuit is equivalent to an open circuit during a discontinuous current period, ZCS or ZVS may be achieved.

Utilisation of electrical resonance is the most common way of satisfying soft switching conditions. However, compared to traditional PWM converters, this has obvious disadvantages. These disadvantages include additional reactive components, higher peak current or voltage ratings, operating frequency uncertainties, and difficulties in controller design. In spite of all these drawbacks, resonant converters are becoming very popular because of their significant contribution to switching loss reduction and better waveform generation. In IPT applications, EMC is a particularly important concern as the track loop or coil is normally large and exposed to the outside world. In consequence, high quality track current waveforms are of great importance so that resonant converter power supplies are desirable.

Resonant converters are generally categorised into load resonant converters and quasi-resonant converters (also named as resonant-switch converters) [12]. They can also be constructed by using resonant links on the source side, or by adding independent commutation circuits [13]. Because an IPT system has an inherent track inductor and requires high quality track current waveforms, load resonant converters that utilise the full resonance of the track resonant circuit are normally the simplest and the most economical choice. Quasi-resonant converters, on the other hand, use local resonance occurring on small soft switching capacitors or inductors near switch transitions to achieve soft switching. They work like PWM converters in the sense that the operating frequency is constant. However, compared to traditional PWM converters, they have less freedom in gate control because the on/off timing of the switching devices is critical to achieving soft switching. Therefore,



InductEV, Inc.
Exhibit 1020
Page 046

a quasi-resonant converter can be regarded as a compromise between a full load resonant converter and a PWM converter.

### 2.3.3 Voltage-Fed and Current-fed Converters

The input source to a power converter can be either a current or voltage source. Accordingly, the converter topologies are grouped as either voltage-fed converters (also named voltage source converters), or current-fed converters (current source converters).

A voltage-fed DC-AC converter/inverter has two basic topologies: full bridge, and half bridge, as shown in Fig. 2-5. The switching network of the full bridge topology has four switches, whereas two of these switches are replaced with two suitably large capacitors in a half bridge topology. As the voltage changes across these capacitors are negligible under steady state conditions, they serve as voltage sources with half the magnitude of the DC power supply. Therefore, the maximum voltage output of the half bridge inverter is $\pm V_d/2$ compared to $\pm V_d$ in the full bridge topology.

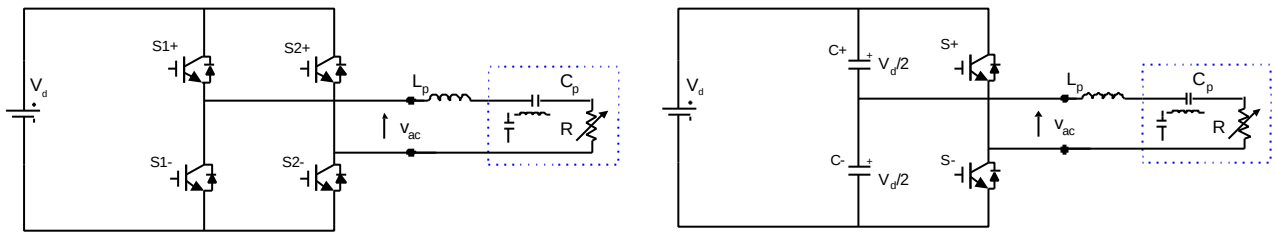


(a) Full bridge (b) Half bridge

**Fig. 2-5: Full bridge and half bridge voltage-fed inverters**

The frequency, magnitude, or phase of the output voltage of a voltage-fed switching converter may be controlled with power switches at their gates. A dead time (also called blanking time) between the turn-on and turn-off of each pair of switches in the same leg is necessary in order to avoid the shorting of the voltage source producing a “short through” failure in the switching devices. The minimum duration of the dead time is determined by the on and off delays of the switching devices, plus a safety factor.

Theoretically, a current-fed resonant converter is the dual of the voltage-fed resonant converter. However, practically, there is a big difference. This results from the fact that a current source cannot stand alone naturally like a voltage source without using superconductivity or a closed loop control. For economic reasons, a large inductor is normally put in series with a voltage source to form a quasi-current source as shown in Fig. 2-6. As the current flowing through the inductor is nearly constant at high frequencies under steady state conditions, it appears like a current source.



InductEV, Inc.
Exhibit 1020
Page 047

However, this inductor and voltage source configuration increases the system order and can cause dynamic problems requiring special circuit control and protection methods [14].

Similar to voltage-fed resonant converters, a full bridge topology and a push pull current-fed topology with a phase splitting transformer dividing the DC current are shown in Fig. 2-6. There are not many differences in the performance of these two topologies, but as will be seen in Chapter 3, the latter does not require isolated high-side gate drives and doubles the resonant voltage.

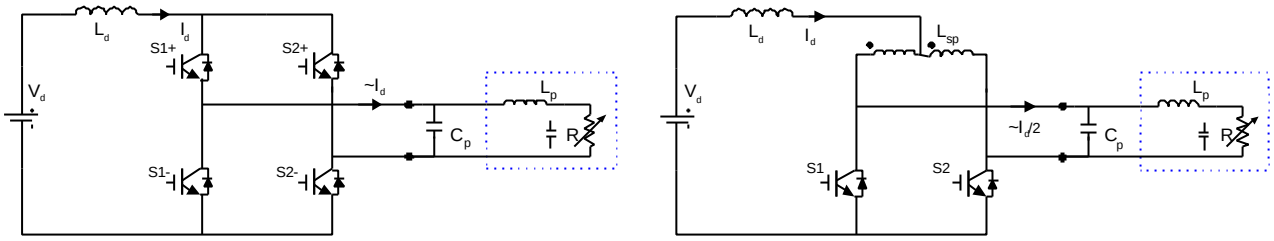


(a) Full bridge (b) Push pull

**Fig. 2-6: Full bridge and push pull current-fed inverters**

Analogous to the protection required to avoid shorting of the voltage source in voltage-fed converters, here the current source must not be broken to avoid the occurrence of high over-voltages. Therefore, at least one leg has to be on over the whole period of operation. However, because the switching devices normally turn on faster than they turn off, practically there may be no need to design an overlap time in gate drives of normal switching devices [15].

A very important aspect needing special attention in the design of voltage or current-fed inverters is the connection between the switching network and the resonant tank. Because two voltage sources cannot be connected in parallel arbitrarily due to the possibility of shorting the sources, the output of a voltage-fed inverter should not be connected to a voltage-source type of load such as a pure capacitor branch. In consequence, a voltage-fed switching network normally matches series tuned (or series-parallel tuned with a series branch in the beginning) types of resonant tanks with at least one inductor being series connected at the input port as illustrated in Fig. 2-5. Similarly, for a current-fed inverter, as two current sources cannot be placed in series arbitrarily due to the possibility of creating over-voltage problems, the output of a current-fed switching network should not be connected to a current source type of load such as a load comprising inductive branches only. Thereby, the current-fed inverting network normally matches parallel-tuned (or parallel-series tuned with a parallel branch first) resonant tanks with at least one capacitive branch connected at the input port as illustrated in Fig.2-6. In the above two situations, a series or parallel connected resistor at the input port will also do, but they are seldom used in practice since this introduces high power losses.



InductEV, Inc.
Exhibit 1020
Page 048

### 2.3.4 Switching Devices

From the appearance of thyristors in 1957 to the development of modern smart power modules, power switching devices have been continuously forcing the advance of power electronics [16]. From circuit design point of view, selecting appropriate switching devices is crucial since they are most likely to fail among all the components of a power converter. The choice mainly relies on a good knowledge of the circuit properties as well as the characteristics of the available power switches. With the development of wafer fabrication techniques, various types of power semiconductor switching devices have been introduced. These mainly include: thyristors (also known as SCRs -Silicon Controlled Rectifiers), triacs, gate turn off (GTO) thyristors, bipolar junction transistors (BJTs), metal-oxide-semiconductor field effect transistors (MOSFETs), insulated gate bipolar transistors (IGBTs), and MOS-controlled thyristors (MCT). These devices may be classified into three types depending on the degree of controllability:

Diode. No separate control gate. On and off states change with the main circuit voltage/current.

Semi-controllable devices. Can be controlled on with a gate signal but turning off is only possible with the aid of the main circuit. Thyristors are typical semi-controllable devices which can latch the “on” state after being fired at gate with a current pulse.

Fully controllable devices. Can be turned on and off by gate control signals. However, it should be noted that for most switches like BJTs, MOSFETs, GTOs, full control is only valid in one “forward” direction while the reverse direction is either blocked or conducts like a diode.

A more detailed investigation of the device switching characteristics shows that the transitions of all switches fall into two basic types: circuit commutated and external signal controlled. A diode is a typical circuit commutated device, while all other devices have gate control abilities. However, due to the technical constraints in wafer fabrication, none of the available power semiconductor switches is completely gate signal controllable like an ideal switch or a relay. A practical switch-mode nonlinear process can be very complex and it is this complexity, combined with the commutation of the semiconductor switches, that makes power electronic circuits very difficult to analyse and control.

Table 2-1 shows some typical specifications and gate control characteristics of several commonly used semiconductor power switches. It can be seen that the traditional power diode and thyristor have the largest power capability, while the MOSFET has the fastest switching frequency. Other



InductEV, Inc.
Exhibit 1020
Page 049

switches like the IGBT have characteristics in between these extremes. Practical IPT track power supply converters normally operate between 10-100kHz, therefore thyristors, and GTOs are too slow for IPT applications. The switching speed of the BJTs is restricted, and like thyristors and GTOs, their gates are current source driven, so they are not preferred either. This leaves MOSFETs and IGBTs as suitable choices for IPT applications. As the maximum voltage ratings of MOSFETs are low, and their on state resistances increase sharply with the increase of its voltage ratings, MOSFETs are only good for low voltage applications up to a level of about 800V. For normal industrial IPT applications at higher voltages, IGBTs are therefore the best choice. It seems that MCTs are also suitable devices for IPT as they are fast, voltage triggered on (with a latching characteristic), and can be turned off using gate signals or via circuit commutation. However, at this time they are not mature enough to compete with the cost and reliability of available IGBTs and MOSFETs. Two new switching devices named IGCTs (Integrated Gate Commutated Thyristors) and IEGTs (Injection Enhanced Gate Transistors) are claimed to have much improved performance such as easy gate drives, faster switching speed, and low conduction losses [17-19], unfortunately they are not commonly available yet. In the long run, silicon carbide (and diamond) power semiconductors seem very promising alternatives to the conventional silicon based switching devices since they have the potential for high-power, high-frequency and low-conduction-drop characteristics [20].

**Table 2-1: Comparison of semiconductor power switching devices**

| *Device Type* | Max Freq. | Typical Max V/A rating | $V_{on}/R_{on}$ | Gate control |
|---|---|---|---|---|
| ***Diode*** | Slow - fast | High, 7kV/5kA | 0.3-1V | Circuit commutation |
| ***Thyristor*** | Slow, 1kHz | High, 3-7kV/5kA | Low, 1-3V | Current pulse triggered on |
| ***Triac*** | Slow, 1kHz | Med, 1kV/50A | Low, 1-3V | Current pulse triggered on |
| ***GTO*** | Slow, 1kHz | High, 6kV/6kA | Low, 1-3V | Current pulse triggered on and off |
| ***MCT*** | Med, 30kHz | Med, 3kV/2kA | Low, 1-2V | Voltage pulse triggered on and off |
| ***MOSFET*** | Fast, 1MHz | Low, 0.2-1kV/1kA | 1mΩ-4Ω | Voltage level controlled on and off |
| ***BJT*** | Med, 10kHz | Low, 1.5kV/1kA | Low, 1V | Current level controlled on and off |
| ***IGBT*** | Med, 80kHz | Med, 1.7-6.5kV/2.4kA | Med, 1-4V | Voltage level controlled on and off |

It is worth noting that the fully controllable devices have promoted the PWM control techniques, however, the development of resonant converters puts forward a new demand for thyristor type switching devices because of their natural commutation properties. Using these devices, soft switching turn-off can be achieved without requiring exact gate control timing. Nevertheless,



InductEV, Inc.
Exhibit 1020
Page 050

traditional thyristors and GTOs are not suitable for IPT resonant converters for the reasons mentioned earlier. In addition, as resonant converters normally deal with oscillatory AC waveforms, they often require fast AC switches with bi-directional control and conduction abilities. Unfortunately, to date fast AC switches are not commercially available. Fig. 2-7 shows two ways of forming these switches using available IGBTs or MOSFETS. The first one combines four fast diodes in a full bridge configuration and an active switch; the second uses two active switches in series. Clearly, the second configuration shown in Fig. 2-7(b) has an advantage of allowing individual control of the switches. The disadvantage of both the types over a single switch option is the larger voltage drop and resultant high conduction losses that are present.

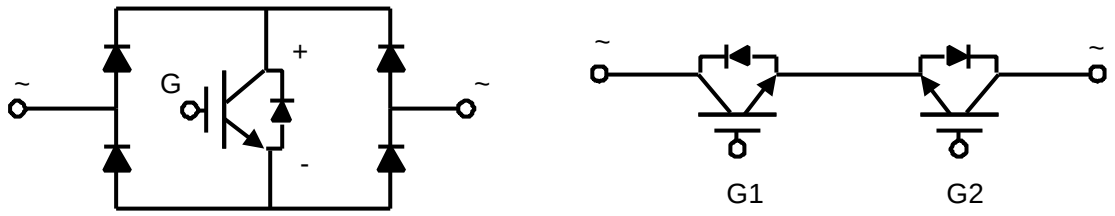


(a) Type 1 (b) Type 2

**Fig. 2-7: Combined bi-directional fully controlled power switches**

Overall, the selection of power switches takes into account the strong interaction between the requirements of the applications and the properties of the switching devices themselves. A new trend in power integration is to embed the switch modules, the gate drive circuitry, as well as the necessary protection circuitry into one block, called a smart-power module [21]. This can greatly simplify the circuit design and improve the general performance of a power converter.

## 2.4 Power Transfer Control and Conditioning

### *2.4.1 Coupling Coefficient and Coupling Factor*

IPT power transfer is based on the mutual magnetic coupling between the primary track coil and the secondary pick-up coil. The mutual inductance between these two coils is determined by the core material, the number of turns, and the geometry. A thorough analysis of magnetic field distribution may yield this parameter, but an easier way is to measure the induced voltage at the pick-up coil, and then determine the mutual inductance with the following formula:

$$M = \frac{V_{so}}{wI_p} \qquad (2\text{-}2)$$



InductEV, Inc.
Exhibit 1020
Page 051

where $V_{so}$ is the magnitude of the open circuit voltage of the secondary pick-up coil as shown in Fig. 2-8, $I_p$ is the primary track current, and ω is the angular frequency.

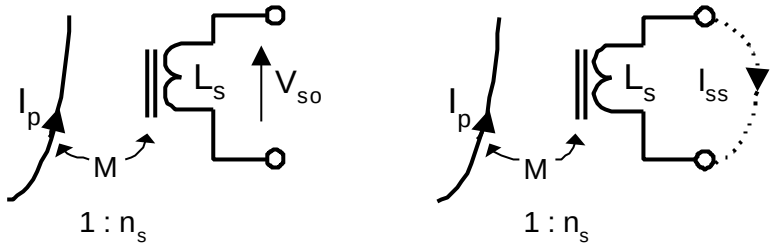


**Fig. 2-8: Open circuit voltage and short circuit current of the pick-up coil**

Traditionally the degree of coupling between two coils is expressed with a coupling coefficient defined as [3]:

$$k = \frac{M}{\sqrt{L_p L_s}} \tag{2-3}$$

where $L_p$ and $L_s$ are self-inductance of the primary coil and secondary coil respectively, M is the mutual inductance.

However, for an IPT system, the pick-up is a lumped coil while the primary track is normally extended over a large area. This makes it difficult to determine the exact part of the track that couples with the pick-up. If the total inductance of the track loop is considered as $L_p$, the resultant coupling factor would be very low and does not properly reflect the real local coupling between the pick-up and the track, since the majority of the track may not be coupled with the pick-up at all. To solve this problem, another parameter, termed "the coupling factor", is introduced in this thesis. It is defined as:

$$k_f = \frac{N_s I_{ss}}{N_p I_p} = n_s \frac{I_{ss}}{I_p} \tag{2-4}$$

where $n_s$ is the turns ratio between the secondary pick-up coil and the primary track, and $I_{ss}$ is the short circuit current as shown in Fig. 2-8 which can expressed as:

$$I_{ss} = \frac{V_{so}}{jwL_s} \tag{2-5}$$

Considering that the open circuit voltage of the pick-up is:

$$V_{so} = jwMI_p \tag{2-6}$$



InductEV, Inc.
Exhibit 1020
Page 052

$I_{ss}$ can be further expressed as:

$$I_{ss} = \frac{M}{L_s} I_p \tag{2-7}$$

It is interesting to see that the short circuit current $I_{ss}$ is independent of the frequency and the ratio between the primary and the secondary currents is similar to a current transformer. In fact, the concept of the coupling factor defined in (2-4) reflects the mmf (magnetic motive force) ratio of this "current transformer". For an ideal current transformer which is completely coupled via an ideal magnetic core, the net magnetising mmf required is zero, thus the primary mmf ($I_pN_p$) and secondary mmf ($I_{ss}N_s$) must be equal in magnitude and opposite in direction. Consequently, the ratio between $I_{ss}N_s$ and $I_pN_p$ is one. For an IPT system, the coupling is not ideal at all. A much larger primary mmf than secondary mmf is required to generate the magnetic field. Owing to the increase of the magnetic resistance in the magnetic path, the weaker the coupling, the larger the difference. Therefore, the ratio shown in equation (2-4) can reflect the real coupling degree between the primary and secondary. From (2-7) and (2-4), the definition of the coupling factor can be further expressed as:

$$k_f = n_s \frac{M}{L_s} \tag{2-8}$$

Because of the fact that the mutual inductance M is proportional to the number of turns, while the self inductance $L_s$ is proportional to its square, the above equation shows that the coupling factor $k_f$ is actually independent of the number of turns and only reflects the coupling caused by the geometry and core material differences in a design. Fig. 2-9 shows three typical coupling types in IPT applications. For a toroid type shown in Fig. 2-9(a), it is very similar to a current transformer with a one turn primary and movable secondary. The coupling factor of this type is very high, typically being larger than 0.95. For a mono-rail trolley application as shown in Fig. 2-9(b), the track conductor is partially enclosed by the pick-up ferrite core, causing a lower coupling factor of about 0.6-0.8. For a typical roadway application such as might be used in roadway electric vehicles, a flat ferrite core layout design as shown in Fig. 2-9(c) allows for a larger vertical and bilateral displacement of the pick-ups [2], but results in a very poor coupling factor of about 0.4 or less. If this design is used for a battery charger with a lumped track coil [5], ferrite cores may also be placed under the track wire to increase the coupling factor at the expense of higher track costs and higher track inductance.



InductEV, Inc.
Exhibit 1020
Page 053

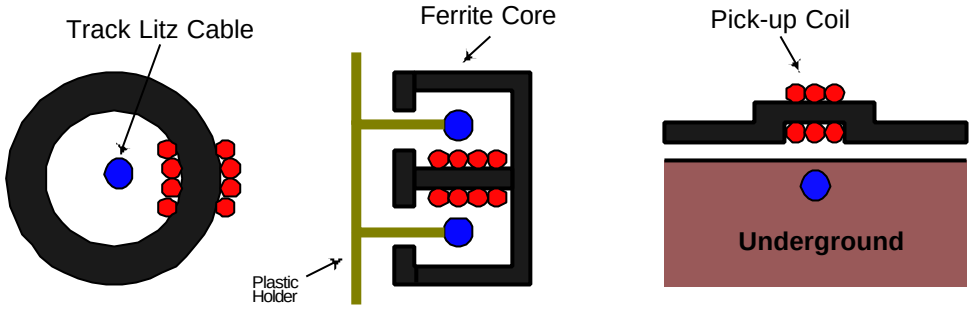


(a) Toroid type (b) Monorail trolley type (c) Roadway type

**Fig. 2-9: Typical coupling configurations between the track coil and the pick-up**

Similar to a current transformer, at a given coupling situation, a larger number turns on the pick-up will result in smaller short circuit current. This can be seen clearly by rewriting equation (2-8) as:

$$I_{ss} = \frac{k_f}{n_s} I_p \tag{2-9}$$

For an ideal current transformer, $k_f$ is equal to one, so that the current ratio is inversely proportional to the turns ratio. In the situation of a loosely coupled IPT system, this inverse relationship still holds but is affected by the coupling factor $k_f$ since the maximum current that can be obtained from the secondary pick-up is also proportional to the coupling factor.

### *2.4.2 Pick-up Tuning and Power Transfer Capacities*

Assuming the track current is constant, then under steady state conditions the induced emf (Electro-Motive Force) in the pick-up of an IPT system is a constant AC voltage source. This voltage source is in series with the self-reactance $\omega L_s$ of the pick-up, so that a Thevinen equivalent of the pick-up circuit can be shown in Fig. 2-10(a). The circuit can be further transformed into a Norton equivalent as shown in Fig. 2-10(b).

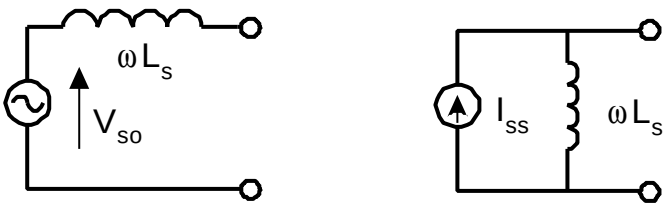


(a) Thevinen equivalent (b) Norton Equivalent

**Fig. 2-10: Equivalent circuits of the pick-up coil**



InductEV, Inc.
Exhibit 1020
Page 054

Power can be transferred to a load R being directly connected to the pick-up. Nevertheless, due to the large internal reactance, the maximum output voltage, current and thus the power will be very limited. The maximum output power occurs when the load resistance R is equal to the internal reactance $\omega L_s$, and this maximum power can be expressed as:

$$P_m = \frac{1}{2} V_{s0} I_{ss} \tag{2-10}$$

where $V_{so}$ is the open circuit voltage and $I_{ss}$ is the short circuit current.

In order to improve the power output capacity, some compensation, or tuning in the pick-up, is necessary. There are two basic tuning topologies: series tuning and parallel tuning as shown in Fig. 2-11 and Fig. 2-12. Some basic power transfer properties of these tuning methods are listed in table 2-2 in comparison with the situation without any compensation. Their voltage and current output characteristics are shown in Fig. 2-13 compared with the situation of no compensation.

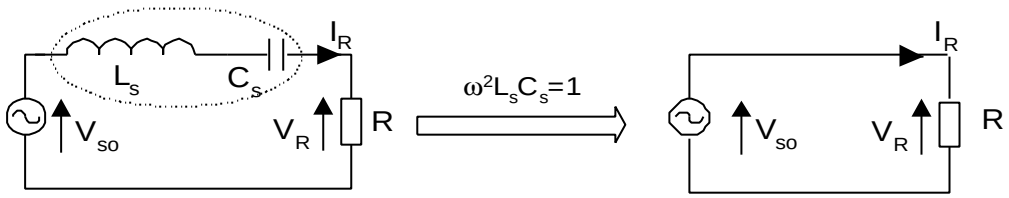


**Fig. 2-11: Series tuned pick-up**

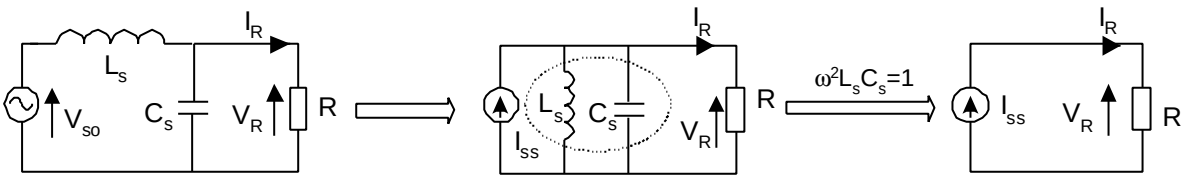


**Fig. 2-12: Parallel tuned pick-up**

**Table 2-2: The output properties of the different pick-up compensations**

| ***Maximum Outputs*** | **No compensation** (at max power condition) | **Series compensation** (fully tuned) | **Parallel compensation** (fully tuned) |
|---|---|---|---|
| ***Voltage*** $V_R$ | $V_{so}/\sqrt{2}$ | $V_{so}$ | $Q_s V_{s0}$ |
| ***Current*** $I_R$ | $I_{ss}/\sqrt{2}$ | $Q_s I_{ss}$ | $I_{ss}$ |
| ***Power*** $P_m$ | $V_{so} I_{ss}/2$ | $Q_s V_{so} I_{ss}$ | $Q_s V_{so} I_{ss}$ |

Note: for series tuning, power factor $Q_s=\omega_0 L/R$; for parallel tuning $Q_s=R/(\omega_0 L)$.

It can be seen that a fully series-tuned pick-up can yield a pure voltage source at the value of the open circuit voltage $V_{so}$. Similarly, Fig. 2-12 shows that a fully parallel tuned pick-up gives a pure



InductEV, Inc.
Exhibit 1020
Page 055

current source at the value of the short circuit current $I_{ss}$. Therefore, theoretically they have unlimited power output capability. However, practically if the load resistance R is too small for the series tuned pick-up, or too large for the parallel tuned one, the quality factor $Q_s$ would be very large. Large $Q_s$ will make the tuning very difficult and tedious, and also make the system too sensitive to parameter variations. Therefore, the maximum power that can be transferred corresponds a specified maximum quality factor $Q_s$, which is normally limited less than 10. Table 2-2 shows the output power of the pick-ups in terms of $Q_s$ and $V_{so}I_{ss}$. It can be seen that the power transfer capability of a fully tuned pick-up can be increased greatly, being $2Q_s$ times higher than the uncompensated one.

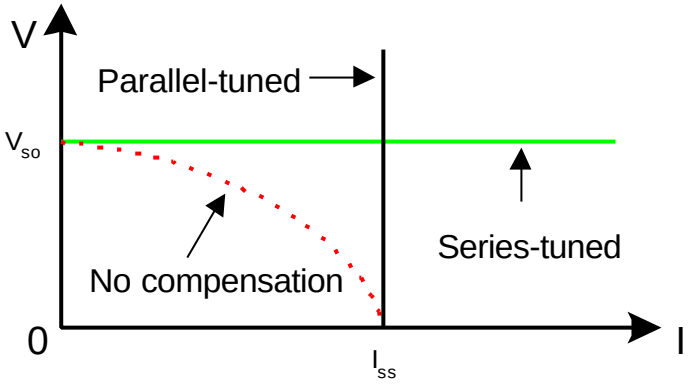


**Fig. 2-13: Pick-up voltage and current characteristics**

Higher power capability as above is obtained as the voltage or the current of the pick-up coil is boosted via tuning. Table 2-2 shows that for series tuning, the output current, being the same as the pick-up coil current, is $Q_s$ times higher than the short circuit current. Similarly, for a parallel tuned pick-up, the output voltage, being the same as the pick-up voltage is increased by $Q_s$ times that of the open circuit voltage. Thus, as pointed out in [22], the true cost of a higher power output capacity is a higher VA rating of the pick-up coil. Nevertheless, in a practical design, individual voltage and current ratings may need to be taken into consideration rather than just the total VA rating. For instance, a coil rated at 5A/100V may be preferred to a coil of 10A/50V since the lower voltage rating variation at this low level makes little difference to the insulation requirements, whereas reducing the current can reduce the coil size and cost considerably.

The output power capacity of the pick-up can be expressed in different ways. By considering the primary current and mutual coupling, the maximum output power equations shown in table 2-2 for fully tuned pick-ups (both series tuned and parallel tuned) can be rewritten as:

$$P_m = \frac{wI_p^{\,2} M^2 Q_s}{L_s} = wI_p^{\,2} Q_s k_f M N_p / N_s \qquad (2\text{-}11)$$



InductEV, Inc.
Exhibit 1020
Page 056

where $k_f$ is the coupling factor determined by the coupling geometry and magnetic material, $N_p$ and $N_s$ are the number of turns of the track and the pick-up. In a practical design, normally the ratio $M^2/L_s=k_fMN_p/N_s$ is designed as high as is practically possible to maximise the power transfer capacity. Note that decreasing $N_s$ does not reduce the maximum power capacity as it is proportional to M. This can also be explained from the fact that as $N_s$ is made smaller the open circuit voltage reduces but the short circuit current increases. As mentioned before, $Q_s$ should not be too large for sensitivity reasons. In consequence, the main design variables are the angular frequency $\omega$ and track current magnitude $I_p$. From equation (2-11), it can be seen that high frequency and high track-current levels are required for high power IPT supplies.

The above analysis assumes that the pick-up circuits are completely tuned so that the full-resonant conditions are met. However, it is known that full resonance is difficult to maintain when the power quality factor is high, and excessive power dissipation at full resonance can lead to poor power efficiency and overheating of the pick-up coils. For this reason, Kelley and Owens tried to avoid full resonance in designing a contactless power supply for an aircraft stereo system [23]. The pick-ups were series-tuned but the tuning capacitors were selected such that sufficient amount of power can be obtained without approaching resonance. System sensitivity to parameter variations was greatly reduced in such a design. However, the total power transfer capacity dropped at the same time. In addition, because the inductance of the pick-up coil was not fully compensated, an additional voltage regulator was required to keep the output voltage constant.

In addition to the basic series and parallel tuning methods discussed previously, more complicated approaches using composite tuning circuits such as that shown in Fig. 2-14, provides more options for pick-up power conditioning. In this circuit, the voltage source $V_{so}$ is transformed to a current source first, then the current source is transformed back into a voltage source. Unlike pure series tuning, the final output voltage $V_{so1}$ can be varied by tuning design according to the following relationship:

$$V_{so1} = \frac{L_{s1}}{L_s} V_{so} = \frac{C_s}{C_{s1}} V_{so} \qquad (2\text{-}12)$$

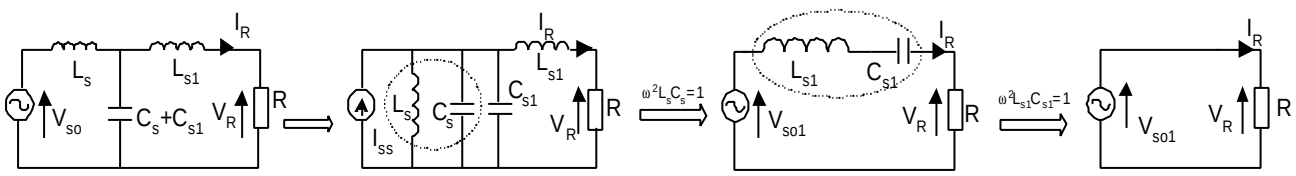


**Fig. 2-14: Composite compensation of the pick-up**



InductEV, Inc.
Exhibit 1020
Page 057

In this tuning circuit, the positions of $C_{s1}$ and $L_{s1}$ can be swapped without changing the output voltage. Following a similar approach, a variable current source output circuit can be constructed. Despite larger passive component number counts, the main disadvantage of these types of passive tuning is their poor transient response due to high order resonance. Using nonlinear components such as saturable inductors may suppress the maximum overshoots, but the circuit operating points have to be designed carefully.

### *2.4.3 Power Transfer Control*

Fig. 2-15 shows four possible ways to control power flow from the primary track to the secondary pick-up. Moving the pick-up away from the track is obviously a direct way to have the two systems decoupled to stop the power flow. Putting a metal shield in the air gap can also block the magnetic coupling. These methods involve mechanical movements which are inconvenient and undesirable in most applications. Alternatively, having the pick-up shorted to screen itself from the magnetic field is a novel way of decoupling. Since the primary track coil is a current source, shorting the pick-up coil directly is not damaging but is a very effective way to control the power flow. When the pick-up coil is shorted with a parallel switch as shown in Fig. 2-15(c), the voltage across the pick-up coil becomes zero. Thus, the magnetic field produced by the short circuit current $I_{ss}$ cancels the magnetic field produced by the primary track current so that the flux linkage in the pick-up coil becomes zero. Consequently, the power flow is blocked. Finally, the power flow can also be controlled in a traditional way as shown in Fig. 2-15(d). In this case, a series switch is used to control the connection between the pick-up coil and the load. When the switch is turned off, although the magnetic coupling and induced voltage still exist in the coil, no power is transferred due to the disconnection of the pick-up circuit. Note that in Fig. 2-15 (c) and (d), the parallel and series switches are drawn for illustration purposes only. Their actual position can be at any suitable place in the pick-up circuitry, and different control strategies may be used to improve the switching conditions.

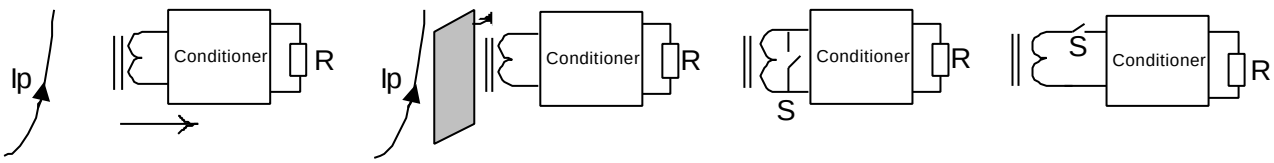


(a) Moving away (b) Shielding (c) Shorting (d) Disconnecting

**Fig. 2-15: Power flow control methods**



InductEV, Inc.
Exhibit 1020
Page 058

The selection of a specific power control strategy should be based on the tuning method employed in a pick-up circuit. For a series tuned pick-up, a series switch may be directly employed to control the output voltage. However, for the parallel tuned pick-up, the circuit is not allowed to be disconnected because of its current source property. Nevertheless, a parallel switch is suitable here to enable current control by shorting the pick-up coil. As the current source can boost the voltage to a very high value as required, it is a very popular technique for applications where the coupling is weak and the induced voltage is low [2,4,5,22]. Fig. 2-16 shows a typical schematic circuit of current-fed boost converter for conditioning the pick-up power. In this circuit, a parallel switch is placed on the DC side enabling a DC switch such as an IGBT or MOSFET to be used directly. A small inductor $L_{s1}$ and a diode D are used to prevent the capacitors $C_s$ and $C_f$ from being shorted. There are two fundamentally different ways of controlling switch S: switching at very high frequency and at very low frequency. These two methods are described in detail in [1]. What is shown in Fig. 2-16 is a simple hysteretic control used for low switching frequency operation. An error band is set up within a very small percentage of a given reference $V_{ref}$. When the output voltage $V_0$ is higher than the error band, the switch is turned on to stop the charging of the capacitor $C_f$. When the voltage is lower than the error band, the switch is turned off enabling power flow so that capacitor $C_f$ is charged up. The actual switching frequency is determined by the width of the error band. Depending on the capacitor size, output voltage, etc., an error band of 5% typically corresponds to a switching frequency of about 10 to 20Hz for a pick-up circuit used in road stud (cats' eyes) application [4].

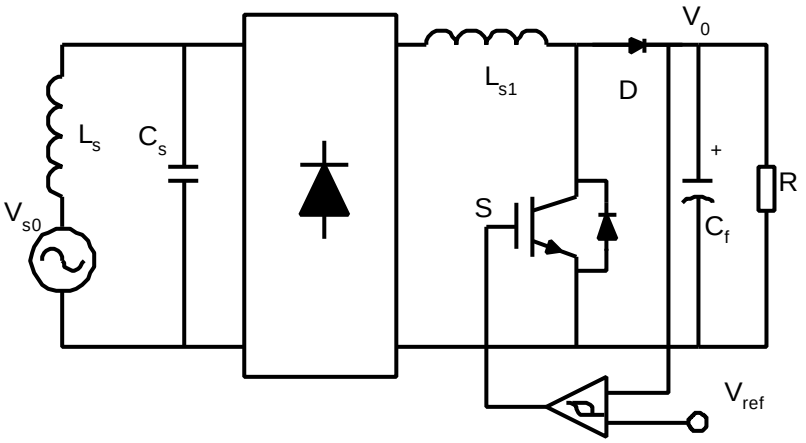


**Fig. 2-16: Pick-up power flow control with a shorting switch**

It is worth noting that when the above self-screening pick-up shorting method is used to control the power flow, the control coil and the power supply coil do not necessarily have to be the same coil. With voltage and current ratios being considered, theoretically two tightly coupled coils can be



InductEV, Inc.
Exhibit 1020
Page 059

modelled as one equivalent coil. In a practical design, changes in voltage and current ratio have a significant effect when selecting suitable power switches. Fig. 2-17 shows a dual coil control scheme used in an inductive battery charger for an electric vehicle [2,5]. The power rating is the same for both the coils, but obviously the high voltage coil $N_{s2}$ has less current than the low voltage coil $N_{s1}$ which is rectified to charge a set of 12V batteries. The charging current from the low voltage coil is up to 250A. If this current is controlled directly, a power switch of at least 250A is required which is very bulky, expensive and inefficient. However, if a high voltage coil is controlled instead with the same power rating, its current would be $N_{s2}/N_{s1}$ times smaller. For example, if the turns ratio is 25:1, then the rating of the control coil will be only 10A/300V. This makes the selection of the power switch much easier. In Fig. 2-17, the high voltage coil is parallel-turned to supply constant current via the low voltage power supply coil. The charging is fully controlled by shorting the control coil in a similar way as for a single parallel-tuned pick-up coil. The difference is that a bi-directional AC switch is used to short the control winding. As discussed in Section 2.3.4, a combined switch with two IGBTs in series (see Fig. 2-7, Type b) can be used for this purpose. These two IGBTs are zero voltage switched so that the stresses and switching losses are minimised.

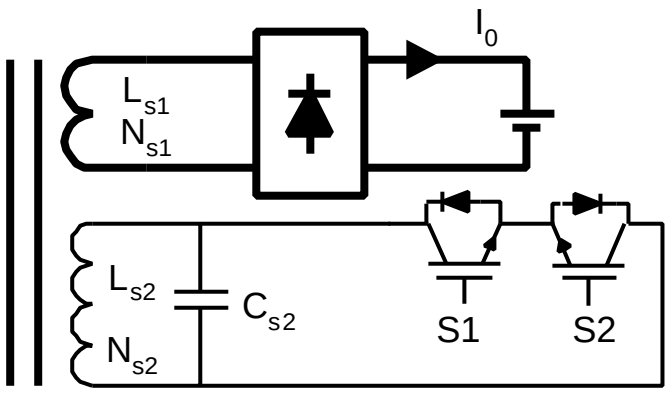


**Fig. 2-17: Dual coil power flow control**

## 2.5 Track Current Control and Stability

### *2.5.1 General Requirements for Track Power Supplies*

As mentioned before, it is desirable to have a current source track power supply for an IPT system to simplify the pick-up design and to allow for multiple pick-up loads. Hence, an IPT track power supply can be regarded as a high frequency AC current generator. In most cases, it is an AC-DC-AC converter/inverter producing a current output at a desired magnitude and frequency. In this



InductEV, Inc.
Exhibit 1020
Page 060

sense, the main objective of an IPT power supply is to ensure high quality track current control against load variations from the pick-ups, circuit parameter drifts, and other disturbances such as the fluctuation of the mains power supply. The power converter used for this purpose should meet the following general requirements:

- Efficient with reduced conduction and switching losses
- Small in size, light in weight, low component counts, and cost effective
- Good steady-state properties as well as fast start-up and load dynamic responses with minimal overshoot
- High input power factor
- Robust and reliable, including minimal EMS (Electromagnetic Susceptibility)
- Low conducted EMI with less harmonics in the current drawn from the mains power supply
- Low radiated EMI.

Moreover, considering the specific features of IPT applications, an IPT track power supply should also meet the following unique requirements:

- Approximate constant magnitude of track current at a level of several tens to several hundreds of amperes
- Approximate constant frequency from several tens of kHz to hundreds of kHz
- Ability to transfer high power levels over a long track length and across a large air gap at voltage levels limited by available semiconductor devices
- Power transfer ability to multiple pick-up loads without mutual power blocking problems
- Ability to keep high power efficiency at required track current magnitude and high operating frequency
- Minimal radiated EMI and direct magnetic field effects of the track loop on its surroundings.

The requirements of a specific application may vary slightly from those listed above. Also, in a practical design, it is desirable but normally impossible to optimise all of the requirements at the same time. For the design of a multi-task system like IPT, some trade-offs are inevitable. The final decision is dependent on the specific application, a user's choice, as well as a designer's judgement. There is no doubt about the existence of objective standards for single items, but at a system level, preferences and priorities have to be taken into consideration in setting up the criteria for system design and evaluation.



InductEV, Inc.
Exhibit 1020
Page 061

### 2.5.2 Basic Track Current Control Strategies

**Fixed Frequency Control and Variable Frequency Control**

Constant and variable frequency control are two main control strategies for IPT track current supplies. For constant frequency control, the frequency is forced with the driving switches at a predetermined value so that it does not vary with the load and circuit parameters. The major advantage of the forced frequency control is that the operating frequency is stable so that the pick-up tuning design as well as EMC filter design is easy. The disadvantage is that the forced operation may impose high voltage and/or current stresses on the switches thus the switching power losses may be high unless some special soft switching techniques are arranged. In the case of variable frequency control, some extent of frequency variation is allowed to follow the circuit resonance. This makes soft switching easy to achieve. Moreover, the system cost, size and power efficiency may be reduced due to unity power factor operation resulting from the frequency variation. Its main disadvantage is that the frequency may vary with the load changes and parameter drifts. Normally, this variation is very small and acceptable for practical applications. However, in some extreme situations, the operating frequency may drift far away from its nominal value, causing system frequency stability problems [1,14].

**Direct Control and Indirect Control**

To keep the track current constant, a feedback control loop can be designed to control the track current directly. This is straightforward but may not always be the best choice. For a multi-task system with many requirements to fulfil and many objectives to achieve at the same time, the concept of indirect control may be utilised to obtain a simple and efficient control system. The basic idea of indirect control meant here is explained below.

If there is a main objective “A”, which is related to an output variable “x”, and there are also other conditions, including sub-objectives “A1”, “A2”, etc., needing to be considered. Variable “x” may be controlled directly to achieve the main objective “A”. However, there may be two problems existing in doing this: firstly, the control may be very difficult or the measurement of variable “x” may be very costly; secondly, even if objective “A” is achieved, other operating conditions may be very poor. In this situation, if the control is changed to target achieving another alternative objective, which may be one of the sub-objectives, say “A1”, then it is called indirect control. The condition of doing indirect control is that a new objective can be found and this alternative objective



InductEV, Inc.
Exhibit 1020
Page 062

must be easy to achieve. In addition, if this objective is achieved, the main object should also be achieved to an acceptable level. At the same time, most other system operating conditions should also be improved and the sub-objectives achieved to a satisfactory extent. As a result, the system obtains a better overall performance than that of the direct control.

The indirect control method can be applied to an IPT system where many requirements have to be taken into consideration at the same time. As discussed before, normally keeping constant track current is the main control objective and can be achieved by a direct closed loop current control. But a complicated controller and a high frequency current sensor including sophisticated signal processing circuits may be required. Moreover, other undesirable operating conditions may result as a consequence of forcing this direct current control. For example, soft switching is difficult to achieve, the current waveforms may contain large harmonic components, etc. For a current-fed resonant converter power supply, an indirect control approach may be employed by doing ZVS control. This is based on the fact that under ZVS conditions the frequency and magnitude of the track current is approximately constant at high quality factor loading conditions. The error is normally quite small and within an acceptable range for practical IPT power converting requirements. This alternative objective is very easy to implement, and doing this also results in many additional advantages required by an IPT power supply, such as low switch stresses, high power efficiency, and improved track current waveforms. Thus in general, indirect ZVS control achieves a very good overall performance. This is a major reason behind its popularity in current-fed resonant converters [1,5,14,24].

**Plant Design and Controller Design**

As noted, indirect control is based on a complete understanding of the properties of a control object, or plant. The purpose of a controller is to change the property of the plant to have new and better characteristics as required. Indirect control is different from normal optimal control. Optimal control combines all the necessary outputs and tries to minimise an optimisation index, while indirect control chooses only one objective to target and leaves the other objectives to be achieved automatically. Clearly the selection of a suitable control objective is the major issue and a good knowledge about the interrelationships between the circuit parameters and variables are of significant importance. Unlike a normal control problem where the plant is given, in the field of power electronics, the plant itself is a nonlinear circuit which needs designing. In fact, there are two aspects involved: one is the controller design, and another is the plant design. These two designs are closely related. In a power electronics circuit, the insertion of a simple diode or a small change in its



InductEV, Inc.
Exhibit 1020
Page 063

location may alter the plant property significantly, thus the controller needs to change accordingly. If a plant can be designed or modified to have a better natural property, then the controller design can be easier. An easy indirect control channel may be found if the property of a power electronics circuit is fully analysed and understood. In some extreme situations, no additional controllers may be required to achieve certain power conversion tasks for a well designed autonomous system. As an example of this, a zero voltage switched DC-AC converter/inverter based on self-sustained oscillation without controllers is proposed in Chapter 7 of this thesis.

### *2.5.3 Pick-up Load Modelling*

When one or more pick-ups exist in an IPT system, each pick-up can be referred back to the primary side as a track load. Normally they can be regarded as series resistors under steady state conditions for approximate power transfer analyses. However, they may affect the track current flow and system stability significantly, therefore a better load model is necessary, particularly if the operating frequency is not constant.

For series tuned pick-ups, under steady state conditions the reflected equivalent impedance is a pure resistor. For parallel tuned pick-ups, even at steady state, this is not true. Fig. 2-18 shows an IPT system with “n” pick-ups configuration. The pick-ups are parallel tuned and each has an equivalent resistive load R. If these “n” pick-ups are not mutually coupled and their parameters are the same, they will be equivalent to a single pick-up system as shown in Fig. 2-19. For each pick-up, the input impedance across the equivalent induced voltage source is:

$$Z_s = jw\,L_s + \frac{1}{jw\,C_s + 1/R} \tag{2-13}$$

where ω is the angular frequency, $L_s$ and $C_s$ are the inductance and its tuning capacitance of each pick-up, and R is the equivalent load resistor.

For a full bridge rectifier connected with a voltage source load (a large capacitive filter in parallel with a load resistor $R_L$), the equivalent AC resistance can be modelled as $R = 8/\pi^2\ R_L \cong 0.81R_L$. Similarly, for a current source load with a large inductor filter after a rectifier, the equivalent resistance is $R = \pi^2/8\ R_L \cong 1.23R_L$ [25].



InductEV, Inc.
Exhibit 1020
Page 064

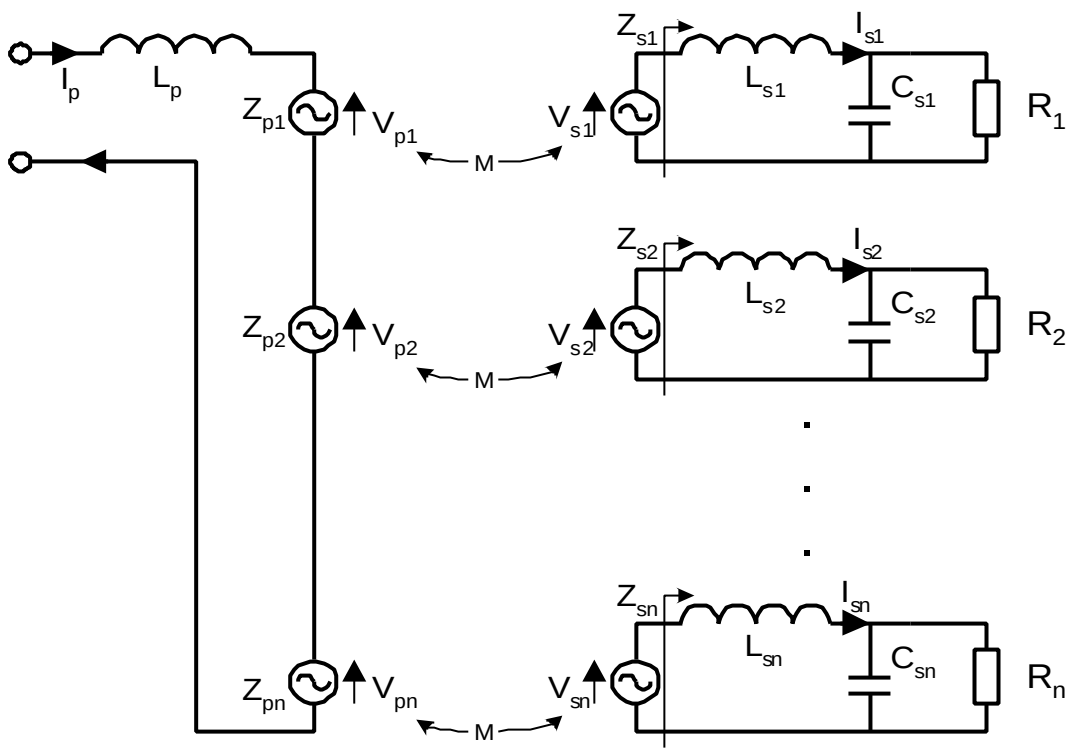


**Fig. 2-18: Load modelling of n parallel tuned pick-ups**

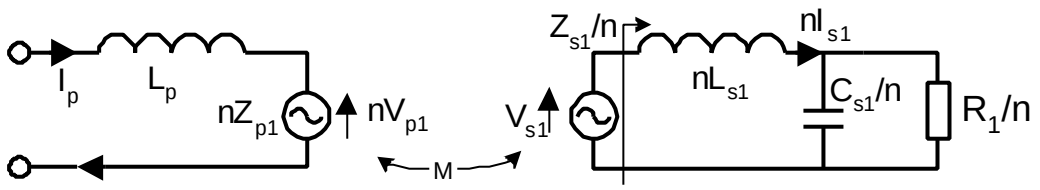


**Fig. 2-19: Equivalent circuit of n parallel tuned pick-ups**

By splitting the real and imaginary parts of the impedance $Z_s$, equation (2-13) can be rewritten as:

$$Z_s = \frac{R}{1+(w\,RC_s)^2} + j(wL_s - \frac{w\,R^2C_s}{1+(w\,RC_s)^2}) \qquad (2\text{-}14)$$

It can be seen that at the nominal undamped resonant frequency $\omega_0 = 1/\sqrt{L_sC_s}$ , the imaginary part of $Z_s$ is not zero. In fact, it can be proven that it has an inductive property.

The reflected impedance of $Z_s$ to the primary track is:

$$Z_p = \frac{V_p}{I_p} \qquad (2\text{-}15)$$



InductEV, Inc.
Exhibit 1020
Page 065

Considering $V_p = \pm jwMI_s$ $I_s = V_s / Z_s$, and $V_s = \mp jwMI_p$ $Z_p$ [*] can be rewritten as:

$$Z_p = \frac{w^2 M^2}{Z_s} \tag{2-16}$$

where M is the mutual inductance. From this equation, it can be seen that the reflected load has the following properties:

If the pick-up impedance $Z_s$ is a pure resistor, the reflected impedance $Z_p$ would also be a pure resistor. This is the case for a fully series tuned pick-up with a resistive load.

If $Z_s$ is inductive, then its reflected impedance $Z_p$ would be capacitive, and vice versa. In the case of a shorted uncompensated pick-up with a self-inductance of $L_s$, its reflection is equivalent to a capacitor with a value of $L_s/(wM)^2$ at steady state.

For a parallel tuned pick-up, even when $L_s$ and $C_s$ are fully tuned, $Z_s$ and thus $Z_p$ are not pure resistors. If the system is running at fixed frequency, then $Z_s$ has an inductive property as mentioned earlier. In consequence, the reflected impedance $Z_p$ will appear to have a capacitive property.

As will be seen in Chapter 5, a capacitive impedance may affect the soft switching operation of voltage-fed resonant converter power supplies.

### *2.5.4 Power Blocking and System Stability Concerns*

An important power transfer concern with the multiple pick-up loads is described as a power blocking problem [1,14]. If the equivalent impedance of a single pick-up $Z_s$ is very small, corresponding to a small load resistance (short circuit for the worst case) in a series tuned pick-up, or a large load resistance (open circuit for the worst case) in a parallel tuned pick-up, the reflected impedance $Z_p$ will be very large, or even becomes infinite as seen from equation (2-16) when $Z_s$ is zero. (Practically the pick-up core material saturation will occur.) This will cause the track current to drop down to a very small value or even to zero under extreme conditions because of the fact that

[*] Note that "+" and "–" signs of $V_p$ and $V_s$ are determined by the polarity dots of the coupling. However, they are opposite in direction regardless of the coupling polarity, thus $Z_p$ is always positive in equation (2-16). This is in consistent with the concept that a passive pick-up circuit only absorbs real power.



InductEV, Inc.
Exhibit 1020
Page 066

no practical converter can supply constant current to an open circuit. Consequently, the power transfer to other pick-ups will be blocked, causing power transfer failure to other pick-ups.

For a series-tuned pick-up with a voltage source output, the power blocking problem is not a big concern under normal working conditions. However, a parallel-tuned pick-up with a current source output property can cause a severe power blocking problem even at no-load conditions. A novel way of solving this problem is to use an active switch as described in section 2.4.3 (see Fig. 2-15c). When the load is removed or if the load resistance becomes too large, the power control switch is turned "on" so that the pick up is shorted and essentially decoupled from the track. Accordingly, the power-blocking problem can be avoided.

Another important concern for a variable frequency controlled IPT power supply is the frequency stability problem. This problem was first found in a current-fed parallel resonant converter for IPT materials handling application [26]. Both the track and the pick-ups are parallel tuned and ZVS control techniques were employed allowing for variable frequency operation. It has been found that when the pick-up number (N) exceeds a certain value, for example, if N>7 in the case investigated, the operating frequency would drift far away from its nominal value, being either too large or too small, causing complete system detuning and loss of power transfer ability. The critical condition of the frequency detuning was found to be [1,26]:

$$N < \frac{L_p L_s}{M^2 Q_s^{\ 2}} \tag{2-17}$$

where N is the pick-up number, M is the mutual inductance, $Q_s$ is the parallel tuned pick-up quality factor, $L_p$ and $L_s$ are the inductance of the track and the pick-up respectively. This relationship was further simplified in terms of voltage and current ratings of the track and the pick-ups, as well as the pick-up output power $P_s$ to give [1]:

$$V_p I_p \geq N V_s I_s \qquad \text{or} \qquad V_p I_p \geq N Q_s P_s \tag{2-18}$$

This equation gives a very concise condition indicating that the primary track VA capacity should be larger than the total pick-up VA capacity, which is $Q_s$ times larger than that of the real power, to avoid the occurrence of the frequency instability and system detuning. However, a further study in Chapter 3 of this thesis will show that (2-17) is an accurate detuning condition only for series tuned track and pick-ups. And (2-18) is only accurate if the VA ratings are replaced with reactive power ratings. These results are approximations for other tuning circuits at high quality factors. The range of the frequency shift at detuning conditions is also analysed in Chapter 3.



InductEV, Inc.
Exhibit 1020
Page 067

## 2.6 Summary

A general overview on the technologies involved in IPT power supplies has been undertaken in this chapter. All the main parts of an IPT system have been discussed systematically.

The primary track of an IPT system can have different layout formats such as in extended parallel cables or in lumped coils depending on the application under consideration. It may be either series or parallel tuned, or tuned in a composite form. The track tuning compensates for the track inductance, functions as a resonant tank of a resonant converter, as well as filters the harmonics between the source and the load. Loose coupling is one of the most outstanding characteristics of an IPT system. As the traditional coupling coefficient can not reflect the accurate local magnetic coupling between the track and the pick-up, a new parameter termed a coupling factor, which is only determined by the geometry and the magnetic material, has been introduced. Common voltage-fed and current-fed topologies of power converters for IPT power supplies, including the property considerations in the selection of power devices, have been discussed. Pick-up tuning methods, power transfer capacities, and power control approaches have been summarised. After analysing the requirements for a track power supply, basic track current control strategies such as fixed frequency and variable frequency operations have been discussed. Special attention has been paid to the concept of indirect converter control via zero voltage switching which may give better overall performance compared with direct converter control. Finally, based on the modelling of the pick-up loads, power blocking problems and system frequency detuning concerns have been discussed.

## 2.7 References

[1] Boys, J. T., Covic, G. A. and Green, A. W.: “Stability and control of inductively coupled power transfer systems,” *IEE Proceedings on Electric Power Applications*, Vol. 147, No.1, pp.37-43, January 2000.

[2] Elliott, G. A. J., Boys, J. T. and Green, A. W.: “Magnetically coupled systems for power transfer to electric vehicles”, *Proceedings of the International Conference on Power Electronics and Drive Systems*, pp.797-800, 1995.

[3] Fink, D. G. and Beaty H. W.: *Standard handbook for electrical engineers*, 13th edition, McGraw-Hill, Inc., New York, 1993.



InductEV, Inc.
Exhibit 1020
Page 068

[4] Boys, J. T. and Green, A.W.: "Intelligent road-studs – lighting the paths of the future", *IPENZ Transactions*, No.24, (1) EMCH, pp.33-40, 1997.

[5] Covic, G. A, Elliott, G, Stielau, O. H. and Green, R. M.: "The design of contact-less energy transfer system for a people mover system", *Proceedings of International conference on power system technology*, Perth, Australia, pp79-84, December 2000.

[6] Juby L., Green, A. and Collinson, A.: "The design of a non-contact charging system for electric vehicles", *European Power Electronics Conference*, pp.573-576, 1997.

[7] Turner, J. B. and Roth, G. W.: "Regulator for inductively coupled power distribution system", *United States Patent*, Patent No: 4,914,539, April 3, 1990.

[8] Ang, S. S.: *Power switching converters*, M. Dekker, New York, 1995.

[9] Green, A.: *Voltage sourced reversible rectifiers*, Ph.D thesis, Electrical and Electronic Department, the University of Auckland, G82, 1990.

[10] Trzynadlowski, A. M.: *Introduction to modern power electronics*, John Wiley & Sons, Inc., 1998.

[11] Boys, J. and Mitchell, B: "Current-forced neutral injection in a three-phase rectifier/converter", *IEE Proc.–Electri. Power Appl.*, Vol. 146, No.4, pp441-446, July 1999.

[12] Kazimierczuk, M. K. and Czarkowski, D.: *Resonant power converters*, John Wiley & Sons, Inc., 1995.

[13] Bellar, M.D., Wu, T.S., Tchamdjou, A., Mahdavi, J., Ehsani, M.: "A review of soft-switched DC-AC converters", *IEEE Transactions on Industry Applications*, Vol. 34, No. 4 , pp. 847 – 860, July-Aug., 1998.

[14] Green, A. W. and Boys, J. T.: "10kHz Inductively coupled power transfer – concept and control", *IEE Power Electronics and Variable Speed Drives Conference*, PEVD, Pub.399, pp.694-699, 1994.

[15] Boys, J. T. and Green, A. W.: "Inductively coupled power transmission – concept, design and application", *IPENZ Transactions*, No.22, (1) EMCH, pp.1-9, 1995.

[16] Bose, B. K.: *Modern power electronics: evolution, technology, and applications*, IEEE Press, New York, 1992.

[17] Bose, B. K., "Energy, environment, and advances in power electronics", *IEEE Transactions on Power Electronics*, Vol.15, No.4, pp.688–701, July 2000.

[18] Tobita, M. and Kushibiki, R.: "Development of new high power converter using IEGT", *IPEC 2000*, Tokyo, pp970-975, 2000.



InductEV, Inc.
Exhibit 1020
Page 069

[19] Ichikawa, K., Shimoura, T., Kawakami, K., Nakajima, R. and Hirata, A.: "New advances high voltage inverters employing IEGTs", *IPEC 2000*, Tokyo, pp994-999, 2000.

[20] Bose. K: *Power electronics and variable frequency drives: technology and applications*, Piscataway, NJ, IEEE Press, 1997.

[21] Benda, V., Gowar, J. and Grant, D. A.: *Power semiconductor devices: theory and applications*, John Wiley & Sons, New York, 1999.

[22] Stielau, O. H., Boys, J.T., Covic, G. A. and Elliot, G. "Battery charging using loosely coupled inductive power transfer." *Eighth European Conference on Power Electronics and Applications*, EPC'99, September 1999.

[23] Kelley, A. W. and Owens, W.R.: "Connectorless power supply for an aircraft-passenger entertainment system", *IEEE Transactions on Power Electronics*, PE-4, (3), pp.348-354, 1989.

[24] Knaup, P. and Hasse, K.: "Zero voltage switching converter for magnetic transfer of energy to movable systems", *European power Electronics Conference*, *EPE'97*, 2, pp.168-173, 1997.

[25] Djemouai, A.: "Prosthetic power supplies", *Wiley Encyclopedia of Electrical and Electronics Engineering Online*, John Wiley & Sons, Inc., December, 1999.

[26] Green, A. W. and Boys, J. T.: "An inductively coupled high frequency power system for material handling applications", *International Power Electronics Conference*, IPEC'93, Singapore, (2), pp.821-826, 1993.



InductEV, Inc.
Exhibit 1020
Page 070

## Chapter 3

# Current-fed Parallel Resonant Converter Power Supplies

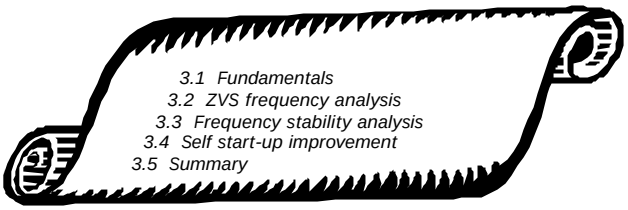


## 3.1 Fundamentals of Current-fed Parallel Resonant Converters

### *3.1.1 Basic Inverting Network Topologies*

As discussed in Chapter 2, the inverting network of a current-fed resonant converter has two basic topologies: the full bridge topology and the push pull topology. Fig. 3-1 and Fig. 3-2 show the current-fed parallel resonant converters based on these two topologies. Both the converter circuits have the same resonant tank consisting of a capacitor C in parallel with an inductor L and a series load R. A DC inductor links a DC power supply $V_d$ and an inverting network which comprises four switching devices for the full bridge topology, or two switching devices and a phase-splitting transformer for the push pull topology. Due to the existence of a capacitor branch at the input port of the resonant tank, the "current source" flowing in the DC inductor can be inverted and injected into the tank without creating a conflict with the current in the resonant inductor L.

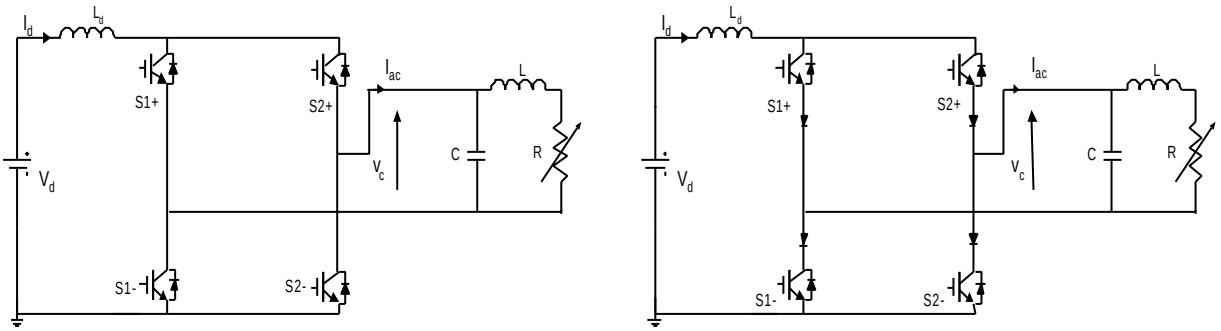


(a) without series blocking diode (b) with series blocking diode

**Fig. 3-1: Full bridge current-fed parallel resonant converters**



InductEV, Inc.
Exhibit 1020
Page 071

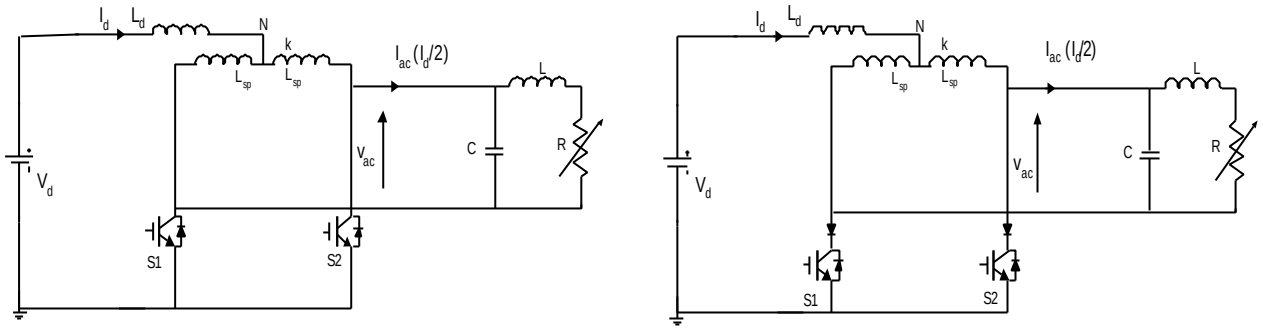


(a) without series blocking diode

(b) with series blocking diode

**Fig. 3-2: Push-pull current-fed parallel resonant converters**

Most commonly used switching devices such as MOSFETs and IGBTs have internally fabricated anti-parallel body diodes [1]. In order to prevent the conduction of these diodes, extra series blocking diodes may be required to be put in series with the active switches as shown in Fig. 3-1 (b) and Fig. 3-2 (b).

As shown, the main difference between the two topologies is that the push-pull has a phase-splitting transformer in place of two upper switches in the full bridge topology. A phase splitting transformer basically divides the DC current in half so that the AC current flowing into the resonant tank is approximately a square waveform with half the magnitude of the DC current under the steady state conditions. Therefore in principle, a push-pull converter has a very similar performance to a full bridge converter, however its gate drives are simpler as no isolation is required if the negative rail of the DC supply is used as a common ground. Moreover, as will be seen later, its resonant voltage is double that of the full bridge topology. This is a very important feature for IPT applications as a higher track coil driving voltage means a longer track can be driven at a certain track current for the same DC voltage supply. The disadvantage of a push pull converter is that its phase-splitting transformer is normally more bulky and expensive than the two switches used in the full bridge topology.

The phase splitting transformer is an essential part of the push-pull topology and potentially an imperfect transformer will cause the push-push system to have inferior performance. Thus transformers have traditionally been made to high standards to minimise leakage inductance – but in fact such care is not required and lower cost methods are perfectly acceptable. For example, Fig. 3-3 shows an equivalent circuit transformation of a phase splitting transformer with self inductance $L_{sp}$ in both sides and a coupling coefficient k. The circuit of Fig. 3-3(a) can be drawn as in Fig. 3-3(b) and this can then be drawn as in Fig. 3-3(c).



InductEV, Inc.
Exhibit 1020
Page 072

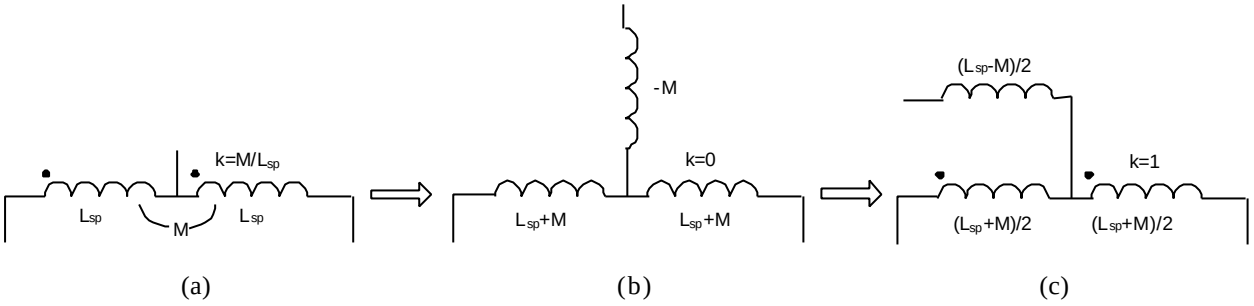


**Fig. 3-3: Equivalent circuits of a phase splitting transformer**

It can be seen that a not fully coupled phase-splitting transformer (with a coupling coefficient k<1) is equivalent to a fully coupled one with a common external leakage inductance. This equivalent leakage inductance $L_{lk}$ can be expressed as:

$$L_{lk} = (L_{sp} - M)/2 = (1-k)L_{sp}/2 \qquad (3\text{-}1)$$

where M and $L_{sp}$ are the mutual inductance and self inductance of the transformer respectively, and k is the coupling coefficient.

Comparing Fig. 3-3 with Fig. 3-2, it can be seen that this leakage inductance can be used advantageously as a part or the complete DC inductance $L_d$ in push pull resonant converters. Therefore, the DC inductor may be reduced - or even eliminated if the leakage is high enough. This finding not only makes the design of a phase splitting transformer much easier, but also can significantly reduce the system cost.

### *3.1.2 Switching Constraints*

For most power electronic circuits, gate control of the switching devices is the main means of achieving the required power conversion. Normally there are certain constraints to the switching process to maintain safe operation of the system. The two main constraints for the current-fed parallel resonant converters shown in Fig. 3-1 and Fig. 3-2 are:

At least one switch (or one upper and one lower switch for the full bridge topology) has to be on to maintain the DC current flow and prevent the occurrence of large over-voltages.

For converters without series blocking diodes, as shown in Fig. 3-1 (a) and Fig. 3-2 (a), the transitions of the switching device have to be at the zero voltage crossings of the resonating voltage, which means ZVS (Zero Voltage Switching) is required. Failing to do this could



InductEV, Inc.
Exhibit 1020
Page 073

result in the resonant capacitor being shorted, and consequently the occurrence of a large over-current.

Fig. 3-4 compares the voltage and current waveforms that show the effect of deviating from the ideal ZVS frequency when no blocking diodes are used. The over-current spikes caused by the shorting of the capacitor voltages are clearly observable under non ZVS operation. If the switching is too fast, ie, the switch is turned on before the resonant voltage $v_c$ drops to zero, $v_c$ will be shorted directly through the newly turned on switch and the body diode of the other switch at the other leg. This can result in a dangerously high instantaneous short current, which may cause the switching devices to fail. On the other hand, if the switching instant is too slow, ie, the switch is turned on after $v_c$ crosses zero, the resonant capacitor is shorted preventing the continuance of normal resonance in the following half cycle. In this situation, a large resonant current will flow through the short circuit path. Even worse, this current has to be switched off later, which again is a potential danger to the switching devices. It can be seen from Fig. 3-4 (b) and (c) that if ZVS is not achieved, the short circuit current can be really large. In addition, the distortions of the waveforms are also large which can cause large EMI.

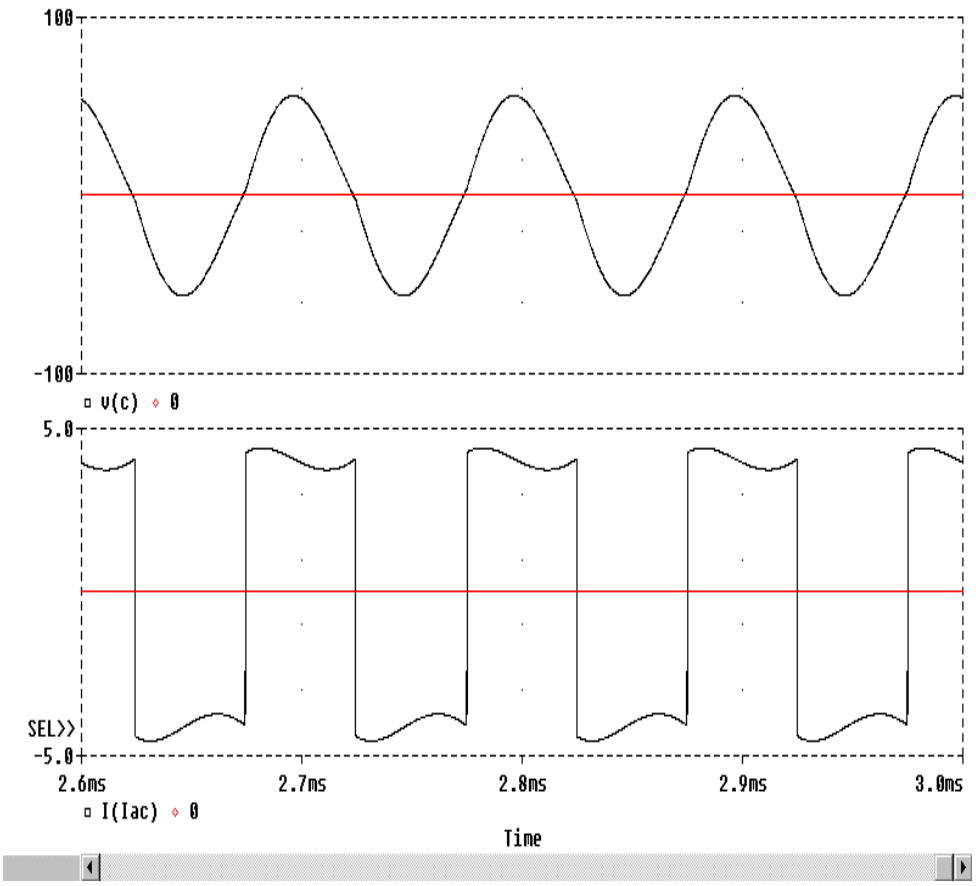


(a) Zero voltage switching



InductEV, Inc.
Exhibit 1020
Page 074

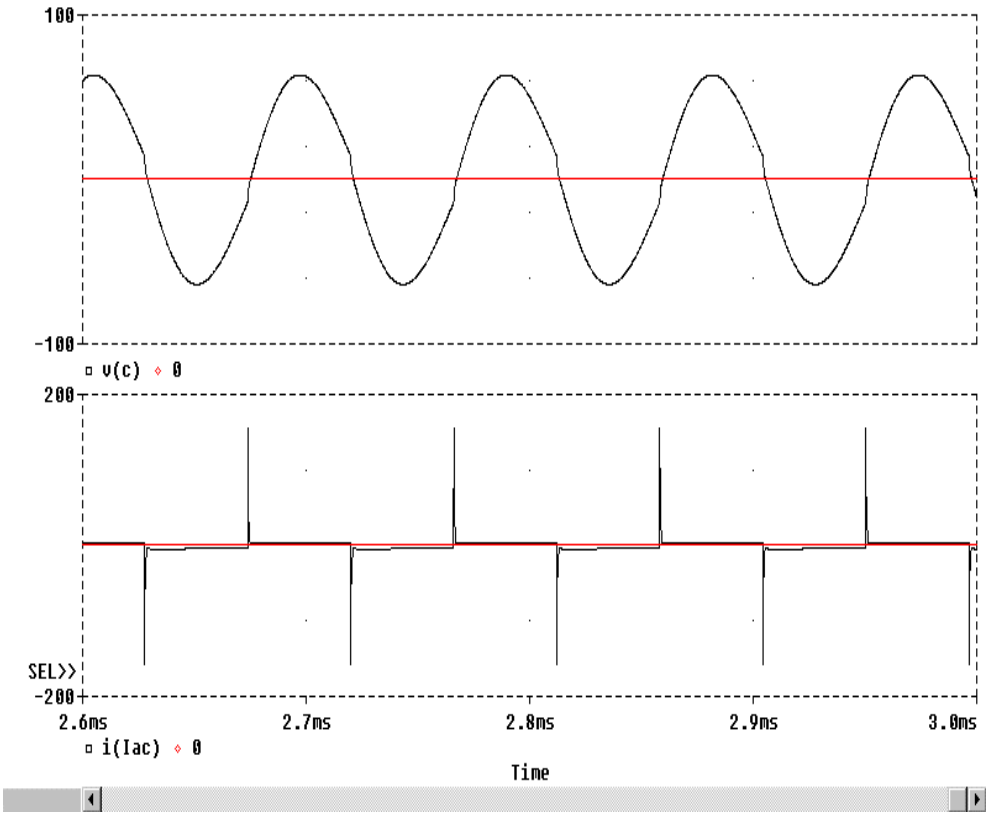


(b) Switching too fast

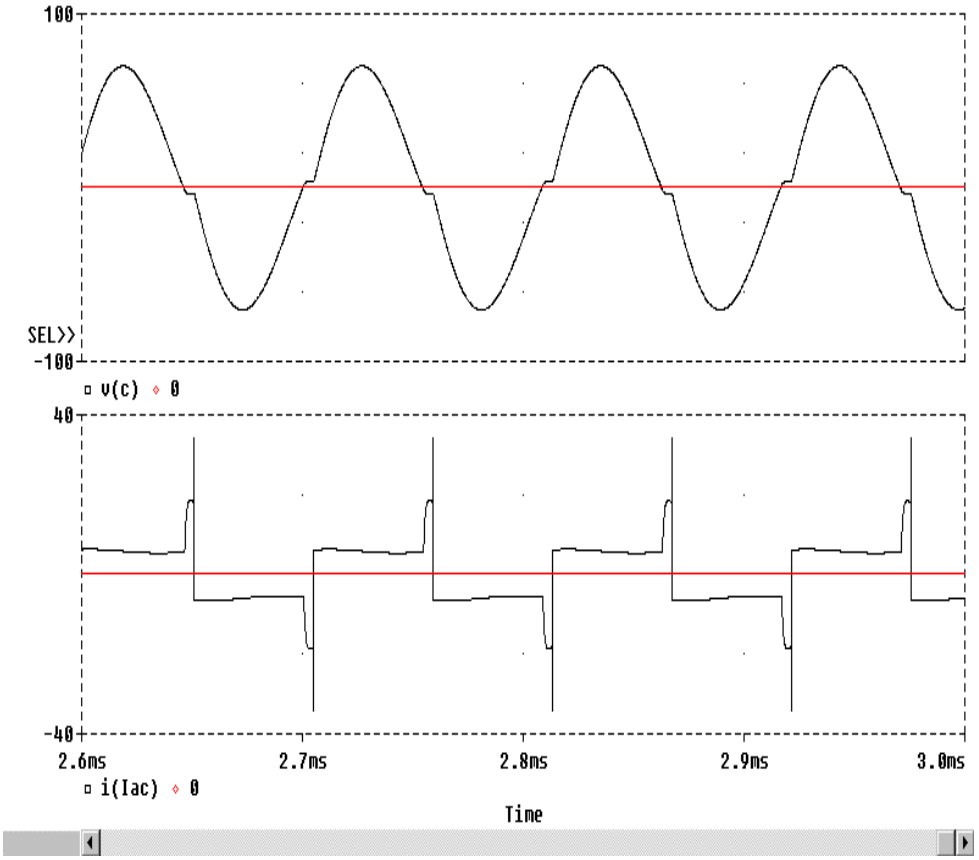


(c) Switching too slow

**Fig. 3-4: Typical voltage and current waveforms without series blocking diodes**



InductEV, Inc.
Exhibit 1020
Page 075

### 3.1.3 DC to AC Voltage Balance Analysis

Take the push-pull topology as an example, Fig. 3-5 (a) shows a generic current-fed resonant converter where Z represents an arbitrary network. From first principles, it can be proven that for a perfect phase splitting transformer (well balanced and fully coupled, ie., $L_{sp1}=L_{sp2}=M$ with a coupling coefficient k=1), then regardless of network Z and the position of the switches (at least one switch should be on at any instant to keep the DC current flow), the instantaneous voltage potential at the central point of the splitter $v_N$ is always equal to the half value of the voltage across the other switch, ie.,

$$v_N = \begin{cases} \frac{1}{2}v_2 \cdots\cdots\cdots S1 = on \\ \frac{1}{2}v_1 \cdots\cdots\cdots S2 = on \end{cases} \tag{3-2}$$

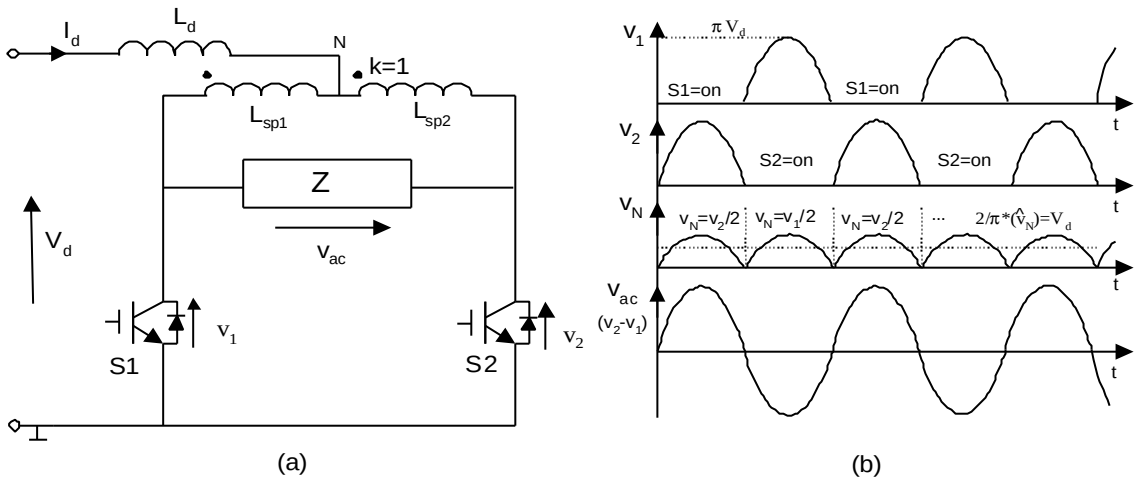


**Fig. 3-5: AC and DC voltage balance of current-fed resonant converter at ZVS condition**

In a steady state condition, the average voltage across the DC input inductor must be zero. Using this simple voltage-seconds rule in this circuit topology, it can be seen that the average value of $v_N$ at the central tap is equal to the DC input voltage $V_d$. Therefore, the AC output voltage $v_{ac}$, which is $v_2$-$v_1$, is linked to the DC input voltage by equation (3-2) in each half switching cycle. This relationship allows the AC voltage generated via the switching network to be calculated.

If Z is a resonant tank, then the resonant voltage $v_{ac}$ is approximately a sinusoidal waveform and can be represented in the form of $\sqrt{2}\,V_{ac}\sin(\omega_0 t)$ provided the harmonics are ignored. When ZVS is achieved with the switches commutated symmetrically at zero voltage instants, the average value of $v_{ac}$ in each half switching cycle divided by two will be equal to the average DC input voltage, which is illustrated in Fig. 3-5 (b). From this relationship, the rms and the peak value of the output AC voltage can be obtained as:



InductEV, Inc.
Exhibit 1020
Page 076

$$V_{ac} = \frac{p\,V_d}{\sqrt{2}} \qquad \hat{V}_{ac} = p\,V_d \tag{3-3}$$

where $V_d$ is the average DC input voltage. It can be seen from this equation that the output AC voltage is directly controlled by the average DC input voltage at steady state. However, it should be noted that under transient conditions, equation (3-2) still holds but not the equalities shown in this equation. Voltage overshoot can occur at start-up and under load transients, which can be a potential danger to the switching devices.

For resonant converters with blocking diodes, if the switching transitions do not occur at zero voltage instants, ie, ZVS is not maintained, then the voltage waveforms $v_1$ and $v_2$ shown in Fig. 3-5(b) will have negative portions in each half cycle. Nevertheless, because the voltage-seconds rule still applies and the DC-AC voltage balance still has to be met, the peak and rms value of the AC output voltage will increase to compensate for the negative part of the voltage. It can be shown that if the harmonics are ignored, the rms and peak value of the output AC voltage will become:

$$V_{ac} = \frac{p\,V_d}{\sqrt{2}\cos q} \qquad \hat{V}_{ac} = \frac{p\,V_d}{\cos q} \tag{3-4}$$

Here θ is the phase shift caused by non-ZVS operation. It can be seen from this equation that the AC voltage can boost up using phase control. However, too large a negative voltage referred back to DC side may lead to very high inrush DC currents. Moreover, if the phase shift is too far away from ZVS condition, eg. near 90 degrees, the system may lose stability since the average AC voltage in each half switching cycle is close to zero and the AC voltage will therefore become dangerously high.

The instantaneous balance (equation 3-2) and the average balance at steady state (equation 3-3 and 3-4) between DC and AC voltages function as a governing rule for current-fed DC-AC converters. It is easy to show that these relationships are also valid for the full-bridge topology except that its output resonant voltage is only half of that in a push pull topology.

No matter which topology is used, for a simple current-fed parallel resonant converter IPT power supply, the network Z shown in Fig. 3-5 is a series-loaded track loop in parallel with a tuning capacitor (as can be seen from Fig. 3-1 and 3-2). Assume the track AC driving voltage is a sine wave and its magnitude is known, then the magnitude of the track current can be determined directly from:



InductEV, Inc.
Exhibit 1020
Page 077

$$I_L = \frac{V_{ac}}{\sqrt{(wL)^2 + R^2}} \approx \frac{V_{ac}}{w_0 L} \frac{Q}{\sqrt{Q^2 + 1}} \tag{3-5}$$

where $V_{ac}$ is the rms value of the AC driving voltage, Q is the quality factor defined as $w_0 L / R$, and ω is the practical operating frequency which is approximately equal to the undamped natural angular frequency $w_0 = 1/\sqrt{LC}$ under normal working conditions with high values of Q. It can be seen from this equation that when the quality factor Q is high, the inductor current is almost completely determined by the resonant voltage and the track impedance. This means that under lightly loaded conditions, the track loop current is approximately constant. It can be calculated from (3-5) that if Q is greater than 3, the current drop from zero to full load will be less than 5.13% [2]. This number is slightly larger than the value of 5% estimated by Green and Boys [3].

### *3.1.4 Fixed Frequency and Variable Frequency Operation*

Since ZVS is not compulsory for current-fed resonant converters with added series blocking diodes, there is greater freedom in choosing their operating frequencies. The system can run at a fixed frequency, or otherwise be variably controlled to regulate the output AC voltage of the inverting network against the input voltage and load variations so as to keep the track current constant. However, as the frequency is very sensitive to the phase-shift between the resonant voltage and current, this phase control method may result in very harsh switching conditions on both the switching devices and the series blocking diodes. Moreover, as discussed earlier, the system dynamic stability becomes a concern if the phase shift is too large.

For current-fed resonant converters without series blocking diodes, ZVS operation is crucial because of the capacitor shorting problem discussed before. It is clear that AC current injection is achieved by commutation of the switches, and ZVS requires an exact match between the switching instants and the zero crossings of the resonant voltage. To achieve ZVS, there are two approaches: one is to tune the circuit dynamically to match a fixed switching frequency, and another is to vary the switching frequency to follow the zero crossing points of the resonant voltage. Although it is feasible to tune the circuit parameters using techniques such as magnetic amplifiers, or switched inductors and capacitors, generally speaking, variable inductors and capacitors at high power levels are very costly. Therefore, they are not economical for most applications. Varying the switching frequency, on the other hand, costs little and is therefore preferred [3-4]. In fact, variable frequency



InductEV, Inc.
Exhibit 1020
Page 078

ZVS operation offers very attractive features for IPT power supplies, particularly when its contribution to reduced switching loss and EMI is considered. Moreover, under ZVS conditions the two (or four for the full bridge topology) series blocking diodes can be eliminated, reducing not only the cost, but also the voltage drop and power losses. This is particularly important for low voltage and high power level applications where minimal voltage drops and power losses are required.

## 3.2 ZVS Frequency Analysis

If a current-fed resonant converter runs at variable frequency ZVS conditions, then of primary theoretical and practical importance is what this ZVS frequency is and how it changes with load and other parameter variations. This section identifies different "resonant" frequencies and analyses the ZVS frequency of a current-fed resonant converter based on a series-loaded parallel resonant tank used in IPT power supplies.

### *3.2.1 Identification of Various Resonant Frequencies*

Fig. 3-6 shows a typical push-pull current-fed DC-AC resonant converter used in IPT power supplies. Switching devices S1 and S2 are turned "on" and "off" at the zero instants of the capacitor voltage thus injecting an approximate square wave current into the parallel resonant tank shown in the dotted block. If multiple pick-ups are supplied by the IPT system, these can be considered as being distributed along the track cable in series with the track inductor L. Therefore, the total load can be approximated with a resistor R with any imaginary part combined into the track inductance. Note this assumption is valid for tuned pick-ups under steady state conditions. When the system is detuned, i.e., the operating frequency shifts away from its nominal value, a more complex model rather than a second order tank must be considered.

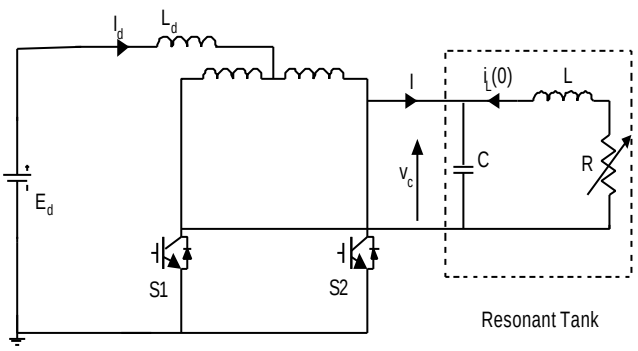


**Fig. 3-6: A push pull current-fed resonant converter**



InductEV, Inc.
Exhibit 1020
Page 079

While oscillation is a natural phenomenon, resonance can be regarded as an extreme oscillatory situation. In an electrical system, the oscillation is due to the circulation of energy between inductors and capacitors, and the resonance may occur at more than one operating condition. For the series-loaded parallel-resonant tank shown in Fig. 3-6, various resonant conditions corresponding to different resonant frequencies are discussed below. They are zero phase angle resonant frequency ($f_r$), maximum inductor current frequency ($f_{iLm}$), maximum capacitor voltage frequency ($f_{vcm}$), natural oscillation frequency ($f_f$), and ZVS frequency ($f_{ZVS}$). The first three frequencies are only valid for sinusoidal AC circuits, the fourth frequency is associated with the circuit free-ringing property, and the fifth frequency is the practical steady state operating frequency of the current-fed ZVS converter. These frequencies, plus the nominal undamped natural frequency ($f_0$), all correspond to common concepts of resonance and are shown together in Fig. 3-7 for comparison.

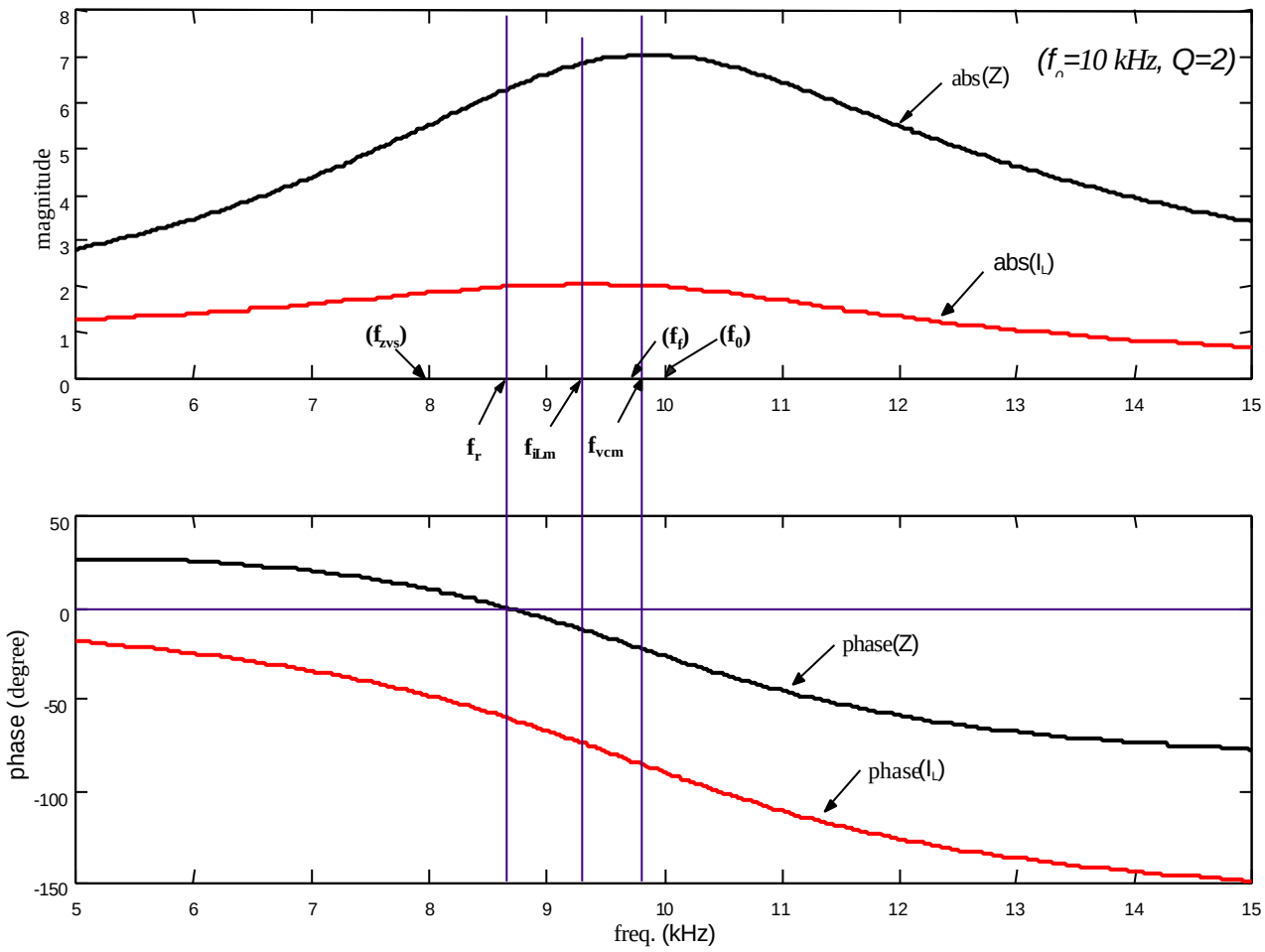


**Fig. 3-7: Various resonant frequencies of a series-loaded parallel-resonant tank**



InductEV, Inc.
Exhibit 1020
Page 080

**Resonant Frequencies under Sinusoidal Excitations**

*Zero Phase Angle Resonant Frequency*

If there is a pure sinusoidal current or voltage source at the input port of the parallel resonant tank (Fig. 3-6), then at a certain frequency the input voltage and current will be in phase under steady state conditions. This frequency is called the zero phase angle resonant frequency. At this frequency, the maximum energies stored in the inductor and capacitor are equal, the reactive power circulates only inside the resonant tank, producing a unity power factor input. In this situation, the source supplies only the real power required by the load resistor.

The zero phase angle resonant frequency of the resonant tank shown in Fig. 3-7 can be expressed as:

$$f_r = f_0\sqrt{1-\tfrac{1}{Q^2}} \tag{3-6}$$

where

$$f_0 = \frac{1}{2p\sqrt{LC}} \tag{3-7}$$

and

$$Q = \frac{1}{R}\sqrt{\frac{L}{C}} = \frac{2pf_0L}{R} \tag{3-8}$$

Note Q is often referred to as the quality factor, but in fact here it is only a defined ratio between the characteristic impedance and the resistance. The exact circuit quality factor at resonance ($Q_r$) should be $2\pi f_r L/R$, and can be expressed in terms of Q as:

$$Q_r = \sqrt{Q^2-1} \tag{3-9}$$

From this equation it can be seen that the circuit quality factor is smaller than Q, however, they are approximately equal when Q is high.

It should be noted that the zero phase angle resonant frequency $f_r$ is the most commonly accepted resonant frequency. In many cases it is simply referred to as the resonant frequency. Unlike the quality factor of a coil, the precise concept of the quality factor of a circuit is only valid at this resonant frequency.



InductEV, Inc.
Exhibit 1020
Page 081

*Maximum Inductor Current Frequency*

Strictly speaking, zero phase angle resonance does not necessarily occur when the current flowing through the resonant inductor reaches its maximum value. If the resonant tank circuit in Fig. 3-6 is excited by a sinusoidal current source, then the steady state maximum inductor current occurs at:

$$f_{i_L m} = f_0 \sqrt{1 - \frac{1}{2Q^2}} \tag{3-10}$$

This frequency is also shown in Fig. 3-7, and corresponds to the peak magnitude of the inductor current $I_L$.

*Maximum Capacitor Voltage Frequency*

Zero phase angle resonance does not guarantee that the oscillation of electric charge, corresponding to the capacitor voltage, reaches its maximum value. Again if a sinusoidal current source is assumed at the input port of the resonant tank, the steady state maximum capacitor voltage of the parallel resonant tank (Fig. 3-6) occurs at:

$$f_{v_c m} = f_0 \sqrt{\sqrt{1 + \frac{2}{Q^2}} - \frac{1}{Q^2}} \tag{3-11}$$

This frequency corresponds to the peak magnitude of the input impedance as shown in Fig. 3-7.

It is interesting to note that at both the maximum inductor current frequency and maximum capacitor voltage frequency, the electric energy stored in the capacitor is larger than the magnetic energy stored in the inductor. This arises because at these frequencies the input impedance is capacitive (a negative phase angle is shown in Fig. 3-7), indicating the capacitor generates reactive power to the source. This is caused by the circuit configuration of the resonant tank where the series load absorbs the circulating energy of the inductor more directly.

**Natural Oscillation Frequency**

If the resonant circuit has some initial energy, for example the resonant inductor has an initial current of $i_L(0)$, or the capacitor has an initial voltage, then even when there is no external excitation, the resonant tank may oscillate naturally. The natural oscillation frequency, sometimes called the free ringing frequency, is determined by the eigenvalues of the differential equations used to describe the resonant circuit. The natural frequency of the parallel resonant circuit used in Fig. 3-6 is:



InductEV, Inc.
Exhibit 1020
Page 082

$$f_f = f_0\sqrt{1-\frac{1}{4Q^2}} \tag{3-12}$$

where $f_0$ and Q have the same meaning as in equation (3-7) and (3-8).

The natural oscillation frequency is the frequency of the transient component of the circuit dynamics. This physical meaning is very different from previous resonant frequencies that assume steady state sinusoidal excitation. For comparison purposes, the natural oscillation frequency $f_f$ at Q=2 is shown in Fig. 3-7.

For a completely lossless resonant tank, i.e. R=0 and Q=∞, the above natural oscillation frequency becomes $f_0$, which has already been shown in (3-6). This frequency is often termed as the undamped natural frequency. In fact, when Q is high, all the resonant frequencies converge to this frequency, corresponding to an ideal no-load resonant condition.

**ZVS Frequency**

As discussed before, for a practical current-fed resonant converter as shown in Fig. 3-6, the commutation of the switching devices is controlled at the zero voltage crossing instants of the parallel resonant capacitor. In consequence, the ZVS operating frequency is the actual operating frequency that is of primary importance [5-6]. Because the resonant tank is neither driven by sinusoidal sources, nor in a free ringing mode, the actual ZVS operating frequency will be different from all of the resonant frequencies discussed before. As such, a more sophisticated analysis is needed to obtain this frequency, as will be discussed in the next section.

### *3.2.2 ZVS Frequency Analysis and Computation*

**The Effect of Harmonics**

For a practical current-fed resonant converter, the inductance of the DC choke and the phase-splitting transformer is normally designed much larger than the resonant inductor L, so that the injection current into the resonant tank is approximately square wave rather than sinusoidal at steady state. Apart from the fundamental, this square wave current includes high order odd harmonic components that can alter the actual zero voltage crossing position. If the fundamental of the injection current is controlled at the zero phase angle resonant frequency $f_f$, then its resultant fundamental voltage will be in phase with this fundamental current. Nevertheless, because there is a unique zero phase angle resonant frequency for a second order resonant circuit, the harmonic



InductEV, Inc.
Exhibit 1020
Page 083

components will not excite circuit resonance at this resonant frequency. As a result, the resultant voltage will be out of phase with the square wave current.

To demonstrate this problem more clearly, Fig. 3-8 shows the effect of the third harmonic. As the resonant tank is capacitive at a frequency that is higher than the zero phase angle resonant frequency, the third harmonic voltage $Vc_3$ is lagging its driving current $I_3$. As a result, the zero crossing points of the total voltage $Vc_1+Vc_3$ will be lagging that of the square wave current. Due to the parallel tuning property of the resonant tank, the switching frequency, which is the same as the frequency of the square wave current, should be reduced to some extent so as to draw the phase back and keep ZVS operation. In consequence, as indicated in Fig. 3-7, the actual ZVS frequency $f_{ZVS}$ will be smaller than the zero phase angle resonant frequency $f_r$.

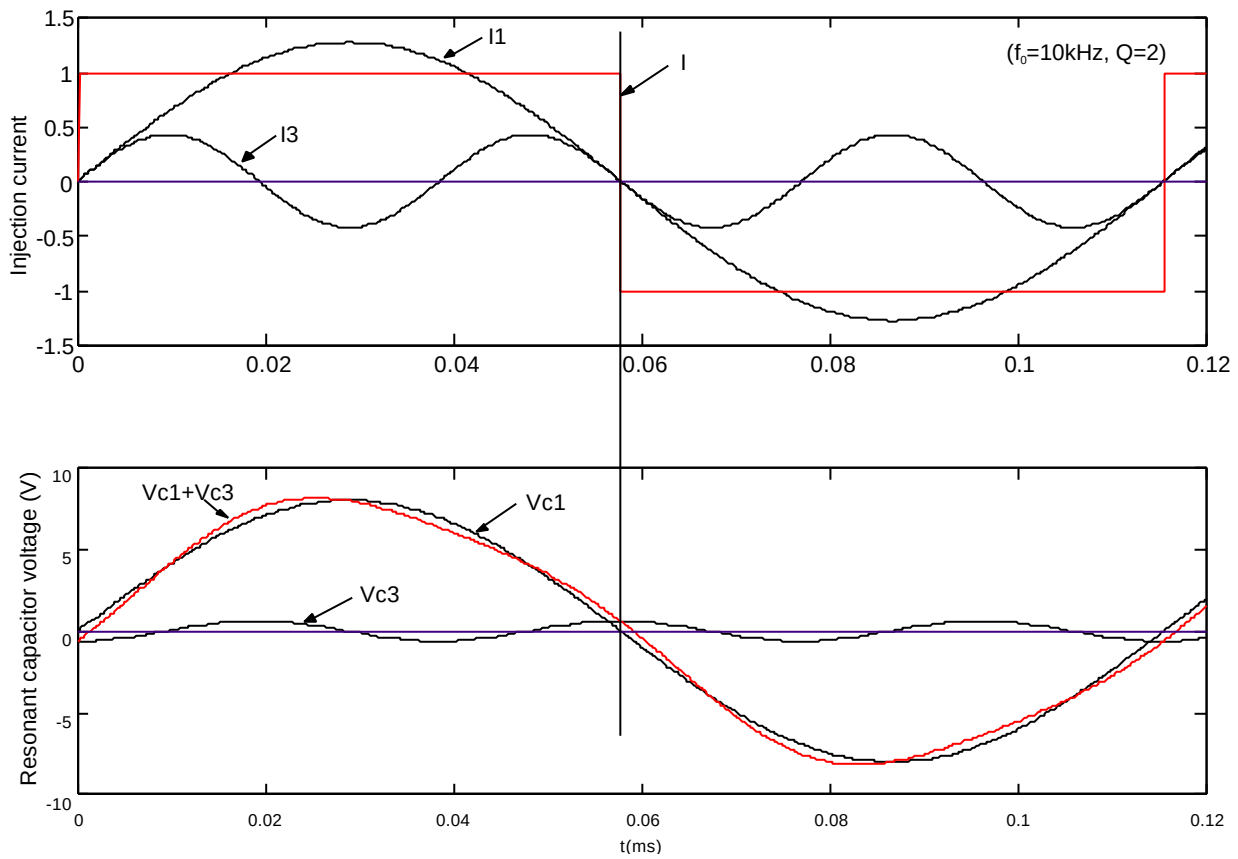


**Fig. 3-8: The effect of the third harmonics on the shift of the zero voltage crossing**

Apparently, the analysis of the ZVS frequency should be based on a complete solution of the capacitor voltage. Such a solution is possible, but the accuracy is limited by the number of harmonics considered. An iterative algorithm based on a complete circuit analysis will therefore give a more accurate solution.



InductEV, Inc.
Exhibit 1020
Page 084

**Iterative Computation Algorithm**

The basis of the analysis method is that the conditions existing in the circuit at the end of a particular switching period are the initial conditions for the start of the next switching period, and these conditions must be identical allowing for changes in polarity caused by the operation of the switches. In each half switching period of the current-fed resonant converter shown in Fig. 3-6, the injection current can be regarded as a step-input source as shown in Fig. 3-9 at the start of the switching period.

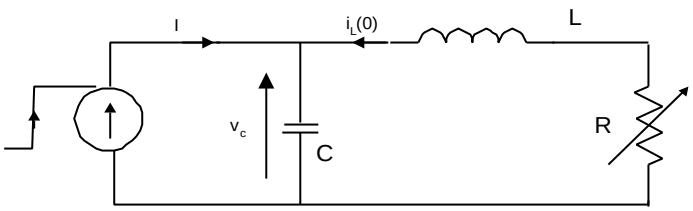


**Fig. 3-9: Step current injection model**

For this step current injection model, the following state space equation can be written:

$$\frac{d}{dt}\begin{bmatrix} i_L \\ v_C \end{bmatrix} = \begin{bmatrix} -\frac{R}{L} & -\frac{1}{L} \\ \frac{1}{C} & 0 \end{bmatrix}\begin{bmatrix} i_L \\ v_C \end{bmatrix} + \begin{bmatrix} 0 \\ \frac{1}{C} \end{bmatrix} I \tag{3-13}$$

If only the variable $v_c$ is considered, the second order ordinary differential equation can be obtained as:

$$LC\frac{d^2 v_c}{dt^2} + RC\frac{dv_c}{dt} + v_c = IR \tag{3-14}$$

Considering the initial condition $v_c(0)=v_c|_{t=0}=0$, $\frac{dv_c}{dt}|_{t=0} = \frac{I+i_L(0)}{C}$, the complete solution of the above equation is:

$$v_c(t) = \frac{IR}{\sin q} e^{-t/T} \sin(w_f t - q) + IR \tag{3-15}$$

where $\omega_f = 2\pi f_f$ is the free ringing angular frequency, T=2L/R is the time constant, and θ is an initial phase angle which can be expressed as:

$$q = \arctan\left(\frac{w_f IRC}{i_L(0) + I(1 - RC/T)}\right) \tag{3-16}$$

Equation (3-15) shows that the complete solution for the resonant capacitor voltage $v_c$ has two parts, as illustrated in Fig. 3-10. The first part is a transient component with oscillatory decay; the second



InductEV, Inc.
Exhibit 1020
Page 085

part is a forced component, which is a DC offset. Because of this offset, the time between the zero crossing points becomes larger than the free ringing half-period $t_f$, as can be seen in Fig. 3-10. Note that in this figure the first half cycle exists from the initial switching instant until the first zero crossing. The second half cycle of the waveform is identical in form but is inverted as shown.

As the ZVS frequency is determined by the zero crossing of the capacitor voltage, substituting $v_c$=0, in equation (3-15) leaves:

$$e^{-t_z/T}\sin(w_f t_z - q) + \sin q = 0 \qquad (3\text{-}17)$$

The solution of this equation is the ZVS half-period $t_z$ as shown in Fig. 3-10. To solve this equation requires the circuit parameters L, C, load R (corresponding to a certain Q), the injection current I, and the initial current $i_L(0)$. In fact, only the ratio $i_L(0)/I$, rather than I and $i_L(0)$ individually, contributes to the solution since equation (3-15) can be rewritten as:

$$q = \arctan\left(\frac{\sqrt{4Q^2-1}}{2Q^2(K_i+1)-1}\right) \qquad (3\text{-}18)$$

where $K_i=i_L(0)/I$, and Q is the quality factor defined in equation (3-5).

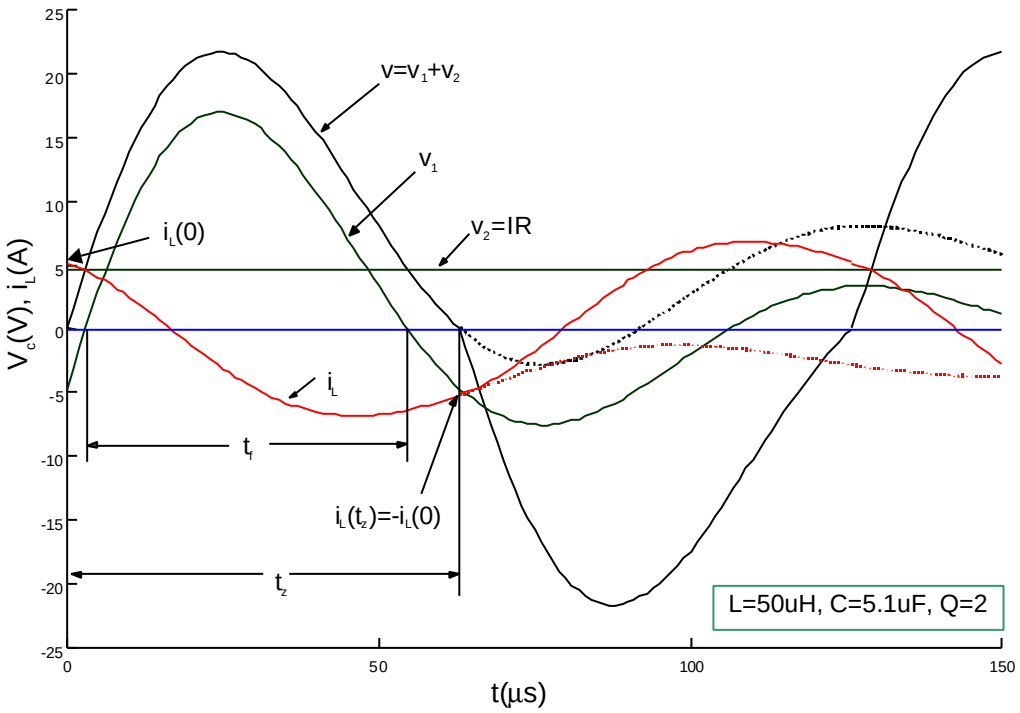


**Fig. 3-10: Complete voltage and current waveforms**



InductEV, Inc.
Exhibit 1020
Page 086

In practice the injection current is a positive or negative square wave at steady state, and the initial inductor current $i_L(0)$ is a dependent value which cannot be defined arbitrarily. To find this initial value, and thus the ratio $K_i$ for a given I, the following complete dynamic current analysis is necessary.

Similar to the voltage solution, the inductor current can be expressed as:

$$i_L(t) = \frac{I+i(0)}{\sin q_i} e^{-t/T} \sin(w_f t + q_i) - I \tag{3-19}$$

where

$$q_i = \arctan\left(\frac{2w_f L(I+i_L(0))}{R(I-i_L(0))}\right) = \arctan\left(\frac{(1+K_i)\sqrt{4Q^2-1}}{1-K_i}\right) \tag{3-20}$$

Because the process is actually repeated each half cycle with only a polarity change, the relationship $i_L(t_z)=-i_L(0)$ must hold (as shown in Fig. 3-10). This condition can be further expressed as:

$$e^{-t_z/T} \sin(w_f t_z - q_i) + \frac{K_i - 1}{K_i + 1} \sin q_i = 0 \tag{3-21}$$

Although an accurate analytical analysis is very difficult, theoretically the solutions of $t_z$ and another variable $K_i$ are governed by equations (3-17) and (3-21) with $\theta$ and $\theta_i$ as interim variables which are associated with the auxiliary equations (3-18) and (3-20). With the help of modern computing techniques, numerical solutions of such problems can be implemented using many available software packages such as MATLAB and C. A computer program based on an iterative computation has been developed to undertake the analysis. Its flow chart and basic algorithm are shown in Fig. 3-11.

The program starts with given circuit parameters L and C, enabling the undamped natural frequency $\omega_0$ and its half-period $t_0$ to be determined. Then load R is chosen allowing Q, time constant T, as well as the free ringing frequency $f_f$ to be calculated. From an input-output power balance analysis it can be shown that the current ratio between $i_L(0)$ and I is approximately equal to Q, therefore Q is a good initial guess of $K_i(0)$ to start the iteration. With $K_i(0)$ known, a numerical solution $t_z$ can be obtained by finding the zero of equation (3-17) around $t=t_0$. With $t_z$ known, $K_i(t_z)=i_L(t_Z)/I$ can be calculated using equation (3-19). The next step is to check whether $K_i(t_z)$ and $-K_i(0)$ have converged to a given error index ($\varepsilon$), e.g. $\varepsilon=10^{-5}$. If the answer is YES, the program terminates with ZVS



InductEV, Inc.
Exhibit 1020
Page 087

frequency $f_{zvs}$ calculated; otherwise, the iteration repeats with $K_i(0)$ updated with half of the error each time until a converged solution is obtained. The algorithm proves to be very fast and robust.

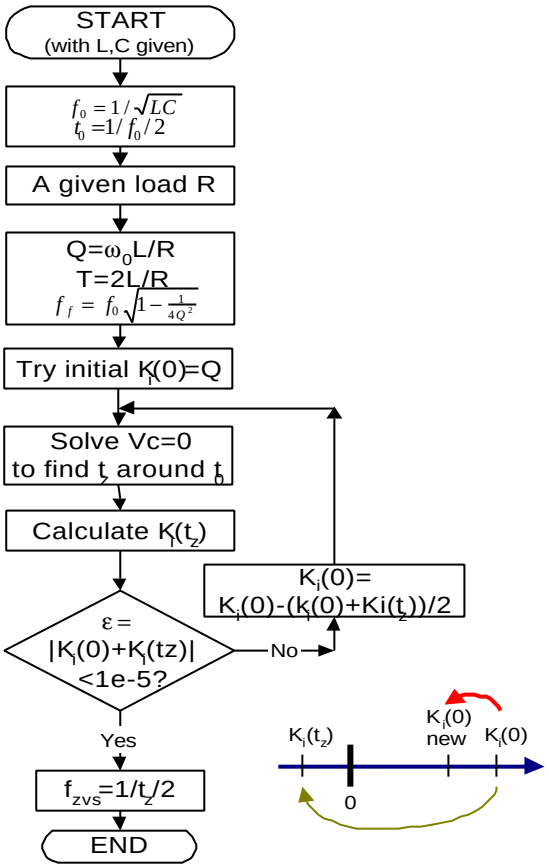


**Fig. 3-11: Iterative numerical analysis**

### Approximate Analytical Analysis

An approximate analytical result can be very helpful in providing a better starting guess of the initial values and the range of the final solutions for the numerical analysis. To achieve such a result, equation (3-17) can be rewritten in the following format:

$$\sin(w_f t - q) = -e^{t/T}\sin q \qquad (3\text{-}22)$$

so that it can be seen that the solution is the intersection point of a sine function curve and an exponential function curve. Using Taylor 's series and ignoring the high order terms: $\sin q = q$ and $e^{t/T} = 1 + t/T$, the following approximate analytical solution can be obtained:

$$t_z = \frac{p + 2q}{w_f - q/T} \qquad (3\text{-}23)$$



InductEV, Inc.
Exhibit 1020
Page 088

Thus, the ZVS frequency can be expressed as:

$$w_z = \frac{w_f - q/T}{1 + 2q/p} \tag{3-24}$$

Furthermore, by considering the input and output power balance, the current ratio can be estimated as:

$$K_i = \frac{4}{p}\sqrt{Q^2 - 1} \tag{3-25}$$

With this estimation, equation (3-18) becomes:

$$q = \arctan\left(\frac{p\sqrt{4Q^2-1}}{8Q^3\sqrt{Q^2-1}+p(2Q^2-1)}\right) \tag{3-26}$$

Equation (3-24) and its auxiliary equation (3-26) give a direct analytical ZVS frequency solution without iterative numeric computation.

### *3.2.3 Analysis Results and Discussion*

Fig. 3-12 shows the ZVS frequency results obtained from the above analyses and results obtained from the PSpice circuit simulations. It can be seen that the numerical analysis is quite accurate as the analysis results are very close to the circuit level PSpice simulation results. Similar to real experiments, frequency shift is allowed in the simulation so that ZVS operation is obtained in the steady state, and then the operating frequency is measured directly from the waveforms.

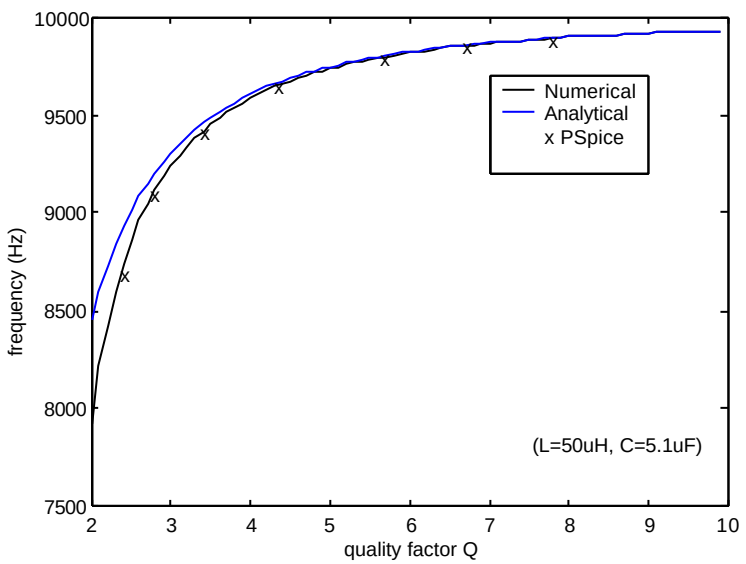


**Fig. 3-12: ZVS frequency results**



InductEV, Inc.
Exhibit 1020
Page 089

Fig. 3-12 also shows that the analytical results are quite good for large Q's, but the error becomes larger when Q is smaller. There are two main reasons for this: the assumption made for Taylor's series for solving the nonlinear equation (3-22), and the estimation of $K_i$ as shown in equation (3-26). Both procedures are only valid for large Q's. Hence the error becomes larger as Q reduces.

To compare different resonant frequencies available for the series loaded parallel resonant tank, these frequencies are drawn on the same graph in Fig. 3-13. It can be seen that all the resonant frequencies tend to converge to the undamped natural frequency (10kHz here) when Q is large. However, the discrepancies become quite large for small values of Q.

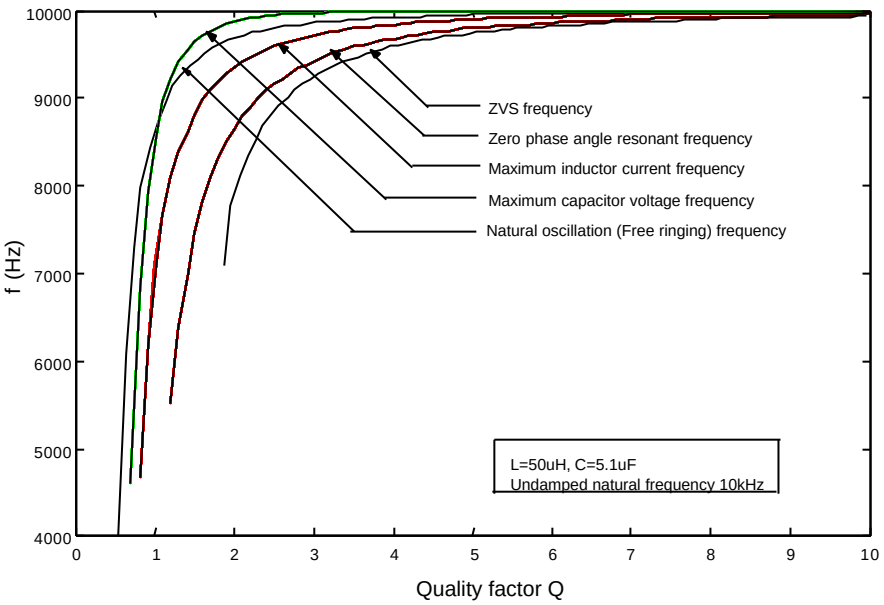


**Fig. 3-13: Resonant frequencies versus Q**

Table 3-1 summarises some important characteristics of the resonant frequencies. It can be seen that apart from the differences in excitation, the critical bounds on Q for maintaining resonance are also different. For example, if Q is equal to or less than 1, it will be impossible to obtain zero phase angle resonance. Due to the DC offset and the decay in a half-switching cycle (see Fig. 3-10), even higher Q is required to maintain the ZVS condition. When Q is smaller than ***1.86***, there is no zero voltage crossing solution, so that ZVS operation is impossible.

It can be seen clearly from Fig. 3-10 that the ZVS frequency is the lowest among all the other resonant frequencies. Table 3-1 shows that it drops to about 79% of its nominal value at Q=2. By comparing equation (3-11) with (3-12) it can be shown that when Q is smaller than $3\sqrt{2}/4$=1.06, the maximum capacitor voltage frequency is smaller than the free ringing frequency. In all other situations, it is the largest resonant frequency.



InductEV, Inc.
Exhibit 1020
Page 090

**Table 3-1: Comparison of different resonant frequencies**

| Name | Excitation | $f/f_0$ at Q=2 | Critical Q |
|---|---|---|---|
| ***Natural oscillation*** | Independent of source | 0.968 | >0.5 |
| ***Max capacitor voltage*** | Sinusoidal AC current source | 0.975 | $> \sqrt{\sqrt{2}-1}$ =0.644 |
| ***Max inductor current*** | Sinusoidal AC current source | 0.935 | $> \sqrt{2}/2$ =0.707 |
| ***Zero phase angle*** | Sinusoidal AC current or voltage source | 0.866 | >1 |
| ***ZVS switching*** | Square wave AC current source | 0.792 | >1.86 |

## 3.3 Frequency Stability Analysis and Stability Enhancing Methods

### *3.3.1 A General Scenario of the Frequency Stability Problem*

As discussed before, a system can run at either a fixed or variable frequency. For economical and practical reasons, particularly the easy realisation of soft switching, variable frequency operation is preferred in many practical IPT systems. However, one main concern is the system detuning problem. As a high order IPT system may have more than one frequency that a variable frequency controller can track, the final operating frequency can be uncertain. If the frequency variations are too large, ie, the practical operating frequency goes beyond an acceptable area, then the pick-up will be detuned so that not enough power can be received. In this situation the power transfer ability drops significantly and the system stability and control issue becomes particularly important [7]. Note that the term “stability” used here is different from the definition in classical linear control theories where a system is considered stable if its output is within a finite bound [8].

Fig. 3-14 illustrates a general block diagram of a simple switch mode variable frequency system. In this diagram, $u_1$ denotes an input source such as a DC voltage source. After the switching network this is changed to another form (eg., an AC voltage or current source $u_2$) suitable for driving a resonant tank. The required output such as a high frequency current for an IPT system is directly obtained from the resonant tank. The operating frequency of the resonant tank is determined by the switching network. However, unlike a fixed frequency system where the frequency is predetermined, the gating of the switching devices in the switching network of such a variable frequency system is governed by one of the state variables of the resonant tank. The required gate drive signals can be from direct zero crossing detection, or other advanced frequency following techniques such as a VCO (Voltage Controlled Oscillator) or a PLL (Phase-Locked Loop).



InductEV, Inc.
Exhibit 1020
Page 091

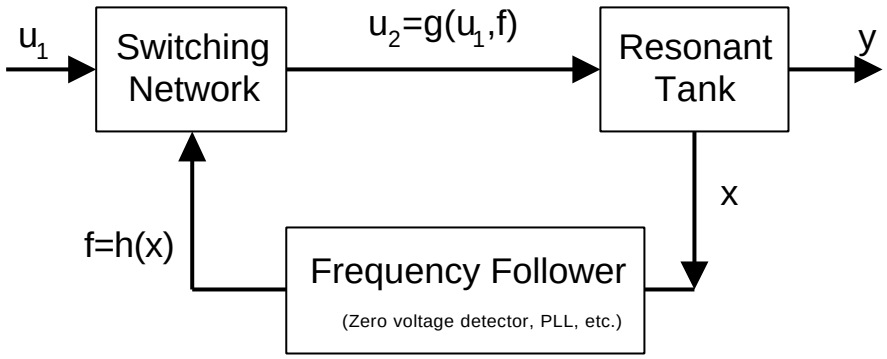


**Fig. 3-14: Variable frequency operation system**

Although a gate controller is used, the system oscillation is virtually autonomous. The complete dynamic analysis of such a nonlinear system is very complex. The solution may be sensitive to initial conditions and parameter variations which may cause uncertainties such as chaos and bifurcation [9].

Despite the complexities involved in the dynamic process, it is normally easier to undertake a steady state analysis to predict the possible steady state operating points regardless of the transient process approaching these points. As such, the frequency stability problem within variable frequency IPT systems is investigated in the following sections using a steady state analysis of the resonant tank.

### *3.3.2 Series Tuned Track and Pick-ups*

To simplify the analysis so as to clearly reveal the essence of the frequency stability problem, a simple situation with a fully tuned track and pick-up as shown in Fig. 3-15 is studied first. As can be seen later, the results drawn from the series tuned situation can be approximately extended to other tuning circuits. If the harmonics generated from the switching network are ignored, the input impedance of the resonant tank can be used to study the system performance. The zero phase angle resonant frequency, corresponding to a unity power factor input, is the main factor affecting the system frequency stability.

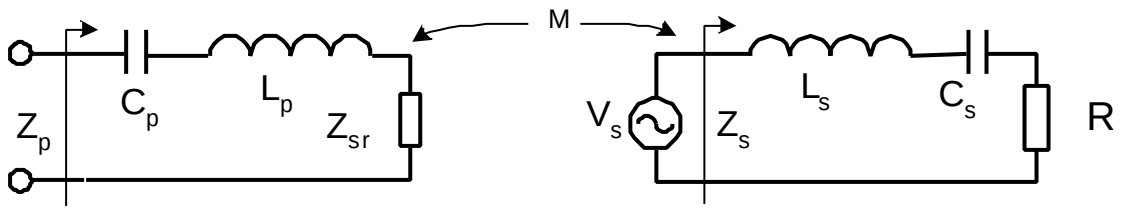


**Fig. 3-15: Input impedance of series tuned track and pick-up circuit**



InductEV, Inc.
Exhibit 1020
Page 092

**Maximum Loading Condition Analysis for a Single Pick-up System**

The input impedance of the network shown in Fig. 3-15 can be expressed as:

$$Z_p = jwL_p + \frac{1}{jwC_p} + Z_{sr} \tag{3-27}$$

where $Z_{sr}$ is the reflected impedance from the pick-up circuit, and can be expressed as:

$$Z_{sr} = \frac{w^2M^2}{Z_s} = \frac{w^2M^2}{jwL_s + \frac{1}{jwC_s} + R} = R_{sr} + jX_{sr} \tag{3-28}$$

Equation (3-27) then can be rewritten as:

$$\begin{aligned} Z_p &= R_{sr} + j(wL_p - \frac{1}{wC_p} + X_{sr}) \\ &= \frac{w^4M^2C_s^2R}{(1-w^2L_sC_s)^2 + w^2C_s^2R^2} + j\left[\frac{(w^2L_pC_p - 1)}{wC_p} - \frac{w^3M^2C_s(w^2L_sC_s - 1)}{(1-w^2L_sC_s)^2 + w^2C_s^2R^2}\right] \end{aligned} \tag{3-29}$$

Letting the imaginary part of $Z_p$ be zero, and considering the tuning condition of the track and the pick-up ($L_pC_p=L_sC_s=1/\omega_0^2$), it can be clearly seen that the nominal operating frequency $\omega_0$ is a solution corresponding to a zero phase angle of $Z_p$. Cancelling the terms $w^2L_pC_p - 1 = w^2L_sC_s - 1$ leaves:

$$\frac{1}{wC_p} - \frac{w^3M^2C_s}{(1-w^2L_sC_s)^2 + w^2C_s^2R^2} = 0 \tag{3-30}$$

Or

$$(1-w^2L_sC_s)^2 + w^2C_s^2R^2 - w^4M^2C_pC_s = 0 \tag{3-31}$$

Considering the quality factor of the pick-up is $Q_s=\omega_0L_s/R$ and the mutual coupling coefficient $k=M/\sqrt{L_pL_s}$, the above equation can be further expressed as:

$$\left[1-\left(\frac{w}{w_0}\right)^2\right]^2 + \frac{1}{Q_s^2}\left(\frac{w}{w_0}\right)^2 - k^2\left(\frac{w}{w_0}\right)^4 = 0 \tag{3-32}$$



InductEV, Inc.
Exhibit 1020
Page 093

$$(1-k)^2\left(\frac{w}{w_0}\right)^4+\left(\frac{1}{Q_s^{\ 2}}-2\right)\left(\frac{w}{w_0}\right)^2+1=0 \qquad (3\text{-}33)$$

If k≠1, two roots exist in the form of:

$$\left(\frac{w_{1,2}}{w_0}\right)^2=\frac{\left(2-\frac{1}{Q_s^{\ 2}}\right)\pm\sqrt{\left(2-\frac{1}{Q_s^{\ 2}}\right)^2-4(1-k^2)}}{2(1-k^2)}.....k\neq 1 \qquad (3\text{-}34)$$

Equation (3-34) can be re-expressed as:

$$\left(\frac{w_{1,2}}{w_0}\right)^2=\frac{\left(2Q_s^{\ 2}-1\right)\pm\sqrt{1+4Q_s^{\ 2}(Q_s^{\ 2}k^2-1)}}{2(1-k^2)Q_s^{\ 2}}.....k\neq 1 \qquad (3\text{-}35)$$

If k=1, which is an unlikely case in a practical system, from (3-33) it is clear that one root occurs at:

$$\left(\frac{w_{1,2}}{w_0}\right)^2=\frac{Q_s^{\ 2}}{2Q_s^{\ 2}-1}.....k=1 \qquad (3\text{-}36)$$

As only real number solutions practically exist, from equation (3-35) it can be seen that in order to avoid the existence of two zero phase angle frequencies which will cause the frequency stability and detuning problems in simple IPT controllers, one of the following two conditions should be met:

$$1+4Q_s^{\ 2}(Q_s^{\ 2}k^2-1)<0 \qquad (3\text{-}37)$$

or

$$\left(2-\frac{1}{Q_s^{\ 2}}\right)\pm\sqrt{\left(2-\frac{1}{Q_s^{\ 2}}\right)^2-4(1-k^2)}<0 \qquad (3\text{-}38)$$

The solution to the first condition is:

$$\frac{\sqrt{1-\sqrt{1-k^2}}}{\sqrt{2}k}<Q_s<\frac{\sqrt{1+\sqrt{1-k^2}}}{\sqrt{2}k}.....k\neq 0$$

And the solution to the second condition is:

$$\left(2-\frac{1}{Q_s^{\ 2}}\right)<0 \text{ or } Q_s<\frac{1}{\sqrt{2}}$$



InductEV, Inc.
Exhibit 1020
Page 094

Which means that if $Q_s$ is smaller than 0.707, the frequency shift is bound not to occur.

It can be proven that when $Q_s>0$ and $0<k<1$, the following equations always hold:

$$1-\sqrt{1-k^2} \le k^2 \qquad \text{or} \qquad \frac{\sqrt{1-\sqrt{1-k^2}}}{k} < 1$$

Therefore, the lower bound of the first solution becomes $Q>1/\sqrt{2}$. As such the two conditions overlap and the full solution can be simplified as:

$$Q_s < \frac{\sqrt{1+\sqrt{1-k^2}}}{\sqrt{2}k} \tag{3-39}$$

Or it can be rewritten as:

$$kQ_s\sqrt{1-\frac{1}{4Q_s^{\,2}}} < 1 \tag{3-40}$$

This equation gives the exact steady state maximum loading condition of a series tuned track and pick-up circuit which have a coupling coefficient of k. If the quality factor $Q_s$ of the pick-up is smaller than a certain value specified in this condition, there will be no extra zero phase angle frequencies except for the nominal resonant frequency $\omega_0$, therefore an IPT system will operate at a stable frequency. Otherwise, multiple zero phase angle frequencies occur and the system can become unstable if a simple controller such as a zero voltage detector is used.

For a large $Q_s$, the left side of (3-40) can be further simplified as $kQ_s$, so that the maximum loading condition before multiple frequencies occur becomes:

$$Q_s < 1/k \tag{3-41}$$

Normally the pick-up tuning quality factor is designed to be as large as possible so as to increase the power transfer capacity. Typical values for $Q_s$ are between 3 and 10, therefore this concise maximum loading condition is normally accurate enough for a practical circuit design.

**Frequency Shift Analysis – From One Zero Crossing to Three Zero Crossings**

If the maximum loading condition as shown in (3-40) is met, ie, $Q_s$ is smaller than what is specified in (3-39), the system will have a single zero phase angle crossing as shown in Fig.3-16 (a) and (b).



InductEV, Inc.
Exhibit 1020
Page 095

Otherwise, the multiple zero phase angle frequencies may occur, and their theoretical values can be determined from equation (3-35) and (3-36).

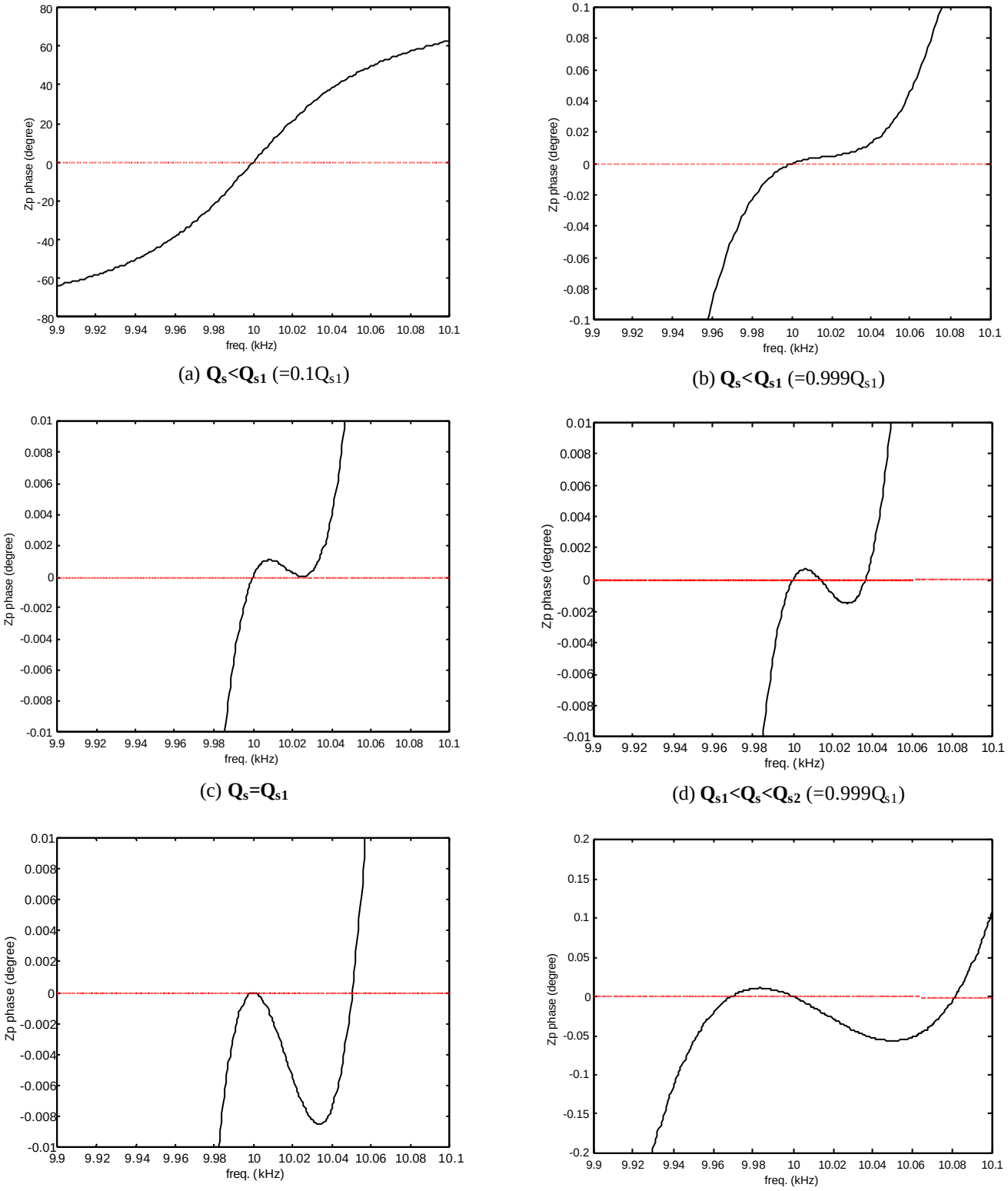


(a) $\mathbf{Q_s<Q_{s1}}$ (=0.1$Q_{s1}$)

(b) $\mathbf{Q_s<Q_{s1}}$ (=0.999$Q_{s1}$)

(c) $\mathbf{Q_s=Q_{s1}}$

(d) $\mathbf{Q_{s1}<Q_s<Q_{s2}}$ (=0.999$Q_{s1}$)

(e) $\mathbf{Q_s=Q_{s2}}$ (=1/k)

(f) $\mathbf{Q_s>Q_{s2}}$ (=1.005$Q_{s2}$)

**Fig. 3-16: Variation of zero phase angle frequency crossings (k=0.1)**



InductEV, Inc.
Exhibit 1020
Page 096

If the frequency increases to the critical condition:

$$Q_{s1} = \frac{\sqrt{1+\sqrt{1-k^2}}}{\sqrt{2}k} \tag{3-42}$$

there is one extra zero phase angle frequency appearing as can be seen in Fig. 3-16 (c). The frequency under this condition can be obtained from equation (3-34) as:

$$w_1 = w_0 \frac{1}{\sqrt[4]{1-k^2}} \tag{3-43}$$

If $Q_s$ increases (corresponding to a load increase), two extra crossing points as shown in Fig. 3-16 (d) appear.

When $Q_s$ increases further to $Q_{s2}$=1/k, it is interesting to note that the number of the extra zero crossings becomes one again. This is because the solutions from equation (3-34) becomes:

$$w_{1,2} = w_0 \sqrt{\frac{(2Q_s^{\ 2}-1)\pm 1}{2(1-k^2)Q_s^{\ 2}}} = w_0, w_0 \frac{Q_s^{\ 2}}{\sqrt{Q_s^{\ 2}-1}} \tag{3-44}$$

Or substituting k for $Q_s$(=1/k) in the above equation gives:

$$w_{1,2} = w_0, w_0 \frac{1}{\sqrt{1-k^2}} \tag{3-45}$$

Which shows that one solution coincides with the nominal frequency $\omega_0$, resulting in only one extra zero phase angle frequency as shown in Fig. 3-16 (e). It can be seen from the diagram that this is a critical point where the slope of the phase angle at the nominal frequency $\omega_0$ becomes zero. Therefore $Q_s$<1/k actually gives a very concise and clear boundary for frequency stability where the slope of the phase angle changes from positive to negative. This maximum loading condition, which is identical to that shown in equation (3-41), can be precisely proven by undertaking a differential operation on the input impedance of the tuned track circuit at $\omega_0$ as shown in Appendix A.

If $Q_s$ increases to a larger value than $Q_{s2}$=1/k, a negative slope will occur at $\omega_0$ causing two extra zero phase angle crossings as clearly shown in Fig. 3-16 (f).



InductEV, Inc.
Exhibit 1020
Page 097

It is interesting to notice that these two extra frequencies tend to remain constant with further increases in $Q_s$. This is because for large $Q_s$, $1/Q_s^2 << 2$, the frequency solutions shown in equation (3-35) and (3-36) can be approximated as:

$$\begin{cases} w_{1,2} = \dfrac{1}{\sqrt{1 \pm k}} w_0 \ldots\ldots\ldots k \neq 1 \\ w_1 = w_0 / \sqrt{2} \ldots\ldots\ldots\ldots\ldots k = 1 \end{cases} \tag{3-46}$$

It can be seen that when k tends to 1, the larger frequency shifts to infinity leaving practically only one lower frequency $\omega_0/\sqrt{2}$, which means for a well coupled large Q system, the practical ZVS operating frequency may be either $\sqrt{2}$ times lower than the tuning frequency or at a much larger value.

Fig. 3-17 shows the magnitude and phase frequency response at $Q_s$=1/k and $Q_s$=5/k respectively. It can be seen that for $Q_s$=1/k, the negative slope at $f_0$=10kHz tends to appear. And for $Q_s$=5/k, the frequency shift range is between 9.53kHz to 10.54kHz, which is the same as can be calculated from (3-46) when the coupling coefficient k=0.1. It is obvious that a larger k will result in a larger frequency shift.

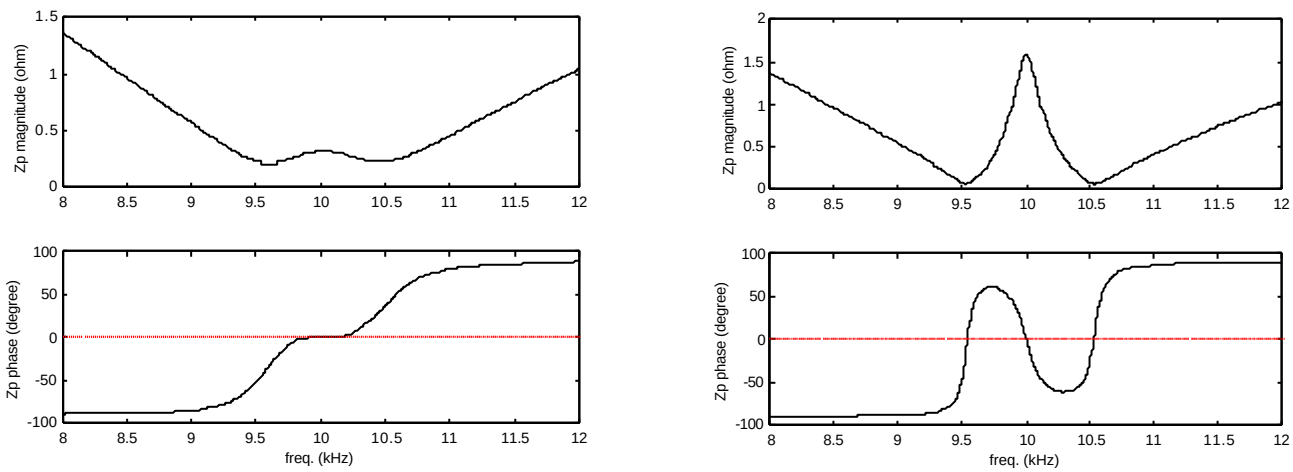


(a) $Q_s$=1/k (b) $Q_s$=5/k

**Fig. 3-17: Zero phase angle frequency shift for series-tuned circuits (k=0.1)**

## Multiple Pick-up System

Practical IPT systems normally have multiple pick-ups coupled with one track loop. In this case, the multiple pick-ups can be transformed to a single equivalent pick-up so that the previous analysis can be applied. For example, if the circuit shown in Fig. 3-15 has N identical pick-ups, then they



InductEV, Inc.
Exhibit 1020
Page 098

will be equivalent to one pick-up with circuit parameters changed to $L_s/N$, $C_sN$, R/N, $\sqrt{N}k$ respectively, while $Q_s$ and M remain the same. Accordingly, all the equations for the single pick-up system can be rewritten and applied to a multiple pick-up system. The frequency stability condition ($Q_s$<1/k) simply becomes:

$$Q_s < \frac{1}{k\sqrt{N}} \tag{3-47}$$

This equation can be rewritten as:

$$N < \frac{L_p L_s}{Q_s^{\,2} M^2} = \frac{1}{Q_s^{\,2} k^2} \tag{3-48}$$

which shows the maximum pick-ups that can be driven before a negative phase angle slope occurs and the system becomes unstable.

The stability criterion shown in equation (3-47) and (3-48) is expressed in circuit parameters. It can also be expressed in the reactive power ratings of the track and the pick-ups. It can be shown that the following equation gives exactly the same frequency stability condition as (3-48):

$$VAr_p > N\,VAr_s = Q_s P_s \tag{3-49}$$

where $VAr_p=\omega_0 L_p I_p^2$ and $VAr_s=\omega_0 L_s I_s^2$ are the reactive circulating powers of the track and each pick-up, and $P_s$ is the real power of each pick-up. This formula indicates that the total reactive power of the track should be higher than the total reactive power of the pick-ups to keep the frequency stable. For high Q systems, the reactive power is much higher than the real power. Therefore the total apparent power can be used to approximate the reactive power to determine the frequency stability. This approximation is the same as that obtained in [7], which states that the total VA rating of the track should be larger than the total rating of the pick-ups to ensure the system frequency stability.

Furthermore, the frequency shift analysis results can be extended easily to multiple pick-up systems. From equation (3-35), a general equation for the calculation of the frequency shift for a coupling coefficient $k \in (0, 1)$ can be obtained as:

$$w_{1,2} = w_0 \sqrt{\frac{\left(2-\frac{1}{Q_s^{\,2}}\right) \pm \sqrt{\left(2-\frac{1}{Q_s^{\,2}}\right)^2 - 4(1-Nk^2)}}{2(1-Nk^2)}} \tag{3-50}$$



InductEV, Inc.
Exhibit 1020
Page 099

For large $Q_s$, this becomes:

$$w_{1,2} = \frac{1}{\sqrt{1 \pm k\sqrt{N}}} w_0 \tag{3-51}$$

Notice the only difference a multiple pick-up system makes is that the coupling coefficient has an additional term of $\sqrt{N}$ compared to that of the single pick-up.

### 3.3.3 Other Tuning Circuits

If the track or the pick-ups are not fully series tuned (or not fully parallel tuned in the dual circuit), the load resistor may affect the zero phase angle at even the nominal frequency $\omega_0$, which is always zero for series tuned track and pick-ups. This makes accurate analysis very difficult. However, for large quality factors, normally certain assumptions can be made to simplify the analysis. For instance, as shown in Fig. 3-18, a practical parallel-tuned pick-up can be approximated as a series tuned circuit under the steady state conditions. The equivalent series resistor and capacitor can be expressed as:

$$C_{seq} = \frac{Q_{sw}^{\ 2} + 1}{Q_{sw}} C_s \approx C_s \tag{3-52}$$

$$R_{eq} = \frac{1}{Q_{sw}^{\ 2} + 1} R \approx R / Q_{sw}^{\ 2} \tag{3-53}$$

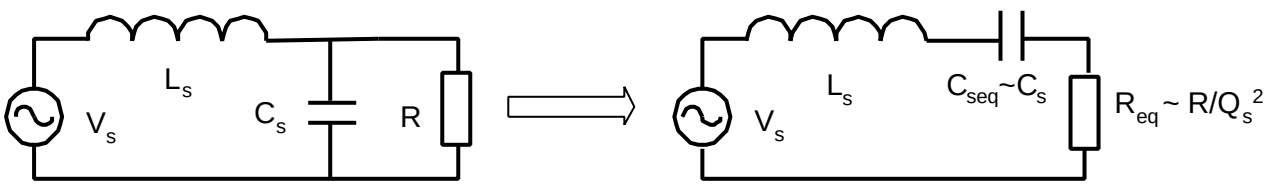


**Fig. 3-18: Approximation of a practical pick-up circuit**

where $Q_{s\omega}=\omega C_s R=R/(\omega L_s)$. Note that here $Q_{s\omega}$ is frequency dependent which is different from $Q_s=R/\sqrt{L_s/C_s}=R/(\omega_0 L_s)=\omega_0 C_s R$. However, if $Q_s$ is large and the practical operating frequency is near $\omega_0$, then $C_{seq}\approx C_s$ and $R_{eq}\approx R/Q_{s\omega}^2\approx R/Q_s^2$. Consequently, the pick-up circuit can be approximately regarded as fully series tuned. Thus the previous frequency shift analysis for the fully tuned pick-up is applicable to this circuit.



InductEV, Inc.
Exhibit 1020
Page 100

Interestingly, a parallel tuned track circuit shown in Fig. 3-19 is actually the dual circuit of the pick-up circuit shown in Fig. 3-18. It can be approximated as a fully tuned parallel circuit with the following parameter transformations:

$$L_{peq} = \frac{Q_{pw}^{2}+1}{Q_{pw}^{2}} L_p \approx L_p \tag{3-54}$$

$$R_{peq} = (Q_{pw}^{2}+1)R \approx Q_{pw}^{2} R_p \tag{3-55}$$

where $Q_{p\omega}=\omega RC_s=R/(\omega L_s)$, and $L_s$ is the total equivalent track inductance with a small part of the reflected pick-up reactance included. Similar assumptions are made for the pick-up circuit, but as the equivalent load $R_p$ is series connected in the track circuit, the definitions of Q are the inverses of those for the parallel connected loads. In this situation, a larger resistor corresponds to a larger portion of real power and therefore a larger quality factor.

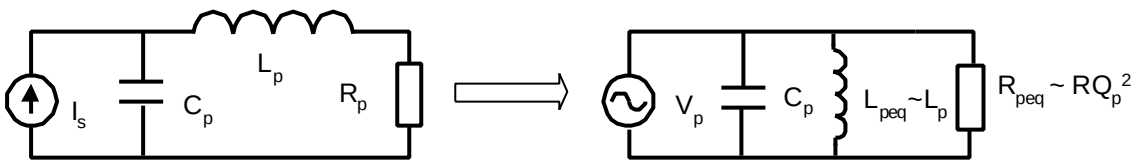


**Fig. 3-19: Approximation of a practical parallel track tuning circuit**

After the above simplification, the same methods used in the series tuned track and pick-ups can be applied for the analysis of the above parallel tuned circuits. Based on the fact that the impedance of a circuit has the same properties as the admittance of its dual circuit, the analysis results obtained from the last section for the series tuned track and pick-ups are also valid here.

To verify the above conclusion, Fig. 3-20 shows the numerical simulation results of the input admittance property of a parallel tuned track and pick-ups. It can be seen from Fig. 3-20 (a) that the maximum loading condition is still the same as $Q_s$=1/k. And it is not difficult to verify that the frequency shift at $Q_s$=5/k is in agreement with the equations obtained for series tuned circuits. If Fig. 3-20 is compared with Fig. 3-17, it can be seen that although there is a small central frequency shift for the parallel tuned circuits, the results are essentially the same for the other two extra zero crossings. For multiple pick-ups, the maximum pick-up numbers that can be loaded before the systems goes unstable has been given by Boys and Green [3,9] showing the same result as equation (3-48). However, from the analysis made here it can be shown that this critical loading condition is accurate for series tuned track and pick-ups (or fully tuned parallel dual circuits), but is only a approximation for the practical parallel-tuned circuits as shown in Fig. 3-18 and Fig. 3-19. A full



InductEV, Inc.
Exhibit 1020
Page 101

parallel tuning is practically impossible as the induced voltages are distributed along the pick-up track windings.

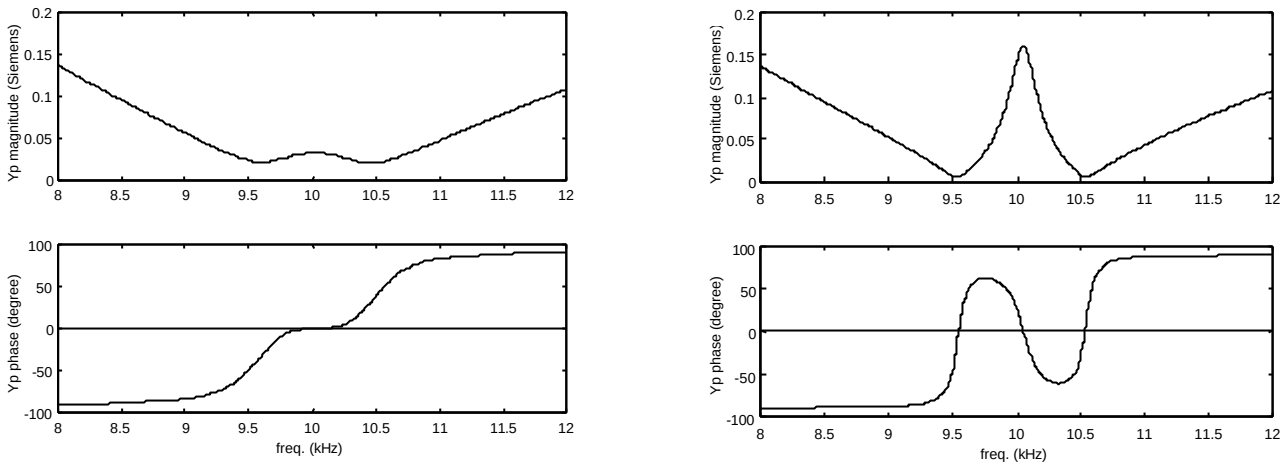


(a) $Q_s=Q_{s2}=1/k$ (b) $Q_s=5Q_{s2}$

**Fig. 3-20: Zero phase angle frequency shift for practical parallel-tuned circuits (k=0.1)**

Besides parallel tuned circuits, other track and pick-up tuning options have also been investigated, and it has been found that the results obtained for the basic series circuit are essentially valid for other types of tuning options. However, the condition is that both the pick-up circuit quality factor $Q_s$ and the equivalent track circuit quality factor $Q_p$ should be high. Note that the quality factors should be correctly defined according to the loading conditions such as series or parallel. The circuit dual properties can be taken into account to simplify the analysis. In fact, detuning is a natural phenomenon of mutually coupled circuits and results obtained reflects the basic properties such as the critical detuning conditions and frequency shifts.

## *3.3.4 Frequency Stability Enhancing Methods*

Based on the analyses made before, the following methods can be employed to enhance the system frequency stability.

### Reducing the Pick-up Quality Factor in Tuning Design

From the frequency stability condition ($\sqrt{N}\,Q_s<k$) obtained, it can be seen that there are two main aspects affecting the system frequency stability: the pick-up tuning property and its coupling effects to the track circuit. The pick-up tuning featured with its tuning quality factor $Q_s$ is largely dependent on its circuit topology, current and the load requirements. For series tuned pick-ups, the quality factor is $Q_s=\omega_0 L_s/R$, whereas for parallel tuned pick-ups $Q_s=R/(\omega_0 L_s)$. In a practical circuit



InductEV, Inc.
Exhibit 1020
Page 102

$Q_s$ should be kept smaller than 10, otherwise the system is too sensitive to parameter variations and tuning can be very tedious.

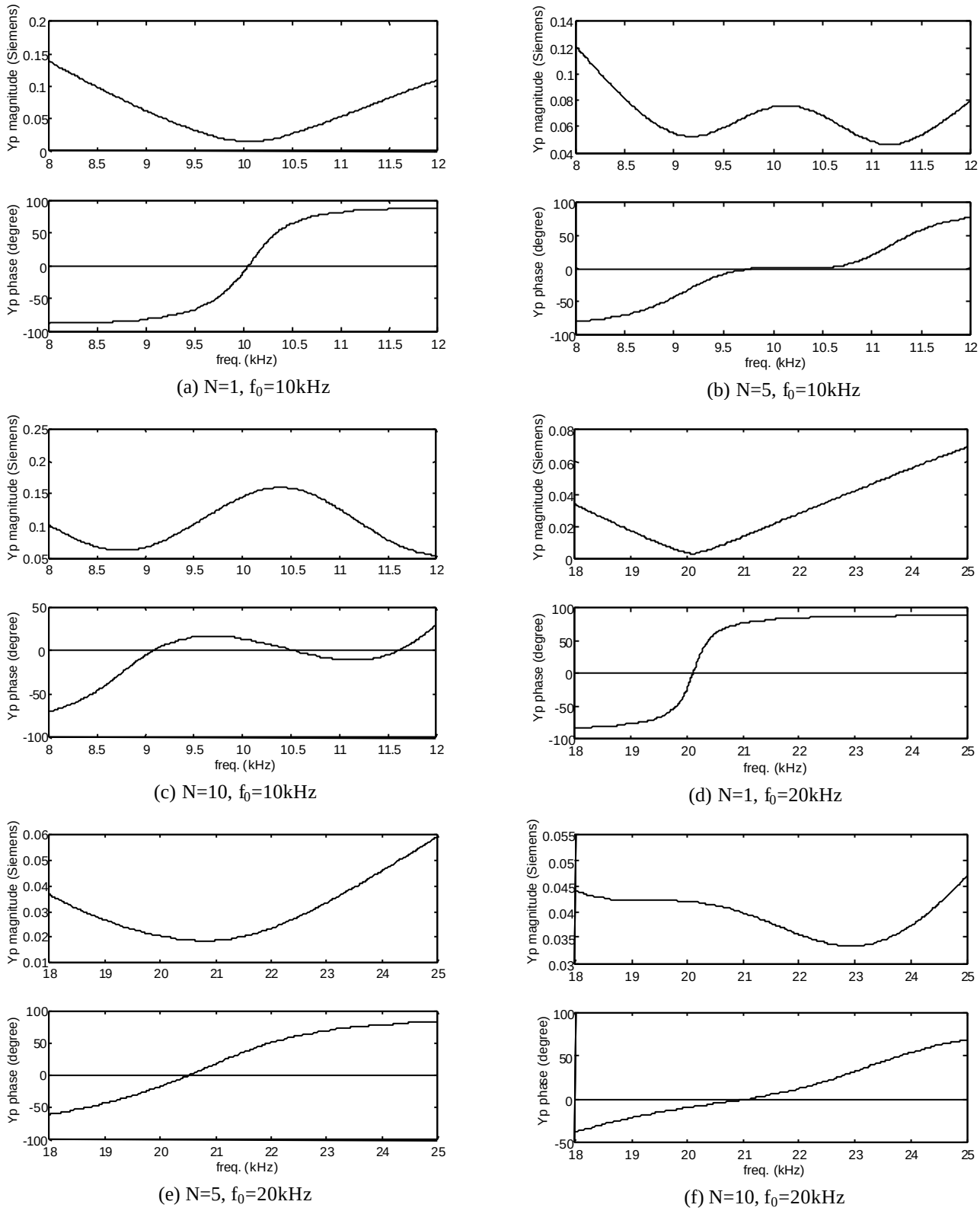


(a) N=1, $f_0$=10kHz

(b) N=5, $f_0$=10kHz

(c) N=10, $f_0$=10kHz

(d) N=1, $f_0$=20kHz

(e) N=5, $f_0$=20kHz

(f) N=10, $f_0$=20kHz

**Fig. 3-21: Increasing the maximum loading by increasing the nominal frequency**

(k=0.1, $Q_s$=4.47 at 10kHz, and $Q_s$=2.23 at 20kHz)



InductEV, Inc.
Exhibit 1020
Page 103

Different pick-up tuning topologies can result in very different circuit properties. The commonly used parallel pick-up tuning circuit (see Fig. 3-18) essentially gives constant current output with a value of $I_p M/L_s$ which is frequency independent. Normally this current is rectified and controlled to boost pick-up voltage to a value suitable for supplying certain loads such as lights and motors. At the maximum load condition, this is approximately equivalent to a certain resistance load R in parallel with the tuning capacitor. In this case, having a higher frequency can reduce the equivalent quality factor $Q_s$ of the pick-up, thus increasing the frequency stability at a given load. This is clearly shown in Fig. 3-21. Fig. 3-21 (a)-(c) show the operation of a 10 kHz system where the maximum pick-up loading number is 5, while Fig. 3-21(d)-(e) show the situation when the designed operating frequency is increased to 20kHz. It can be seen that by just increasing the nominal frequency, the maximum number of pick-ups that can be driven increases. Although it is known that increasing the track current reduces the equivalent pick-up quality factor (for a controlled constant voltage output system) and thus improves the system stability [9], increasing the operating frequency may be the simplest and most cost-effective way in a particular design. For standard fully tuned series circuits, theoretically the maximum loading capacity should increase by four times the original pick-up number simply by doubling the operational frequency. However, large load variations can cause a larger nominal frequency shift as shown in Fig. 3-21(f) where the zero crossing frequency is shown to shift to about 21kHz although the slope of the phase angle is still positive. Note this problem does not exist for fully tuned track and pick-up circuits.

From the definition of the quality factor of a parallel tuned pick-up $Q_s=R/(\omega_0 L_s)$, it can be seen the quality factor can also be reduced by increasing the pick-up coil inductance $L_s$. However, due to the fact that the self inductance $L_s$ is proportional to the square of the number of turns, while the mutual inductance M is approximately proportional to the number of turns, increasing the turns on the pick-up reduces the short circuit current and thus the current output ability.

For a series tuned pick-up, the situation is just the opposite. A lower frequency reduces $Q_s$ and improves the frequency stability. Having more turns on the pick-up coil increases the quality factor and worsens the frequency stability problem. But too few turns reduce the open circuit voltage and consequently reduce the maximum voltage output level.

**Weakening the Relative Coupling Effect by Increasing the Track VAr Rating**

For a second order track circuit, it is clear that frequency detuning is caused by the coupling effect of the pick-ups. Besides the improvements in the pick-up circuit tuning design, weakening the coupling coefficient k can reduce the total effect of the pick-up on the track. From the definition of



InductEV, Inc.
Exhibit 1020
Page 104

k, there are three design parameters to be considered. One is the mutual inductance M, reducing the value of this parameter can definitely weaken the coupling effect and ease the detuning problem but may reduce the power transfer ability greatly. Therefore, normally M is designed as large as possible. Another parameter to consider is $L_s$, for the same reason as mentioned before regarding the relationships between the number of turns and the mutual inductance and the self inductance, the number of turns on $L_s$ does not affect k. This leaves only one parameter - the track inductance $L_p$ to design. For an IPT system, normally only a small part of $L_p$ couples with the pick-up coil, so k actually does not reflect the local coupling situation. As discussed before, local coupling is only determined by the geometry and magnetic materials and is more accurately defined by the coupling factor $k_f$. However, the coupling coefficient $k_f$ does reflect the overall relationship between the primary and the secondary circuits, therefore it is more suitable for the frequency stability analysis here. Increasing $L_p$ means weakening the relative effect of the pick-up circuit. Considering the tuning together, a series LC network as shown in the dotted block in Fig. 3-22 (a), or its dual (a parallel LC network) as shown in Fig. 3-22 (b), may be inserted for this purpose.

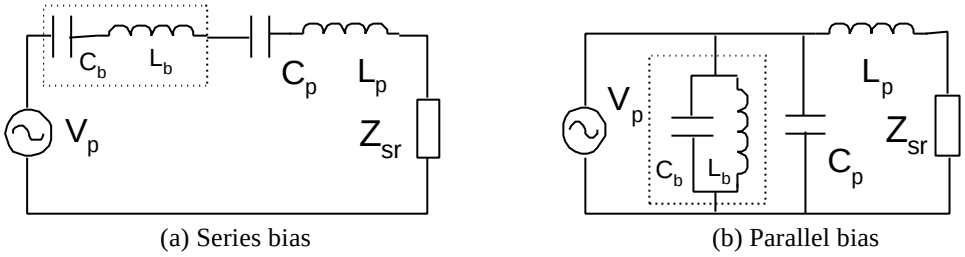


(a) Series bias (b) Parallel bias

**Fig. 3-22: Adding bias network to increase the system frequency stability**

The additional LC tank is also called reactive bias. When the system operates at the nominal resonant frequency these bias tanks have almost no effect as the inductor and the capacitor cancel out. However, they help to prevent the resonant frequency dynamically shifting away from the desired value. This method is simple and reliable, but an obvious disadvantage is the larger size and higher cost required by the extra VArs. The concept used here is in agreement with the stability condition (3-49) considered from the reactive power balance point of view. The added LC tank increases VAr rating of track circuit thus increasing the total system frequency stability. In fact, this concept is also valid for other composite track tuning circuits such as those used in improved voltage and current-fed resonant converters which are discussed in Chapters 4 and 5.

### Dynamic Parameter Tuning

The above two methods for enhancing frequency stability are based on circuits with fixed parameters. Another approach to solving the frequency detuning problem is to change the circuit



InductEV, Inc.
Exhibit 1020
Page 105

parameters dynamically. The complete dynamic circuit analysis can be very complex if the value of one parameter such as an inductor or a capacitor changes with loading conditions. However, by and large the resonant frequency is determined by the L and C of a tuned circuit. A large L or C value corresponds to lower resonant frequency. Based on this simple fact, the average operating frequency can be kept constant using a proper dynamic controller.

The problem is how to implement this dynamic parameter tuning. Variable capacitors based on ceramic oscillation are available for radio systems applications, but their power level is too low for high power circuits. Magnetic amplifiers can result in variable inductance, however they are too bulky and inefficient and are therefore not preferred. It seems that having a continuous variable inductor or capacitor at high power levels is not very feasible and a new approach is required.

A novel approach is to use switching devices to vary the reactance in a discontinuous mode. Proper location of the tuning circuit and easy implementation need to be considered in a particular design. As shown in Fig. 3-23 (a), Boys and Green put capacitors at the input port of a parallel resonant tank. The capacitors are then controlled to be inserted in or disconnected according to the frequency changes [10]. This method is simple to implement and comparatively cheap as no extra VArs are required. However, the frequency dynamically varies during operation, which can result in random EMI. Nevertheless, an extra advantage is that the AC noise is mitigated due to the frequency dithering effect.

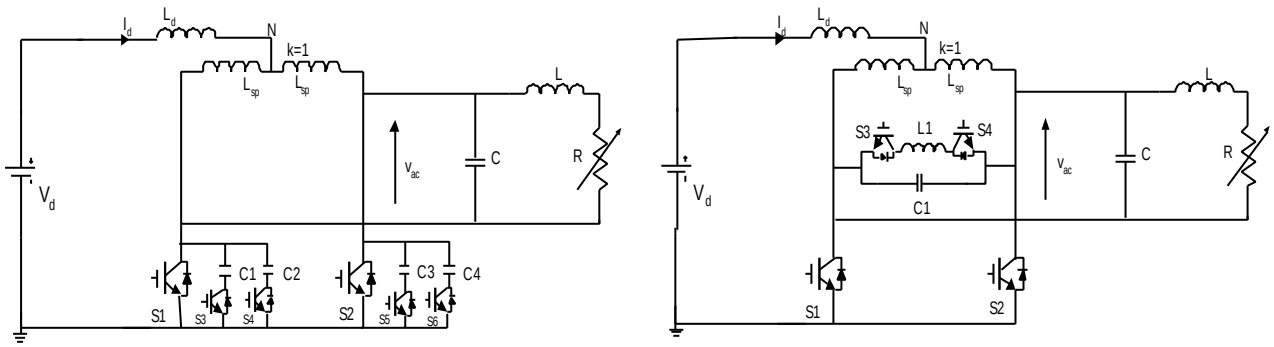


(a) Dynamic capacitor switching

(b) Dynamic reactance regulator

**Fig. 3-23: Dynamic parameter tuning methods**

Alternatively, Fig. 3-23 (b) shows another method of dynamic tuning. The trigger angle of the current flowing through inductor L1 is controlled with two MOSFETs or IGBTs (forming a fast AC switch) so that the average current is under control. Therefore, the equivalent inductance is varied accordingly. This “variable inductor” can also be placed in series with the track inductor. With the configuration shown in Fig. 3-23 (b), a single-phase full bridge switching device package available



InductEV, Inc.
Exhibit 1020
Page 106

commercially can be employed easily. In this circuit, a parallel resonant tank is formed using an additional capacitor C1, or a part of the resonant capacitor C. As discussed before, this resonant tank is beneficial for frequency stabilisation. Compared to switched capacitors, this method can achieve smooth tuning so that the operating frequency can be set to a stable value rather than jumping from one point to another. The firing angle can move between $0^0$ to $90^0$ to control the current flowing through the inductor. In fact, thyristor type switches are ideal for this application as they can turn off naturally so that no exact turn-off timing is required.

## 3.4 Improved Power Supply with Dynamic ZVS Start-up

### *3.4.1 Zero Voltage Crossing Problems at Start-up*

To achieve ZVS, a basic question that needs to be answered is whether the resonant voltage oscillates to zero, ie, whether zero crossing points exist or not [11]. For practical current-fed resonant converters as shown in Fig. 3-24, normally the inductance of the DC inductor (including the phase-splitter leakage inductance for push–pull converter) is much larger than that of the resonant inductor L, thus at normal operation at steady state conditions, the DC current is constant and the switching network injects an approximate AC square wave current into the resonant tank. But on start-up this is not the case. Fig. 3-24(a) shows a start-up equivalent circuit when only the switches in one leg of the inverter are turned on to start the system. Its state space equation can be written as:

$$\frac{d}{dt}\begin{bmatrix} i_d \\ i_L \\ v_C \end{bmatrix} = \begin{bmatrix} 0 & 0 & \frac{1}{L_d} \\ -\frac{R}{L} & 0 & \frac{1}{L} \\ \frac{1}{C} & -\frac{1}{C} & 0 \end{bmatrix}\begin{bmatrix} i_d \\ i_L \\ v_C \end{bmatrix} + \begin{bmatrix} \frac{1}{Ld} \\ 0 \\ 0 \end{bmatrix} V_d \qquad (3\text{-}56)$$

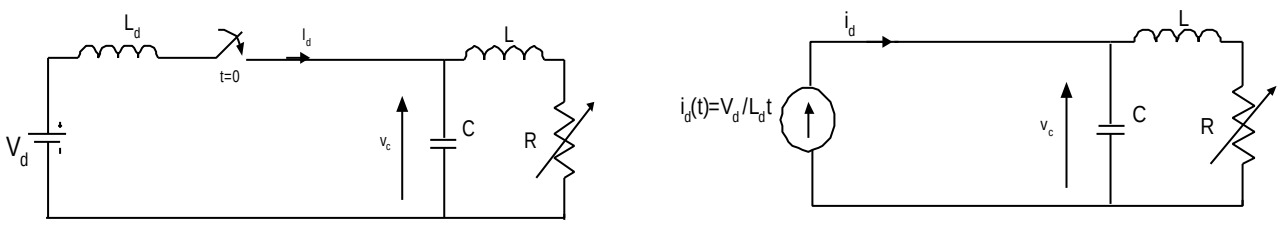


(a) Equivalent circuit

(b) Ramp current input model

**Fig. 3-24: Equivalent circuit and ramp current input model**



InductEV, Inc.
Exhibit 1020
Page 107

If the circuit parameters are known, the numeric solution of the resonant voltage $v_t(t)$ can be easily obtained from available software packages such as MATLAB. But it is not easy to reach a general conclusion suitable for all situations. Considering the existence of the large DC inductance (and also the inductance of the phase-splitter for the push pull topology) and a small $v_c$ initially, the injection current actually ramps up almost linearly with a slope of $V_d/L_d$. This can be modelled as a ramp up current input into the resonant tank as shown in Fig.3-24 (b). Thus, a second order differential equation can be written as:

$$LC\frac{d^2v_c}{dt^2} + RC\frac{dv_c}{dt} + v_c = \frac{V_d}{L_d}Rt + V_d \qquad (3\text{-}57)$$

Considering the initial conditions $v_c|_{t=0}=0$ and $\frac{dv_c}{dt}|_{t=0}=0$, the solution of the resonant voltage can be obtained as:

$$v_c(t) = \frac{V_d}{\sin q}(1-R^2C/L_d)e^{-t/T}\sin(w_f t - q) + \frac{V_d R}{L_d}t + V_d(1-R^2C/L_d) \qquad (3\text{-}58)$$

where $\omega_f$ is the natural free ringing frequency:

$$w_f = \frac{1}{w_0}\sqrt{1-\left(\frac{1}{2Q}\right)^2} \qquad (3\text{-}59)$$

and $\omega_0=1/\sqrt{LC}$ is the undamped natural frequency, $Q=\omega_0 L/R$ is the circuit quality factor, $T=2L/R$ is the time constant, and $\theta$ is an initial phase angle which can be expressed as:

$$q = \arctan\left(\frac{w_f L_d T(1-R^2C/L_d)}{RT(RC/T-1)-L_d}\right) \qquad (3\text{-}60)$$

At an ideal oscillation condition where the equivalent load resistor R=0, the time constant $T=\infty$, and the initial phase angle $\theta=-90^0$, the resonant voltage can be expressed as:

$$v_c(t) = V_d(1-\cos w_f t) \qquad (3\text{-}61)$$

From this equation it can be seen that even under ideal conditions where no damping exists, $v_c(t)$ is always greater than or equal to zero. At normal load the oscillation is damped so it is clear that a zero voltage crossing point does not exist.



InductEV, Inc.
Exhibit 1020
Page 108

For a practical resonant converter, Fig. 3-25 shows the injection current and resonant voltage waveforms at ideal no load and a typical loaded condition. The numerical solution of the original third order equation (3-56) and the analytical solution of (3-58) based on the ramp current injection model are compared. It can be seen that the results are very close, meaning that analytical analysis based on the ramp current input model is valid and the general conclusion that no zero crossing point exits is correct.

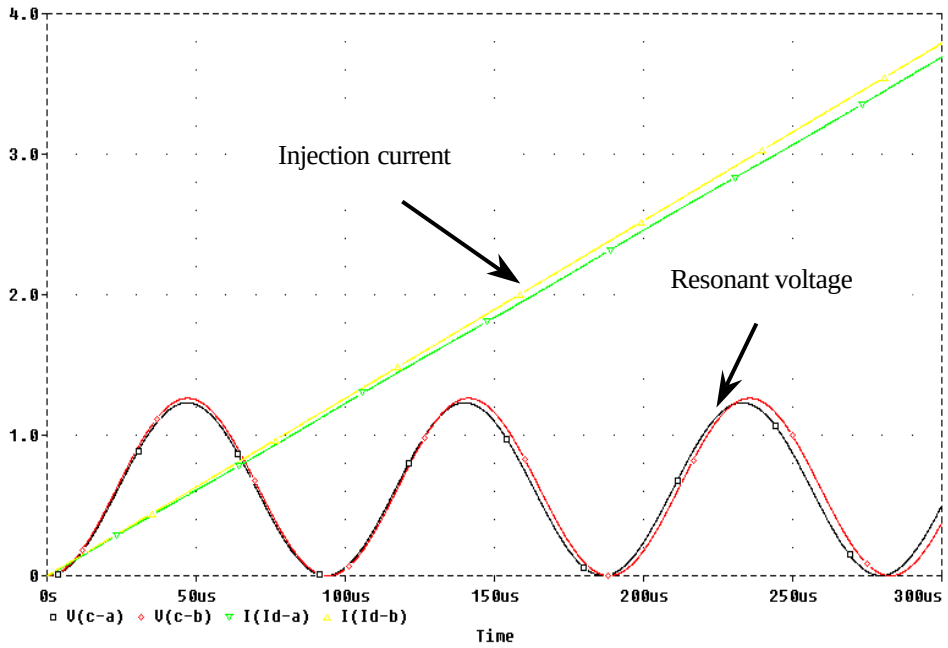


Ideal No-load Condition (Q=∝)

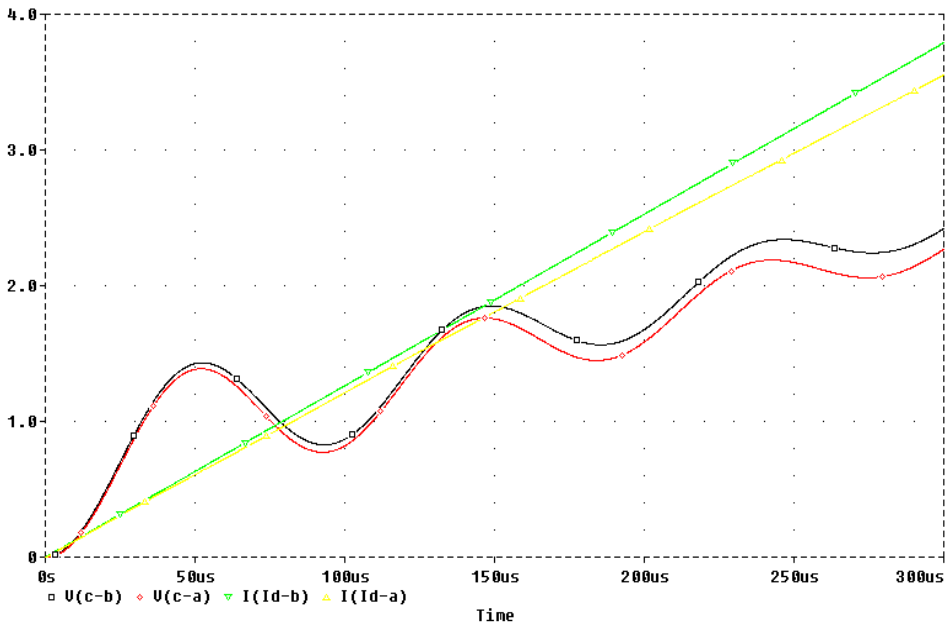


Load Condition (Q=6.28)

(V(c-a) and I(Id-a): numerical solutions; V(c-b) and I(Id-b): analytical solutions)

**Fig. 3-25: Voltage and current waveforms after the first switch is on**

Therefore, if the turn-on of the switches is alternated so as to build up the energy in the resonant tank and start the system, ZVS is impossible, as the voltage does not go to zero. As a result,



InductEV, Inc.
Exhibit 1020
Page 109

externally forced clocking is a must and momentary capacitor shorting is inevitable if no blocking diodes are used. As discussed before, this short circuit current is a great danger to the switching devices, especially for high voltage and current level applications. This explains why in some practical situations the switching devices blow up before the system can reach steady state without an appropriate start-up control circuit.

### *3.4.2 Initially Forced DC Current Solution*

The main reason that the voltage does not go to zero is that the injection current ramps up from zero and there is no initial energy in the tank at start-up. If energy can be injected into the resonant tank prior to starting, ie. giving the resonant capacitor an initial voltage, or the resonant inductor an initial current, system oscillation may occur with zero voltage crossing, but doing this requires additional charging circuitry. An alternative option is to give the DC inductor an initial current. In a current-fed resonant converter, if the switches at both legs are controlled to be "on" for a short time $t_1$, the DC inductor current will ramp up to a certain value $I_d(o)$. If the switch in one of these legs is then turned "off", the injection current into the resonant tank will have an initial value $I_d(o)$. Provided $I_d(o)$ is much greater than the current increase $\Delta I_d$ in the first half cycle of the oscillation, the starting process is approximately equivalent to a step current input response. Thus (3-57) becomes:

$$LC\frac{d^2v_c}{dt^2} + RC\frac{dv_c}{dt} + v_c = I_d(0)R \qquad (3\text{-}62)$$

And the complete solution of $v_c$ is:

$$v_c(t) = \frac{I_d(0)R}{\sin q}e^{-t/T}\sin(w_f t - q) + I_d(0)R \qquad (3\text{-}63)$$

where the initial phase angle is:

$$q = \arctan\left(\frac{w_f RC}{1 - RC/T}\right) \qquad (3\text{-}64)$$

Under ideal oscillation conditions with an equivalent load resistor R=0, time constant T=∞, and initial phase angle θ=0, the resonant voltage can be expressed as:

$$v_c(t) = \frac{I_d(0)}{w_f C}\sin(w_f t) \qquad (3\text{-}65)$$



InductEV, Inc.
Exhibit 1020
Page 110

Comparing (3-65) with (3-61) it can be seen that under ideal zero damped conditions, the ramp up current injection and the step input current injection have quite different oscillation properties. The former oscillates above zero with a DC offset $V_d$, while the latter oscillates around zero, therefore zero voltage instants exist as required. For practical circuits with damping, zero crossing is conditional and proper design is necessary to ensure that ZVS exists at start-up.

### *3.4.3 Zero Voltage Crossing Conditions*

There are several factors that make the voltage difficult to go to zero. The first obvious factor is that the injection current is a step input plus a ramp up input rather than a pure step input. But if the initial current $I_{d(0)}$ is much larger than the current increase $\Delta I_d$ in the first half-switching cycle, then this effect will be very small.

Another factor which is worthy of special concern is the effect of load R. For a given system at a certain frequency, heavier load means smaller quality factor Q. From (3-59) it can be seen that in order to achieve zero voltage crossing, a minimum requirement is that the quality factor Q is larger than 0.5 (note that the condition for zero phase angle resonance is Q>1), otherwise the circuit is not oscillatory and ZVS is impossible. Furthermore, as shown in (3-63) and illustrated in Fig. 3-26, the complete voltage solution includes two parts: $v(c_1)$ and $v(c_2)$, even when Q>0.5, there is still a competition between the DC offset of the forced component and the decay in the natural component to determine whether the voltage can go to zero. Considering the complete voltage solution shown in (3-63), it can be found that the point corresponding to the minimum voltage occurs at:

$$w_f t_{\min} = \arctan(w t) + p + q \tag{3-66}$$

and the minimum voltage can be expressed as:

$$v_{c\min} = -I_d(0) R Q e^{-t_{\min}/T} + I_d(0) R \tag{3-67}$$

Thus in order to guarantee $v_{cmin}$ smaller than zero, the following condition should be met:

$$e^{-t_{\min}/T} > 1/Q \tag{3-68}$$



InductEV, Inc.
Exhibit 1020
Page 111

which means in order to achieve zero voltage crossing during start-up, the time constant T should be large enough to keep the percentage of the voltage decay smaller than 1-1/Q before reaching its minimum value.

Considering the relationship of $\omega_0 T=2Q$, and the fact that the minimum voltage time $t_{min}$ occurs approximately at $(3\pi/2)/\omega_f \approx (3\pi/2)/\omega_0$, then the condition shown in (68) can be rewritten as:

$$Q \ln Q > 3p/4 \tag{3-69}$$

It is easy to solve the above equation numerically and this results in the following requirement for Q:

$$Q > 2.54 \tag{3-70}$$

This is not a difficult condition to meet as normally Q is designed larger than 3 to keep the resonant current and frequency approximately constant as the load varies [3,10]. In applications of magnetically coupled load such as IPT, the resonant track current builds up very slowly at start-up so that the equivalent dynamic load of the pick-ups is very small. Therefore, ZVS start-up should not be a problem even under heavy loads.

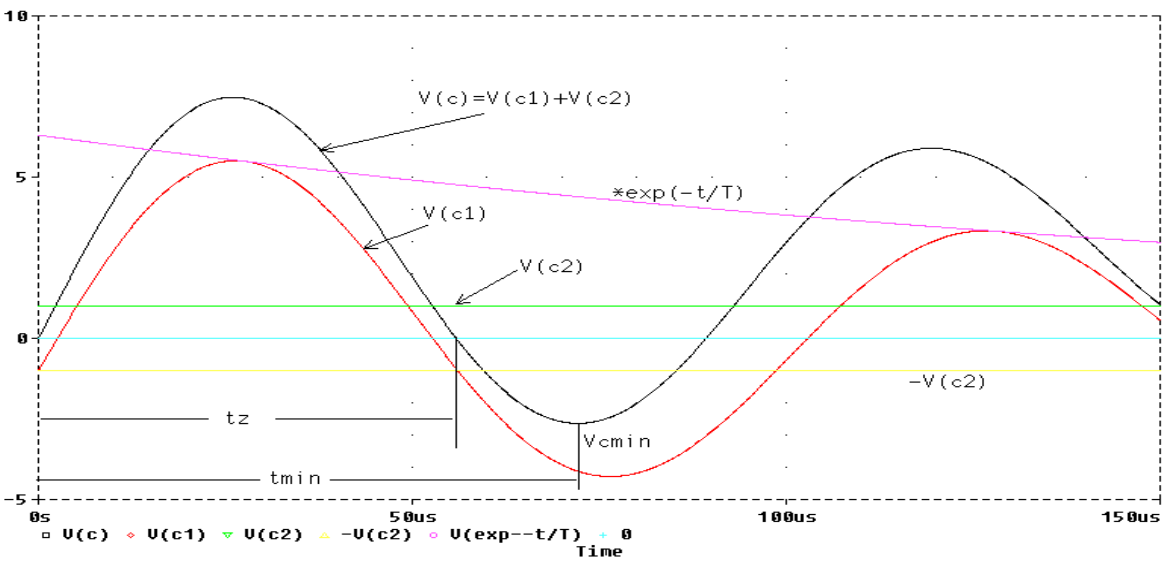


**Fig. 3-26: Zero voltage crossing analysis during start-up**

### *3.4.4 Simulation and Experimental Results*

Fig. 3-27 (a) shows a typical PSpice simulation result of a push pull converter with the data shown in table 3-2. First the DC supply $V_d$ is assumed to be a step input and the switches at both legs S1 and S2 are controlled to be on for a period of $t_1$=0.2ms (which is much larger than the half



InductEV, Inc.
Exhibit 1020
Page 112

switching period which is about 50us) to boost a DC initial current. S2 is then switched "off" with S1 still "on", the resonant voltage oscillates to zero and normal zero voltage detection control scheme can be employed. Fig. 3-27 (a) shows that ZVS is completely achieved but there are voltage and current over shoots.

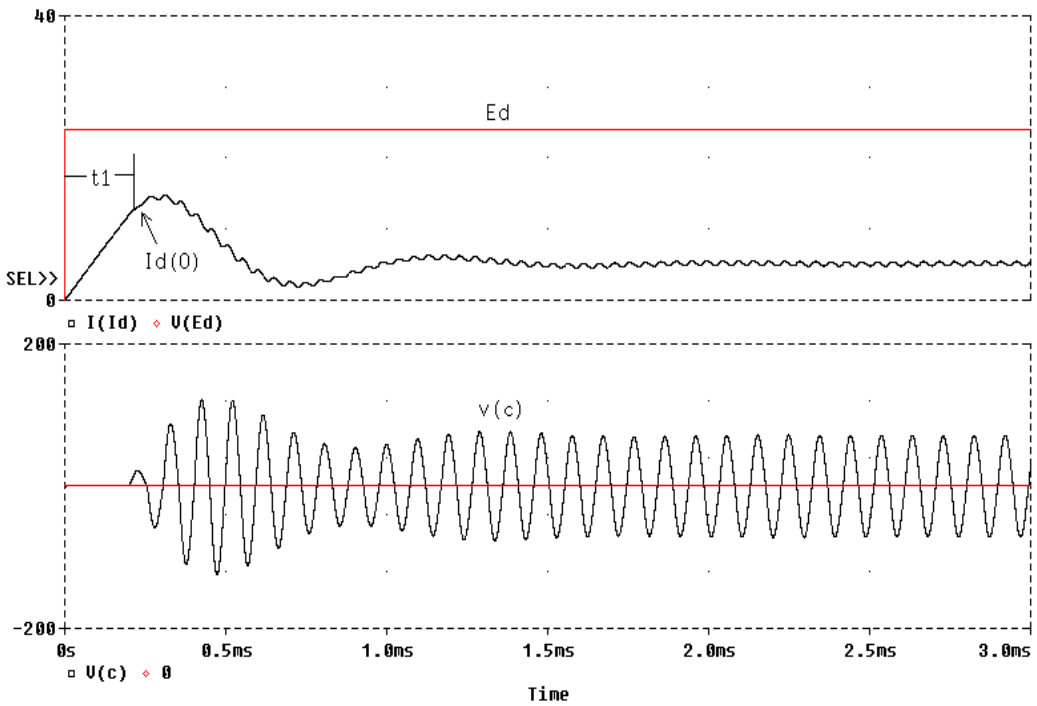


(a) Step input DC supply

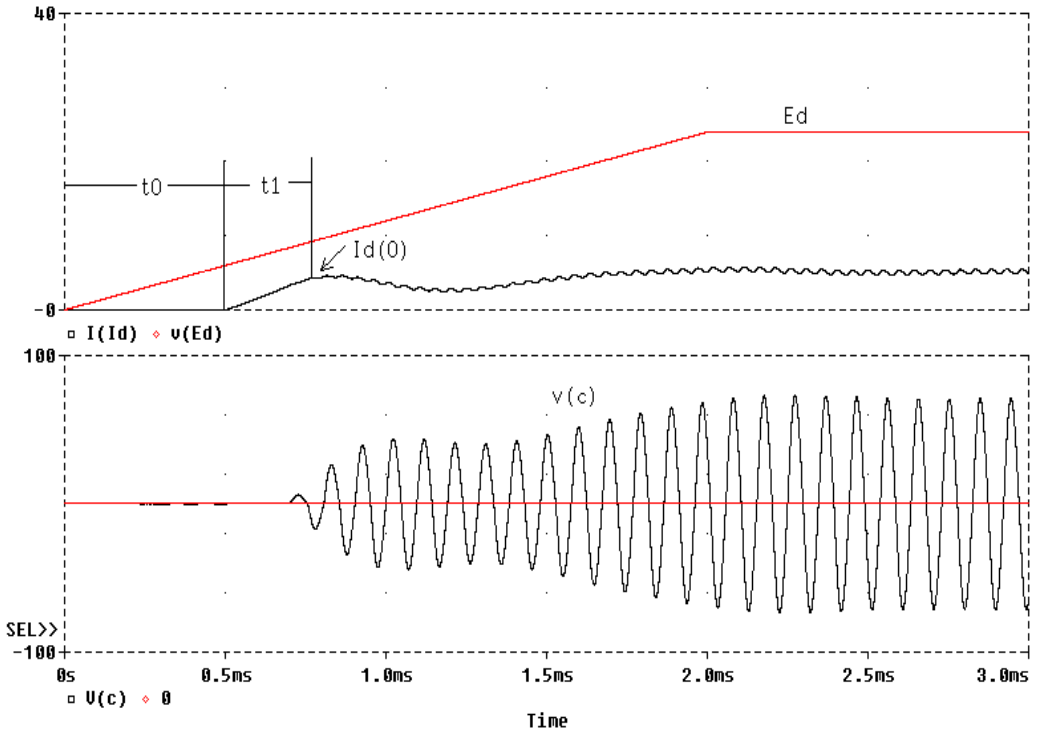


(b) Ramp DC supply

**Fig. 3-27: PSpice simulation results of ZVS start-up**



InductEV, Inc.
Exhibit 1020
Page 113

**Table 3-2: Converter data for the ZVS dynamic start-up**

| | | | |
|---|---|---|---|
| Inductor L | 50μH | DC power supply $V_d$ | 24V |
| Capacitor C | 4.5μF | Inverted AC voltage $V_c$ (rms) | 53V |
| DC inductor $L_d$ | 200μH | Undamped natural frequency $f_0$ | 10kHz |
| Phase-splitter inductance $L_{sp}$ | 1.9mH×2 | Load resistor R | 0.5Ω |
| Coupling factor k | 0.824 | Quality factor Q | 6.28 |

In many situations because of the main switch delay and/or capacitor charging process, at start-up the DC power supply is not a pure step input but ramps up slowly. Fig. 3-27 (b) shows a PSpice simulation result when the delay of $V_d$ is assumed to be 2ms. It can be seen that in this situation a delay $t_0$ can be used to time the starting point of $V_d$ before it goes to its maximum value, thus the start-up overshoot can be contained or eliminated.

Practical ramping times for $V_d$ can be very long. The measured delay of a normal manual switch is about 100ms to 150ms. Fig. 3-28 (a) shows typical experimental results of resonant voltage and DC current waveforms on start-up and at steady state. It can be seen that besides dynamic ZVS, complete overshoot free control has been achieved.

The controller design can be very simple. The major points to be concerned with are the firing point $t_0$ to set the starting $V_d$, and the pre-energising period $t_1$ to determine the initial DC current $I_{d(0)}$. None of these are critical because of the slow change of $V_d$. Normal timing control or comparative threshold control can be employed for the implementation.

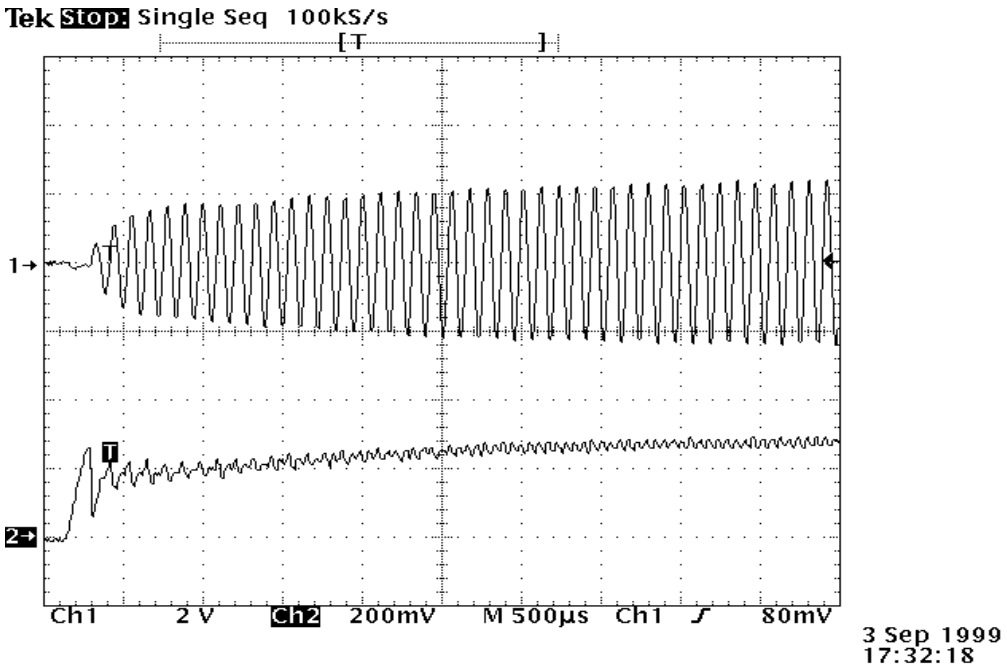


(a) Start up



InductEV, Inc.
Exhibit 1020
Page 114

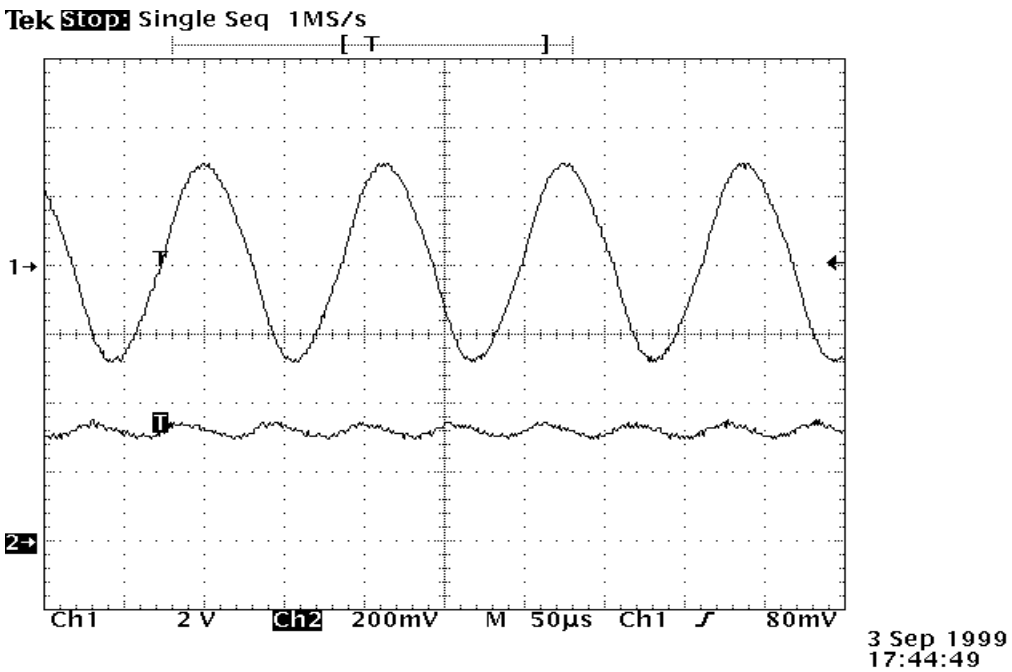


(b) Steady state

**Fig. 3-28: Experimental voltage and current waveforms**

## 3.5 Summary

In this chapter, the fundamental properties and performance improvements of basic current-fed parallel resonant converters for IPT power supplies have been investigated.

First, the full bridge and push pull topologies of the current-fed resonant converters have been discussed with the switching constraints of the switching devices stressed. It has been found that the leakage inductance of a phase-shift transformer can be used advantageously to partially or fully replace the DC inductor of a push pull current-fed converter. Transient and steady state DC and AC voltage balance relationships before and after the inverting networks have been developed to define the governing rules for current-fed resonant converters.

ZVS operation is a basic requirement as well as a control strategy for reliable and efficient operation of current-fed resonant converters. Various resonant frequencies available for a series loaded parallel resonant tank have been identified. Their resonant conditions and dependencies upon the circuit parameters characterised by quality factor Q and the undamped natural frequency are clarified. Based on a complete dynamic analysis of a step current injection model, a numerical computation algorithm has been developed for the ZVS frequency analysis of a current-fed resonant converter. It has been found that the ZVS frequency is the smallest frequency among all the resonant frequencies and it drops very fast at low Q's. Moreover, a minimum bound on Q that



InductEV, Inc.
Exhibit 1020
Page 115

ensures ZVS operation has been defined for both steady state (*Q>1.86*) and transient start-up (*Q>2.54*) process. The analysis has developed a new theoretical limit for the design of current-fed resonant converters used in IPT power supplies where quality factor Q is normally designed at a low value to reduce the system cost and size.

The frequency stability problem has been analysed in a closed form for a fully series tuned track and pick-up circuit. The maximum loading conditions as well as the zero phase angle frequency range are identified for both single and multiple pick-up systems. When the quality factors are high, the results can be extended to other tuning circuits, such as practical parallel-tuned track and pick-ups. Several frequency stability enhancing methods such as simply varying the system operating frequency have been proposed.

After analysing the start-up process of a resonant converter based on a ramp current model, a simple, low cost ZVS start-up method has been proposed and verified with both simulation and experimental results.

## 3.6 References

[1] Ramshaw, R.: *Power electronics semiconductor switches*, 2nd edition, Chapman & Hall, 1993.

[2] Hu, A.: "Theory and development of IPT power supplies", *Proceedings of the 5th Annual New Zealand Engineering and Technology Postgraduate Conference*, Palmerston North, New Zealand, pp.246-251, November 1998.

[3] Boys, J. T. and Green, A. W.: "Inductively coupled power transmission – concept, design and application", *IPENZ Transactions*, No.22, (1) EMCH, pp.1-9, 1995.

[4] Hasse, K. and Knaup, P.: "Zero voltage switching converter for magnetic transfer or energy to movable systems", *European Power Electronics Conference*, 1997.

[5] Hu, A., Boys, J. and Covic, G. A.: "Frequency analysis and computation of a current-fed resonant converter for IPT power supplies", *Proceedings of IEEE-PES/CSEE 2000 International conference on power system technology*, Perth, Australia, Vol. 1, pp327-332, December 2000.

[6] Boys, J. T., Hu, A. P., and Covic,G. A.: "Critical Q analysis of a current-fed resonant converter for ICPT applications", *IEE Electronics Letters*, Vol.36, No.17, pp.1440-1442, August 2000.



InductEV, Inc.
Exhibit 1020
Page 116

[7] Boys, J. T., Covic, G. A. and Green, A. W.: "Stability and control of inductively coupled power transfer systems," *IEE Proceedings of Electric Power Applications*, Vol. 147, No.1, pp.37-43, January 2000.

[8] D'Azzo, J. J. and Houpis, C. H.: *Linear control system analysis and design: conventional and modern*, McGraw-Hill, 4th edition, New York, 1995.

[9] Glendinning, P.: *Stability, instability, and chaos: an introduction to the theory of nonlinear differential equations*, Cambridge University Press, 1994.

[10] Green, A. W. and Boys, J. T.: "10kHz Inductively coupled power transfer – concept and control", *IEE Power Electronics and Variable Speed Drives Conference*, PEVD, Pub.399, pp.694-699, 1994.

[11] Hu, A., Boys, J. and Covic, G.: "Dynamic ZVS direct on-line start up of current-fed resonant converter using initially forced DC current", *Proceedings of 2000 IEEE International Industrial Symposium on Industrial Electronics*, Vol. 1, pp.312-317, Puebla, Mexico, December 2000.



InductEV, Inc.
Exhibit 1020
Page 117

## Chapter 4

# Improved Current-fed CLC Parallel-Series Resonant Converter Power Supplies

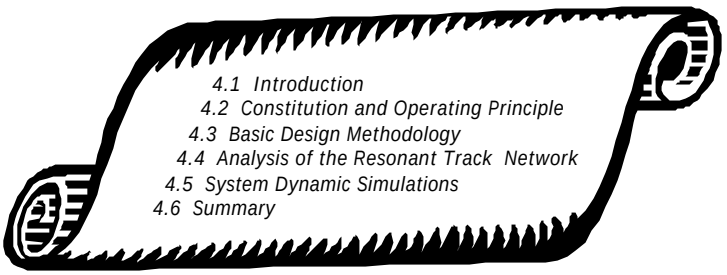


## 4.1 Introduction

IPT power supplies based on current-fed parallel resonant converters as discussed in the previous chapter have been developed and were the first of such devices to be placed in industrial applications. As such these converters were labelled as generation one (G1) power supplies at the University of Auckland. Voltage-fed series quasi-resonant converters were later used in IPT power supplies because of their ability to drive long tracks. As such these power supplies have been termed generation two (G2) power supplies and will be discussed in detail in the next chapter.

The G1 supply is based on a parallel resonant converter that provides a voltage controlled current source for the track. It is called a voltage controlled current source because the magnitude of the current injected into the resonant tank is actually dependent on the input DC voltage for a given load. The main advantages of the G1 supply are: 1) the track current is a good sine wave so that the harmonics and radiated EMI are low; 2) both the conduction and switching losses are low because only the load current goes through the main switches and ZVS implementation is relatively easy to achieve so that the power efficiency is high; 3) it has a good turn down ratio for the DC input voltage as this voltage can vary over a large range enabling easy control over the track current magnitude without losing ZVS operation.



InductEV, Inc.
Exhibit 1020
Page 118

However, the disadvantages of the G1 supply include: 1) the track length is limited by the available voltage, typically 100m with available semiconductor voltage ratings; 2) the track current varies with the load; 3) the operating frequency varies with the load, and detuning problems may occur at heavy loads where the frequency may be unstable; 3) to keep variations in the track current and the frequency small, the track quality factor Q has to be high so that the maximum power transfer ability is limited by the installed VA capacity of the reactive components.

This chapter proposes a new IPT power supply, namely the generation three (G3) power supply, which can overcome the above disadvantages and improve the system performance significantly. It is based on a current-fed parallel-series resonant converter with an additional trans-conductance CLC π network introduced at the output of the supply feeding the track loop and load.

## 4.2 Constitution and Operating Principles

### *4.2.1 Basic Structure of the Proposed Power Supply*

A schematic diagram of the proposed G3 power supply is shown in Fig. 4-1. Similar to a G1 supply, the inverting network of a G3 supply can be a full-bridge topology or a push-pull topology. Fig. 4-1 shows a push-pull configuration. The converter comprises a DC input supply $V_d$, a DC chopper including S3 and D3, a DC inductor $L_d$, a phase splitting transformer $L_{sp}$, two IGBT switches S1 and S2, a bias network with $L_b$ and $C_b$ in parallel, two short-circuit protection blocking diodes D1 and D2, two over voltage protection diodes D4 and D5 that are connected to a DC voltage source $V_c$, a trans-conductance CLC π network consisting of $C_p$, $L_{s1}$ and $C_{p1}$, and a series resonant track including the track inductor $L_s$, its tuning capacitor $C_s$ and equivalent resistor R with the track resistor $R_s$ and the equivalent load resistor $R_L$ together.

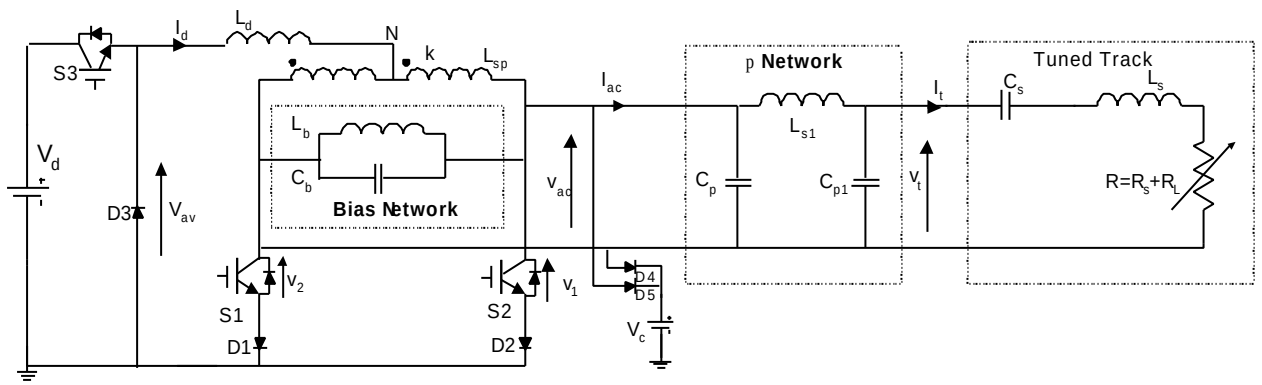


**Fig. 4-1: Proposed CLC parallel-series resonant converter**



InductEV, Inc.
Exhibit 1020
Page 119

In essence the circuit is very similar to a G1 supply but with an added CLC network between the converter and the (series) tuned track. The properties of this network make a significant change to the characteristics of the power supply. The CLC network has some resonant current and there is an extra tuned circuit (called a bias network) added as shown to provide extra VArs thereby improving the ZVS characteristics of the converter.

The DC power supply shown in the diagram can be obtained directly from a three phase AC mains supply after a full bridge rectifier and an LC filter. The DC chopper acts as a "buck" converter to control the voltage-fed parallel resonant circuit. The DC inductor keeps the DC current constant. The phase splitting transformer divides the DC current into two branches, and the two main switches alternate the direction of the charging current into the resonant circuit. The bias network increase the reactive circulating energy in the network and helps to hold the resonant frequency approximately constant; it also improves the waveform of the oscillating voltage and current. The track inductor $L_s$ is completely tuned by the series capacitor $C_s$. The CLC $\pi$ network plays the most important role in the system: it transforms the low input impedance of the track to a high impedance suitable for being driven by a voltage source converter at unity power factor. It transforms the voltage source $v_{ac}$ into the current source $\dot{I}$, and it also works as a band filter to absorb the harmonics and make the track current waveform almost a pure sine wave. The blocking diodes D1 and D2 are used to prevent momentary short-circuiting of the parallel capacitors, and clamping diodes D4 and D5 can offer a very effective way of over-voltage protection across the main switching devices.

In brief, the circuit works in such a way that by controlling the input DC voltage the track current is controlled, and the $\pi$ network does the necessary impedance and voltage to current transformations and filters the harmonics produced by the resonant converter. The CLC $\pi$ network also supplies the basis of ZVS for S1 and S2 by acting as a source of resonant VAr capacity for the whole system.

Overall, there are basically five sub-systems in a G3 power supply:

***The DC power supply.*** The DC chopper is used to reduce the input DC voltage, which is normally derived from rectification of a 3-phase mains supply, to a controlled DC voltage to feed the main resonant converter. As discussed before, the resonant output voltage and therefore the track current is proportional to the DC input voltage provided that ZVS is maintained. Therefore, accurate control of the chopper is essential to keep the resonant voltage and the track current constant against mains supply variations and other disturbances.



InductEV, Inc.
Exhibit 1020
Page 120

***The resonant converter/inverter network***. The resonant converter network takes controlled DC voltage from the DC chopper and converts it to a required resonant voltage. The converter has a high impedance (current source) at the resonant frequency since the track network is fully tuned and any current changes must come through the DC inductor. As the output voltage varies, the current in the DC inductor varies producing a voltage controlled current source characteristic for the inverter. Apart from the necessary short circuit and over voltage protection, the only control strategy possible is to vary the switching instants. Similar to a G1 power supply, there are two options to control the system to reach a ZVS operation: either switching at a variable frequency allowing for the load and parameter variations, or switching at a constant frequency provided the circuit parameters are dynamically tuned to maintain a constant ZVS frequency.

***The CLC*** $p$ ***network***. As discussed, this network performs all the impedance transformations while not affecting the ZVS frequency or track tuning. The properties of the $\pi$ network needed in this application are analysed in detail in the next section of this chapter.

***The bias network***. The bias network is relatively independent. It basically has two functions: the first function is to increase the total reactive circulating power rating compared with the real power, so that the dynamic effects of the load change or other parameter drifts within the system can be reduced; the second function is to filter the harmonic distortions so that the waveforms of the resonant voltage and current are improved. In general, the bias network keeps the system running at the tuned frequency but may cause a slower dynamic system response. In fact a G3 supply can run without a bias network, but having a bias factor* of 0.5 to 1 helps to improve the system resonant performance and stability.

***The tuned track***. The track inductor $L_s$ is fully tuned with series capacitor $C_s$, so that the track length can be extended with an available resonant AC voltage.

### *4.2.2 Significant Property Improvements*

A track circuit with a $\pi$ network connected to a series tuned track of a current-fed G3 power supply is shown in Fig. 4-2. By doing three things at the same time, the CLC $\pi$ network improves the network properties significantly. It compensates the network, undertakes a conversion from a

* The bias factor is defined as the ratio between the bias network current and the track current. A larger bias factor means a larger VA rating of the bias network.



InductEV, Inc.
Exhibit 1020
Page 121

voltage source to a current source, as well as functions as a band-pass filter. Consequently, it leads to the following features that are ideal for IPT track power supplies: a unity power factor, a constant track current independent of load, and low distortion in the track current. These features are determined analytically below.

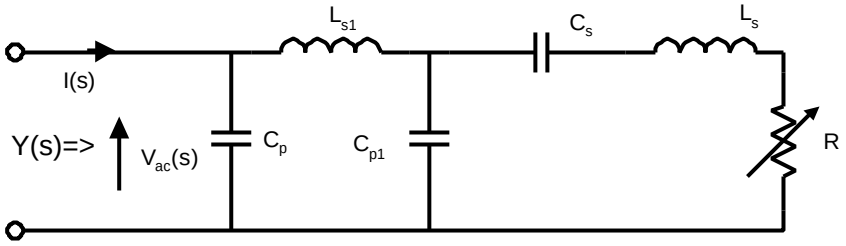


**Fig. 4-2: Current-fed G3 Track Network**

**Unity Power Factor Input**

The input admittance of the network shown in Fig. 4-2 can be written in Laplace form as:

$$Y(s) = \frac{s^3 L_s C_s C_{p1} + s^2 C_s C_{p1} R + s(C_s + C_{p1})}{s^4 L_s C_s L_{s1} C_{p1} + s^3 C_s L_{s1} C_{p1} R + s^2 (L_s C_s + L_{s1} C_s + L_{s1} C_{p1}) + s C_s R + 1} + s C_p \qquad (4\text{-}1)$$

If the track system is completely tuned, ie., $C_s=1/(\omega_0^2 L_s)$, $C_{p1}=C_p=1/(\omega_0^2 L_{s1})$, then equation (4-1) becomes:

$$Y(s) = \frac{s[s^4 L_s + s^3 R + s^2 w_0^{\,2}(3L_s + L_{s1}) + 2s w_0^{\,2} R + w_0^{\,4}(2L_s + L_{s1})]}{w_0 L_{s1}[s^4 Ls + s^3 R + s^2 w_0^{\,2}(2L_s + L_{s1}) + s w_0^{\,2} R + w_0^{\,4} L_s]} \qquad (4\text{-}2)$$

At the nominal frequency $\omega_0$, the input admittance is:

$$Y(jw_0) = RC_{p1}/L_{s1} = R/z_0^{\,2} = R/(w_0 L_{s1})^2 = R/X_{Ls1}^{\,2} \qquad (4\text{-}3)$$

where $z_0 = \sqrt{L_{s1}/C_{p1}} = w_0 L_{s1} = X_{Ls1}$ is the characteristic impedance of the π network.

The magnitude and phase frequency response of the admittance expressed in equation (4-2) is shown in Fig. 4-3. This diagram and equation (4-3) show that at the nominal frequency $\omega_0$ the admittance is purely real at any load resistance. This means that the network has a unity power factor input characteristic provided the system is fully tuned. As such the input current is always in phase with the input voltage (provided they are pure sine waves) as required for ZVS of current-fed resonant converters. This property can also be obtained by undertaking an AC circuit equivalent



InductEV, Inc.
Exhibit 1020
Page 122

circuit transformation. Fig. 4-4 clearly shows that the π network presents a purely resistive load to the driving source in the steady state.

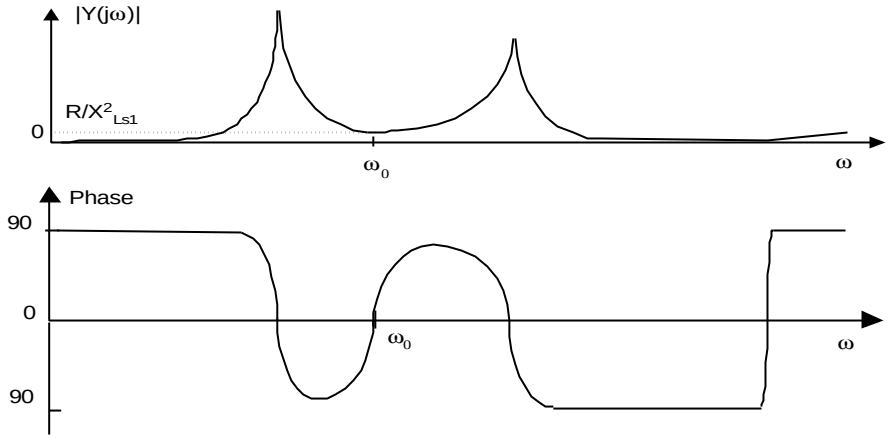


**Fig. 4-3: Frequency response of the input admittance**

For an IPT system, the characteristic impedance of the π network is normally designed to be much larger than the equivalent load resistance. Therefore, the π network performs an impedance transformation such that low impedance loads on the output appear as a high impedance at the input.

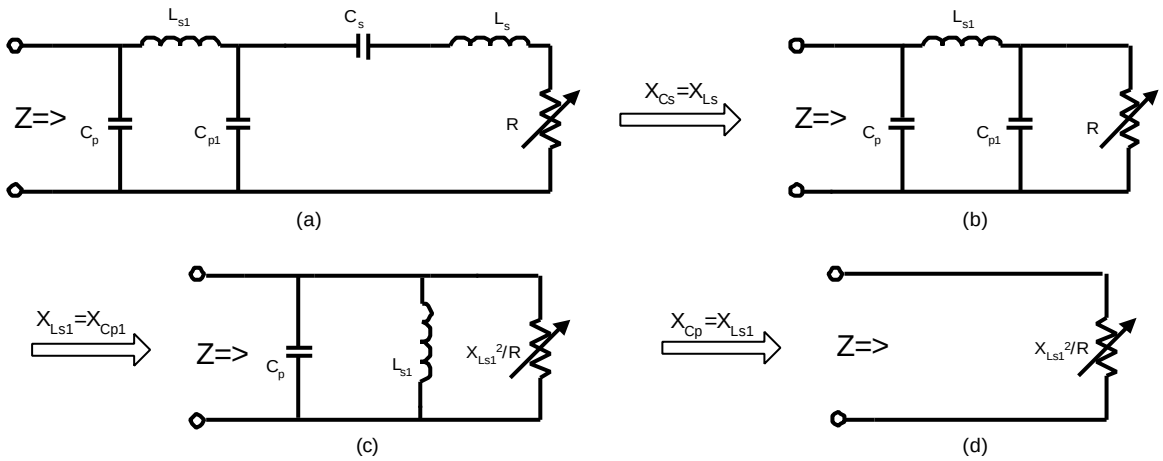


**Fig. 4-4: Unity power factor input transformation**

### Constant Track Current Output

The general form of the transfer function from the input voltage to the output track current (the trans-admittance) can be derived from the track network (Fig. 4-2) and reduced to:

$$G(s)=\frac{I_t(s)}{V_{ac}(s)}=\frac{sC_s}{s^4L_sC_sL_{s1}C_{p1}+s^3L_sL_{s1}C_{p1}R+s^2(L_sC_s+L_{s1}C_s+L_{s1}C_{p1})+sC_sR+1} \qquad (4\text{-}4)$$



InductEV, Inc.
Exhibit 1020
Page 123

For a completely tuned system [$C_s=1/(\omega_0^2 L_s)$, $C_{p1}=C_p=1/(\omega_0^2 L_{s1})$], equation (4-4) can be simplified to:

$$G(s)=\frac{sw_0^{\ 2}L_{s1}}{s^4L_sL_{s1}+s^3L_{s1}R+s^2w_0^{\ 2}L_{s1}(2L_s+L_{s1})+sw_0^{\ 2}L_{s1}R+w_0^{\ 4}L_sL_{s1}} \qquad (4\text{-}5)$$

At the nominal frequency $\omega_0$ the transfer function becomes:

$$G(jw_0)=I_t(jw_0)/V(jw_0)=1/(jX_{LS1}) \qquad (4\text{-}6)$$

For a given sine wave input $V_{ac}$ at $\omega_0$, this means that in the steady state the track current can be expressed as:

$$I_t=V_{ac}/(jX_{LS1}) \qquad (4\text{-}7)$$

This current is independent of the track impedance including the load resistor R. It is always 90 degrees lagging the input voltage, and its value is completely controlled by the input voltage magnitude in conjunction with the characteristic impedance of the π network. For a constant input voltage, the output current is constant. This transformation can be seen clearly in Fig. 4-5 by undertaking a circuit transformation from the source side. As noted, *the track current is independent of the track impedance and is constant for a constant input voltage.* This is a significant feature of G3 power supplies.

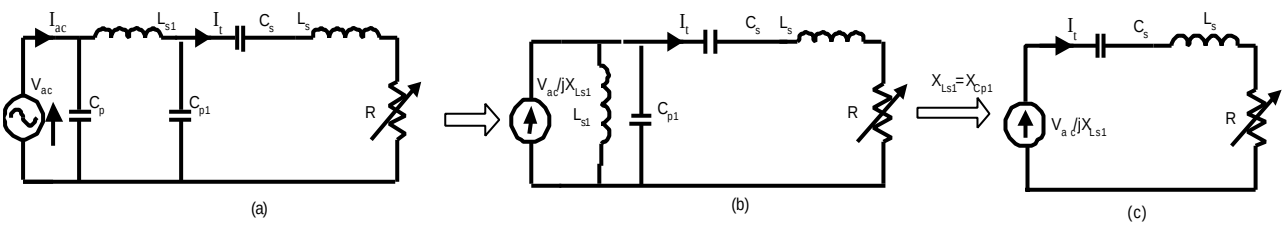


**Fig. 4-5: Constant track current transformation**

p **Network Filtering between the Input and Output**

A typical magnitude and phase frequency response of the trans-admittance transfer function expressed in equation (4-4) is shown in Fig. 4-6. It can be seen that there is a flat area for the trans-conductance G (ω) around $\omega_0$ and its magnitude at both very high and very low frequencies is small. This result is very significant. It shows that the trans-admittance is highly stable for small variations in frequency around $\omega_0$, so that the tolerance on the π network components is acceptable and small variations will not cause excess sensitivity in the track current. In addition, the network



InductEV, Inc.
Exhibit 1020
Page 124

only works over a finite bandwidth, so that harmonics will not propagate; in other words, the π network is a very effective band-pass filter.

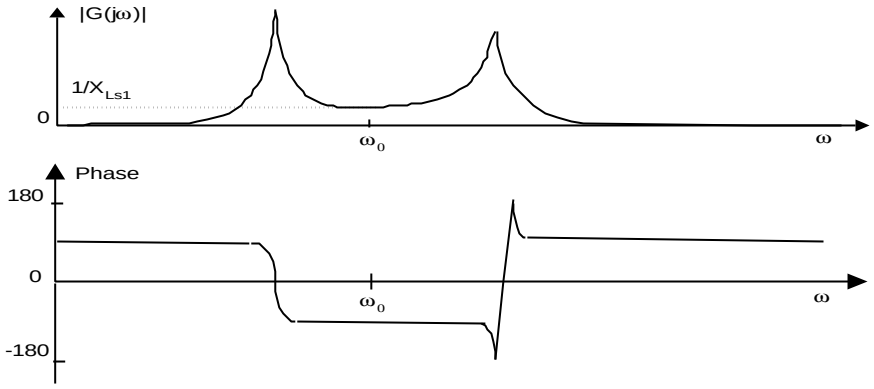


**Fig. 4-6: The frequency response of the trans-conductance $G(jw)=I_t(jw)/V_{ac}(jw)$**

In addition to the above improvements, the G3 power supply has enhanced frequency stability due to its increased VArs in the track network. For a practical G1 power supply used in a typical monorail overhead IPT trolley with a track current of 80A/15kHz, Boys and Green found that the maximum number of the power pick-ups that the system can drive is 7, which can be approximately determined by the total VA balance between the primary track and secondary pick-up circuits [1]. If the pick-up number is larger than 7, say 8 as the case shown in Fig. 4-7(a), the track circuit will have less VA than the pick-ups so that the system will have multiple zero phase crossings and the actual operating frequency can be significantly higher or lower than the nominal frequency (which is 10kHz in this case). The resultant frequency shift causes slight track current variation in magnitude as shown in Fig. 4-7, but more importantly, it detunes the power pick-up circuits causing significant reduction in power transfer capability. Compared to the G1 supply, the π network of the G3 supply can supply extra VArs so that the total VA rating of the track network increases and consequently the G3 supply can drive more power pick-ups. Fig. 4-7(a) shows that when the pick-up number is 8, the G1 supply has obvious multiple zero phase angle crossings and the frequency shift can be large. However, there exists only one zero phase angle crossing for the G3 supply around the nominal frequency and the frequency shift is much smaller. Fig. 4-6 (b) shows that possible zero phase angle frequency change for both the supplies increases with the number of the pick-ups but multiple zero phase angle crossings of the G3 supply only appear when the pick-up number is increased over 20. This number is more than double that of the G1 supply because the VA rating of the G3 is increased by more than 100% because of the contribution of the π network.

In essence, instability or bifurcation in the G1 supply occurs as the power supply cannot supply VArs switching as it does on zero voltage crossings. The G3 supply has extra VArs so it can drive



InductEV, Inc.
Exhibit 1020
Page 125

more pick-up loads corresponding to not only more output power but also more VArs. If blocking diodes are used in series with the main switching devices (as discussed in section 3.1.1), both the power supplies will be able to run at a non zero phase crossing so that VArs can also be supplied at the input of the track network. However, in these conditions the devices will be switching an increased current.

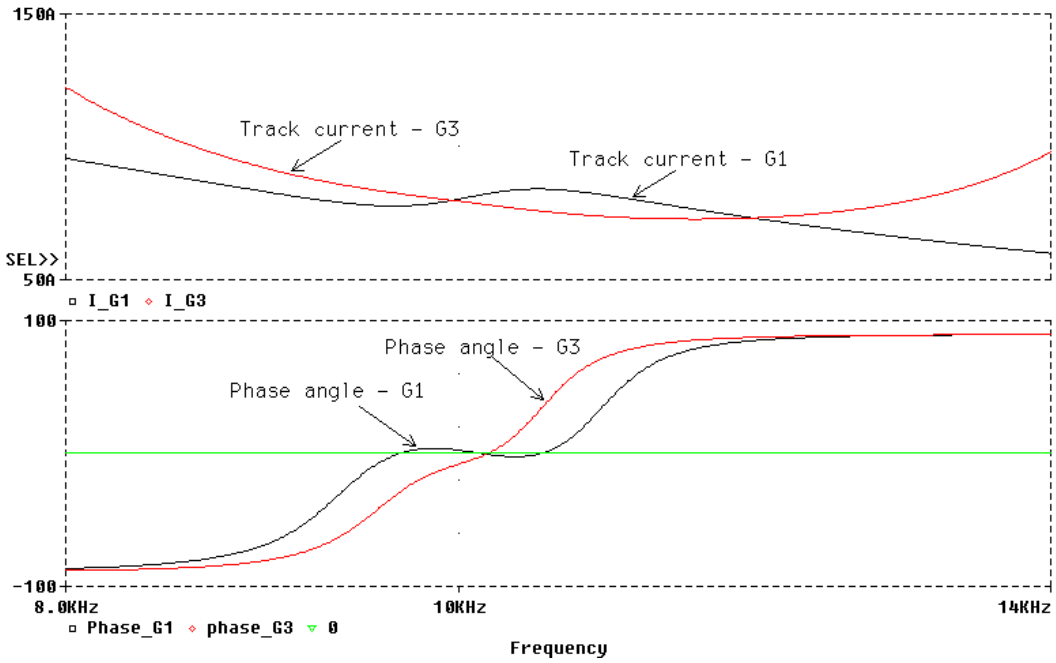


pick-up number N=8

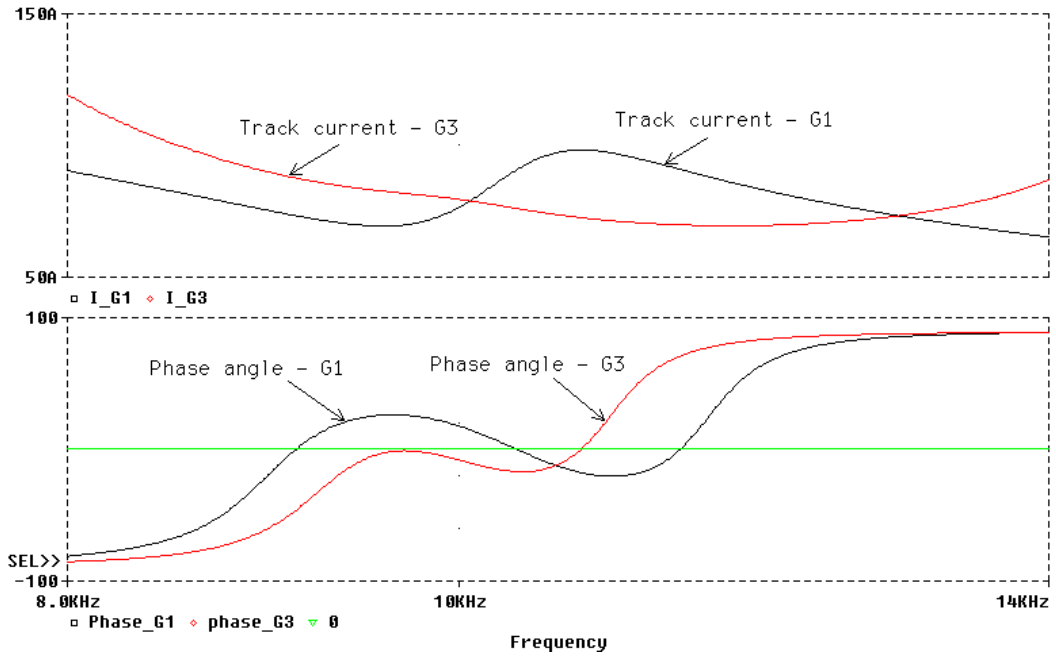


pick-up number N=20

**Fig. 4-7: Improved frequency stability of the G3 supply**



InductEV, Inc.
Exhibit 1020
Page 126

## 4.3 G3 Power Supply Design Methodology

### *4.3.1 Design Concepts and Practical Considerations*

The proposed G3 power supplies must operate within the limits of the components and the availability of the power sources. For example, typically semiconductor switches with peak voltages less than 1700V, a three phase 400V 50/60Hz utility supply with a 10% variation, a known track current requirement and power level have to be considered. For a push pull current-fed converter power supply, to produce 200 kW with a track current of 250A at 15kHz, a typical specification may be:

| | |
|---|---|
| Input DC voltage: | 600V max |
| Average DC chopper output: | 450V |
| Nominal resonant voltage: | 1000V rms, 1414V peak |
| Track current: | 250A |
| Bias current: | 125A |
| Maximum track power: | 200kW |
| $\pi$ network impedance: | 4Ω [1000V/250A] |

The duty cycle of the DC chopper is controlled to keep the average DC input voltage constant (450V) against AC mains variation. As discussed before, the resonant AC voltage out of a push-pull inverter is essentially controlled by the average output of the DC chopper with a proportion of $\pi/\sqrt{2}$ provided ZVS is achieved. Therefore, its rms value is approximately constant at 1000V with a peak value of 1414V, so that 1700V switching devices can be used. The $\pi$ network transforms this voltage source into a constant track current of 250A by a division of track impedance of 4Ω. Thus in a real system design with a given track current requirement, a resonant voltage is controlled within the maximum limit of the switching devices using a DC chopper, and the impedance of the $\pi$ network is determined accordingly.

At a given frequency, for example, 15kHz, the series capacitor $C_s$ is used to tune the equivalent track inductor completely, the capacitor $C_{p1}$ in the $\pi$ network is tuned with the inductor $L_{s1}$ for constant current transformation, and the capacitor $C_p$ in the $\pi$ network is also tuned with the inductor $L_{s1}$ for ZVS purposes. Therefore, it can be seen that these three capacitors are not independent design variables. They are used to tune the inductors.



InductEV, Inc.
Exhibit 1020
Page 127

Unlike a G1 power supply, because a high track current can be obtained by designing a smaller π network impedance, a high resonant voltage is no longer a top priority to drive a long track. Therefore, a full bridge topology converter which provides a lower resonant voltage can be used. In fact, because the semiconductor switches can become both cheaper and smaller than the reactive components such as a phase splitting transformer at the same power level, the full bridge option may be preferable. This is especially true for high power applications where the isolated gate drive required for a full bridge topology accounts for only a very small portion of the whole system cost.

In the above situation, if a full-bridge topology converter is used, lower rated voltage switching devices (eg. 1200V) can be used. An average DC voltage of 540V is normally obtained from a 400V mains power supply, which gives a resonant voltage of 600V rms without using a DC chopper, or 848.2V peak which is lower than 1kV even if a variation of 10% is taken into account. On the other hand, because the nominal resonant voltage is reduced from 1kV rms to 600V rms after using a full-bridge topology, the characteristic impedance of the π network should be reduced proportionally form 4Ω to 2.4Ω so as to produce the required track current of 250A rms.

The resonant bias network (comprising an inductor and a capacitor in parallel) is relatively independent of other components. To reduce the size and cost, the power supply may be designed without using a bias network. However, as noted having a bias current in the order of half the track current, helps to stabilise the resonant frequency and improves the voltage and current waveforms.

### *4.3.2 Basic Design Procedure and Equations*

**Determination of the resonant voltage**

For a full bridge topology, the resonant AC driving voltage in rms is:

$$V_{ac} = \frac{pV_d}{2\sqrt{2}} \tag{4-8}$$

where $V_d$ is the average DC voltage applied to the inverting network. As discussed, a push-pull topology doubles the output resonant voltage. A DC chopper can be employed to maintain the input DC voltage, and therefore the output resonant voltage, constant. The minimum duty cycle of the DC chopper is the ratio between the average DC voltage required by the inverter and the maximum voltage of the DC power supply.



InductEV, Inc.
Exhibit 1020
Page 128

**Tuning the track with a series capacitor**

At the nominal frequency $\omega_0=2\pi f_0$, the equivalent series track tuning capacitor as shown in Fig. 4-1 can be determined from:

$$C_s = 1/(w_0^{\ 2} L_s) \tag{4-9}$$

The total track reactance $X_{Ls}$ and susceptance $X_{cs}$, when fully tuned, are equal:

$$X_{Ls} = X_{Cs} = w_0 L_s \tag{4-10}$$

and the voltages across them are:

$$V_{Ls} = V_{Cs} = X_{Ls} I_t \tag{4-11}$$

**The design of the p network**

With a given AC input voltage and track current, the impedance of each component of the π network (see Fig. 4-1) should be equal:

$$X_{Cp} = X_{Cp1} = X_{Ls1} = V_{ac} / I_t \tag{4-12}$$

Therefore, the inductance and capacitance of the π network should be:

$$L_{Ls1} = X_{Ls1} / w_0 \tag{4-13}$$

$$C_{p1} = C_p = 1/(w_0^{\ 2} L_{s1}) \tag{4-14}$$

The voltage across the tuning capacitor $C_p$ is the AC voltage $V_{ac}$ out of the inverting network, and its current is equal to the track current $I_t$. But the voltage and current for $C_{p1}$ vary with the track loading condition and are equal to $I_tR$ and $I_tR/X_{cp1}$ respectively with a fully series-tuned track.

The voltage and current of the π network inductor $L_{s1}$ also varies with the track impedance, and their magnitudes can be much larger than the rated AC voltage ($V_{ac}$) and the track current ($I_t$) at heavy loading conditions. They can be expressed as:

$$V_{Ls1} = \sqrt{V_{ac}^{\ 2} + V_t^{\ 2}} = V_{ac}\sqrt{1 + (R/X_{Ls1})^2} \tag{4-15}$$

$$I_{Ls1} = \sqrt{I_t^{\ 2} + I_{cp1}^{\ 2}} = I_t\sqrt{1 + (R/X_{Cp1})^2} \tag{4-16}$$



InductEV, Inc.
Exhibit 1020
Page 129

**Determination of the Bias $C_b$ and $L_b$**

The bias circuit (as shown in Fig. 4-1) affects the system dynamic properties and can be designed with a predetermined bias factor n. With this factor known, the bias current flowing through $L_b$ and $C_b$ can be calculated directly from the track current:

$$I_{Lb} = I_{Cb} = I_t \times n \tag{4-17}$$

Then the inductance and capacitance of the bias network can be designed as:

$$L_b = I_{Ls1} / n \qquad C_b = C_p \times n \tag{4-18}$$

**Calculation of the equivalent load resistance and DC current**

The maximum equivalent load resistance referred from the pick-ups is:

$$R_L = P_0 / h_p / I_t^{\ 2} \tag{4-19}$$

where $P_0$ is the pick-up power, and $\eta_p$ is the efficiency of the pick-ups. The total track resistance is:

$$R = R_L + R_s \tag{4-20}$$

where $R_s$ is the equivalent series resistance of the track loop.

The total maximum track power is therefore:

$$P_t = I_t^{\ 2} R \tag{4-21}$$

If all other losses within the inverter are ignored, the DC current at full load is:

$$I_d = P_t / V_d \tag{4-22}$$

This DC current flows through the DC chopper and the DC inductor and is then switched at 50% duty cycle via the main power-switches. A larger DC inductance $L_d$ helps to keep the DC current smooth so that the current injection into the resonant tank resembles a square wave. However, if $L_d$ is large, the system transient response will be slower and the stored energy in the inductor may cause high voltage surges to the switching devices.

Applying the above procedure and equations, a current-fed full-bridge G3 power supply rated at 250A/200kW has been designed. The system was designed for use in an IPT powered electric train



InductEV, Inc.
Exhibit 1020
Page 130

application as described in Chapter 1 of this thesis (see Fig. 1-3b). The system data is given in Appendix B.

## 4.4 Analysis of the Resonant Track Network

### *4.4.1 Poles and Zeroes of the Admittance Transfer Function*

For a completely tuned track network, the admittance transfer function (equation 4-2) at the input can be expressed in normalised form using $s_0=s/\omega_0$ as a substitution for s:

$$Y(s_0)=\frac{s_0[s_0^{\ 4}+s_0^{\ 3}\frac{1}{Q}+s_0^{\ 2}(k+3)+s_0\frac{2}{Q}+(k+2)]}{w_0L_{s1}[s_0^{\ 4}+s_0^{\ 3}\frac{1}{Q}+s_0^{\ 2}(k+2)+s_0\frac{1}{Q}+1]} \qquad (4\text{-}23)$$

Here $Q=\omega_0L_s/R=1/(\omega_0C_sR)$, and coefficient $k=L_{s1}/L_s=C_s/C_{p1}$.

At the nominal frequency $\omega_0$, the above equation gives $Y|_{s=j\omega 0}=Y|_{s0=j}=R/(\omega_0L_{s1})^2$, meaning that the voltage and current are in phase at steady state provided they are pure sine waves. However, the dynamic response of the system is much more complex and its performance is closely related to the locations of the poles and zeroes of the transfer function.

It should be noted that the transfer function showing the relationship between the input current and voltage of the track resonant network can be expressed in either admittance or impedance form. Here an admittance form is used implying that the voltage is assumed to be the input and the current the output. Conversely, if the current is considered as the input and the voltage the output, then an impedance transfer function should be employed. The difference is that if an impedance transfer function is used, the zeroes and poles will be swapped and the system order (the number of poles) will increase from 4 to 5. This is because the capacitor $C_p$ is in parallel with the voltage source causing a decrease of the system order by one. In fact, the output of the switching network of a current-fed converter is neither a current source nor a voltage source. However, as analysed before if ZVS is achieved, the output of the switching network is nearly a sine wave voltage source whose magnitude is only determined by the DC power supply under steady state conditions. In this sense, using an admittance transfer function is more appropriate in a track network analysis.

If it is assumed that $Q=\omega_0L_s/R=\infty$, ie, the system has no load and there is no track loss, then the item 1/Q in equation (4-23) becomes zero, and the poles and zeroes can be solved respectively from:



InductEV, Inc.
Exhibit 1020
Page 131

$$s_0^{\ 4} + s_0^{\ 2}(k+2) + 1 = 0 \tag{4-24}$$

$$s_0[s_0^{\ 4} + s_0^{\ 2}(k+3) + (k+2)] = 0 \tag{4-25}$$

The resultant four poles are all on the imaginary axis:

$$s_0 = \pm j \qquad \text{and} \quad s_0 = \pm j\frac{\sqrt{k+4}-\sqrt{k}}{2} \tag{4-26}$$

One zero is obviously $s_0$=0, and the other four zeroes are also on the imaginary axis:

$$s_0 = \pm j \qquad \text{and} \qquad s_0 = \pm j\sqrt{k+2} \tag{4-27}$$

For practical Q's, it is more difficult to solve these equations. To get the poles, the denominator of the transfer function expressed in equation (4-23) can be rewritten as:

$$(s^2 + s_0\tfrac{1}{2Q} + 1)^2 - (\tfrac{1}{4Q^2} - k)s_0^{\ 2} = 0 \tag{4-28}$$

The four resulting poles can be obtained in the following form:

$$s_0 = \frac{-\left(\frac{1}{2Q} \pm \sqrt{\frac{1}{4Q^2} - k}\right) \pm \sqrt{\frac{1}{2Q^2} + \frac{1}{Q}\sqrt{\frac{1}{4Q^2} - k} - (k+4)}}{2} \tag{4-29}$$

Except for $s_0$=0, the other four zeroes are very difficult to solve in a closed form. Nevertheless, numerical solutions are easy to obtain provided the circuit parameters Q and k are known.

For a practical IPT track power supply with a 400m long track and 16 pick-ups as specified in Appendix B, the coefficient $k=L_{s1}/L_s$=25.456mH/620mH=0.041. The loads are modelled as pure resistors to simplify the track network analysis. At no load, the track equivalent resistor $R_s$ is 0.3Ω, so that $Q=X_{Ls}/R_s$=58.434/0.3=194.78, and the normalised transfer function equation can be obtained as:

$$Y(s_0) = \frac{s_0(s_0^{\ 4} + 0.005134s_0^{\ 3} + 3.041s_0^{\ 2} + 0.010268s_0 + 2.041)}{2.4(s_0^{\ 4} + 0.005134s_0^{\ 3} + 2.041s_0^{\ 2} + 0.005134s_0 + 1)} \tag{4-30}$$

At full load, $Q=X_{Ls}/(R_s+R_L)$=58.434/(0.3+2.7)=19.48, the normalised transfer function becomes:

$$Y(s_0) = \frac{s_0(s_0^{\ 4} + 0.05134s_0^{\ 3} + 3.041s_0^{\ 2} + 0.10268s_0 + 2.041)}{2.4(s_0^{\ 4} + 0.05134s_0^{\ 3} + 2.041s_0^{\ 2} + 0.05134s_0 + 1)} \tag{4-31}$$



InductEV, Inc.
Exhibit 1020
Page 132

Using analytical and/or numerical methods, the poles and zeroes of 4-30 and 4-41 can be computed. The results are shown in table 4-1. The result under ideal no load conditions (Q=∞) is also shown in the same table for comparison. When the track length is extended from 400m to 1500m, then k becomes $L_{s1}/L_s$=25.456mH/2325mH=0.01095. Using the same method, the poles and zeroes are calculated and also shown in table 4-1. To see the results more clearly, all the zero and pole locations of the tuned track network are drawn in Fig. 4-8.

**Table 4-1: Poles and zeroes of a practical parallel-series tuned track network**

| Situation | | At no load ($Q=w_0L_s/R$=194.78) | At full load (Q=19.478) | Assume Q=¥ |
|---|---|---|---|---|
| ***400m track ($k=L_{s1}/L_s$ =0.041)*** | Poles | -0.0014 ± j1.1063,<br>-0.0012 ± j0.9039 | -0.0141 ± j1.1054,<br>-0.0116 ± j0.9045 | ±j1.1064,<br>±j0.9039 |
| | Zeroes | 0,<br>-0.0001 ± j1.4286,<br>-0.0025 ± j1.0000 | 0,<br>-0.0010 ± j1.4286,<br>-0.0247 ± j0.9997 | 0,<br>±j1.4286,<br>±j |
| ***1500m track (k=0.01095)*** | Poles | -0.0014 ± j1.0537<br>-0.0012 ± j0.9491 | -0.0046 ± j1.0535<br>-0.0041 ± j0.9492 | ± j1.0537<br>± j0.9490 |
| | Zeroes | 0,<br>0.0000 ± j1.4181<br>-0.0025 ± j1.0000 | 0,<br>-0.0001 ± j1.4181<br>-0.0086 ± j1.0000 | 0,<br>± j1.4181<br>±j |

The results show that if Q=∞, the poles and zeroes have only imaginary parts, the system will oscillate around the nominal frequency $\omega_0$ ($s_0$=j) without damping. When the track load increases, Q decreases accordingly, the real components of the poles and zeroes become larger so that the system gets more damping. On the other hand, when the track length increases, Q increases, consequently the system gets less damping. It is interesting to note that the real parts of the poles and zeroes are approximately inversely proportional to Q. However, the imaginary parts of each pair of poles and zeroes almost do not change with Q at a given track length. This means that the natural frequency corresponding to each pair of poles and zeroes of the tuned track network is almost constant and does not change with the load. If the track length increases, the imaginary parts of the poles decrease slightly. Therefore, a longer track length (larger inductance) helps to stabilise the frequency to its nominal value. For a high order system like this, the complete system response will be determined by the combined effects of the poles and zeroes on the complex plane. A knowledge of their location is useful for system dynamic analysis and controller design.

It is clear that the poles and zeroes are only determined by the Q of the series-tuned track and the ratio between the π network inductance and the track inductance. For a long track system, the ratio k is much smaller than one. From equation (4-23) it can be seen that the effect of k is negligible since the factors (k+2) and (k+3) approximately equal to 2 and 3 respectively. In this situation, the poles and zeroes will only be determined by the quality factor Q.



InductEV, Inc.
Exhibit 1020
Page 133

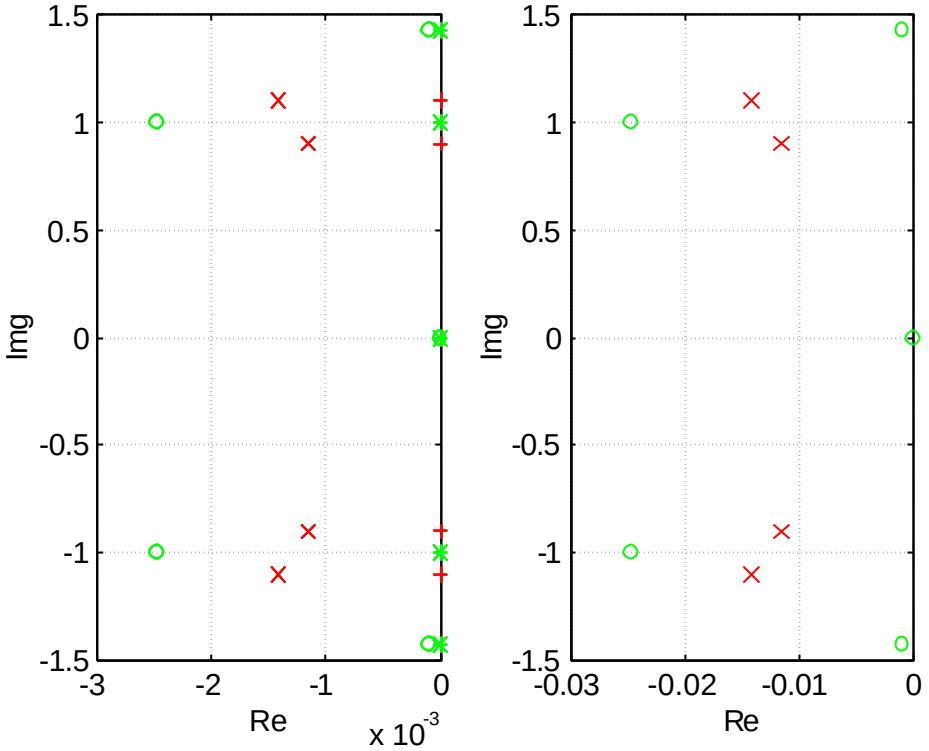


(1) Q=194.78 (at no load) and Q=∞ (2) Q=19.478 (at full load )

**(a) 400m tuned track (´ /o: poles/zeroes, but +/* for Q=¥)**

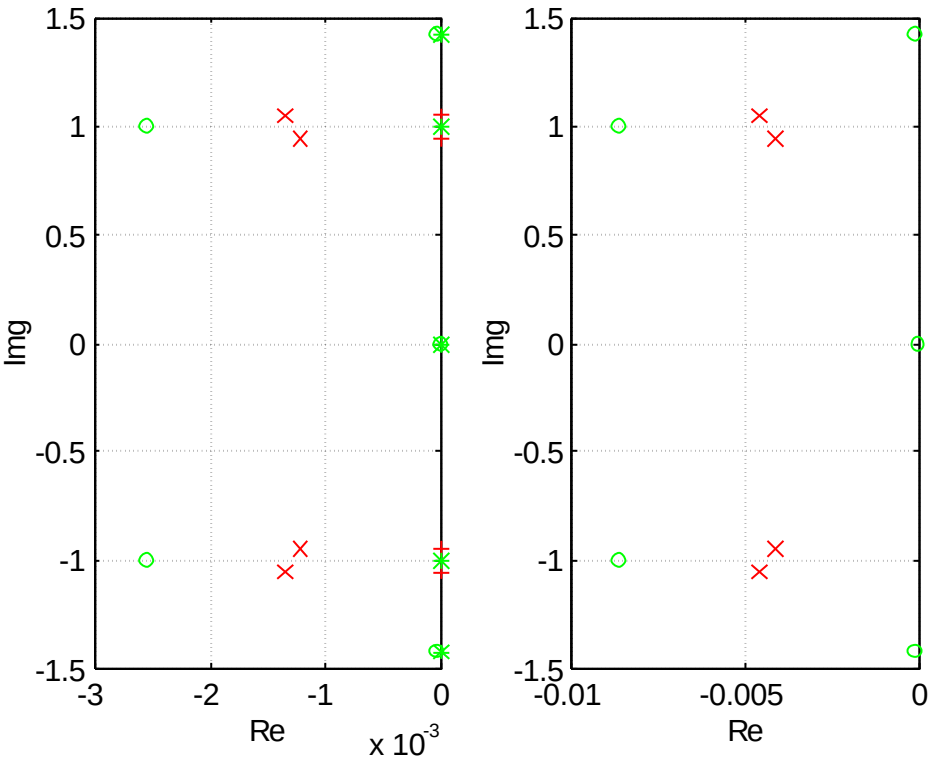


(1) Q=194.78 (at no load) and Q=∞ (2) Q=57.29 (at full load )

**(b) 1500m tuned track (´ /o: poles/zeroes, but +/* for Q=¥)**

**Fig. 4-8: Zeroes and poles location of a current-fed G3 track network**



InductEV, Inc.
Exhibit 1020
Page 134

### 4.4.2 Sensitivity Analysis

**Nominal Values and Variations of the Circuit Parameters**

The previous analyses on the track network were based on ideal components without considering circuit parameter variations. In a practical system, the components are non-ideal and parameter variations may deteriorate the circuit performance greatly. Therefore, sensitivity analyses are needed for system design and component selection purposes.

Fig. 4-9 shows a tuned track network to be analysed. The ESRs (Equivalent Series Resistances) of the reactive components are considered and the detailed data can be found in Appendix B. The pick-up load is modelled as an equivalent resistance to simplify the analysis. Its maximum value is 2.7 Ω, corresponding to a total load of 160kW with an efficiency of 95% at a track current of 250A. Considering a series track resistance of 0.3Ω, the total track resistance R varies over the range of 0.3Ω to 3Ω from unloaded to fully loaded conditions.

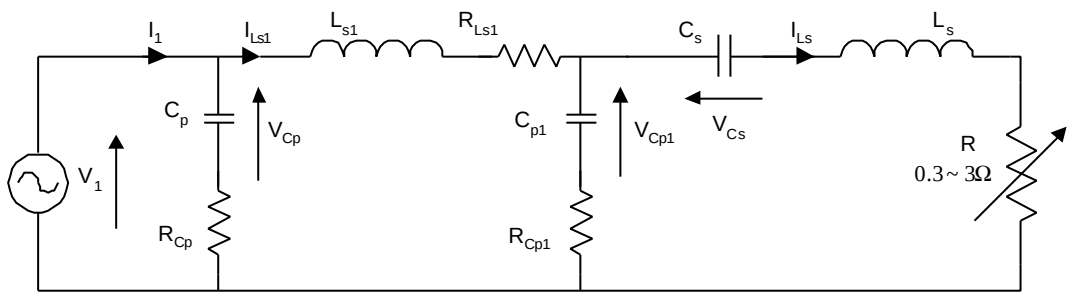


**Fig. 4-9: Tuned track network for sensitivity analysis**

To analyse the effect of the load variations, the track resistor R is regarded as having a nominal value of 1.65Ω and a maximum tolerance of ±81.82%, ie, it varies from the middle value to the maximum and minimum limits. This assumption is only made to investigate the effect of the load variation. At the nominal AC input voltage of 600V rms, the nominal capacitor voltages and inductor currents at 15kHz are calculated and shown in table 4-2.

**Table 4-2: Nominal values of the tuned track network**

| Variables | $I(L_s)$ | $V(C_s)$ | $V(C_{p1})$ | $I(L_{s1})$ | $V(C_p)$ | $I_1$ |
|---|---|---|---|---|---|---|
| *Magnitude* | 249.97A | 14.61kV | 412.45V | 303.39A | 600.00V | 172.08A |
| *Phase* | -89.98° | -179.98° | -89.98° | -55.46° | -0.014° | 0.057° |

Note: The nominal condition is based on $V_1=600\angle 0^0$V rms, $f_0$=15kHz, and R=1.65Ω.



InductEV, Inc.
Exhibit 1020
Page 135

It can be seen from the table that the track current $I(L_s)$ is slightly smaller than 250A, and also there are some slight phase errors. This is caused by the ESRs of the reactive components which were not considered in the preliminary design. Because these resistances are much smaller than their corresponding impedances, it can be seen that their effects are in fact very small.

In a practical system, all the parameters may drift away from their nominal values to some extent. These errors may exist independently of each other within a so-called "device tolerance", such as those caused in component production; or they may track each other and vary simultaneously within a so-called "lot tolerance", such as variations caused by temperature changes. For the tuned track network as shown in Fig. 4-9, while the tolerance of the load resistor is set at ±81.82% to reflect the full load range, the tolerances of the reactive components $C_p$, $C_{p1}$, $L_{s1}$, $C_s$, and $L_s$ are set at ±2%, ±5%, and ±10% respectively to investigate their effects. To simplify the analysis, only device tolerances are considered, which means that the component values can vary independently within a given maximum tolerance.

**Sensitivity and Worst Case Analysis at Forced Frequency**

As discussed earlier, there are two quite different schemes to drive the tuned track network of a G3 IPT power supply: to force the switching frequency, or to vary the switching frequency to achieve ZVS operation. A fixed frequency at the nominal frequency of 15kHz is assumed first to analyse the sensitivity of the tuned track network.

In principle, the sensitivity reflects the degree of output changes caused by parameter variations. It can be expressed in either a relative or absolute form. In general, if there is a function F(x, y, z ...), then the relative sensitivity of F with respect to x is defined as [2]:

$$S_x^F = \frac{x}{F}\frac{\partial F}{\partial x} = \frac{\partial F / F}{\partial x / x} \tag{4-32}$$

Normally it is very difficult to get a closed form expression of the sensitivity for a complicated circuit. However, with the help of simulation softwares such as PSpice [3], it is easy to obtain numerical solutions of the sensitivity at a given operating point. They can be expressed in a relative form in percentage ratios, or in an absolute form with values such as ΔF with respect to Δx.

For the tuned track circuit, the sensitivity and worst case results obtained from PSpice simulations are shown in table 4-3. These results show that:



InductEV, Inc.
Exhibit 1020
Page 136

$C_p$ hardly has any effect on the variables of interest except for the input current $I_1$. This is because $C_p$ is in parallel with the input voltage source and it is mainly used to compensate the reactive power and therefore correct the power factor. A 1% variation in $C_p$ will cause the input current to increase by 0.013% and a phase shift of 0.833°.

The most sensitive component affecting the track current $I(L_s)$ is $L_{s1}$, the relative sensitivity is nearly -1, meaning that a 1% increase in $L_{s1}$ will cause about a 1% drop in the track current. In fact, $L_{s1}$ is the component which determines the track current level when the input voltage is given. It is tuned with $C_{p1}$ to supply a constant current to the track. Exactly how these $L_{s1}$ and $C_{p1}$ should be tuned is related to the track equivalent impedance. The results show that at about the half load condition (R=1.65Ω) the effect of other parameters including $C_{p1}$ on the track current variation is very small. This is because the impedance of the equivalent parallel branch of $L_{s1}$ and $C_{p1}$ is much greater than the equivalent tuned track impedance after the voltage source is converted to a current source (see Fig. 4-5b). Under worst case conditions, the combined effects cause a larger track current variation. With maximum device tolerances of ±10%, ±5% and ±2%, the track current may decrease by as much as 43.9%, 15.36% or 1.75% respectively. It is clear that the component tolerance, particularly that of the π network inductance, should be controlled so as to minimise the track current variation.

The most sensitive component affecting the track tuning capacitor voltage $V(C_s)$ is $L_{s1}$ and $C_s$ itself. This is because the variation of $L_{s1}$ directly affects the track current magnitude and $C_s$ determines the impedance and therefore the voltage drop. The relative sensitivity of both is about -1.

The most sensitive components affecting the track driving voltage $V(C_{p1})$ is also $L_s$ and $C_s$ because they may cause track detuning and consequently a large increase in equivalent track impedance. The relative sensitivity of both is about 6. The load also affects the track driving voltage. The sensitivity of $V(C_{p1})$ with respect to the load resistance is about 1.

The most sensitive components affecting the π network inductor current $I(L_{s1})$ are again $L_s$ and $C_s$. The detuning of $L_s$ with $C_s$ will cause large current changes in $L_{s1}$. The relative sensitivity of $I(L_{s1})$ with respect to both $L_s$ and $C_s$ can be as high as approximately –16.



InductEV, Inc.
Exhibit 1020
Page 137

The magnitude of the input current $I_1$ is mostly affected by $L_s$ and $C_s$, the sensitivity is about 6 in both cases. $L_s$ and $C_s$ also contribute to the largest phase shift of $I_1$. A 1% increase in $L_s$ or $C_s$ may cause a phase shift of around 20 degrees. Under worst case conditions, the combined effect of the component variations on the phase shift is very high. The shift can be as high as 82 degrees even when the maximum tolerance is limited to ±2%. The high sensitivity of the phase angle with respect to the component variations explains why ZVS operation is difficult to maintain in a practical constant frequency system.

**Table 4-3: Sensitivity and worst case analysis results of parallel-series tuned track at 15kHz**

| Variables | D**I($L_s$)** | D**V($C_s$)** | D**V($C_{p1}$)** | D**I($L_{s1}$)** | D**V($C_p$)** | D**$I_1$** |
|---|---|---|---|---|---|---|
| ***$L_s$ +1%*** | +6.1E-5A<br>(+2.44E-5%)<br>-9.3E-3° | +2.93E-3V<br>(+2.0E-5%)<br>-9.3E-3° | +25.12V<br>(+6.091%)<br>+19.49° | -47.82A<br>(-15.76%)<br>+7.75° | +0V<br>(+0%)<br>+0° | +10.46A<br>(+6.08%)<br>+19.47° |
| ***$C_s$ +1%*** | +6.1E-5A<br>(+2.44E-5%)<br>-9.21E-3° | -144.62V<br>(-0.9901%)<br>-9.22E-3° | +24.64V<br>(+5.974%)<br>+19.31° | -47.37A<br>(-15.61%)<br>+7.66° | +0V<br>(+0%)<br>+0° | +10.26A<br>(+5.96%)<br>+19.30° |
| ***$C_p$ +1%*** | +0A<br>(+0%)<br>+0° | +0V<br>(+0%)<br>+0° | +0V<br>(+0%)<br>+0° | +0A<br>(+0%)<br>+0° | +0V<br>(+0%)<br>+1.43E-4° | +0.219A<br>(+0.013%)<br>+0.833° |
| ***$C_{p1}$ +1%*** | -6.47E-3A<br>(-2.59E-3%)<br>-0.394° | -0.3789V<br>(-2.59E-3%)<br>-0.39° | -0.0107V<br>(-2.6E-3%)<br>-0.394° | +0.97A<br>(+0.32%)<br>-0.127° | +0V<br>(+0%)<br>+0° | -4.5E-3A<br>(-2.6E-3%)<br>-0.394° |
| ***$L_{s1}$ +1%*** | -2.479A<br>(-0.992%)<br>-0.39° | -144.86V<br>(-0.992%)<br>-0.39°° | -4.09V<br>(-0.9917%)<br>-0.39° | -3.0A<br>(-0.992%)<br>-0.39° | +0V<br>(+0%)<br>+0° | -3.39A<br>(-1.97%)<br>+0.451° |
| ***R +1%*** | -1.14E-3A<br>(-4.58E-4%)<br>+0° | -0.0664V<br>(-4.55E-4%)<br>+0° | +4.1226V<br>(+0.9995%)<br>+9.16E-5° | +0.976A<br>(+0.322%)<br>+2.67° | +0V<br>(+0%)<br>+0° | +1.718A<br>(+1.0%)<br>-9.1E-5° |
| ***Worst Case (±10%)*** | -109.76A<br>(-43.91%)<br>+119.72° | +4.52kV<br>(+30.93%)<br>-3.7° | +1.19kV<br>(+289.2%)<br>+89.12° | +1.697KA<br>(+559.36%)<br>+133.5° | +0V<br>(+0%)<br>+1.43E-3° | +568.7A<br>(+330.5%)<br>+88.44° |
| ***Worst Case (±5%)*** | -38.384A<br>(-15.36%)<br>+5.55° | +1.69KV<br>(+11.57%)<br>-3.01° | +943.5V<br>(+228.75%)<br>+87.5° | +717.2A<br>(+236.4%)<br>+107.94° | +0V<br>(+0%)<br>+7.16E-4° | +422.3A<br>(+245.4%)<br>+87.03° |
| ***Worst Case (±2%)*** | -4.3788A<br>(-1.75%)<br>+1.697° | +613.82V<br>(+4.2%)<br>-1.47° | +516.41V<br>(+125.2%)<br>+82.85° | +302.49A<br>(+99.7%)<br>+55.67° | +0V<br>(+0%)<br>+2.86E-4° | +233.04A<br>(+129.6%)<br>+82.83° |

**Note:** 1. Both the absolute and relative sensitivities of the magnitudes of the variables are shown in the table.



InductEV, Inc.
Exhibit 1020
Page 138

2. Only the absolute sensitivity of the phase angles is shown. This is because the relative ones are not very meaningful when the nominal angle is near zero.
3. For all the worst-case analyses, the tolerance of R is ±81.82% to cover the full load variation.

### Monte Carlo Analysis at Forced Frequency

It should be noted that the PSpice worst case analysis undertaken in the previous section is not an optimisation process; it does not search for the set of parameter values which result in the true worst case. In fact, the result is obtained by varying each parameter as far away from its nominal value as allowed by its tolerance in a direction where a specified collating function (such as maximum variation, minimum value, zero phase angle crossing edge, etc.) tends to its "worst". There is no guarantee that the result is the true worst-case unless the collating function is monotonic with all the parameter variations. Usually it is difficult to check whether a collating function is monotonic for a multiple variable system. Therefore, it is doubtful that the result will be the absolute worst case, although normally it is indeed near the limit since all the parameters are individually varied to their "worst" limits.

In order to overcome the shortcoming of the worst-case analysis, Monte Carlo analysis has been undertaken. In a Monte Carlo analysis, component values are varied randomly according to a specified distribution (uniform, Gaussian, or user defined) within their specified tolerance. In this way, statistical data on the impact of a device parameter's variance can be obtained and a general picture can be shown. In a practical simulation there is a trade-off in choosing the number of Monte Carlo runs and the accuracy of the results. More runs provide better results, but need larger computer overheads and take a longer simulation time. As the number of runs increases, the output distribution is shown more precisely so that the true worst-case can be approached more closely.

The magnitude of the track current $I(L_s)$ and the phase angle of the input current $I_1$ (with respect to the input voltage, being the same as the phase angle of the input admittance) are the most two important values of concern in a IPT power supply. Their distributions at different parameter tolerances have been obtained from Monte Carlo analyses. As an example, Fig. 4-10 shows the situation when the tolerance is ±2%. The number of runs is set to be 300 and the default uniform distribution is selected in PSpice.

Most Monte Carlo analysis results are in good agreement with those obtained from the worst case analysis discussed in the previous section. However, as expected they do reveal some more severe cases. For instance, when the tolerance is ±2%, Fig. 4-10 shows that the maximum track current



InductEV, Inc.
Exhibit 1020
Page 139

variation is 260.304-250=10.304A (4.12 % of the rated value), which is larger than the figure of 4.3788A (1.75 %) shown in table 4-3.

Fig. 4-10 further shows that the maximum phase angle deviation of the track network input current can be more than 80 degrees even when the component tolerance is only 2%. As such, ZVS operation is difficult to achieve at a fixed frequency unless some complex parameter self-tuning methods are employed to correct the power factor dynamically. Alternatively, variable frequency control can be utilised to shift the operating frequency slightly.

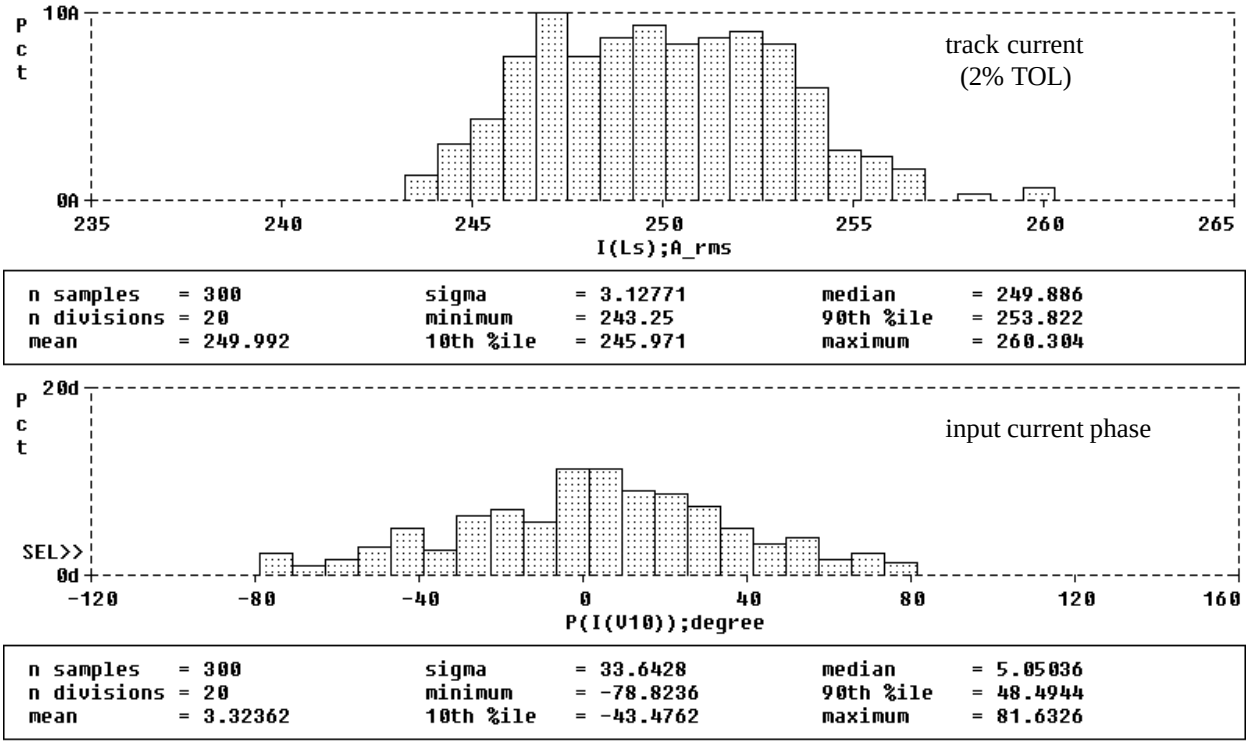


**Fig. 4-10: Monte Carlo analysis of the track current and input current phase (Tolerance: ±2%)**

### Frequency Shift Sensitivity Analysis

Several variable frequency shift control methods, such as a zero voltage crossing detector, a VCO (voltage controlled oscillator) frequency controller using voltage or current spike errors, and PLL (phase-locked loop) techniques are available. No matter what control method is used, an important concern is how circuit components variations will affect the ZVS frequency shift. As such a frequency shift sensitivity analysis is required to answer this question.

Normal sensitivity, worst-case, and Monte Carlo analyses have been undertaken individually to evaluate both the increase and decrease of the central zero phase angle frequency shift of the input



InductEV, Inc.
Exhibit 1020
Page 140

current where the voltage and current are in phase. Table 4-4 shows the sensitivity and worst-case analysis results. To see the results more clearly, the sensitivities (caused by a 1% change in parameter variations) of the track current magnitude and the track network input current phase angle around the nominal frequency 15kHz are shown in Fig. 4-11. As an example, a "worst-case" situation corresponding to a "maximum" frequency shift at a ±2% tolerance is shown in Fig. 4-12(a) compared with an AC sweep under nominal working conditions shown in Fig. 4-12(b). In addition, the Monte Carlo histogram is shown in Fig. 4-13.

**Table 4-4: Sensitivity and worst-case analysis result of the frequency shift**

| *Variables* | Df | *Variables* | Df | *Variables* | Df (HI) or Df (LO) |
|---|---|---|---|---|---|
| $L_s$ *+1%* | -73Hz (-0.486%) | $C_{p1}$ *+1%* | +1Hz (+9.5E-3%) | ***Worst Case (±10%)*** | +1.668kHz (+11.12%) or –1.45kHz (-9.67%) |
| $C_s$ *+1%* | -73Hz (-0.486%) | $L_{s1}$ *+1%* | -2Hz (-0.0109%) | ***Worst Case (±5%)*** | +790Hz (+5.27%) or -790Hz (-5.27%) |
| $C_p$ *+1%* | -3Hz (-0.020%) | *R +1%* | ≈0 (-1.2E-5%) | ***Worst Case (±2%)*** | +306Hz (+2.04%) or -313Hz (-2.088%) |

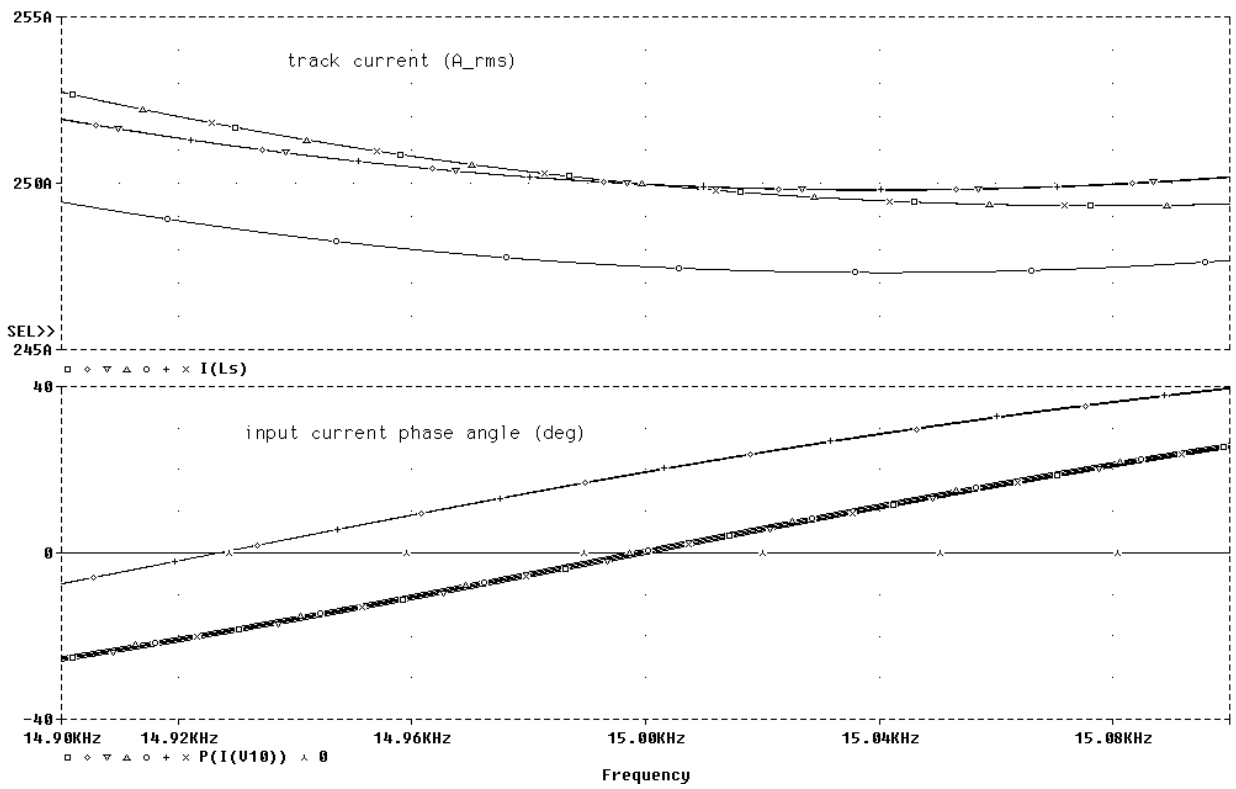


ð....Nominal ◊...$C_s$ +1% ∇...$C_{p1}$ +1% Δ...$C_p$ +1%
o ...$L_{s1}$ +1% +...$L_s$ +1% ×...R +1%

**Fig. 4-11: Frequency shifts caused by a 1% increase of the circuit components**



InductEV, Inc.
Exhibit 1020
Page 141

Fig. 4-11 further shows that the most sensitive component to the variation of the magnitude of the track current is the π network inductor $L_{s1}$. However, it can be seen that $L_{s1}$ is not sensitive to the frequency shift at all. The most sensitive components with respect to the frequency shift are obviously the track inductor $L_s$ and its tuning capacitor $C_s$. Table 4-4 and Fig. 4-10 show that a 1% increase in their values causes about a 73 Hz drop (around 0.5%) in the zero impedance phase angle frequency. The results also show that other parameters, particularly the resistive load, have little effect on the frequency shift.

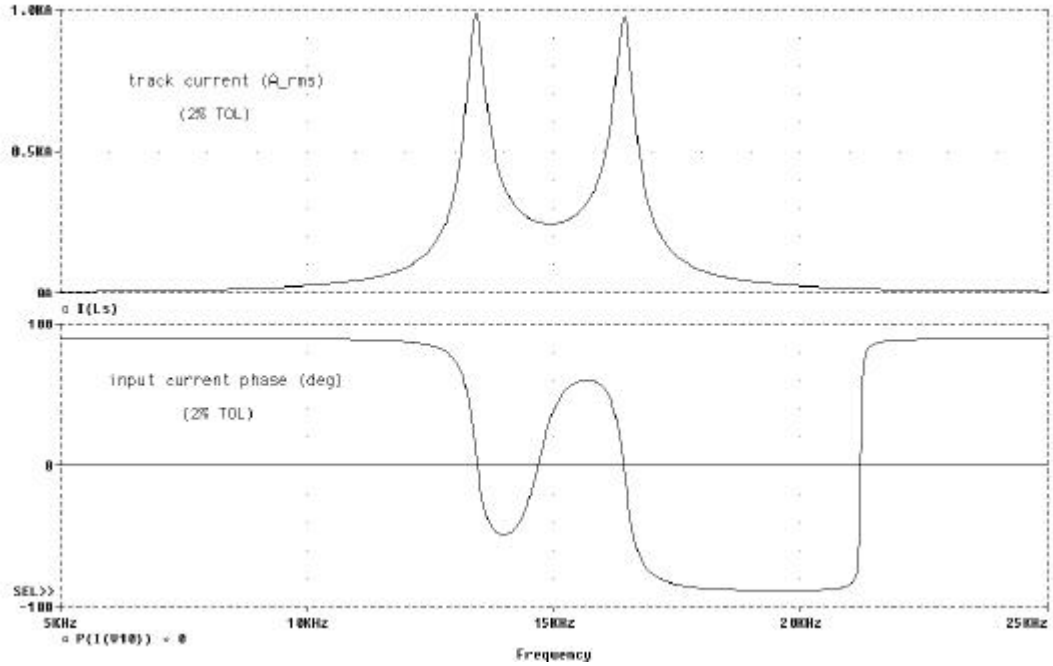


(a) Worst case frequency response at a ±2% tolerance



InductEV, Inc.
Exhibit 1020
Page 142

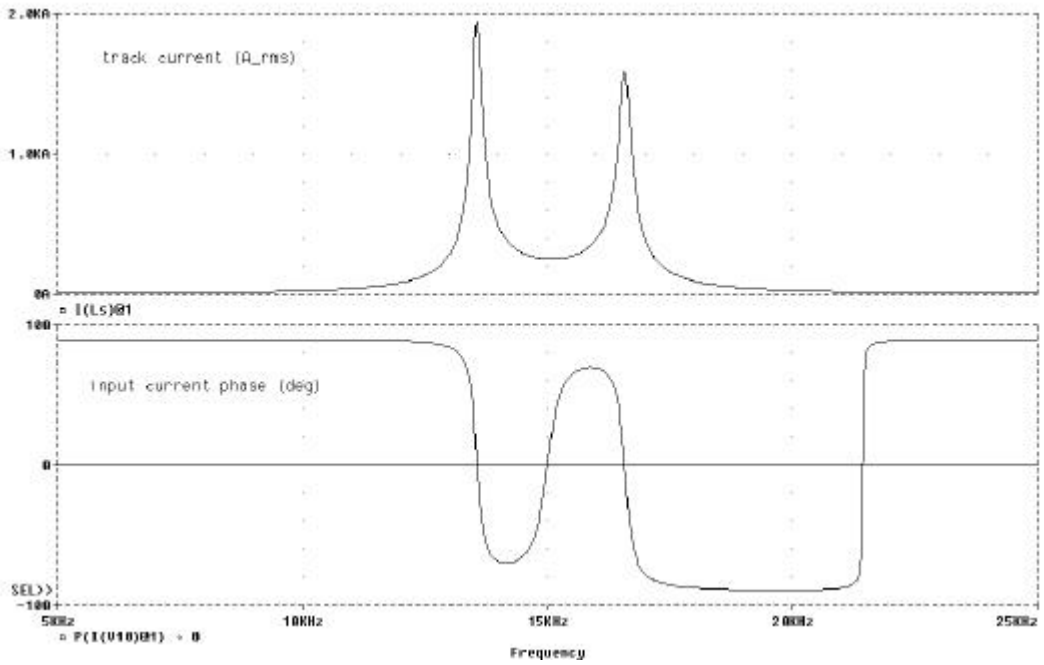


(b) Nominal frequency response (AC sweep)

**Fig. 4-12: Worst case frequency shift AC sweep compared with the nominal situation**

The results obtained from the worst case analysis and the Monte Carlo analysis show that the maximum percentage zero phase angle frequency shift is close to the specified component tolerances. It has been found that when the tolerance is ±10%, the maximum frequency shift is about 11%; when the tolerance is ±5%, the maximum frequency shift is about 5.3%; and when the tolerance is ±2%, the sensitivity and worst-case analysis results (table 4-4 and Fig. 4-12) show that the maximum frequency shift is about 2% of the nominal frequency. The Monte Carlo analysis (Fig. 4-13) gives a similar result showing a maximum shift of approximately 2.7%.



InductEV, Inc.
Exhibit 1020
Page 143

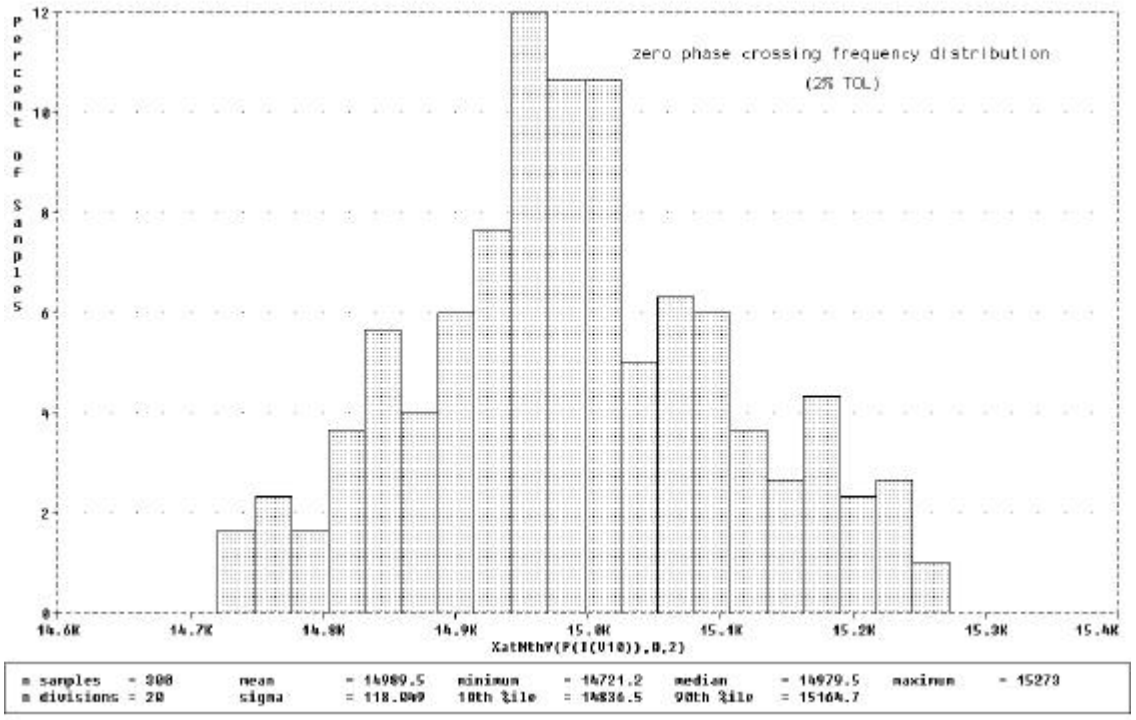


**Fig. 4-13: Monte Carlo analysis of the zero phase angle frequency shift of the CLC track network**

It should be noted that the zero phase angle (resonant) frequency discussed here is not exactly the same as the ZVS frequency of the current-fed G3 power supply under variable frequency operation. The analysis is totally based on the track network circuit with a pure resistive load (Fig. 4-2) using sinusoidal steady-state AC circuit theory. Due to the effects of the switching process of a practical inverting network and the power pick-up control, the harmonic components will affect the actual ZVS frequency. The accurate analysis of such a high-order switch-mode nonlinear system is very difficult. However, if the reactive power in the track network, including that of the bias network, is much larger than the real power, the effect of the harmonics will be very small and modelling power pick-ups as a pure resistor will not introduce significant errors. Consequently, the zero phase angle frequency of the track network will be very close to the practical ZVS frequency.

## 4.5 System Dynamic Simulations

### *4.5.1 A Typical Current-fed G3 IPT System*

To investigate the validity and dynamic properties of the proposed current-fed G3 power supply, various simulations have been undertaken for an electric train application in Wampfler AG, Germany [4-5]. Fig. 4-14 shows the schematic diagram of a current-fed G3 IPT system (without bias network) being investigated. The system specifications include:



InductEV, Inc.
Exhibit 1020
Page 144

| | |
|---|---|
| Nominal frequency: | 15kHz |
| Nominal track current magnitude: | 250A rms |
| Maximum output power: | 200kW |
| Track length: | 400m |
| Maximum number of pick-ups: | 16 |
| Nominal DC power supply voltage: | 540V |
| DC output battery voltage: | 640V |

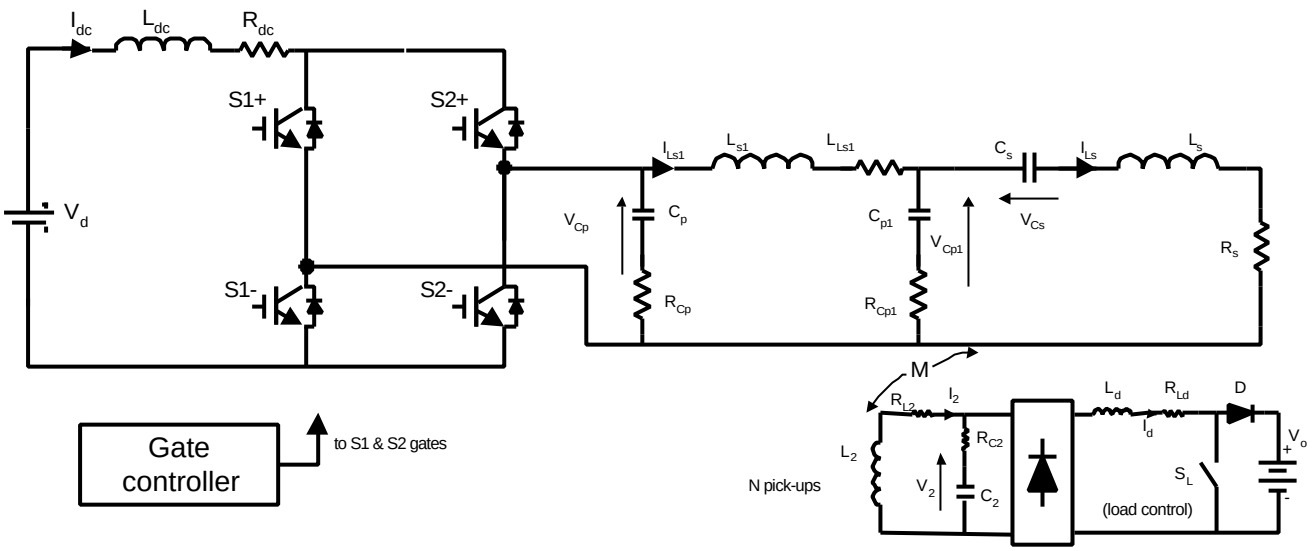


**Fig. 4-14: Schematic diagram of a current-fed G3 IPT system (zero bias)**

Practical power pick-up loads are considered in the study. Each pick-up coil is parallel-tuned, and after a full-bridge rectifier it supplies an approximately constant DC current output. The power flow is controlled using a shorting switch $S_L$ as shown in Fig. 4-14. When $S_L$ is "off", the DC current flows directly to the load so that a battery bank (650V) for the train power supply is charged. On the contrary, if $S_L$ is controlled "on", the pick-up coil is shorted therefore the load is essentially decoupled from the primary track power supply. In the pick-up circuit, diode D is used to prevent the shorting the battery output voltage $V_0$ when $S_L$ is turned "on", while inductor $L_d$ provides a choke input filter for the rectifier bridge and prevents high surge currents damaging the switch when it turns on.

The track is series-tuned and the $\pi$ network is designed according to the methods discussed earlier in this chapter. A PSpice schematic diagram of the current-fed full-bridge G3 IPT system with a 400m track length and 16 pick-ups are shown in Appendix C. Detailed system data, including the



InductEV, Inc.
Exhibit 1020
Page 145

pick-ups and the measured equivalent series resistors of the reactive components, is shown in Appendix B.

Both the push-pull and full-bridge are feasible topologies for the application. As discussed in Chapter 3, a push-pull inverter can generate twice as much the AC voltage as that of a full bridge topology, and it may not require isolated gate drives. However, high voltage generation at the inverter side is no longer a big concern for current-fed G3 power supplies as the $\pi$ network can boost the track driving voltage easily. Moreover, since two semiconductor switches are relatively cheaper and smaller, and the isolated gate drives account for little cost in a high power system, the push-pull topology as shown in Fig. 4-14 is preferred for this application.

Similar to a current-fed G1 power supply, the gate drives of a current-fed G3 power supply can be controlled at a constant frequency (15kHz) or a variable ZVS frequency. ZVS operation can be obtained by detecting the voltage and current errors in the switching network. A controller based on voltage errors is illustrated in Fig. 4-15. In this diagram two series blocking diodes D1 and D2 are inserted in series with the main power switches. Under non-ZVS operation, there will be negative voltage spikes existing across the diodes. These negative voltage spikes are detected and gated through two analogue switches. The pulses with double switching frequency are used to control the analogue switches and the outputs of the analogue switches are integrated to shift the frequency such that these spike errors tend to zero so that ZVS operation can be achieved. A simple VCO (Voltage Controlled Oscillator) circuit (such as CD4046) can be used to vary the frequency, while two analogue switches are controlled to select the integral direction based on whether the switching is too fast or too slow. The VCO used in Fig. 4-15 limits the frequency variation in a small range between $f_1$ and $f_2$, so that the switching frequency is limited between $f_1/2$ to $f_2/2$ (typically 14.5kHz~15.5kHz). As a result, the system does not run away from the nominal operating point. This is particularly important for high order systems that have multiple frequency modes. For this reason, simple controllers based on direct zero voltage detection are not suitable for the proposed G3 power supply.



InductEV, Inc.
Exhibit 1020
Page 146

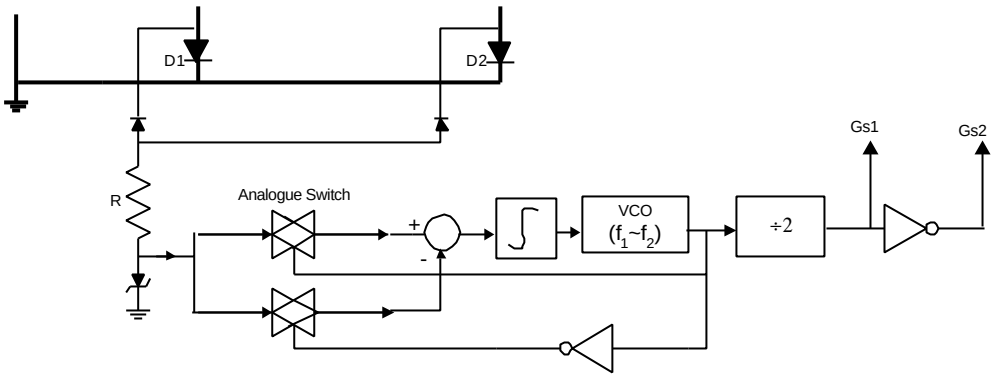


**Fig. 4-15: Variable frequency control based on voltage errors**

If there are no blocking diodes in series with the main switches, there will be current spikes in the loop of the switching network when ZVS is not achieved. Similar to voltage spikes, these current errors contain useful information as to whether the switching is too fast or two slow. Therefore, they can be used to control the system to achieve ZVS. In fact, a ZVS controller based on current errors has been developed in Wampfler AG based on various simulations by the author [4]. Due to commercial confidentiality, it is not shown here. An advantage of the controller based on the current error is that no series blocking diodes are required. However, the controller must be fast and accurate enough to suppress the dynamic current errors during transients. Otherwise, as discussed in Chapter 3, the high shorting currents may damage the switching devices.

### *4.5.2 Simulation Results and Discussion*

The PSpice simulation package has been used extensively to evaluate the system dynamic performance [6-7]. Typical load-increase and load-decrease transient response of a 400m/16pick-ups track power supply controlled at a fixed frequency (15kHz) is shown in Fig. 4-16 (a) and Fig. 4-17 (b) respectively. A larger track length of 1500m is also considered and the transient response is shown in Fig. 4-16 (b) and Fig. 4-17 (b) for comparison. To observe the system dynamic response, the pick-up loads were switched “on” and “off” at certain intervals. In Fig. 4-16, the system starts up at no load (all the pick-up switches are “on”), after which 12.5% of the full load is added, and then the load is stepped up to 50% of the full load, and finally the full load (all the pick-up switches are “off”) is applied; whereas in Fig. 4-17 the load steps are reversed from full load down to no load. All transient voltage and current waveforms can be observed from the simulation results, but of particular interest are the DC inductor current (equal to the current flowing through the semiconductor switches), the inverted AC voltage (equal to the voltage on the semiconductor



InductEV, Inc.
Exhibit 1020
Page 147

switches), the track inductor current, the total track driving voltage, as well as the track tuning capacitor voltage. And these waveforms are displayed in Fig. 4-16 and Fig.4-17.

Fig. 4-16 shows that with each increasing load, there is a noticeable current surge to supply the extra power required. At the same instants, the inverted resonant voltage $V_{cp}$ experiences similar (but inverted) transients. The transient is more severe when the load is removed as expected because the system damping is reduced with decreasing load. The typical transient time at full load is about 2 to 3ms. Fig. 4-17 shows that the DC input current drops when the load is reduced. It again shows that the oscillation is more severe at no load conditions due to reduced damping.

From Fig. 4-16 it can be seen that there is essentially no over-voltage existing on load increase. However, in Fig. 4-17 the voltage surge is obvious when the load decreases. For a 400m track length, an over voltage of around 20% of the nominal voltage value can arise when half of the load (8 pick-ups) is removed suddenly. This voltage surge is a potential danger to the switching devices and therefore requires protection circuits to be employed. The main reason behind the over voltage is that when the load is reduced suddenly, the DC current has to decrease accordingly to keep the power balance. This means that part or all of the energy stored in the DC inductor has to be discharged into the resonant tank causing the voltage rise. For this reason, the most effective way to prevent the over voltage is to dynamically control the energy to flow back to the source or to be consumed in a braking resistor [1]. As the DC inductor current can not be disconnected by the main control switches, additional semiconductors and/or voltage clamping circuits, such as those shown in Fig. 4-1, are required for this purpose.

Comparing the results obtained at two different track lengths of 400m and 1500m, it can be seen that the start-up DC current surge of the 1500m track power supply is much higher than that of the 400m track power supply. This is because the 1500m track network needs much more initial energy to start up. However, once it gets started, the network can maintains a more stable oscillation so that the load transients are smother. Due to the increased track length, the transient ringing frequency is smaller. Moreover, it is obvious that when the load is removed suddenly, its inverted AC voltage surges are smaller. From 50% of the full load to no load, the over-voltage surge is only around 10%. Also, as the equivalent series resistance of the 1500m track is proportionally increased, it can be observed that when the load is removed completely, the system damping is obviously larger compared to the 400m track power supply.



InductEV, Inc.
Exhibit 1020
Page 148

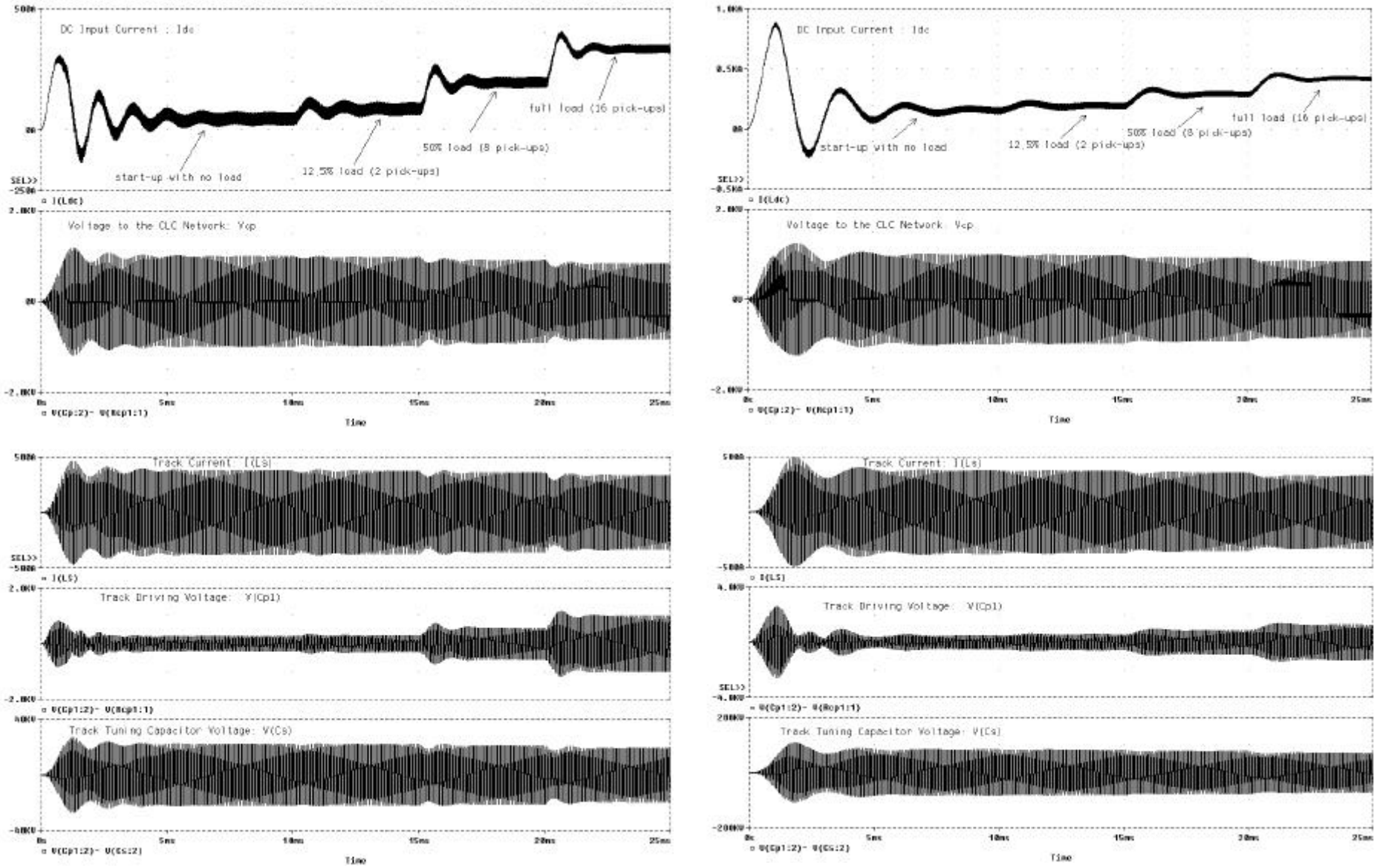


(a) 400m track length (b) 1500m track length

**Fig. 4-16: Load increase transient response**



InductEV, Inc.
Exhibit 1020
Page 149

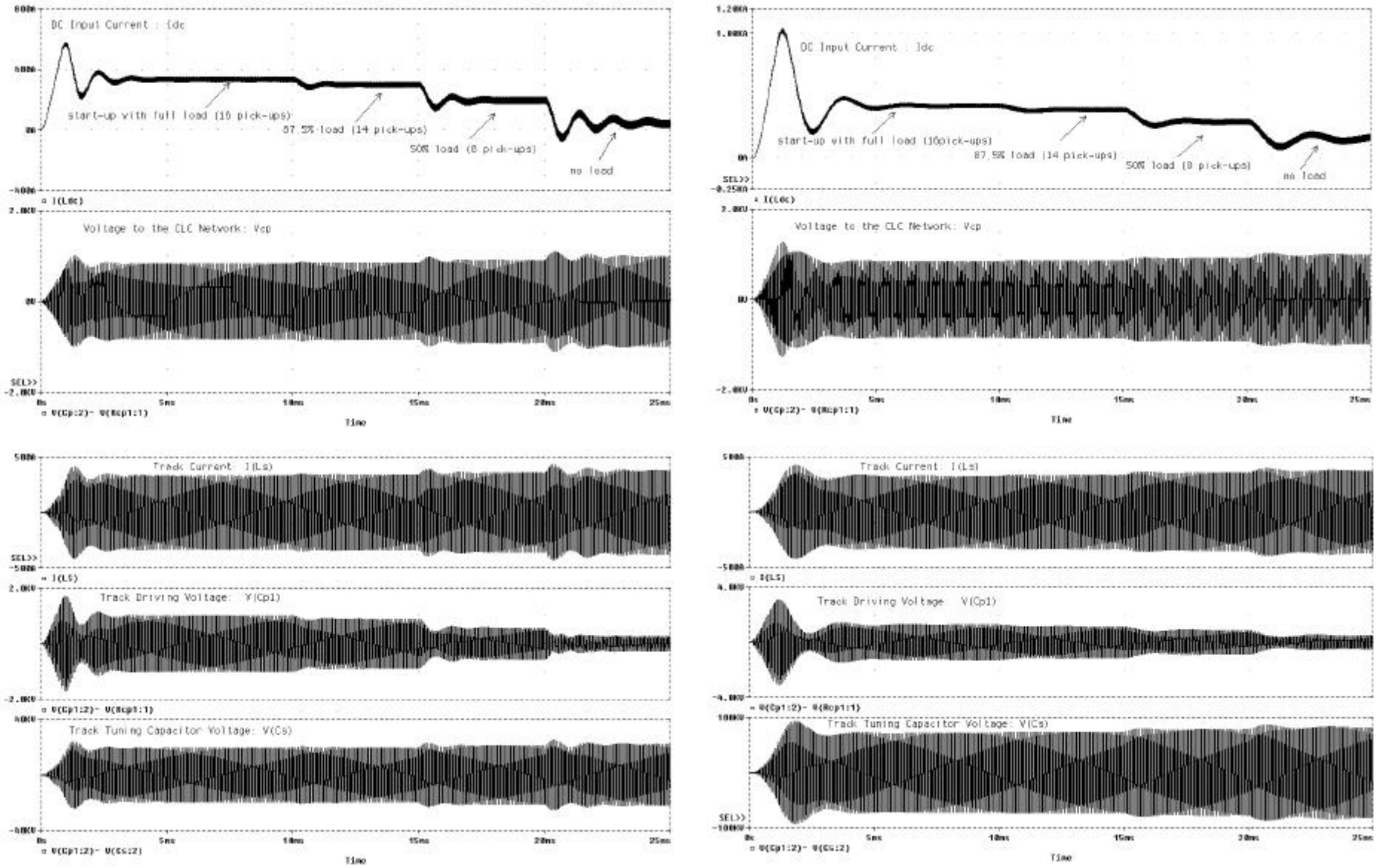


(a) 400m track length (b) 1500m track length

**Fig. 4-17: Load decrease transient response**



InductEV, Inc.
Exhibit 1020
Page 150

As expected, a nice feature of the new power supply is that the track current is approximately constant under steady state conditions. Fig. 4-16 and Fig. 4-17 show that this is essentially true for both 400m track and 1500m track power supplies. When the load varies, the track driving voltage $V_{cp1}$ adjusts automatically so that the track current is kept almost constant. The small track current drop is mainly due to the switch-mode harmonic distortion and the voltage drop across the equivalent resistance of the reactive components and power switches. It can be seen from the simulation results that the inverted voltage $V_{cp}$ drops slightly at full load conditions. This is very normal considering the magnitude of the currents (around 410A at full load) flowing through the DC inductor and power switches.

Theoretically, there is no limit to the power level and the track length of a G3 power supply since a high track current can be obtained with limited driving voltage from the inverter output. However, practically a large load may require very high voltage/current ratings for the reactive components, so that the system may be very bulky and costly. For example, in the case of the 400m track, it can be seen from the simulation results that the total equivalent track tuning capacitor voltage is about 21kV in peak. If the track length is extended to 1500m, this voltage will increase to about 80 kV! Another limitation which has not been taken into account at present is the wave propagation problem. If the track length is comparable to the electromagnetic wavelength (20km at 15kHz), a more complex approach, rather than a lumped parameter track model, has to be considered for IPT system design.

## 4.6 Summary

This chapter has proposed a new current-fed parallel-series resonant converter with improved properties for a new generation of IPT power supplies (G3). The current-fed G3 power supplies have the following obvious advantages:

The track current is constant and independent of the track impedance. This is essentially true if the DC input voltage is constant and the harmonics are negligible.

It is easy for the converter to achieve ZVS operation since the resonant tank provides a unity power factor load to the switching network. The fundamental components of the input current and the driving voltage are in phase if the network is fully tuned, therefore the actual frequency shift required to achieve ZVS is very small.



InductEV, Inc.
Exhibit 1020
Page 151

The track current is nearly a pure sine wave owing to the band filtering function of the track network. Therefore, the radiated EMI is low.

Innovation in the G3 power supply involves the adoption of a CLC π network between the series tuned track and the inverting network. The π network matches the impedance, filters the harmonics, and converts the voltage source to a current source. A detailed study on the properties of the tuned track network has been undertaken in this chapter. The poles and zeroes of the admittance transfer function have been presented. It has been found that for a long track the location of the poles and zeroes of the admittance transfer function are mainly determined by the quality factor of the series tuned track circuit. The real parts of the poles and zeroes are approximately inversely proportional to Q. However, the imaginary parts of each pair of poles and zeroes hardly change with load, so that the natural oscillating frequency remains almost constant as a result.

The sensitivity analyses, including worst-case and Monte Carlo analyses, have shown that the π network inductor is the most sensitive component affecting the magnitude of the track current, while the track inductor $L_s$ and its tuning capacitor $C_s$ are the most sensitive components with respect to the input phase angle and thus the frequency shift. These results are of great importance for system design and component selection.

The basic design concept and design equations of G3 track power supplies have been presented. The validity and system dynamic properties of a current-fed G3 IPT power supply for an electric train application have been investigated using PSpice simulations. It has been observed that high over-voltages can occur when the load is removed suddenly. The over-voltage is mainly caused by the energy stored in the DC inductor, therefore a dynamic energy discharge control circuit may be required. The G3 power supply makes very high power transfer over a long track distance possible. Nevertheless, the voltage and current stresses on the reactive components may be very high which can greatly increase the system cost and size. Moreover, wave propagation problems need to be investigated if very long track lengths are required.

## 4.7 References

[1] Boys, J. T., Covic, G. A. and Green, A. W.: “Stability and control of inductively coupled power transfer systems,” *IEE Proceedings of Electric Power Applications*, Vol. 147, No.1, pp.37-43, January 2000.

[2] Qiu, G. Y.: *Network analysis*, Science Press, China, 1980.



InductEV, Inc.
Exhibit 1020
Page 152

[3] Al-Hashimi, B.: *The art of simulation using PSpice – Analog and Digital*, CRC Press, 1995.

[4] Hu, A. and Boys, J.: "Series-parallel resonant converters, Stage I: Current-fed, single ended, series-parallel converter simulation", *Research Report of Auckland Uniservices Ltd for Wampfler AG, Germany, and Daifuku Ltd, Japan*, 52 pages, June 1998.

[5] Hu, A. and Boys, T: "Current sourced CLC, G3 IPT track power supply, Stage II: Research and development investigation", *Research Report of Auckland Uniservices Ltd for Wampfler AG, Germany*, 78 pages, March 1999.

[6] Ramshaw, R. and Schuurman D.: *PSpice simulation of power electronics circuits – an introductory guide*, Chapman & Hall, 1997.

[7] Kraus, R. and Mattausch, H. J.: "Status and trends of power semiconductor device models for circuit simulation", *IEEE Transactions on Power Electronics*, Vol.13, No. 3, May 1998.



InductEV, Inc.
Exhibit 1020
Page 153

## Chapter 5

# Voltage-fed Resonant Converter Power Supplies

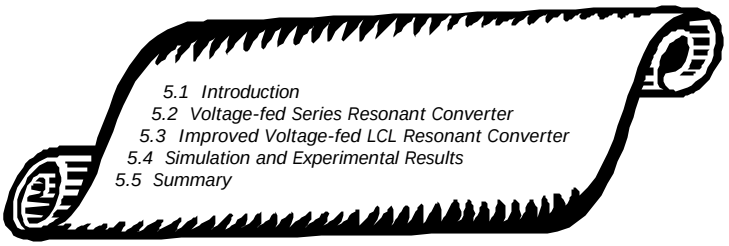


## 5.1 Introduction

Chapters 3 and 4 focused on current-fed resonant converters. In practice however a constant current source cannot stand alone like a voltage source without using superconductivity techniques that are not yet mature. A closed loop current controller can be used to produce an accurate constant current source, but it is not a common choice for high power applications due to economical reasons. Thus a large DC inductor in series with a voltage source is widely used in a practical current-fed resonant converter power supply as it can generate a relatively “constant” current in comparison with the fast changing AC variables. However, as discussed previously, such a configuration increases the circuit order and worsens the system dynamic properties. It also results in poorer control and protection options in the switching network of the inverter because the current in the DC inductor has to be maintained during the operating period [1-2].

In comparison, a voltage source is more readily accessible and voltage-fed resonant converter power supplies are easier to control. However, their resonant networks normally require series-tuning at the input port (to meet voltage transition requirements), which is not ideal for high reactive current circulation because the current has to flow through the switching devices. In fact, as will be seen later, the voltage-fed and current-fed resonant converters used for IPT power supplies are essentially dual circuits. They both have obvious shortcomings and strengths but the overall performance is comparable. As such both are used in practical applications depending on each system’s particular requirements.



InductEV, Inc.
Exhibit 1020
Page 154

This chapter is concerned with voltage-fed resonant converter power supplies. Phase shift PWM control and soft-switching operation of a basic voltage-fed series-resonant converter power supply (called a generation two or G2) is analysed first. Then its improved version – a series-parallel LCL resonant converter power supply (a voltage-fed generation three or G3) is proposed and discussed.

## 5.2 Voltage-fed Series Resonant Converter Power Supplies

### *5.2.1 Elements and Structure of the Converter*

As discussed in Chapter 2, voltage-fed converters have two basic configurations: a full bridge topology using four switches and a half bridge topology where two switches from the full bridge are replaced by two large capacitors. Due to the price drop of the semiconductor switches, the full bridge topology becomes more popular. Fig. 5-1 shows a typical full bridge voltage-fed series resonant converter for use in IPT applications. It comprises a DC voltage source $V_d$, an inverting network comprising four switching devices in a full bridge, and a series tuned resonant tank. The track coil is modelled as a lumped inductor $L_p$ and the load is represented by an equivalent resistor R. A series capacitor $C_p$ is used to tune the track depending on the track length. In a practical application, $C_p$ may be distributed at certain positions along the track so as to limit the maximum voltage on the track. The four capacitors in parallel with the switches are used for soft switching purposes as will be discussed later. The parasitic output capacitances of the switches are combined into these four capacitors so they are utilised advantageously.

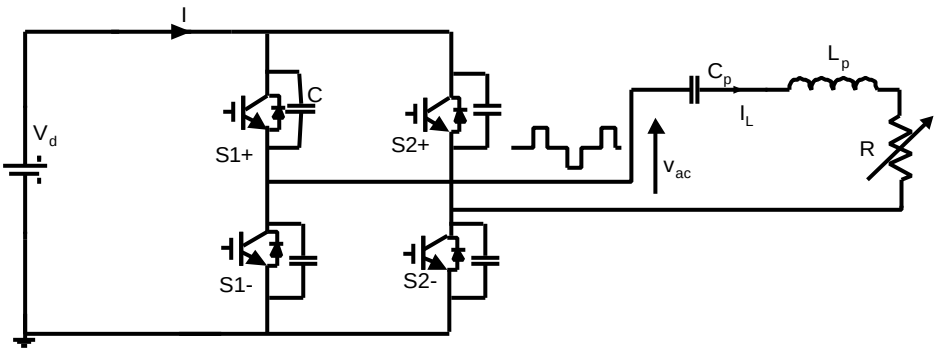


**Fig. 5-1: A typical voltage-fed series resonant converter power supply (G2)**

### *5.2.2 Phase Shift Regulation of the Track Current*

Unlike a current-fed resonant converter whose output AC voltage is mainly determined by the average DC input voltage under ZVS conditions, the output voltage of a voltage-fed inverting



InductEV, Inc.
Exhibit 1020
Page 155

network is completely under the control of the switching devices of the inverting network. In consequence, the track current can be regulated by duty cycle control. One control strategy is to shift the phase of the gate signals. In Fig. 5-1, the switches S1+ and S1-, S2+ and S2- are complementarily controlled, ie, when S1+ is "on", S1- is "off", similarly when S2+ is "on", S2- is "off", and vice versa. If both the upper switches S1+ and S2+ (or both the lower switches S1- and S2-) are "on", the AC output voltage from the inverting network is zero. Otherwise, the output voltage will be either positive $V_d$ or negative $V_d$, depending on the state of the switches. Because of this, phase-shift duty cycle control can be utilised to regulate the output voltage and consequently the track current. Fig. 5- 2 shows a situation when the gate signals of S2+ and S2- are lagging S1+ and S1- by 120 degrees. In this case, the output voltage is a PWM square wave with a duty cycle of 2/3. It is obvious that if S1+ (S1-) and S2+ (S2-) are completely in phase, ie, the phase shift is zero, the output voltage will be zero. On the other hand, if the switching is completely out of the phase, ie, the phase shift is 180 degrees, then the output voltage reaches its maximum value with a fundamental magnitude (rms) given by:

$$V = \frac{4}{p\sqrt{2}} V_d \qquad (5\text{-}1)$$

where $V_d$ is the DC input voltage.

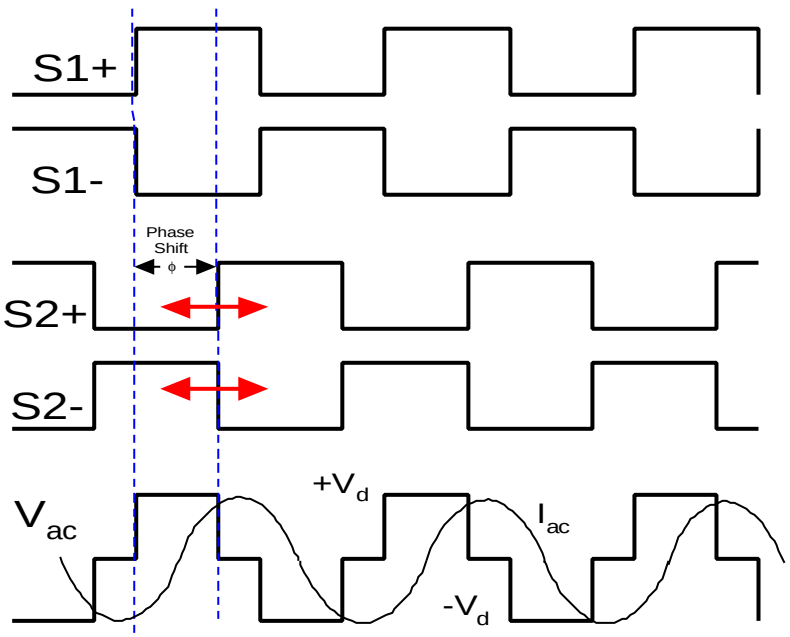


**Fig. 5-2: Phase shift control**

In a more general case where the phase shift angle ϕ is between zero degrees and 180 degrees, this voltage can be expressed as:



InductEV, Inc.
Exhibit 1020
Page 156

$$V = \frac{4}{p\sqrt{2}} V_d \cdot \sin\left(\frac{f}{2}\right) \tag{5-2}$$

or

$$V = \frac{4}{p\sqrt{2}} V_d \cdot \sin\left(\frac{pD}{2}\right) \tag{5-3}$$

where D=ϕ/π is the duty cycle of the output voltage. A duty cycle of 2/3, corresponding to a phase shift of 120 degrees, is a preferable operating point where the harmonic distortion is the lowest for a square waveform output [3-4].

In a practical circuit, because the switching devices turn off more slowly than they turn on, a dead time is necessary to prevent momentarily short-circuiting the DC voltage source. Therefore, a blanking out period exists so that the actual PWM phase shift control range is slightly larger than zero degrees and smaller than 180 degrees. As a result, the maximum output voltage is slightly smaller than the ideal value given in equation (5-1).

To achieve a constant track current output, a closed loop control (shown in Fig. 5-3) is normally used. A current sensor such as a toroidal current transformer or a LEM device can be used to measure the instantaneous track current. As the measured current changes with time at a relatively high frequency, a process of obtaining the average rms value or the peak envelope curve of the track current is required. There are many technical options to fulfil this signal processing task, for example, using phase shift amplifiers or sample and hold techniques. A novel method is to monitor the energy stored in the resonant circuit to estimate the track current. Using this method, simple integral circuits can be used to avoid expensive analogue multipliers [4-5]. After the dynamic track current magnitude has been obtained, it is compared with a current reference and the error is sent to a PI regulator. The output of the regulator is then used for PWM phase-shift control of the inverting network, so that finally the track current can be regulated to the right value as set by the reference.

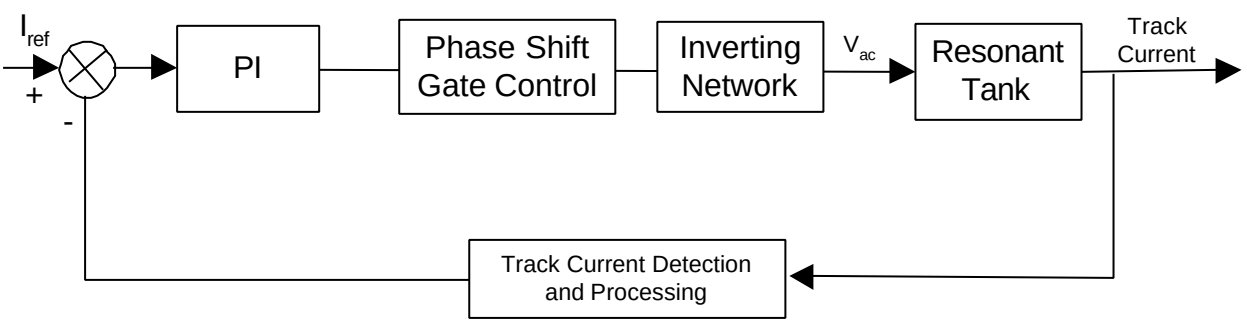


**Fig. 5-3: Closed loop track current regulation**



InductEV, Inc.
Exhibit 1020
Page 157

### 5.2.3 Soft Switching Operation Analysis

In a voltage-fed series resonant converter, the track is usually tuned in such a way that its inductance is not completely compensated by the series capacitor but leaves a net inductive residue, so that the track current lags behind the voltage at steady state as shown in Fig. 5-2. In this case, the track current goes through the corresponding body diodes of the switches before the switches are tuned on. Therefore, ZVS turn-on is achieved naturally. This is the preferred situation when operating above resonance where ideal turn-on conditions arise for both the switches and diodes [6]. However, when the switches are turned "off", a high current exists at high voltage. If there are no soft switching capacitors across the switches, the turn-off losses can be high.

Employing parallel soft switching capacitors helps to eliminate or contain the turn-off losses. When the dead-time considerations are added, the necessary gate control signals and resultant voltage and current waveforms are illustrated in Fig. 5-4. The switching process of the active switches under the steady state conditions can be divided into eight states, and their corresponding equivalent circuits are shown in Fig. 5-5, where the inductor $L_r$ represents the net residue inductance of the tuned track. These eight states are described in detail below:

Assume the first state starts at $t_0$ when switch S1+ turns on. As both S1+ and S2- are on (S1-and S2+ off), the output voltage is positive and equals to $V_d$. Owing to the above-resonance tuning (lagging power factor), the track current lags the fundamental of the driving voltage and changes its direction after a certain time. In the beginning, the current flows through the antiparallel body diodes of S1+ and S2-, and then switches S1+ and S2- themselves begin to conduct after the current changes direction.

State 2: t1 - t2. S2- turns off at t1 before S2+ turns on at t2, leaving the required dead time. Because of the existence of the capacitor C2-, the voltage across S2- cannot increase suddenly. During the short switch-off time of S2-, the voltage remains almost zero therefore zero voltage turn-off is approximately achieved. Later, C2+ is discharged and C2-is charged gradually resulting in a ramped voltage change across the track. If the voltage across C2+ is completely discharged corresponding to fully charging C2- from zero to $V_d$, then D2+ begins to conduct to keep the continuity of the track current. The track voltage drops to near zero (about –1V).



InductEV, Inc.
Exhibit 1020
Page 158

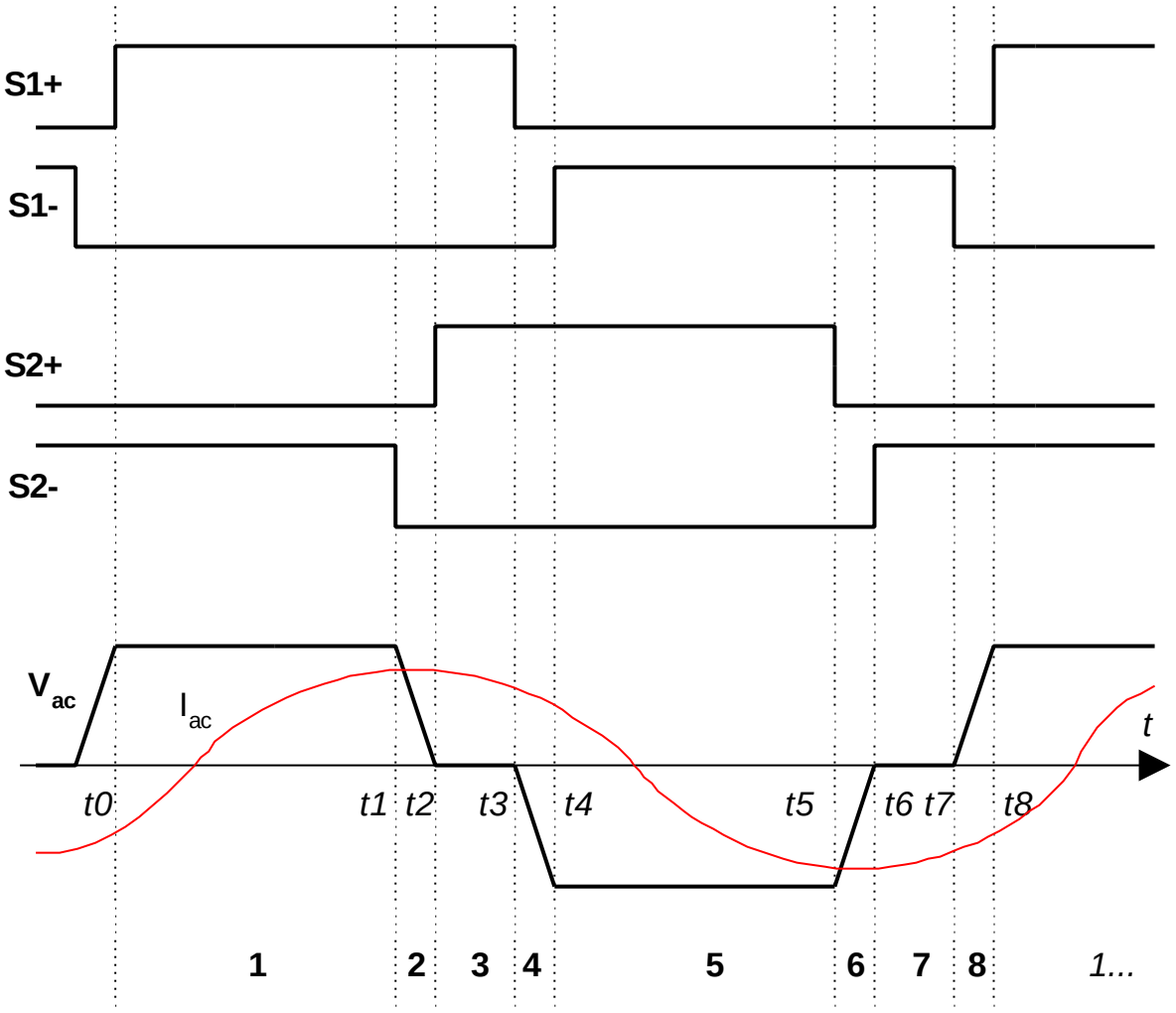


**Fig. 5-4: Soft switched waveforms of a voltage-fed series resonant converter**

State 3: t2-t3. S2+ is switched on at t2. If D2+ conducts, it clamps the voltage across S2+ to almost zero so that zero voltage switch-on of S2+ is achieved. In fact, S2+ is also switched "on" at zero current because it does not conduct before the current changes direction. Therefore, an ideal "soft" turn-on condition is obtained.

State 4: t3 - t4. S1+ switches off at t3. Similar to state 2, zero voltage switch-off of S1+ is achieved because the voltage across C1+ increases slowly. When C1- is fully discharged, D1+ begins to conduct.

State 5: t4 - t5. S1- is switched on at t4. If D1- conducts, then zero voltage switch-on of S1- is achieved. As both S1- and S2+ are on, the output track voltage is $-V_d$. In this period, similar to state 1, the current changes direction. In the beginning, the body diodes conducts, then the switches S1- and S2+ begin to conduct after the current changes direction.



InductEV, Inc.
Exhibit 1020
Page 159

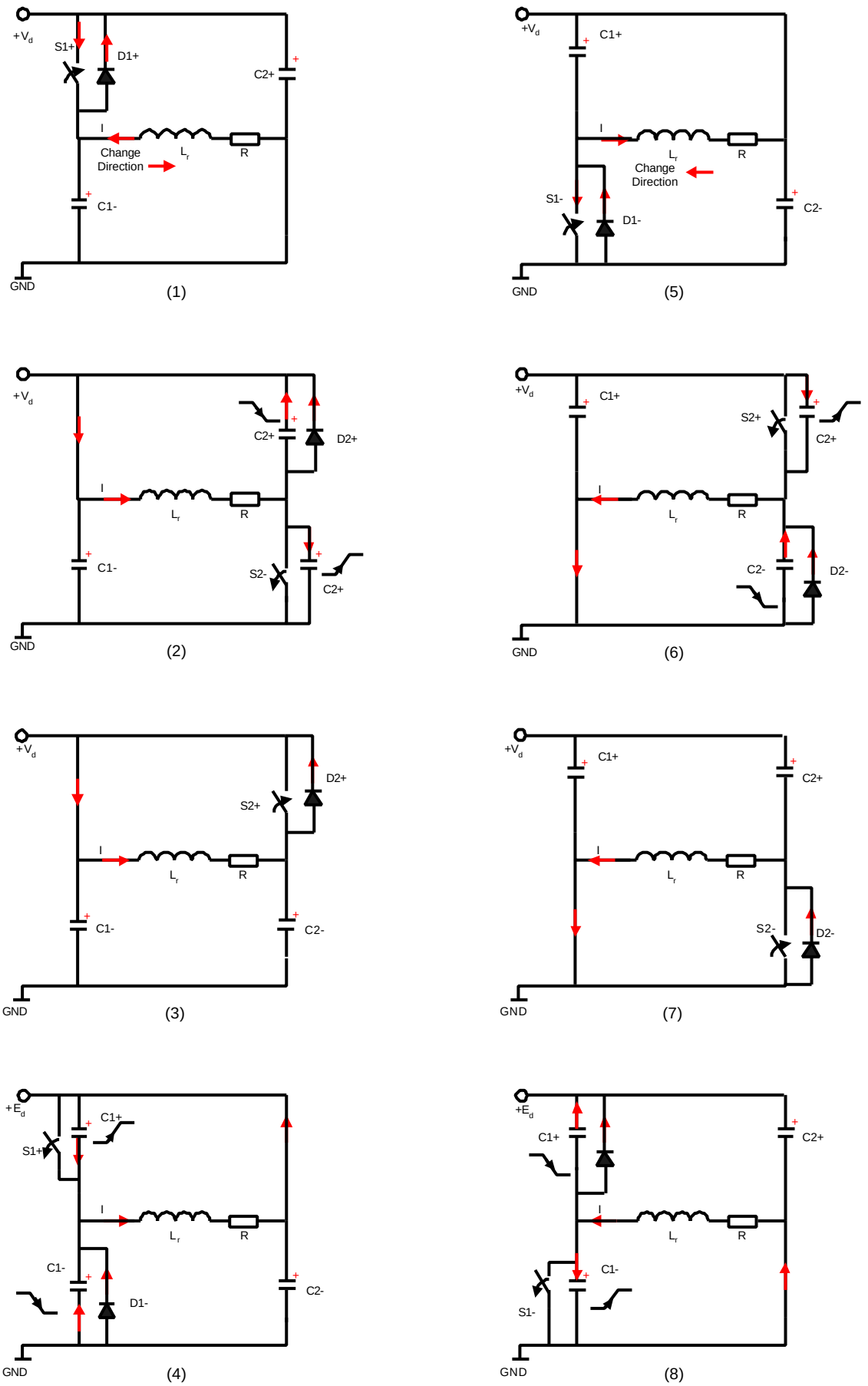


**Fig. 5-5: The soft switching process of a voltage-fed converter**



InductEV, Inc.
Exhibit 1020
Page 160

State 6: t5 - t6. S2+ is switched off at t5. The process is very similar to state 2 and 4, ZVS during "off" state is achieved for S2+. When C2- is fully discharged, D2- begins to conduct offering a zero voltage turn-on condition for S2-.

State 7: t6 - t7. S2- is switched on at t6. D2- conducts and clamps the voltage across S2- almost to zero so that zero voltage switch-on of S2 is achieved. Similar to other turn-on situations, after S2+ is switched on, it does not begin to conduct immediately since the current has not changed direction.

State 8: t7 - t8. S1- is switched off at t7. Zero voltage switch-off of S1+ is achieved due to the slow charge up of C1-. When C1+ is fully discharged, D1+ begins to conduct. After this, S1+ can be switched on at zero voltage and the switching cycle repeats from state 1.

From the above analyses it can be seen that due to the charging/discharging of the soft switching capacitors, the PWM output voltage waveform is trapezoidal rather than square wave. Switching occurs at zero voltage or zero current instants so that the switching losses are essentially eliminated. Moreover, the stresses on the semiconductor devices are alleviated as all the transitions are "soft" at the switching instants. There are essentially no reverse recovery problems for the diodes. Compared to direct hard switching methods, an additional advantage of this soft switching technique is that electromagnetic interference is reduced due to reduced dv/dt, di/dt and improved resultant track current waveforms.

However, the above analysis also shows that this soft switching is conditional. Specifically, the turn-on of the switches is critical. If the soft switching capacitors are not completely charged/discharged during the dead time, the residue voltage will be shorted by the switches during turn-on, which may cause the switching devices to fail. The essential issue here is that the track must be tuned above resonance which ensures the track impedance is inductive and the current has the right polarity to charge/discharge the capacitors. Also, the inductive energy stored in the track in the residual inductance needs to be large enough to charge/discharge the capacitors fully to avoid shorting these capacitors during turn on.

Assuming the track current is constant at $I_L$ during the dead time, the charging/discharging process can be modelled with the simple circuit shown in Fig. 5-6. Considering the initial conditions $V_{c1}(0)=V_d$ and $V_{c2}(0)=0$ when switch S is tuned off at time t=0, the voltage across the capacitor C1 during its discharging period (before the diode D starts to conduct) can be expressed as:



InductEV, Inc.
Exhibit 1020
Page 161

$$v_{c1} = V_d - \frac{I_L}{2C} t \tag{5-4}$$

where C1=C2=C, and $V_d$ is the DC power supply voltage. If the dead time is given as Δt, from this equation, it can be shown that the following condition should be met to guarantee safe soft switching operation

$$C < I_L \frac{\Delta t}{2V_d} \tag{5-5}$$

when designing the soft switching capacitors. If the capacitance is too large, the track residual inductor will not be able to fully charge/discharge it. As a result, their parallel switches at turn-on will short circuit the capacitors. However, if the capacitance is too small, the capacitor voltages will increase too fast during the turn-on time and the soft switching will be practically impossible. Therefore, there is a trade-off between a desirable zero voltage switching condition and avoiding device failure.

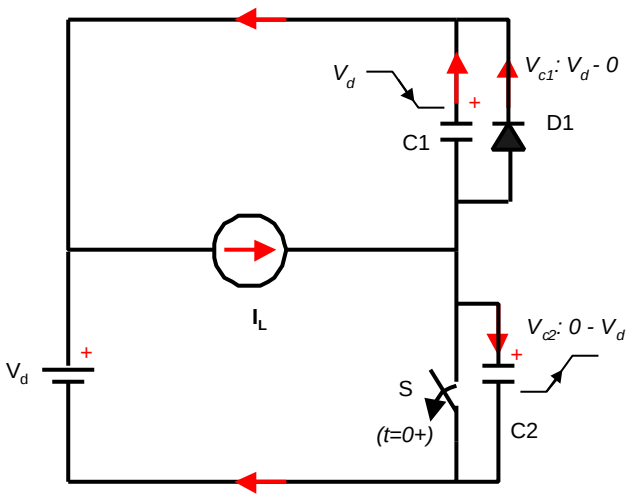


**Fig. 5-6: Equivalent circuit of capacitor charging and discharging during dead time**

On the other hand, from the track network side proper track tuning is required to achieve soft switching. A basic requirement is that the track network should be able to supply enough inductive energy to charge up the soft switching capacitors. In practical operation, the parameters of the track inductor and its tuning capacitors may cause some variation in the residue inductance $L_r$. In addition, load changes also affect the track current value $I_L$ during the dead time period. Therefore, it is a non-trivial task to maintain the soft switching performance without compromising system security. Dynamic parameter tuning may be a solution, but a more economical approach is to allow the frequency to vary during operation. A self-sustained frequency control technique ensuring



InductEV, Inc.
Exhibit 1020
Page 162

above-resonant operation has been presented by Humberto, et al [7]. However, as large frequency variations can cause detuning problems in the pick-ups of an IPT system, these frequency variations should be carefully controlled in IPT applications, and careful circuit analysis and design are essential.

## 5.3 Improved Series-Parallel Resonant Converter Power Supplies

### *5.3.1 Dual Circuit Transformation from CLC Network to LCL Network*

For a fully tuned track at the nominal resonant frequency and under the steady state conditions, its equivalent impedance can be regarded as a pure resistor R. In this situation, a current-fed resonant tank with a CLC π matching network can be directly transformed into a voltage-fed dual circuit. Fig. 5-7 illustrates how the transformation is implemented. The basic process of the dual circuit transformation is to choose a node in each loop (see A, B, and C in Fig. 5-7) plus a common node O outside the circuit first, and then try to connect these nodes with their dual elements [8]. A direct conversion between a current source and a voltage source, an inductor and a capacitor can be carried out. A resistor branch is kept resistive after conversion but its resistance is inverted, or viewed in another way, its conductance is made equal to the original resistance value. In general, the rule is to replace the impedance of each branch with its inverse value. Note that after the dual circuit conversion, all the parallel and series relationships change. Fig. 5-7 shows that how a current-fed CLC π network is transformed into a voltage-fed LCL T network.

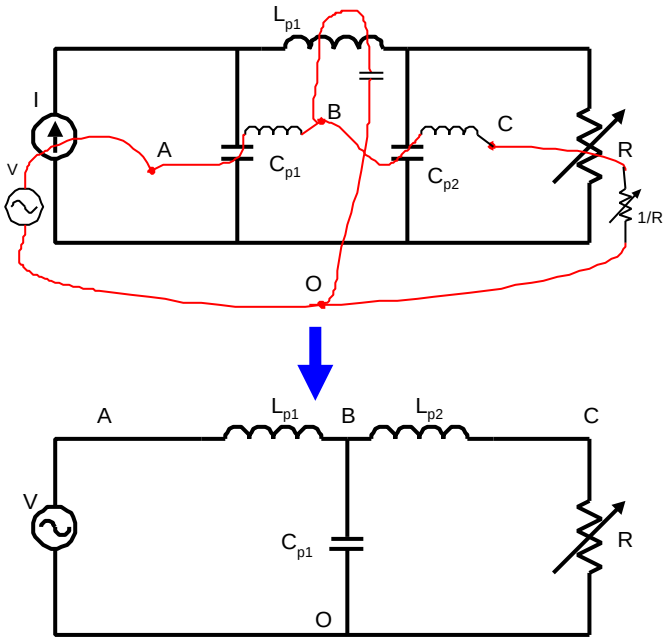


**Fig. 5-7: Dual transformation from current-fed CLC network to voltage-fed LCL network**



InductEV, Inc.
Exhibit 1020
Page 163

Because of the dual-circuit properties, the input admittance of the LCL network is the same as the input impedance of its dual CLC network. As such, all the good features of the CLC network used for the current-fed resonant converter also exist here for the LCL network.

Firstly, from the track output side, the track current is constant provided the input voltage is constant. This is true as long as $L_{p1}$ is fully tuned with $C_{p1}$ at the nominal frequency regardless of whether $L_{p2}$ is tuned. The reason is that $L_{p1}$ and $C_{p1}$ cancel each other out after a Norton equivalent circuit transformation from a voltage source to a current source, leaving a constant current source output with an infinite output impedance as shown in Fig. 5-8 (a)-(b).

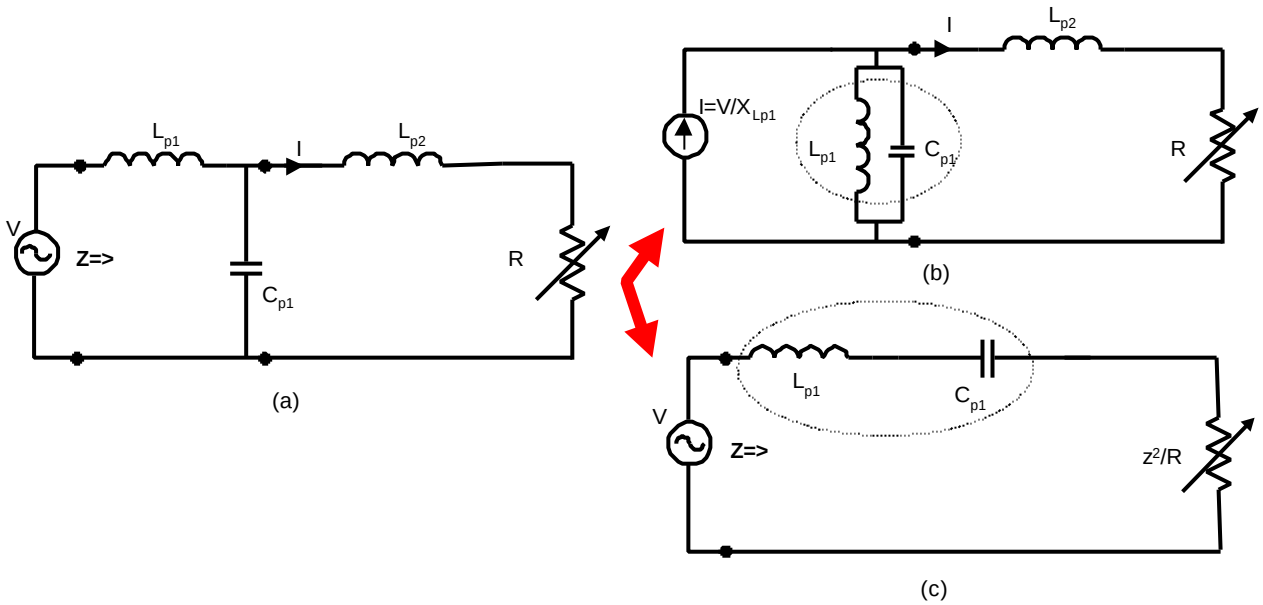


**Fig. 5-8: Constant track current and unity power factor properties of the LCL network**

Secondly, the phase angle of the input admittance is zero if the network is fully tuned. This feature can be illustrated with an impedance transformation as shown in Fig. 5-8 (a)-(c). The transformation is based on the fact that *the input impedance of a resonant circuit comprising a parallel capacitor and an inductor with a series resistor is equivalent to a single branch comprising a capacitor in series with a resistor*. It can be shown that the equivalent capacitor value does not change, while the equivalent resistor is equal to:

$$R_{eq} = \frac{L}{RC} = \frac{z^2}{R} \qquad (5\text{-}6)$$

where z= $\sqrt{L/C}$ is the characteristic impedance of the circuit which is also equal to the reactance of each tuned reactive element. As the equivalent capacitor after the above transformation cancels the



InductEV, Inc.
Exhibit 1020
Page 164

inductor $L_{p1}$ (as shown in Fig. 5-8(c)), the final input impedance of the network will be a pure resistor with unity power factor.

Similar to the current-fed CLC network, the LCL network also functions as a good band filter filtering the noise between the input power source and the track current output. Consequently, the system EMI is alleviated.

### *5.3.2 Zero Current Switching Operation*

Using the above transformation, a voltage-fed converter with series-parallel LCL network as shown in Fig. 5-9 can be formed. The IPT power supply based on this converter is named a voltage-fed G3 power supply because it is transformed from the current-fed G3. However, It should be noted that the voltage-fed G3 is not exactly the dual circuit of the current-fed G3 when the series track tuning is considered. This is because in an exact dual circuit transformation, the standard series tuned track (series loaded) will become a standard parallel tuned track (parallel loaded). Although this does not make any difference at steady state for a fully tuned track, the system dynamic property may be varied.

The voltage-fed G3 can be regarded as a voltage-fed series resonant converter with a LCL T network inserted in the middle. This network improves the system performance greatly. A direct advantage of this configuration over the current-fed one is that part of the track inductance may be used for $L_{p2}$ so that practically $L_{p2}$ may not be required. As such, the system cost and size can be reduced. It is worth noting that if $L_{p2}$ is considered as part of the track, the voltage-fed G3 can also be viewed as a G2 power supply with an LC filter at the input to the track network.

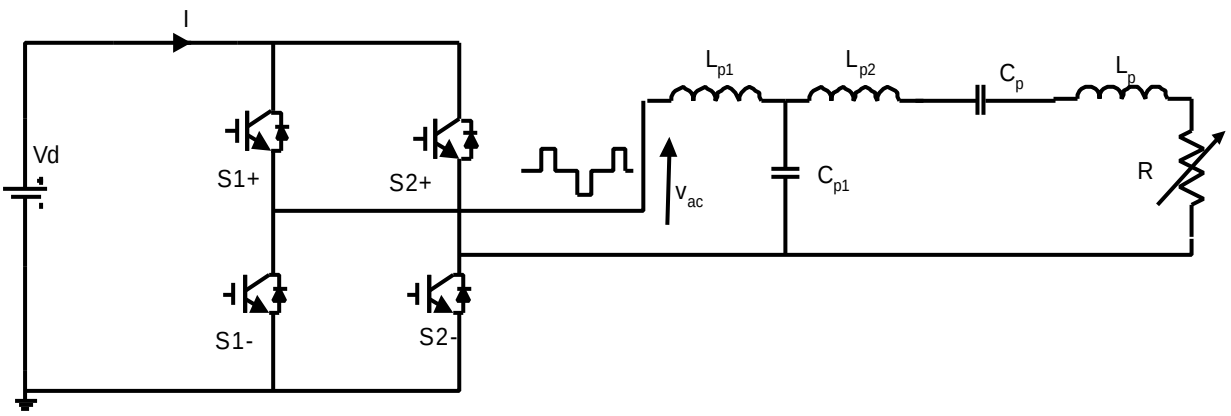


**Fig. 5-9: Improved voltage-fed series-parallel resonant converter (G3)**



InductEV, Inc.
Exhibit 1020
Page 165

There are several ways to run this voltage-fed resonant converter. Analogous to ZVS operation in the current-fed G3 power supplies, ZCS (Zero Current Switching) operation may be achieved for voltage-fed G3 power supplies. As the input admittance/impedance phase angle of the tuned track network is zero, the fundamentals of the voltage and current waveforms are in phase. Therefore, voltage commutation can be controlled at zero current instants and ZCS operation around the nominal resonant frequency is feasible in principle.

However, for a practical voltage-fed converter, a dead time must be considered for safe operation, ie, a blanking period must exist between switch transitions. This makes accurate ZCS impossible at high operating frequencies due to the rapid increase in current magnitude during the dead time. For practical switches with anti-parallel body diodes, at least one switching state, either during turn-on or turn-off will not occur at zero current instants. Therefore, strictly speaking ZCS cannot be fully achieved. However, at low frequencies, the dead time is relatively short compared with the switching period so that ZCS can be approximately achieved.

### *5.3.3 Duty Cycle Track Current Regulation and Soft switching Operation*

An obvious advantage of the voltage-fed resonant converters over the current-fed resonant converters is the duty cycle control. For G2 power supplies, as discussed, the phase-shift duty cycle control is a basic means of keeping the track current constant. As for the LCL voltage-fed G3 power supplies, since the network converts the voltage source to a current source, theoretically no control is required to keep the track current constant. However, practically the input power supply voltage may vary and the system parameters may shift away from their nominal values. Therefore, a track current controller may be required and this can be done via duty cycle regulation. Nevertheless, compared to the basic voltage-fed parallel resonant converter where the voltage has to vary in accordance with the load, the duty cycle regulation required for the LCL series-parallel resonant converter can be very small owing to the improved network property.

For similar reasons as discussed in the previous section, the effect of the dead-time and the need for duty cycle regulation makes ZCS operation at full resonance impossible. To solve this problem, soft switching techniques used for G2 power supplies may also be employed in voltage-fed G3 power supplies. If the LCL network is not fully tuned but leaves a residue inductance, soft switching may be achieved by adding additional soft switching capacitors in parallel with the switching devices. This can be regarded as combining both conventional PWM and resonant techniques. The main idea is to utilise “local resonance” around the switching transitions so as to improve the switching



InductEV, Inc.
Exhibit 1020
Page 166

conditions. As such, the flexibility of PWM control and the advantages of soft switched resonant converters are combined.

As little duty cycle regulation is required for voltage-fed G3 power supplies, the soft switching condition is easier to meet and less affected by the loading conditions at steady state. However, due to the increased system order, the system dynamics become complex to analyse so that it is very challenging to guarantee soft switching operation during system transients such as at start-up and load changes. If soft switching is not achieved, the momentary shorting of the soft switching capacitors that results may cause switching devices failure.

Note that if the track is not fully tuned, leaving an impedance of R+jX, then it can be shown that the referred impedance to the input port of the LCL network is:

$$Z_{eq} = \frac{z^2}{R + jX} \tag{5-7}$$

where $z = \sqrt{L_{p1} / C_{p1}}$ is the characteristic impedance of the LCL network. This equation means that the LCL network can change the track impedance property from inductive to capacitive, and vice versa. Therefore, in order to ensure the net inductance at the input port of the track network appears inductive, the track itself (excluding the part used as an inductor of the LCL network) should be tuned to have a capacitive property.

## 5.4 Simulation/Experimental Results and Discussion

### *5.4.1 Basic voltage-fed series resonant converter power supply*

A voltage-fed series resonant converter (see Fig. 5-1) used in a practical G2 IPT power supply with a maximum rating of 2kW/2km for a road stud (cat's eye) application [9-10] has typical parameters shown in table 5-1. In place of each power switch (S1+, S1-, S2+, and S2-) shown in Fig. 5-1, two MOSFETs (IRFP460, 500V/20A/0.27Ω) are put in parallel to increase the current handling capability. The positive temperature coefficient property of the MOSTETs balances the current sharing automatically thus makes the direct parallelling feasible. Two 10Ω resistors are connected at the gates of the paralleled MOSFETs individually to eliminate possible circuit oscillations.

Component level PSpice simulation of this power supply has been undertaken and Fig. 5-10 shows the gate drive signals and track voltage/current waveforms at a 700W load (3.6Ω). Note that the



InductEV, Inc.
Exhibit 1020
Page 167

track current is enlarged by 10 times in the same plot in order to view it alongside the track driving voltage. To get the 14A rms (about 20A peak) track current at a load of 700W, the duty cycle required is approximately 0.68, corresponding to a phase shift of $122.7^0$. It can be seen from this result that the track driving voltage drops to zero completely during the dead time (shown between the dotted vertical line in Fig. 5-10), which means ZVS operation is obtained as analysed previously.

**Table 5-1: Converter data of a voltage-fed parallel resonant IPT power supply**

| Symbol | Value | Notes |
|---|---|---|
| f | 38.4kHZ | Operating frequency |
| $V_d$ | 300V | DC power supply voltage |
| L | 326µH | Track inductance, being distributed along a track length of about 600m (0.54µH/m) |
| $X_L$ | 78.7Ω | Reactance of the track inductor |
| $I_L$ | 14A rms | Track current under the phase shift control |
| $V_{max}$ | 243V rms | Maximum track driving voltage from 300V DC power supply |
| \|Z\| | 17.4Ω | Maximum track impedance magnitude $\|Z\|=Vmax/I_L$ |
| Δt | 1.3us | Dead time to prevent momentary shorting of the switches |
| $C_p$ | 0.066µF | Track series tuning capacitor, 10 sets of 2 paralleled 0.33µF |
| $X_c$ | 62.8Ω | Susceptance of the tuning capacitor |
| Z | 3.6+j15.9Ω ($16.3\angle 77.2^0\Omega$) | Net impedance of the tuned track, at a 700W load |
| $L_r$ | 66.0µH | Equivalent net residue track inductance after the series tuning |
| V | 228V rms | Required track voltage for 700W load |
| C | 22nF | Capacitors for soft switching |

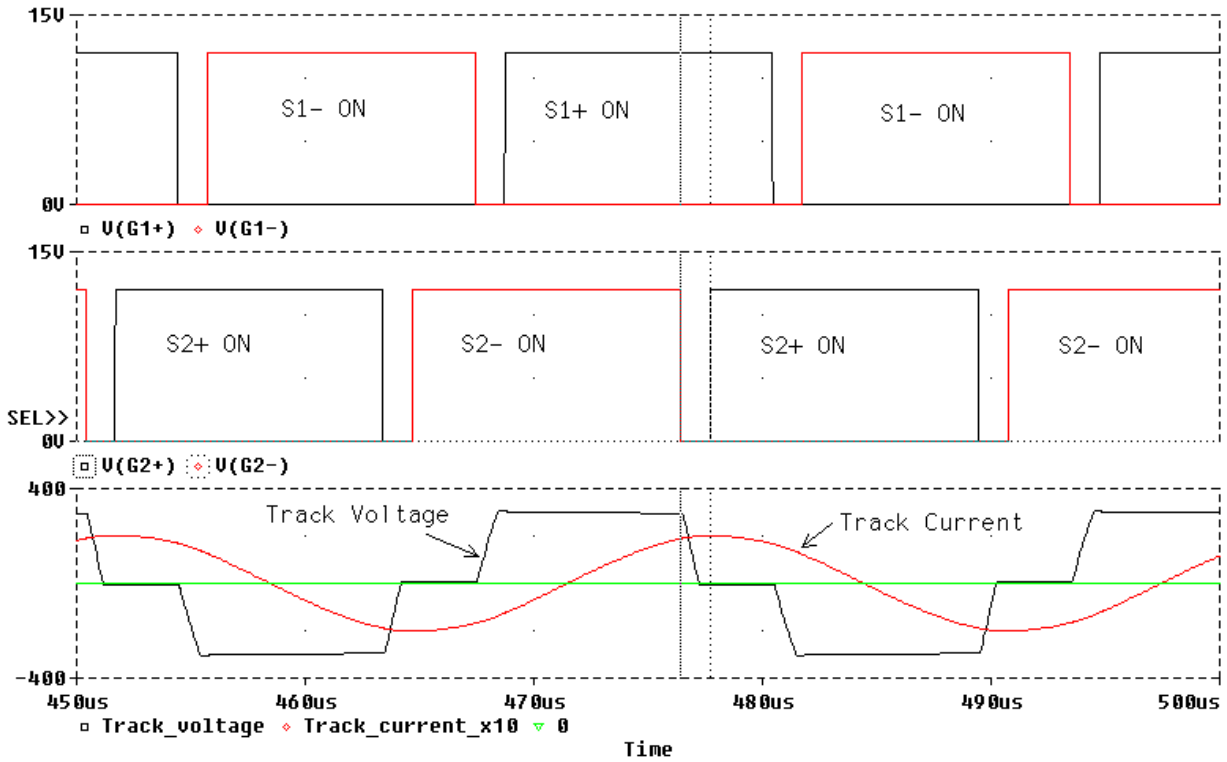


**Fig. 5-10: Simulated switching waveforms of a G2 power supply**



InductEV, Inc.
Exhibit 1020
Page 168

From the soft switching condition expressed in equation (5-5) it is easy to calculate that the maximum soft switching capacitance should be smaller than 30.3nF with the parameters given in table 5-1. Because 22nF is used in practice, soft switching operation is achieved safely even when the parasitic output capacitor of the MOSFET which is about 870pF is considered. To observe this operation more clearly, Fig. 5-11 shows the switching waveforms for one switch (S1-). Its gate signal, the charge/discharge current of the soft switching capacitor, and the voltage and current are all shown. It can be seen that before S1- turns on, its soft switching capacitor has already fully charged and its body diode is on (reverse current), so that S1- turns on at a zero voltage. The actual current transition from the body diode to this power switch occurs naturally when its current changes direction. During the turn-off period when the current goes to zero as shown, the voltage across the switch is very small owing to the slow charging process of the soft switching capacitor. Therefore, the desired soft switching operation is achieved and the switching stresses and power losses are minimised.

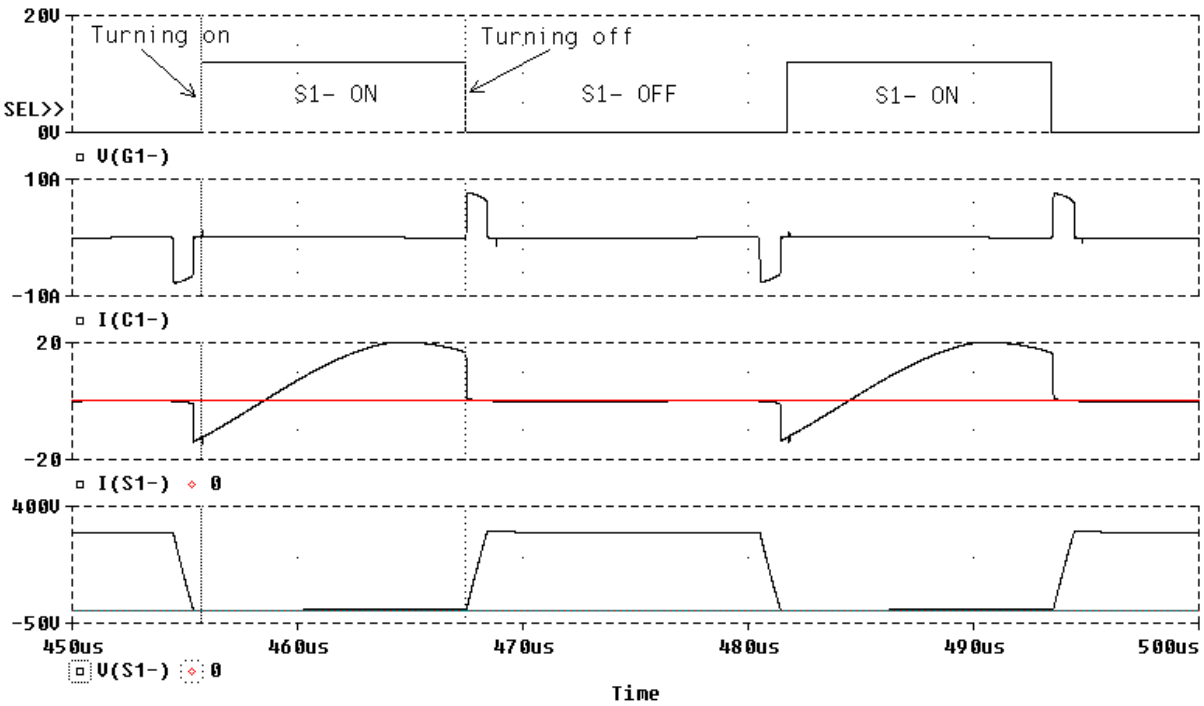


**Fig. 5-11: Gate signal and switching waveforms of one of the switches**

Measurements on a practical experimental supply are shown in Fig. 5-12. A Tektronix high voltage differential probe P5200 with a voltage ratio of 1V/500V, and a Rogowski Coil current waveform transducer CWT1B with a sensitivity of 20.0mV/A have been used for the measurement. It can be seen that the peak track driving voltage reading (channel 1) is 300V, the peak track current reading



InductEV, Inc.
Exhibit 1020
Page 169

(channel 2) is about 20A (14A rms), and the operating frequency is 38.5kHz. The practical waveforms are in good agreement with analysis and simulation results.

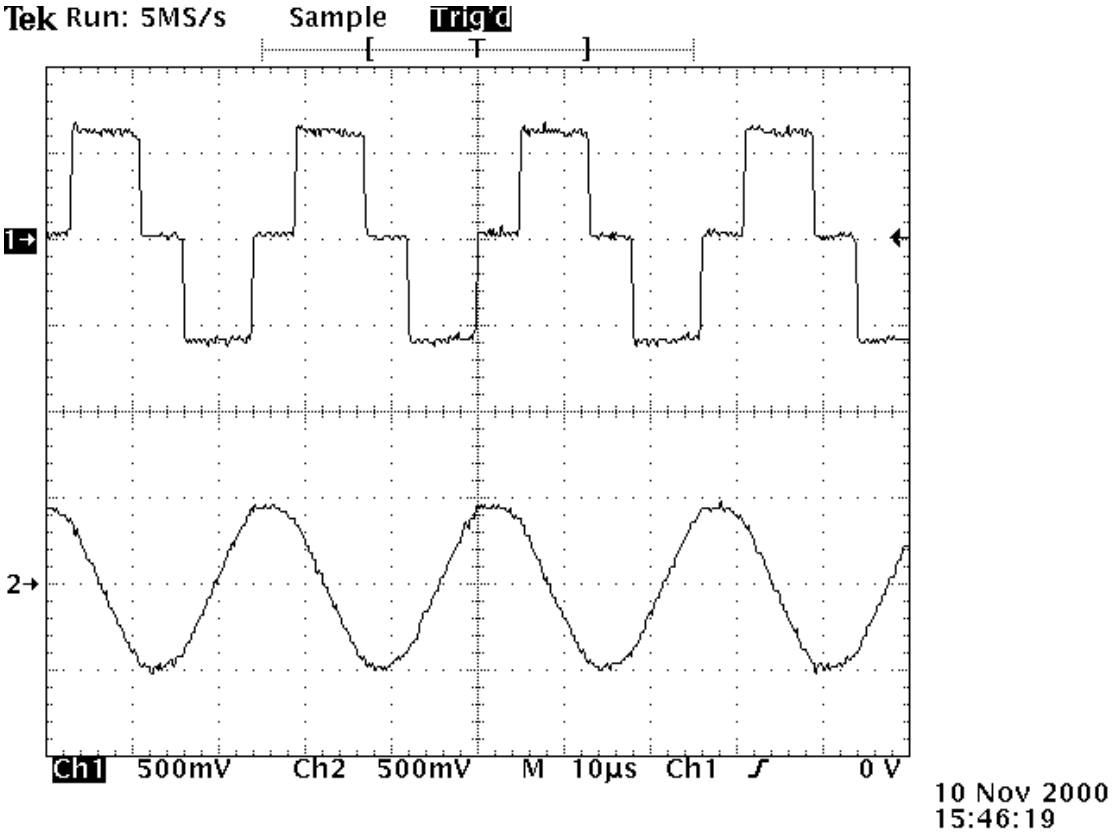


**Fig. 5-12: Measured voltage and current waveforms of a practical G2 power supply**

### *5.4.2 Discussion on the voltage-fed G3 power supply*

The above basic voltage-fed series resonant converter can be easily developed into a series-parallel resonant converter by inserting an LCL network (Fig. 5-9). Based on the data of the basic parallel resonant converter (Table 5-1), the LCL network parameters are designed to obtain the required track current at a certain driving voltage out of the inverter, in this case, it is 14A rms at 270V rms fundamental at a nominal frequency of 38.4kHz. The newly modified parameters are shown in Table 5-2. The basic design procedure and equations are very similar to those used for the current-fed G3 power supplies due to the dual circuit property. Note that no soft switching capacitors are used, and the track is fully tuned at the nominal resonant frequency.

If the operating frequency is forced at the nominal resonant frequency 38.4kHz, the designed track current of 14A rms is obtained at the given load of 700W as shown in Fig. 5-13. However, the input current waveform can be very poor. The voltage (square wave) and the current zero crossings are not in phase even at steady state. As a result, ZCS is not achieved and the stresses and switching



InductEV, Inc.
Exhibit 1020
Page 170

losses are high. In fact, Fig. 5-13 shows that the current does not go to zero naturally in this case although the system is running at the zero phase angle frequency of the linear track network. Unlike a second order network, it is difficult to determine the zero current crossing conditions for this converter, because the dynamic effects of the harmonics is difficult to analyse in such a high order system. The situation is worse if soft switching capacitors are added and duty cycle control is employed. Similar to the current-fed G3 power supplies, adding a reactive bias network may help to achieve ZCS and improve the waveform quality.

**Table 5-2: Parameter modifications for the improved voltage-fed G3 power supply**

| Symbol | Value | Notes |
|---|---|---|
| $C_p$ | 52.7nF | Track tuning capacitor , fully tuned with the equivalent track inductance of 326µH |
| $L_{p1}$=$L_{p2}$ | 79.9µH | Inductors of the LCL network, $L_{p2}$ can be part of the track inductor |
| $C_{p1}$ | 0.215µF | Capacitor of the LCL network, fully tuned with $L_{p1}$ and $L_{p2}$ |
| $X_{LCL}$ | 19.3Ω | Reactance of the LCL network, determined by the full AC voltage and the track current |
| Vmax | 270V rms | The maximum AC output voltage from the inverter at a 300V DC power supply |
| R | 3.6Ω | The equivalent load resistor at a 700W load |

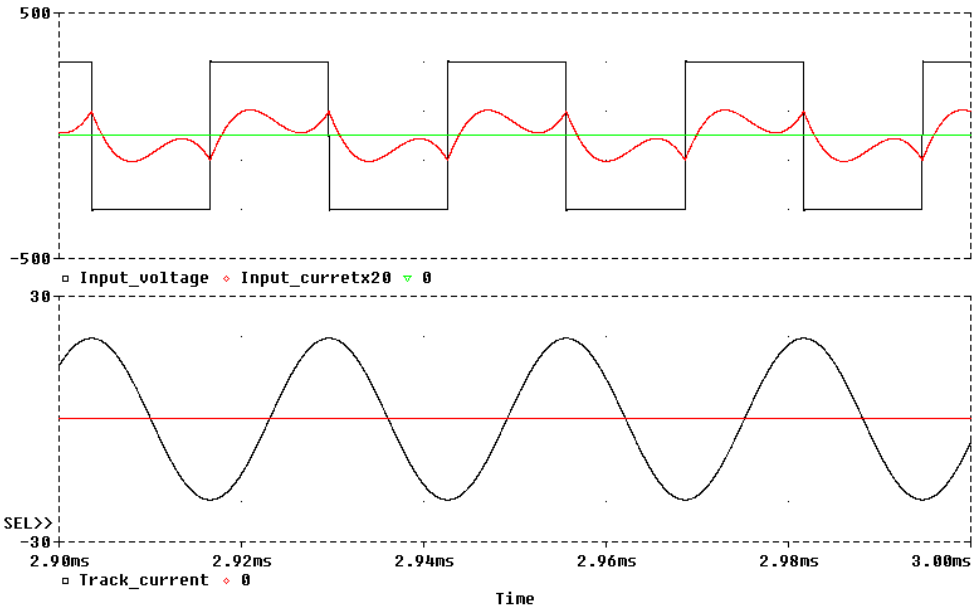


**Fig. 5-13: Voltage-fed LCL resonant converter running at nominal frequency**

If the power switches are dynamically controlled to track the zero crossing instants of the input current, then ZVS operation as shown in Fig. 5-14 can be obtained. Due to dead time requirements, the voltage transition does not occur exactly at zero current instants, but the error is negligible. Note that the actual operating ZCS frequency, which is about 28.6kHz, is smaller than the nominal resonant frequency 38.4kHz, so that the whole system, including the LCL network, is detuned. The resultant track current is much higher (about 225A peak, 160A rms) than its nominal value 14A



InductEV, Inc.
Exhibit 1020
Page 171

rms. This means that the ZCS frequency drifts away so that the system is found to operate naturally at another “mode”. Other ZCS frequencies may exist owing to chaos and bifurcation features of the nonlinear system. In a normal resonant converter design, the system parameters are only tuned at the nominal frequency. However, for a high order system, this may be unnecessary since the circuit tuning could be designed for operation at other resonant modes, and such a design may significantly reduce the system size and cost. While this is a very interesting problem worth investigating, it is beyond the scope of this thesis.

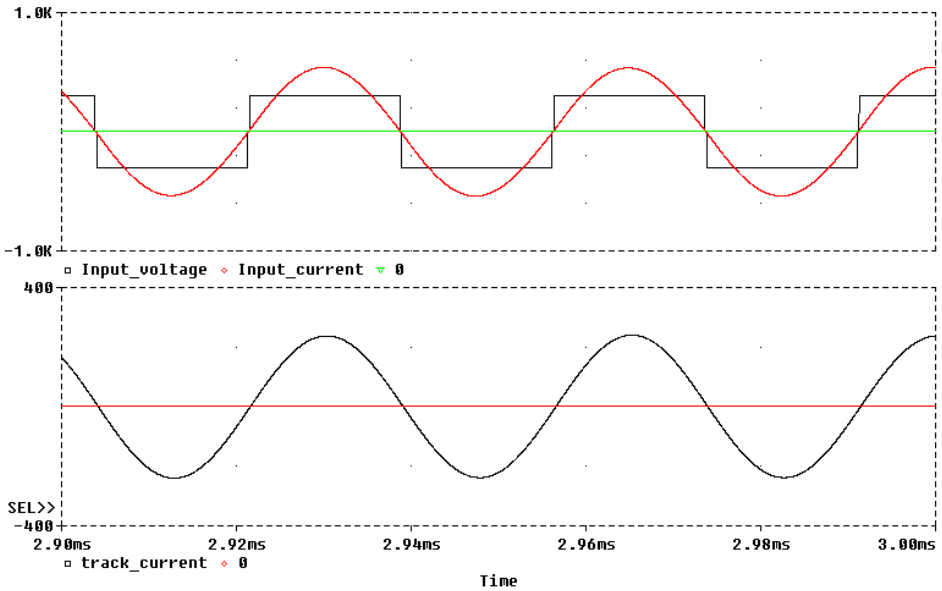


**Fig. 5-14: Detuned ZCS operation of a voltage-fed LCL resonant converter**

## 5.5 Summary

In this chapter, the voltage-fed resonant converters have been shown to have greater freedom in control compared to the current-fed resonant converters. The chapter has focussed on the analyses of two voltage-fed resonant converter power supplies. In particular, basic voltage-fed series resonant converter IPT power supply (G2) as well as its improved version - a voltage-fed G3 power supply, have been discussed.

The mechanism of the closed-loop phase-shift control of the track current has been analysed first. Then, an in-depth analysis of the soft switching operation of the G2 power supply has been undertaken with detailed switching sequences and waveforms presented. The soft switching condition has been determined using a simplified capacitor charge/discharge model. The validity of the analysis has been backed up with simulations and experimental measurements.



InductEV, Inc.
Exhibit 1020
Page 172

Using a dual circuit transformation, the current-fed G3 power supply was developed into a voltage-fed G3 power supply with the adoption of an LCL T network. Similar to the CLC π network used in the current-fed G3 power supply, the LCL network improves the system properties significantly. It supplies a constant track current from a constant voltage, offers a unity power factor input at the nominal frequency, and functions as an EMC filter. Theoretically, a voltage-fed G3 power supply can run at a fixed frequency without using phase-shift duty cycle control. The simulation results have proven that it is very easy to obtain a desirable constant track current. However, achieving soft switching operation is challenging due to the complexities involved in the dynamics of the high order system. It has been found that the system may operate at other resonant modes away from nominal frequencies. These operation modes may be used advantageously in system tuning and controller design.

## 5.6 References

[1] Trzynadlowski, A. M.: *Introduction to modern power electronics*, John Wiley & Sons, 1998.

[2] Hu, A. and Boys, T: "Current sourced CLC, G3 IPT Track Power Supply, Stage II: Research and Development Investigation", *Research Report of Auckland Uniservices Ltd* for Wampfler AG, Germany, 78 pages, March 1999.

[3] Irwin, J. D.: *Basic engineering circuit analysis*, 4th edition, Maxwell Macmillan International, 1993.

[4] Wilkinson, J: "Series tuned IPT – A hemi J Perspective", *Research Report of Auckland Uniservices Ltd*, the University of Auckland, 1996.

[5] Green, A. W. and Boys, J. T.: "10kHz Inductively coupled power transfer – concept and control", *IEE Power Electronics and Variable Speed Drives Conference*, PEVD, Pub.399, pp.694-699, 1994.

[6] Jiang, H. J., Maggetto, G. and Lataire, P.: "Steady-state analysis of the series resonant DC-DC converter in conjunction with loosely coupled transformer - above resonance operation", *IEEE Transactions on Power Electronics*, Vol.14, No.3, May 1999.

[7] Pinheiro, H., Jain, P. K., and Joós, G.: "Self-sustained oscillating resonant converters operating above the resonant frequency", *IEEE Transactions on Power Electronics*, Vol.14, No.5, September 1999.

[8] Skilling, H. H.: *Electric Networks*, John Wiley & Sons, Inc., 1974.



InductEV, Inc.
Exhibit 1020
Page 173

[9] Gurr, W: "Hardings road studs: 2kW series tuned IPT power supply", *Research Report of Auckland Uniservices Ltd, the University of Auckland*, 1997.

[10] Boys, J. T. and Green, A.W.: "Intelligent road-studs – lighting the paths of the future", *IPENZ Transactions*, No.24, (1) EMCH, pp.33-40, 1997.



InductEV, Inc.
Exhibit 1020
Page 174

## Chapter 6

# Mathematical Modelling of a Current-fed IPT System

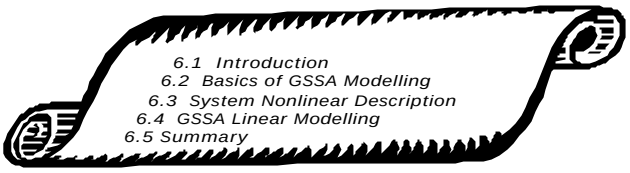


## 6.1 Introduction

With the development of numerical techniques and fast advances in computer software and hardware technologies, circuit simulation has become very popular. Being regarded as a "cheap experiment", it is widely used to check the validity of circuit designs before actual implementation. Nevertheless, such simulations often give little physical insight into the inter-relationships between the system parameters, so that the analysis and design of large and complex systems may remain a tedious "trial and error" exercise. This is particularly true for power electronic circuits where non-linearity is an inherent feature. In this respect, obtaining good mathematical models continues to be invaluable in revealing the circuit properties and guiding the system design. For this reason, considerable effort has been invested into the development of suitable mathematical models for nonlinear circuits, among which the state space averaging method developed by Middlebrook and Cuk appears the most successful [1]. The basic averaging technique has been widely used for DC-DC converter analysis and design [2], however, it is not valid for modelling resonant converters since one of its major assumptions is that the state variables of the converter should be slowly time-varying compared with the switching frequencies. This is clearly not true for resonant converters whose variables exhibit predominantly oscillatory behaviour. A modified state space averaging approach proposed by Xu and Lee [3] partially relaxed the constraints on the input variables of the state space averaging model so that it could be used for modelling quasi-resonant converters, but this approach is still not applicable for full resonant converters.



InductEV, Inc.
Exhibit 1020
Page 175

A generalised state space averaging (GSSA) method proposed by Sanders et. al. is valid for modelling a wider range of converters [4] although its modelling process is more difficult. It is particularly suited to full resonant converters which inherently generate quasi sine wave voltage and current waveforms at an approximately constant frequency. Compared to other resonant converter modelling techniques such as, approximate steady-sate AC analysis [5], Fourier series superposition [6], state-plane description [7-8], time-domain differential equation solutions [9-10], etc, this GSSA method is unique in representing state variables over a windowed view that is applicable to both slow time-varying "DC" variables and fast oscillatory "AC" variables. The method is valid for both steady state and dynamic analysis, and the order of a GSSA model can be arbitrarily determined according to the variable characteristics and the required accuracy. Green [13] has successfully employed this method in modelling a parallel resonant converter with a second order resonant tank. However, to date no work has been reported on modelling high order IPT power supplies with loosely coupled power pick-ups.

In this chapter, a complete 9$^{th}$ order current-fed G3 IPT power supply, including 16 pick-up loads, is modelled using GSSA. The basic properties of this current-fed G3 supply has been studied in Chapter 4 of this thesis by means of approximate steady-state AC analyses and computer simulations. Here it is taken as an example of applying the GSSA modelling technique. As the current-fed G3 is a further development of the current-fed G1 supply discussed in Chapter 3, the models developed in this chapter are fully applicable to G1 IPT power supplies. The basic modelling method is also valid for voltage-fed resonant converter power supplies discussed in Chapter 5 which are, in fact, easier to model due to the direct track voltage driving properties and reduced system order.

## 6.2 Basics of GSSA Modelling

As illustrated in Fig. 6-1, the GSSA (Generalised State Space Averaging) modelling method is based on a sliding window representation of dynamic variables. The basic concept results from the fact that any waveform x(t) on a time interval [t : t+T] can be expressed in Fourier series as:

$$x(t) = \tfrac{1}{2}a_0 + \sum_{n=1}^{\infty}(a_n \cos wnt + b_n \sin wnt) \qquad (6\text{-}1)$$

where $\tau \in [0,T]$, $\omega=2\pi/T$, and T is a chosen period of a sliding window. It is called a sliding window because the position of the window moves with time. The variable x(t) is not necessarily periodic



InductEV, Inc.
Exhibit 1020
Page 176

but can be imagined so by assuming the window repeats over all the time span. As such, a Fourier series (6-1) exists and its coefficients can be determined from:

$$a_n = \tfrac{2}{T}\int_t^{t+T} x(t)\cos(nwt)dt \qquad b_n = \tfrac{2}{T}\int_t^{t+T} x(t)\sin(nwt)dt \qquad (6\text{-}2)$$

Note that these coefficients are time dependent, meaning that the average value $a_0/2$ and the amplitude $\sqrt{a_n^{\,2}+b_n^{\,2}}$ of each component change with time when the window moves. In other words, the coefficient $a_n$ and $b_n$ can reflect the envelope of the original signal x(t). However, since $a_n$ and $b_n$ are independent with the phase angle of each component unknown, using $a_n$ and $b_n$ to represent the original variable x(t) can result in many mathematical difficulties which makes mathematical modelling practically impossible. An alternative approach is to express the Fourier series in a complex number exponential form as:

$$x(t) = \langle x\rangle_0 + \sum_{n=1}^{\infty}\langle x\rangle_n e^{jwnt} + \sum_{n=1}^{\infty}\langle x\rangle_{-n} e^{-jwnt} = \sum_{n=-\infty}^{\infty}\langle x\rangle_n e^{jwnt} \qquad (6\text{-}3)$$

where the complex number coefficients exist in conjugates and can be expressed as:

$$\langle x\rangle_n = \tfrac{1}{2}(a_n - jb_n) = \tfrac{1}{T}\int_t^{t+T} x(t)e^{-jwnt}dt$$
$$\langle x\rangle_{-n} = \langle x\rangle_n^{*} \qquad n=0,1,2... \qquad (6\text{-}4)$$

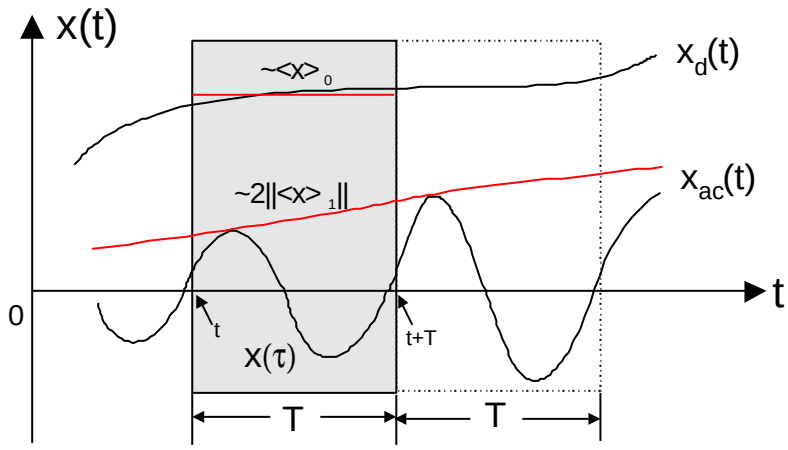


**Fig. 6-1: Illustration of the GSSA (Generalised State Space Averaging) modelling method**

Note that $\langle x\rangle_n$ are time-dependent complex variables. After such a transformation, the original time domain variable x(t) is expressed with new conjugated complex variables. If these variables are



InductEV, Inc.
Exhibit 1020
Page 177

solved, the time domain waveform $x(\tau)$ in any window $\tau \in [0, T]$, and consequently the original signal x(t) over the whole time range, can be obtained.

The required accuracy can be obtained from the above transformation by including sufficient high order terms in the Fourier series. However, this may lead to too many variables and eventually too high an order in the resultant model. Practically, if the period of the sliding window is well chosen, only one or two coefficient variables will be sufficient to represent the dominant components and the real time waveforms. For example, in Fig. 6-1, $<x>_0=a_0/2$ is normally good enough to represent the moving average of a slow varying signal $x_d(t)$ where the DC component dominates. In fact, this applies with conventional state space averaging modelling.

For resonant converters, besides slow time varying DC variables, many variables are quasi-sinusoidal, therefore, if the period T of the sliding window is chosen to be equal to or near the oscillation period of a waveform, the fundamental term of the variable in each sliding window will be a good representation of this waveform. Since $<x>_1$ and $<x>_{-1}$ are conjugates, $<x>_1$ is sufficient to represent the original variable. From equation (6-4) it can be seen that the envelope of the original signal can be approximated with $2\|<x>_1\|$ as illustrated in Fig. 6-1. Here $\|<x>_1\|$ denotes the second norm or modulus of the complex coefficient $<x>_1$.

In short, the main concept of GSSA modelling is to replace the real time domain variables with their complex Fourier coefficient variables over a sliding window. For a resonant converter, such a transformation may linearlise the nonlinear resonant circuit and lead to a dynamic linear model. The solution to the linear model can directly reflect the envelope of the original variables. It can also be transformed back to obtain the complete time domain waveforms of the original variables.

In a practical transformation, the following basic operations on the complex Fourier coefficients are normally required:

$$< x+u >_n = < x >_n + < u >_n \tag{6-5}$$

$$\frac{d < x >_n}{dt} = < \frac{dx}{dt} >_n - jw\, n < x >_n \tag{6-6}$$

$$< xu >_n = \sum_i < \mathrm{x} >_{n-i} < \mathrm{u} >_i \qquad i = 0, \pm 1, \pm 2 \cdots \tag{6-7}$$

where x and u are time domain variables and $<\bullet>_n$ denotes their nth order complex Fourier coefficients. In (6-7), the sum is taken over all integers, but in many cases only a few low order items of interest are taken into account since the high order items are negligibly small.



InductEV, Inc.
Exhibit 1020
Page 178

In addition, an existence function s(t) and a sign function sgn(x) can be useful in modelling the switching process of power electronics circuits. The existence function is defined in such a manner that it represents a train of square wave pulses with a magnitude of 1 or -1, while the sign function gives the sign of the input variable, i.e., the output is 1, 0, and -1 when the input is positive, zero, and negative respectively. The operation of these two functions is shown below:

$$\langle s(t)\rangle_n = \begin{cases} 0 & n = 0,2,4... \\ \dfrac{-2j}{np}\sin(\dfrac{pD}{2}) & n = 1,3,5... \end{cases} \tag{6-8}$$

$$< \mathrm{sgn}(x) >_1 = \frac{2}{p} e^{j\angle\langle x\rangle_1} \tag{6-9}$$

Here D is the duty cycle of the existence function s(t) in each half period.

## 6.3 Non-linear Description of a Current-fed G3 Supply

A current-fed full-bridge G3 IPT power supply with a 400 m track length and 16 pick-ups as described in Chapter 4 (see Fig. 4-13) is chosen as an example system for GSSA modelling. Each pick-up has a 650V battery load to drive a 10kW electric train. In this section the nonlinear switching process of the supply is represented mathematically allowing GSSA to be applied in the following section.

### *6.3.1 Circuit Representation with Controlled Sources*

Fig. 6-2 shows a representation of the current-fed G3 power supply. As the switching network of the primary track power converter simply inverts the voltage and current directions between the DC input side and the AC resonant side in each half switching cycle, therefore an existence function s(t) with a period of T and duty cycle of one is used to represent the switching process. In this way, the relationship between the DC and AC side can be described using controlled voltage and current sources as shown in the first dotted block in Fig. 6-2. Similarly, for a naturally commutated full bridge diode rectifier used in the pick-up battery charging circuits of this current-fed G3 supply, the



InductEV, Inc.
Exhibit 1020
Page 179

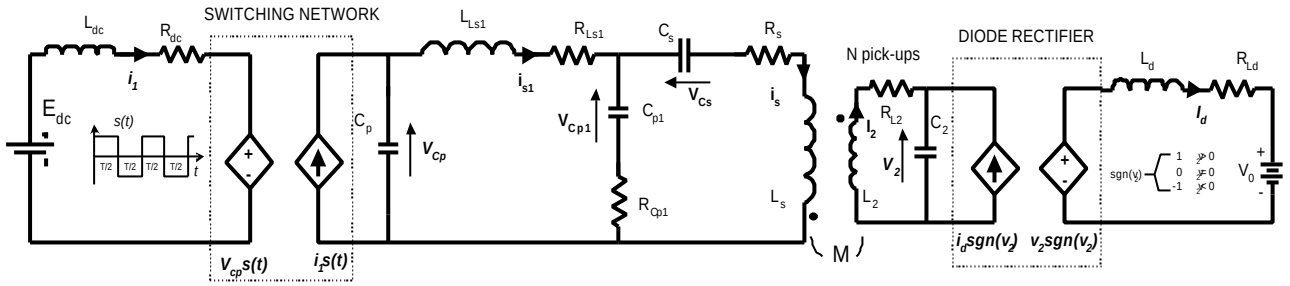


**Fig. 6-2: Equivalent circuit of a current-fed G3 IPT power supply**

switch transitions are determined by the polarity change of the resonant voltage $v_2$. Consequently a sign function sgn($v_2$) can be used to represent the circuit commutation as shown in the second dotted block in Fig. 6-2. After such a representation, the complete current-fed G3 power supply system including the pick-ups is simplified as an equivalent circuit shown in Fig. 6-2. In this circuit, all the switches are replaced with controlled voltage/current sources to simplify the mathematical modelling process.

Note that the following assumptions are made in the above representation:

***Switching devices are ideal***. The switching device voltage drops and transition times are ignored so that ideal voltage-controlled voltage-source and current-controlled current-source can be used to model the switching network and the diode rectifier of the current-fed G3 supply as shown in Fig. 6-2. Using ideal switches greatly simplifies the modelling process but does not cause significant error in the system dynamic analysis provided fast and low voltage drop switching devices are used.

***The battery charging current $i_d$ is continuous in the pick-up circuit***. This assumption ensures that the natural commutation of the full-bridge diode rectifier occurs when the polarity of the AC input voltage $v_2$ changes. Thus the relationship between the currents before and after the rectifier can be expressed as $i_{da}$=sgn($v_2$)$i_d$, where sgn($v_2$) is the sign function of $v_2$. In addition, the relationship between the voltages before and after the rectifier can be expressed as $v_{2d}$=$v_2$ sgn($v_2$)=|$v_2$|, where |$v_2$| denotes the absolute value of $v_2$.This assumption is essentially true due to the current-source output property of the parallel tuned pick-up and the existence of the output DC inductor $L_d$.

***Two equivalent series resistances are ignored***. It can been seen from Fig. 6-2 that the equivalent series resistances of the track network input tuning capacitor $C_p$ and the pick-up tuning capacitor $C_2$ are ignored. The reason for doing so is to simplify the circuit representation without causing much error as the voltage across the track and pick-up resonant capacitors $C_p$ and $C_2$ are relatively constant and low. The equivalent resistance $R_{cp1}$ is left in the equivalent circuit since the track



InductEV, Inc.
Exhibit 1020
Page 180

driving voltage across the capacitor $C_{p1}$ can be very high at heavy loads causing a large current and high power loss in $R_{cp1}$.

### 6.3.2 Nonlinear Differential State Space Equations

Choosing inductor currents and capacitor voltages in the equivalent circuit of Fig. 6-2 as state variables, the nonlinear time-variant 9th order state-space equations can be set up following standard techniques [11] as:

$$\begin{cases} \dfrac{di_1}{dt} = -\dfrac{R_{dc}}{L_{dc}} i_1 - \dfrac{1}{L_{dc}} s(t) v_{cp} + \dfrac{1}{L_{dc}} e_{dc} \\ \dfrac{dv_{cp}}{dt} = \dfrac{1}{C_p} s(t) i_1 - \dfrac{1}{C_p} i_{s1} \\ \dfrac{di_{s1}}{dt} = \dfrac{1}{L_{s1}} v_{cp} - \dfrac{r_1}{L_{s1}} i_{s1} - \dfrac{1}{L_{s1}} v_{cp1} + \dfrac{R_{cp1}}{L_{s1}} i_s \\ \dfrac{dv_{cp1}}{dt} = -\dfrac{1}{C_{p1}} i_{s1} + \dfrac{1}{C_{p1}} i_s \\ \dfrac{dv_s}{dt} = \dfrac{1}{C_s} i_s \\ \dfrac{di_s}{dt} = \dfrac{L_2 R_{cp1}}{\det} i_{s1} + \dfrac{L_2}{\det} v_{cp1} - \dfrac{L_2}{\det} v_s - \dfrac{L_2 r_2}{\det} i_s + \dfrac{NMR_2}{\det} i_2 + \dfrac{NM}{\det} v_2 \\ \dfrac{di_2}{dt} = \dfrac{-MR_{cp1}}{\det} i_{s1} - \dfrac{M}{\det} v_{cp1} + \dfrac{M}{\det} v_s + \dfrac{Mr_2}{\det} i_s - \dfrac{L_s R_2}{\det} i_2 - \dfrac{L_s}{\det} v_2 \\ \dfrac{dv_2}{dt} = \dfrac{1}{C_2} i_2 - \dfrac{1}{C_2} \mathrm{sgn}(v_2) i_d \\ \dfrac{di_d}{dt} = \dfrac{1}{L_d} \mathrm{sgn}(v_2) v_2 - \dfrac{R_d}{L_d} i_d - \dfrac{1}{L_d} v_0 \end{cases} \tag{6-10}$$

where $\det = L_s L_2 - NM^2$, $r_1 = R_{cp1} + R_{Ls1}$, $r_2 = R_s + R_{cp1}$, $di_s/dt$ and $di_2/dt$ items are split from the following equations which link the N pick-ups and the track network:

$$\begin{cases} L_s \dfrac{di_s}{dt} + NM \dfrac{di_2}{dt} = R_{cp1} i_{s1} + v_{cp1} - v_s - r_2 i_s \\ M \dfrac{di_s}{dt} + L_2 \dfrac{di_2}{dt} = -R_2 i_2 - v_2 \end{cases} \tag{6-11}$$

## 6.4 GSSA Linear Modelling and Analysis



InductEV, Inc.
Exhibit 1020
Page 181

### 6.4.1 Continuous Linear Model

A linearised continuous model can be obtained in terms of the variables of interest using equations 6-5 through to 6-9. This transforms the real time variables in equation (6-10) to their complex Fourier coefficient variables, and the result can then be reduced to a standard form as:

$$\dot{\underline{x}} = \underline{A}\underline{x} + \underline{B}\underline{u} \tag{6-12}$$

where $\underline{A} =$

$$\begin{bmatrix}
\frac{-R_{dc}}{L_{dc}} & \frac{-j2}{pL_{dc}} & \frac{j2}{pL_{dc}} & 0 & 0 & 0 & 0 & 0 & 0 & 0 & 0 & 0 & 0 & 0 & 0 & 0 \\
\frac{-j2}{pCp} & -jw & 0 & \frac{-1}{Cp} & 0 & 0 & 0 & 0 & 0 & 0 & 0 & 0 & 0 & 0 & 0 & 0 \\
\frac{j2}{pCp} & 0 & jw & 0 & \frac{-1}{Cp} & 0 & 0 & 0 & 0 & 0 & 0 & 0 & 0 & 0 & 0 & 0 \\
0 & \frac{1}{L_{s1}} & 0 & \frac{-r_1}{L_{s1}} - jw & 0 & \frac{-1}{L_{s1}} & 0 & 0 & 0 & \frac{R_{cp1}}{L_{s1}} & 0 & 0 & 0 & 0 & 0 & 0 \\
0 & 0 & \frac{1}{L_{s1}} & 0 & \frac{-r_1}{L_{s1}} + jw & 0 & \frac{-1}{L_{s1}} & 0 & 0 & 0 & \frac{R_{cp1}}{L_{s1}} & 0 & 0 & 0 & 0 & 0 \\
0 & 0 & 0 & \frac{-1}{C_{cp1}} & 0 & -jw & 0 & 0 & 0 & \frac{1}{C_{cp1}} & 0 & 0 & 0 & 0 & 0 & 0 \\
0 & 0 & 0 & 0 & \frac{-1}{C_{cp1}} & 0 & jw & 0 & 0 & 0 & \frac{1}{C_{cp1}} & 0 & 0 & 0 & 0 & 0 \\
0 & 0 & 0 & 0 & 0 & 0 & 0 & -jw & 0 & \frac{1}{C_s} & 0 & 0 & 0 & 0 & 0 & 0 \\
0 & 0 & 0 & 0 & 0 & 0 & 0 & 0 & jw & 0 & \frac{1}{C_s} & 0 & 0 & 0 & 0 & 0 \\
0 & 0 & 0 & \frac{L_2 R_{cp1}}{\det} & 0 & \frac{L_2}{\det} & 0 & \frac{-L_2}{\det} & 0 & \frac{-L_2 r_2}{\det} - jw & 0 & \frac{NMR_2}{\det} & 0 & \frac{NM}{\det} & 0 & 0 \\
0 & 0 & 0 & 0 & \frac{L_2 R_{cp1}}{\det} & 0 & \frac{L_2}{\det} & 0 & \frac{-L_2}{\det} & 0 & \frac{-L_2 r_2}{\det} + jw & 0 & \frac{NMR_2}{\det} & 0 & \frac{NM}{\det} & 0 \\
0 & 0 & 0 & \frac{-MR_{cp1}}{\det} & 0 & \frac{-M}{\det} & 0 & \frac{M}{\det} & 0 & \frac{Mr_2}{\det} & 0 & \frac{-L_s R_2}{\det} - jw & 0 & \frac{-L_s}{\det} & 0 & 0 \\
0 & 0 & 0 & 0 & \frac{-MR_{cp1}}{\det} & 0 & \frac{-M}{\det} & 0 & \frac{M}{\det} & 0 & \frac{Mr_2}{\det} & 0 & \frac{-L_s R_2}{\det} + jw & 0 & \frac{-L_s}{\det} & 0 \\
0 & 0 & 0 & 0 & 0 & 0 & 0 & 0 & 0 & 0 & 0 & \frac{1}{C_2} & 0 & -jw & 0 & \frac{-2}{pC_2} \\
0 & 0 & 0 & 0 & 0 & 0 & 0 & 0 & 0 & 0 & 0 & 0 & \frac{1}{C_2} & 0 & jw & \frac{-2}{pC_2} \\
0 & \frac{j2}{pL_{dc}} & \frac{j2}{3pL_{dc}} & 0 & 0 & 0 & 0 & 0 & 0 & 0 & 0 & 0 & 0 & \frac{2}{pL_d} & \frac{2}{pL_d} & \frac{-R_d}{L_d}
\end{bmatrix}$$



InductEV, Inc.
Exhibit 1020
Page 182

$$\underline{B}=\begin{bmatrix} \frac{1}{L_{dc}} & 0 \\ 0 & 0 \\ 0 & 0 \\ 0 & 0 \\ 0 & 0 \\ 0 & 0 \\ 0 & 0 \\ 0 & 0 \\ 0 & 0 \\ 0 & 0 \\ 0 & 0 \\ 0 & 0 \\ 0 & 0 \\ 0 & 0 \\ 0 & 0 \\ 0 & 0 \\ 0 & \frac{-1}{L_d} \end{bmatrix} \qquad \underline{x}=\begin{bmatrix} \langle \mathbf{i_1} \rangle_0 \\ \langle \mathbf{v_{cp}} \rangle_1 \\ \langle \mathbf{v_{cp}} \rangle_{-1} \\ \langle \mathbf{i_{s1}} \rangle_1 \\ \langle \mathbf{i_{s1}} \rangle_{-1} \\ \langle \mathbf{v_{cp1}} \rangle_1 \\ \langle \mathbf{v_{cp1}} \rangle_{-1} \\ \langle \mathbf{v_s} \rangle_1 \\ \langle \mathbf{v_s} \rangle_{-1} \\ \langle \mathbf{i_s} \rangle_1 \\ \langle \mathbf{i_s} \rangle_{-1} \\ \langle \mathbf{i_2} \rangle_1 \\ \langle \mathbf{i_2} \rangle_{-1} \\ \langle \mathbf{v_2} \rangle_1 \\ \langle \mathbf{v_2} \rangle_{-1} \\ \langle \mathbf{i_d} \rangle_0 \end{bmatrix} \qquad \text{and} \qquad \underline{u}=\begin{bmatrix} < e_{dc} >_0 \\ < v_0 >_0 \end{bmatrix} \approx \begin{bmatrix} E_{dc} \\ V_0 \end{bmatrix}$$

In the above model, only $<\bullet>_0$ terms (corresponding to the moving average) are considered for DC variables $i_1$ and $i_d$, while $<\bullet>_1$ and $<\bullet>_{-1}$ terms (corresponding to the fundamental) are considered for other AC oscillating variables. As the input variables $E_{dc}$ and $V_0$ are essentially constant, real time domain values can be used in the place of their moving averages.

In the above transformation process, one important step is taken to process the pick-up resonant voltage $v_2$ so as to obtain the linear model. By analysing the phase shift relationships in the circuit shown in Fig. 6-2, it can be shown that $v_2$ essentially leads the track driving voltage $v_{cp}$ by 90 degrees. As $v_{cp}$ is basically a sine wave in phase with the existence function s(t) (with a zero initial angle), $v_2$ is essentially a cosine waveform. As a result, $<v_2>_1$ *is essentially real* and can be expressed solely as $a_1 \cos wt$ ($a_1>0$) in equation (6-4) without introducing significant error. Consequently $<v_2>_1=<v_2>_{-1} \cong a_1/2$, and the phase angle of $<v_2>_1$ is $0^0$ rather than $180^0$ because $a_1$ is positive. Therefore, from equation (6-9) the following operation can be undertaken:

$$\langle \mathrm{sgn}(v_2) \rangle_1 = \langle \mathrm{sgn}(v_2) \rangle_{-1} = \frac{2}{p} e^{j0} = \frac{2}{p} \qquad (6\text{-}13)$$

Based on equation (6-7), the transformation of the following product items in the nonlinear model (6-10) can be implemented:



InductEV, Inc.
Exhibit 1020
Page 183

$$\langle \mathrm{sgn}(v_2) i_d \rangle_1 = \langle \mathrm{sgn}(v_2) i_d \rangle_{-1} = \frac{2}{p} \langle i_d \rangle_0 \tag{6-14}$$

$$\langle \mathrm{sgn}(v_2) v_2 \rangle_0 = |v_2| = \frac{2}{p} \langle v_2 \rangle_1 + \frac{2}{p} \langle v_2 \rangle_{-1} \tag{6-15}$$

These two equations reveal the basic voltage and current relationships before and after the full bridge diode rectifier. In fact, equations (6-14) reflects a ratio of $4/\pi$ ($2\times2/\pi$) between the amplitudes of the fundamental and the square waveform, while equations (6-15) illustrates that the amplitude of a sine waveform is $\pi/2$ times its average value over a half period. These results are conceptually correct.

### *6.4.2 Discrete Linear Model*

Based on the continuous linear model expressed in equation (6-12), a discrete model can be obtained with a chosen sampling period $T_s$. Note that $T_s$ is different from the sliding window period T for GSSA modelling. The discrete model can be written in a general format as:

$$\underline{x}(k+1) = \underline{\Phi}\, \underline{x}(k) + \underline{\Gamma}\, \underline{u}(k) \tag{6-16}$$

where k=0,1,2…, corresponding to t=0, $T_s$, $2T_s$,…, $\underline{u(k)}$ and $\underline{x(k)}$ represent the sampled inputs and state variables respectively. $[\Phi, \Gamma]=f(A, B, T_s)$ is transformed from the continuous model with a chosen sampling period $T_s$. Although an analytical process of doing such a transformation can be very complex, or nearly impossible for high order systems, numerical methods can be employed to fulfil this task. For instance, various algorithms available in MATLAB [12] or other software package can be used to perform this transformation from equation (6-13) to (6-16) directly. The required system parameters are shown in Appendix B.

It should be noted that the discrete equation (6-16) is represented as complex coefficients. This makes it very difficult to use the model for practical controller design using micro-computers or other embedded systems. In fact as conventional control theories requires the system parameters to be real [11], this model with complex-coefficients cannot be easily analysed to determine system stability bounds. However, as will be shown in the following section, both the continuous and discrete models are very effective for system steady state and dynamic analyses.



InductEV, Inc.
Exhibit 1020
Page 184

### 6.4.3 Steady State and Dynamic Analysis Using the Linear Models

The steady state and dynamic solutions of the example current-fed G3 IPT power supply can be obtained directly from the GSSA models as shown below.

**Steady State Analysis**

Under steady state conditions, the derivatives of the state variables ($\dot{\underline{x}}$) are zero in the continuous linear model (6-12), and discrete variables $\underline{x}(k+1)$ are equal to $\underline{x}(k)$ in the discrete linear model (6-16). In consequence, the steady state solutions for the state variables can be obtained easily from:

$$\underline{X}_{ss}=-\underline{A}^{-1}\,\underline{B}\,\underline{u} \qquad (6\text{-}17)$$

or

$$\underline{X}_{ss}=(\underline{I}-\underline{\Phi})^{-1}\,\underline{B}\,\underline{u} \qquad (6\text{-}18)$$

where I is an identity matrix with the same dimension as $\Phi$.

The steady state solutions from the above equations can be directly transformed to time domain solutions. For example, the peak inverted AC resonant voltage $V_{cp}=2\|<V_{cp}>_1\|$, and the DC battery charging current $I_d=<I_d>_0$. Power efficiency can also be calculated from the steady state input and output power calculation. Table 6-1 shows some important steady state results for the voltage-fed G3 power supply.

**Table 6-1: Steady state results based on the linear GSSA models**

| Load Conditions | Track Current $I_s$ (A, rms) | AC Voltage $V_{cp}$ (V peak) | Pick-up Output DC Current $I_d$(A) | Input DC Current $I_1$(A) | Efficiency h= P_out/P_in (kW/kW) |
|---|---|---|---|---|---|
| ***N=16, $V_0$=650V*** | 249.24 | 846.43 | 16.02 | 382.08 | 166.7/206.3= 80.8% |
| ***N=16, $V_0$=0*** | 249.86 | 847.90 | 16.20 | 70.30 | 0/38.0= 0% |
| ***N=10, $V_0$=650V*** | 247.47 | 846.98 | 16.04 | 264.87 | 104.3/143.0= 72.9% |
| ***N=10, $V_0$=0*** | 249.86 | 847.9 | 16.19 | 69.52 | 0/37.8= 0% |
| ***N=0 (no pick-ups)*** | 249.86 | 847.90 | 16.19 | 69.52 | 0/37.5= 0% |

Note: f=15kHz, step DC input $E_{dc}$=540V, track equivalent resistor $R_s$=0.6Ω

The steady state analysis results of Table 6-1 show that the track current is essentially a constant current source at its rated value 250A rms, while the output voltage of the inverting network $V_{cp}$ is approximately equal to its nominal value 848.23V peak, or 600V rms as designed in Chapter 4. The DC input current increases with load as predicted by equation (4-22). And the pick-up output DC



InductEV, Inc.
Exhibit 1020
Page 185

current is around 16A, which is consistent with the nominal pick-up short circuit current 14.6A rms after taking a ratio of around 1.1 between the average and rms value (caused by the AC-DC conversion via the diode rectifier) into consideration. These results are in good agreement with the original system design and simulation results presented in Chapter 4 of this thesis.

With the equivalent resistors of the reactive components known and the currents flowing through them solved from the GSSA models, the total power losses can be calculated. Table 6-1 shows that the track takes up the most power losses of all the reactive components. The track loss is approximately constant at 37.5kW when an equivalent load resistor $R_s$ is 0.6Ω, while the total system loss is about 40 kW at full load. The efficiency is about 81% at full load, and 73% at 62.5% load (10 pick-ups). If $R_s$ is reduced to 0.3 Ω, then the track losses are halved so that the maximum efficiency reaches about 88.8% at full load. Note that the conduction and switching losses of the semiconductor devices are not taken into account as ideal switches have been assumed for GSSA modelling.

**Dynamic Analysis**

Apart from the steady state solutions, a system dynamic analysis can also be undertaken by solving the linear differential equation models of 6-12 and 6-16. Again, numerical approach has to be employed due to complexities involved in the complex numbers and the high system order. Note that it is incorrect to split the coefficient matrices of the models into real and imaginary parts, solve the resultant equations separately, and add the results together to obtain the final solution. This is because the superposition theorem is about the addition of the inputs and outputs of a liner system rather than the addition of a coefficient matrix which is determined by the system itself.

After the complex variables have been solved using standard numerical packages such as MATLAB [12], their corresponding time domain variables can be recovered from the following equations:

$$\begin{cases} x_d(t) = \langle x \rangle_0 \\ x_{ac}(t) = \langle x \rangle_1 e^{jwt} + \langle x \rangle_{-1} e^{-jwt} = 2(\mathrm{Re}\langle x \rangle_1 \cos wt - \mathrm{Im}\langle x \rangle_1 \sin wt) \end{cases} \quad (6\text{-}19)$$

where $x_d$ and $x_{ac}$ represent the DC and AC variables, and $\mathrm{Re}\langle x \rangle_1$ and $\mathrm{Im}\langle x \rangle_1$ denote the real part and imaginary part of $\langle x \rangle_1$ respectively. It is obvious that the envelopes of the AC variables can be obtained from $2\|\langle x \rangle_1\|$.

As an example, Fig. 6-3(a) shows a typical dynamic result obtained from the continuous linear model when the system starts at no load and the full load (16 pick-ups) are added at t=0.1s. In this



InductEV, Inc.
Exhibit 1020
Page 186

diagram, the DC input current $i_1$, the envelopes and the complete waveforms of the resonant AC voltage $v_{cp}$ and the track current $i_s$ are displayed.

To verify the validity of the GSSA model, a dynamic PSpice simulation result is shown in Fig. 6-3 (b) for comparison. It can be seen that the general dynamic responses shown in Fig. 6-3 (a) and Fig. 6-3 (b) are in fairly good agreement although there are some transient errors which are

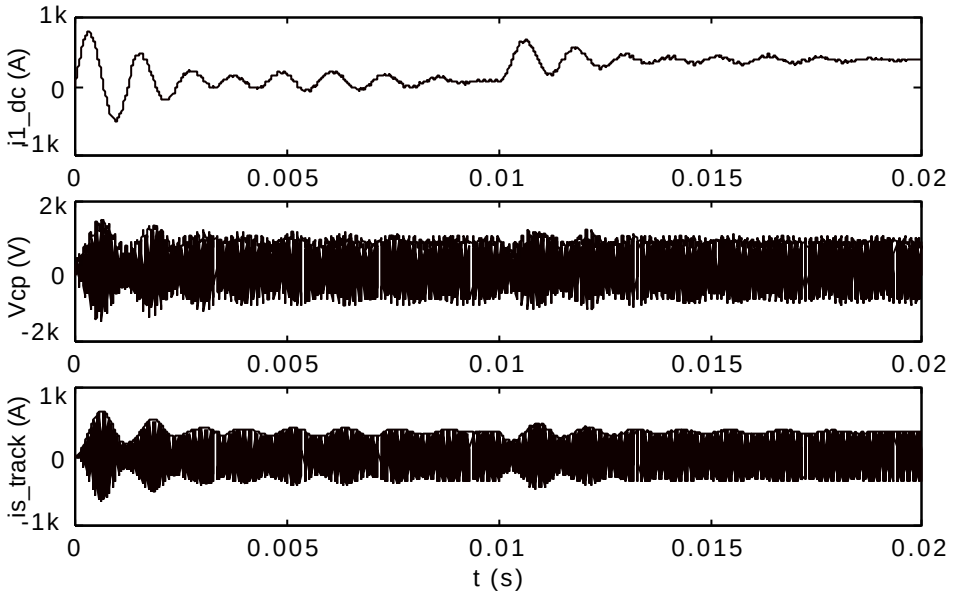


Result from the continuous GSSA model

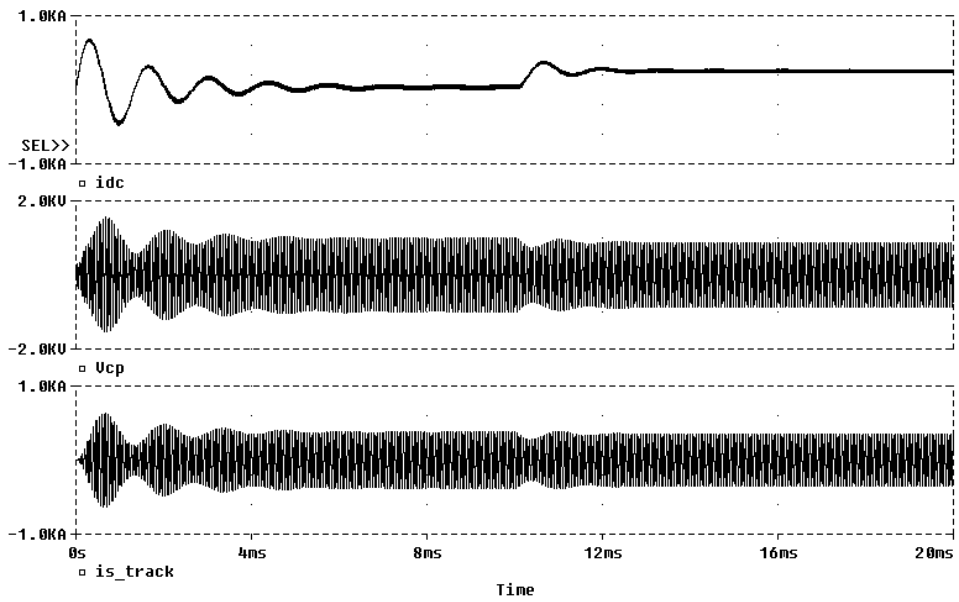


Result from PSpice simulation

**Fig. 6-3: Load increase transient response obtained from GSSA model and PSpice simulation**



InductEV, Inc.
Exhibit 1020
Page 187

mainly caused by the system dynamic ZVS frequency variations. In addition, due to the assumption made for the modelling that the switching devices (including the diodes) are ideal, the GSSA model shows less damping than PSpice simulation results where practical voltage drops and switching transition delays are considered.

Fig. 6-3 shows that the waveforms from the GSSA model are not as smooth as those obtained from the PSpice simulation, in particular the envelope of the output AC voltage $v_{cp}$ from the inverting network has clearly observable glitches. This is mainly because of the discrepancy between the switching frequency (the same as the sliding window frequency used in the GSSA model) and the practical ZVS resonant frequency. When the sliding window period chosen for the GSSA modelling is not exactly the same as the actual zero voltage crossing frequency of $v_{cp}$, ZVS will not be achieved accurately so that $v_{cp}$ is not a good sine wave and has significant harmonic distortion. In this situation, using only the fundamental components $<v_{cp}>_1$ and $<v_{cp}>_{-1}$ in GSSA modelling may cause a large error. This is particularly true during transients when the ZVS frequency varies. Obviously slight dynamic frequency shifts may improve the results, but the difficulty is that the exact ZVS frequency is not known for this $9^{th}$ order system so that a trial and error approach such as that used by Green has to be adopted [13]. A full ZVS analysis of a current-fed resonant converter under the steady state conditions has been undertaken by the author for a second order resonant tank [14], but more work is needed for the analysis of dynamic and high order systems. Fortunately, the actual frequency shift of a current-fed G3 power supply in normal operation, particularly under the steady state conditions, is very small compared to G1 power supplies due to the increased reactive power (VArs) in the track network. Therefore, choosing the fixed nominal frequency as the sliding window frequency does not cause significant error. An alternative approach which results in improved accuracy is to take more Fourier series harmonic components into account in the model. For example, the second harmonics of the “DC” variables and the third harmonics of the AC variables could be added into the model as these are normally the next most significant components. However, this approach increases the order and therefore the complexity of the model. It has been observed that while helpful, the improvement is not significant if the harmonic component order is increased only by one in GSSA modelling.

Despite the above mentioned shortcomings, the analysis based on the GSSA model is more convenient and faster compared to PSpice or any other numerical simulation technique. The whole IPT system can be solved in a closed form without using complicated iterative algorithms, and the full dynamic solutions can be obtained in less them one minute compared to two to four hours for a complete PSpice simulation. In addition, there is no need to set up schematic circuit diagrams as



InductEV, Inc.
Exhibit 1020
Page 188

well as their simulation options, and the convergence problems are completely eliminated. Therefore, the GSSA linear model is very useful for analysing the circuit performance and checking the validity of a circuit design.

### The Effect of the Sampling Time on the Discrete Model

For the discrete model, choice of sampling time is important. Two typical results are shown in Fig. 6-4 where the system starts up at full load and the load is removed suddenly at t=0.01s. It is observed that if the sampling frequency is two times faster than the sliding window frequency, reasonably good results can be obtained. According to Shannon's sampling theorem this result is to be expected [11]. Fig. 6-4 (a) shows the situation when the sampling frequency is four times faster, which in fact gives as good results as that of the continuous model. Furthermore, it has been observed that even when the sampling frequency is slightly slower than the switching frequency, eg. 1.5 times slower as in the case of Fig. 6-4 (b), some waveforms, particularly their envelopes are still in good agreement with the results obtained from the continuous model. It can be seen from Fig. 6-4 (b) that the dc input current and the track current are in quite good agreement with what are shown in Fig. 6-4 (a). Although the time domain waveform (the lower curve) of the resonant voltage $V_{cp}$ is no longer correct, its envelope (the upper curve) still contains some basic transient and steady state information that may be useful. This means that if a discrete controller is to be designed for a current-fed G3 IPT power supply, a slower sampling frequency may be able to chosen, which is preferable for practical implementations as the speed and memory requirement for the control system can be reduced.

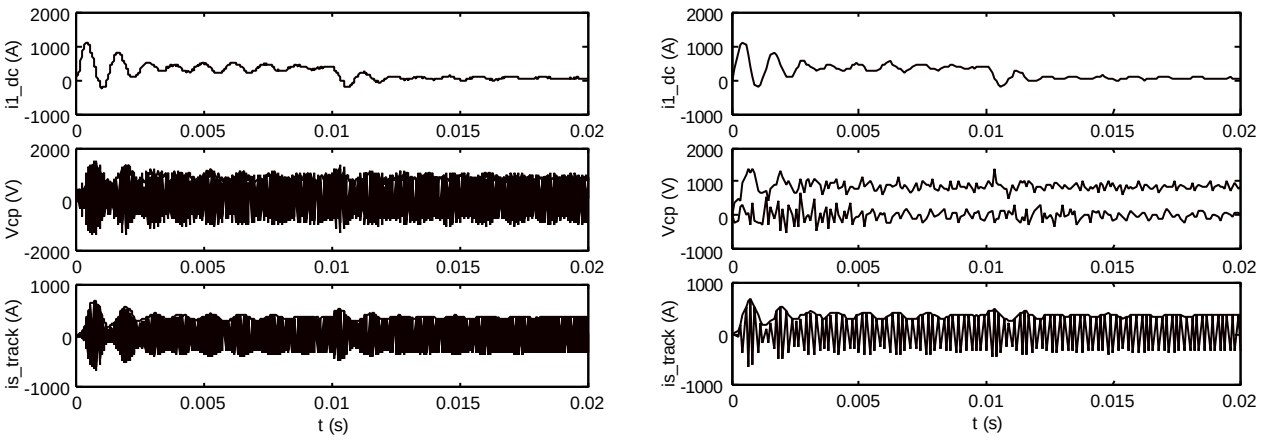


(a) Fast sampling ($T_s$=T/4)

(b) Slow sampling ($T_s$=1.5T)

**Fig. 6-4: Load transient response from the discrete GSSA linear model using different sampling times**



InductEV, Inc.
Exhibit 1020
Page 189

## 6.5 Summary

In this chapter, GSSA (Generalised State Space Averaging) is described and has been successfully employed in modelling a large current-fed G3 power supply with 16 tuned pick-ups.

First, the switching network of the primary power converter and the diode rectifiers of the pick-up circuit were represented with voltage and current controlled sources using an existence function and a sign function, so that a simplified equivalent circuit is obtained. Then the complete system was described with a 9th order nonlinear differential equation based on the equivalent circuit. By transforming the real time variables of the nonlinear differential equation model into Fourier complex number variables, continuous and discrete models with a 16x16 complex number coefficient matrix have been derived and used for the system analysis. These models have made both the steady state and dynamic analyses very convenient and fast. Despite some transient errors, the results obtained from the models are in good agreement with the original system design and PSpice simulation results.

For the discrete model, the effect of the sampling time on performance has also been investigated. As expected, the discrete model gives good results provided that the sampling frequency is two times faster than the basic switching frequency. Furthermore, it has been observed that even when the sampling frequency is chosen slower than the switching frequency, eg, the sampling time is 1.5 times longer, the solution to the discrete model can still contain some basic information about the envelope of the system dynamics which may be useful for discrete control design of a current-fed G3 IPT power supply.

It has been shown that the basic concept of the GSSA method involves a mathematical transformation between time domain variables and their complex Fourier series representations within a sliding window. While effective, one major limitation of using the GSSA technique to model the current-fed G3 power supply is that the actual ZVS operating frequency of the system may vary and is difficult to determine. As such it is difficult to choose a sliding window period exactly in agreement with the actual resonant frequency. The mismatch may cause errors when only the significant variables such as DC and AC fundamental components are considered. This is particularly true for the resonant AC voltage which is the direct output from the switching network. Another disadvantage is that the obtained models are in complex form, which makes the conventional theory difficult to apply and consequently complicates the controller design.



InductEV, Inc.
Exhibit 1020
Page 190

## 6.6 References


[1] Middlebrook, R. D. and Cuk, S.: "A general unified approach to modelling switching power converter stages", *IEEE PESC Rec.*, pp.18-34, 1997.

[2] Middlebrook, R. D. and Cuk, S.: *Advances in switched-mode power conversion*, Pasadena, CA, TESLA CO., 1983.

[3] Xu, J. and Lee, C. Q.: "A Unified averaging technique for the modelling quasi resonant converters", *IEEE Trans., Pwr. Elect*, Vol.13, No.3, May 1998.

[4] Sanders, S. R., Noworolski, J. M., Liu, X. Z. and Verghese, G. C.: "Generalised averaging method for power conversion circuits", *IEEE Transactions on Power Electronics*, Vol.6, No.2, April,1991.

[5] Wang, C. S., Stielau, O. H. and Covic, G. A.: "Load models and their applications in the design of loosely coupled inductive power transfer systems", *Proceedings of International conference on power system technology*, December, 2000, Perth, Australia.

[6] Bhat, A. K. S.: "A generalised steady state analysis of resonant converters using two-port model and Fourier-series approach", *IEEE Transactions on Power Electronics*, Vol.13, No.1, January, 1998.

[7] Lee, C. Q., Siri, K., Fang, S. J.: "State plane approach to frequency response of resonant converters", *IEE Proceedings -G.*, Vol.138, No.5, October 1991.

[8] Kutkut, N. H., Lee, C. Q., and Batarsesh, I.: "A generalised program fro extracting the control characteristics of resonant converters via the state-plane diagram", *IEEE Transactions on Power Electronics*, Vol.13, No.1, January 1998.

[9] Shenkman, A. L., Axelrod, B. and Chudnovsky, V.: "A new simplified model of the dynamics of the current-fed parallel resonant inverter", *IEEE Transactions on Industrial Electronics*, Vol.47, No.2, pp.282-286, April, 2000.

[10] Eghtesadi, M. "Inductive power transfer to an electric vehicle - analytical model", *IEEE Vehicular Technology Conference*, 40, pp.100-104, 1990.

[11] Zhou, Q., Li, P. and Gao G.: *Automatic control theory*, Huanai University of Technology Press, 1988.

[12] Etter, D. M.: *Engineering problem solving with MATLAB*, Prentice Hall, 1993.

[13] Green, A. W.: "Modelling a push-pull parallel resonant converter using generalised state-space averaging", *IEE Proceedings-B*, (6), 140, pp.350-356, 1993.




InductEV, Inc.
Exhibit 1020
Page 191

[14] Hu, A., Boys, J. T. and Covic, G.: "Frequency analysis and computation of a current-fed resonant converter for IPT power supplies", *Proceedings of IEEE-PES/CSEE 2000 International Conference on Power System Technology*, pp.327-332, Perth, Australia, December 2000.



InductEV, Inc.
Exhibit 1020
Page 192

## Chapter 7

# Innovative Resonant Converters and Practical Implementation

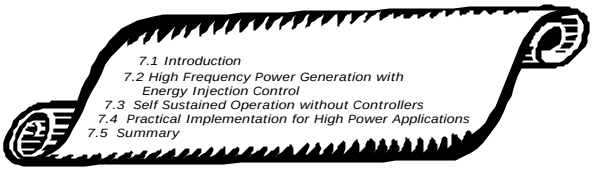


## 7.1 Introduction

In proceeding chapters, conventional voltage and current-fed resonant converters as well as their improved versions used for IPT power supplies have been discussed. As noted, an IPT power supply is mainly to provide contactless power transfer to movable pick-up loads. With more IPT power supplies being put into applications, there have been increasing concerns as to how to fulfil this power transfer task more efficiently and cost effectively. Since a loose magnetic coupling is employed in an IPT system, generation of relatively high frequency (typically 10 – 100 kHz) AC currents in a track coil or extended track loop is essential. To fulfil this task, new power converters are investigated in addition to the conventional IPT power supplies.

This chapter introduces two novel resonant converters that can be used for IPT applications. The first converter is based on free oscillation and energy injection control whereby a high frequency, high magnitude track current can be generated with low switching frequencies and low voltage inputs. The second one is a converter that relies solely on self-sustained oscillation with no external controllers required for the converter operation. These two new power converters are analysed, simulated and experimentally verified. Moreover, practical aspects regarding their high power applications in IPT power supplies are discussed. In particular, EMI concerns of a direct AC-AC converter using energy injection control, and the gate driving problems of the self-sustained converter at high voltage levels are addressed. Finally, a practical 80A/10kHz IPT power supply using PLL (Phase locked loop) and direct ZVD (Zero Voltage Detection) techniques are implemented and their advantages and drawbacks in performance are discussed.



InductEV, Inc.
Exhibit 1020
Page 193

## 7.2 High Frequency Power Generation with Energy Injection Control

### *7.2.1 Basic Concept of Free Oscillation and Energy Injection Control*

Traditional converters used for IPT power supplies are driven continually by a voltage or current source via power switches. High frequency track currents are generated by switching of these voltage or current fed power supplies. In consequence, the switching frequency has to be equal to the actual system operating frequency irrespective of load conditions. Furthermore, the circuit transient process involved in these power supplies is normally very complex and difficult to analyse, so unpredicted voltage and current overshoots during start-up and load transients can damage the switching devices or other components. For this reason, additional soft starters or dynamic controllers are often required [1].

In fact, if a network is oscillatory, it will be able to oscillate naturally at its free ringing frequency as long as there is some energy stored in it. Ideally a lossless electric network will oscillate continuously with the same voltage and current magnitudes at an existing energy level. Unfortunately a practical circuit has various losses resulting from normal loads, non-superconducting cables, etc., so that the oscillation cannot be sustained naturally. However, if the energy losses were continually compensated, the oscillation would continue. Therefore, in principle the track oscillation could be maintained by energy injection control. This concept can be used to develop a new type of resonant converter for IPT applications.

There are two major issues involved in designing a practical power converter using this concept: an oscillatory network and an appropriate energy injection technique. A basic rule is that the energy injection control should be able to compensate for the power losses promptly and smoothly without affecting the natural circuit oscillation characteristics, such as the frequency and magnitude of the track current, significantly. The fundamental process is analogous to mechanical oscillation – for example a pendulum clock that oscillates at near constant frequency and magnitude with little adverse effect from the external force which is used to continually compensate any energy loss.

### *7.2.2 Proposal and Analysis of a Simple DC-AC Converter*

Fig. 7-1 shows a simple and novel example of a DC-AC converter/inverter based on free oscillation and energy injection control. Normally the switch S2 is “on” and S1 is “off” (State 1) so that the track inductor $L_s$, its series tuning capacitor $C_s$ and the equivalent resistor R form a free oscillation



InductEV, Inc.
Exhibit 1020
Page 194

network. If switch S2 is controlled "off" and S1 "on" (State 2) during the positive period of the track current, then the energy will be brought into the network from the DC power supply $V_d$. The differential equation expressed in the track current (i) for both of these two states can be written as:

$$LC\frac{d^2i}{dt^2}+RC\frac{di}{dt}+i=0 \qquad (7\text{-}1)$$

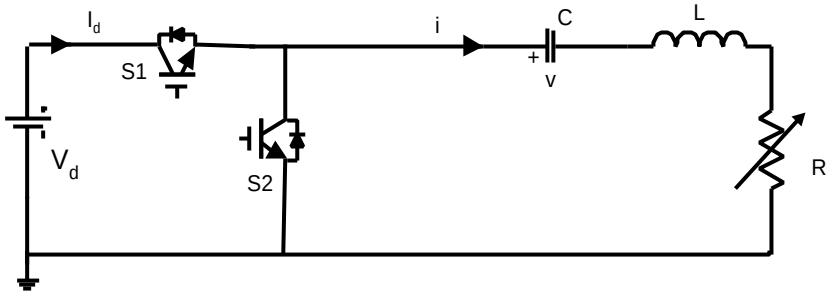


**Fig. 7-1: A simple inverter based on free oscillation and energy injection control**

Therefore, the oscillation frequency of the track current is not affected by the energy injection process. By solving equation (7-1), it can be shown that this free ringing frequency is:

$$w=w_0\sqrt{1-z^2}=w_0\sqrt{1-\left(\tfrac{1}{2Q}\right)^2} \qquad (7\text{-}2)$$

where $\omega_0=1/\sqrt{LC}$ is the undamped natural frequency, $\zeta=R/(2\sqrt{L/C})$ is the damping factor, and $Q=\omega_0 L/R$ is the network quality factor.

Note that the free ringing frequency, also termed the natural oscillation frequency, is different from the zero phase angle resonant frequency corresponding to a unity power factor at the input. For a standard series tuned track circuit shown in Fig. 7.1, the zero phase angle frequency is the same as the undamped natural frequency $\omega_0$ which is independent of the load. However, equation (7-2) shows that Q must be greater than 0.5 to ensure that the circuit has a free ringing frequency otherwise the network will be overdamped, so that no free oscillation exists. Equation (7-2) also shows that the free ringing frequency is almost constant at high Q values. For example if Q>3 the frequency variation will be less than 1.4% from no load to the full load.

During the free ringing period (S1 is "off" and S2 is "on"), the complete solution of the track current can be found from equation (7-1) and expressed as:

$$i=\frac{-v(0)}{wL}e^{-\frac{t}{t}}\sin wt+i(0)\frac{w_0}{w}e^{-\frac{t}{t}}\cos(wt+q) \qquad (7\text{-}3)$$



InductEV, Inc.
Exhibit 1020
Page 195

where v(0) and i(0) are the initial voltage of the tuning capacitor $C_s$ and the initial current of the track inductor respectively.

$$t = 2L / R \tag{7-4}$$

is the time constant of the decay of the track current envelope (theoretically if R=0, then $\tau=\infty$, and there would be no decay), and

$$q = \arctan\left(\frac{1}{wt}\right) = \arctan\left(\frac{1}{2Q}\right) = \arctan(z) \tag{7-5}$$

is a phase shift caused by the load resistor. When Q is high, the damping factor $\zeta$ is small and $\theta \approx 0^0$.

If the switching transitions occur at zero current crossing points, then the initial current i(0) is zero, and the corresponding initial voltage of the tuning capacitor $C_s$ will be around its peak value, which can be denoted as v(0). Under such a condition, the second term of equation (7-3) becomes zero, resulting in a simple current equation given by:

$$i = \frac{v(0)}{wL} e^{-\frac{t}{t}} \sin wt \tag{7-6}$$

In Fig. 7-1, if S2 turns “off” and S1 turns “on” only at positive zero crossing instants of the track current (in an actual circuit, a small dead-time is necessary to prevent a momentary short-circuit of the DC supply), then the positive track current in the following half cycle flows through the DC voltage source and brings a certain amount of energy into the network. During each energy injection period, the track current can be solved from equation (7-1) and expressed as:

$$i = \frac{V_d + v(0)}{wL} e^{-\frac{t}{t}} \sin wt \tag{7-7}$$

Comparing equation (7-6) with equation (7-7) it can be seen that they both demonstrate decaying sinusoidal oscillation properties except that the magnitude of the track current is larger during the energy injection period because of the effect of the DC input voltage $V_d$. However, for long track and high current applications as in the example of the IPT power supply for an electric train given in Appendix B, $|v(0)| >> V_d$ (here v(0) is approximately equal to the peak value of the total tuning capacitor voltage which is $14.6\text{kV}\times\sqrt{2}\approx 21\text{kV}$ compared with $V_d$=540V), therefore the current surge caused by the energy injection is actually very small. As an example, Fig. 7-2 shows a PSpice simulation result for this application using the proposed converter (Fig. 7-1). Here the energy stored



InductEV, Inc.
Exhibit 1020
Page 196

in the network is controlled at a reference of 38.75 J, corresponding to a track current of 250A rms (354A peak) as required for a track length of 400m/620µH. The result shows that the track current fluctuation is quite small and the start-up and the load transient responses are very smooth, although the energy injection is undertaken only in positive half cycles of the track current to achieve ZCS operation. It is clear that the average value of the injection current changes automatically with the load, consequently the track current is kept approximately constant. Fig. 7-2 shows that if the load is decreased at t=3ms, the frequency of the current injection decreases accordingly with almost no current overshoots.

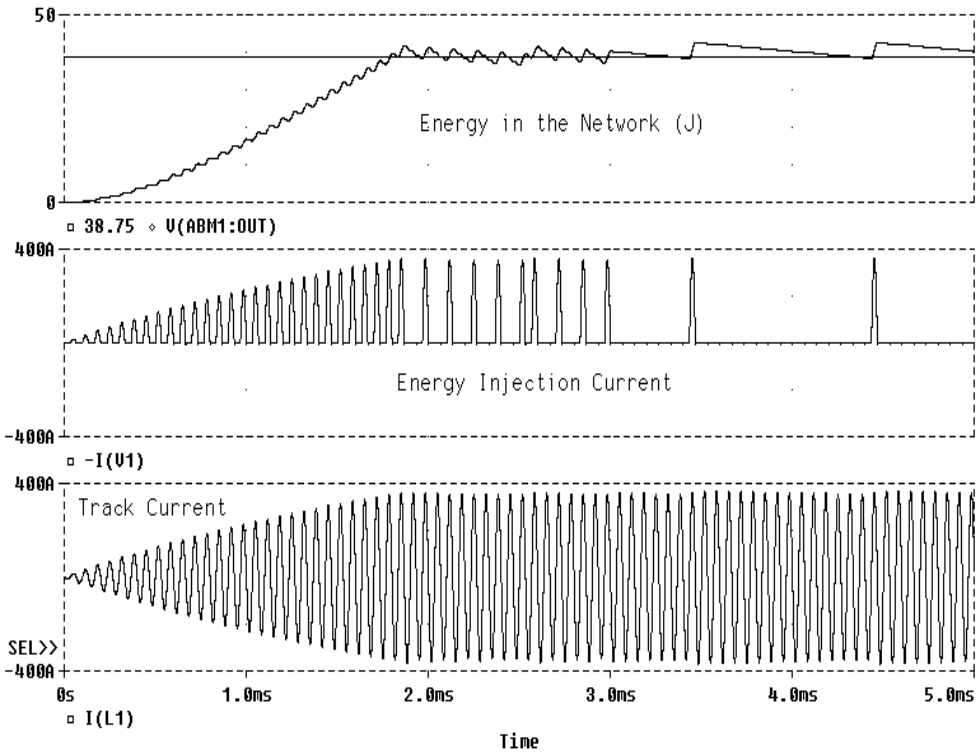


**Fig. 7-2: Transient response of a DC-AC converter based on direct energy injection control**

When S1 is on (S2 turns off) during every positive half cycle of the track current, the converter reaches its maximum power capacity which can be expressed as:

$$P_{\max} = \frac{\sqrt{2}}{p} IV_d = 0.45\, IV_d \qquad (7\text{-}8)$$

Here I is the track current rating in rms, and $V_d$ is the DC input voltage. In the above example IPT application (I=250A rms and $V_d$=540V), the maximum power that can be supplied is about 60 kW. If a full bridge topology is used in place of S1 and S2 (Fig. 7-1), the control process will be similar but the maximum power capacity will double because the energy can be pumped into the resonant circuit in both the positive and negative half cycle of the track current.



InductEV, Inc.
Exhibit 1020
Page 197

### 7.2.3 Experimental Results and Discussion

Based on the concept of free oscillation and energy injection control, many practical methods can be used to generate a required track current. For instance, a simple ZCS strategy is to control the transitions of S1 and S2 by detecting the instantaneous peak value of the track current. When the peak track current is detected to be lower than a predetermined reference, switch S1 is controlled "on" (S2 should be "off" slightly earlier allowing for a short dead time) in the following positive half cycle of the track current. In order to investigate the effectiveness of this technique, an experimental converter with the main circuit as shown in Fig. 7-1 was constructed and its simulated and measured gate drive voltage and track current waveforms are shown in Fig. 7-3.

To simplify the circuit, this converter has a DC power supply of 12V so that a pair of low voltage P and N channel MOSFETS could be used as the control switches eliminating the gate drive isolation requirements. A toroidal current transformer is used to detect the current. The controller is particularly simple and it has been implemented using only standard IC chips such as the MC14011 and LM393. It can be seen that the simulated and the measured results are in very good agreement. They show that the track current is controlled constant at a frequency of 23kHz whereas the switching frequency is three times smaller at a load of one third of its maximum value. If the load increases, this switching frequency will also increase to give more energy injection to compensate for the power consumption.

There are two main concerns regarding the quality of the track current waveform in the design of such converters: one is the decay speed during the free ringing period (S2 on, S1 off); and the other is the current surge during the energy injection. The former is related to the damping factor $\zeta$ (=1/2/Q), or the quality factor Q of the network. If Q is too small, the decay will be too fast which may result in a poor track current waveform. It can be shown that if Q is larger than $\pi$, then the decay time constant $\tau$ will be greater than the free ringing period so that the track current distortion will not be very large. As for the current surge during energy injection, it is mainly determined by the ratio between $V_d$ and the v(0) as shown by equation (7-7). If this ratio is too high, the energy injected each time will be large compared to the energy stored in the track network, in consequence, the track current fluctuation and harmonics will be high. For this reason, a large track inductance and a high current rating are preferable. On the other hand, this current surge problem can be alleviated by reducing the amount of energy that is injected each time. For example, S1 can be switched "on" later than the positive zero crossing (of the track current) or switched "off" earlier



InductEV, Inc.
Exhibit 1020
Page 198

than the negative zero crossing without utilising the complete half cycle. However, either the ZCS "on" or ZCS "off" conditions has to be compromised. Considering the two factors together, it can be concluded that in general a high reactive circuiting power is required to both maintain the oscillation and suppress any current surges. These requirements are often met in IPT applications where long tracks, high frequency, and high currents are required simultaneously.

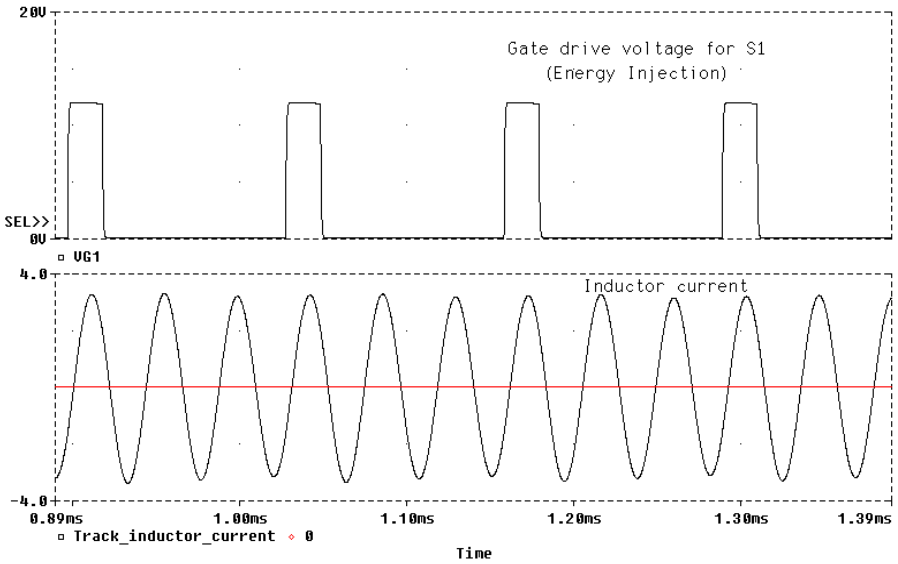


Simulation result

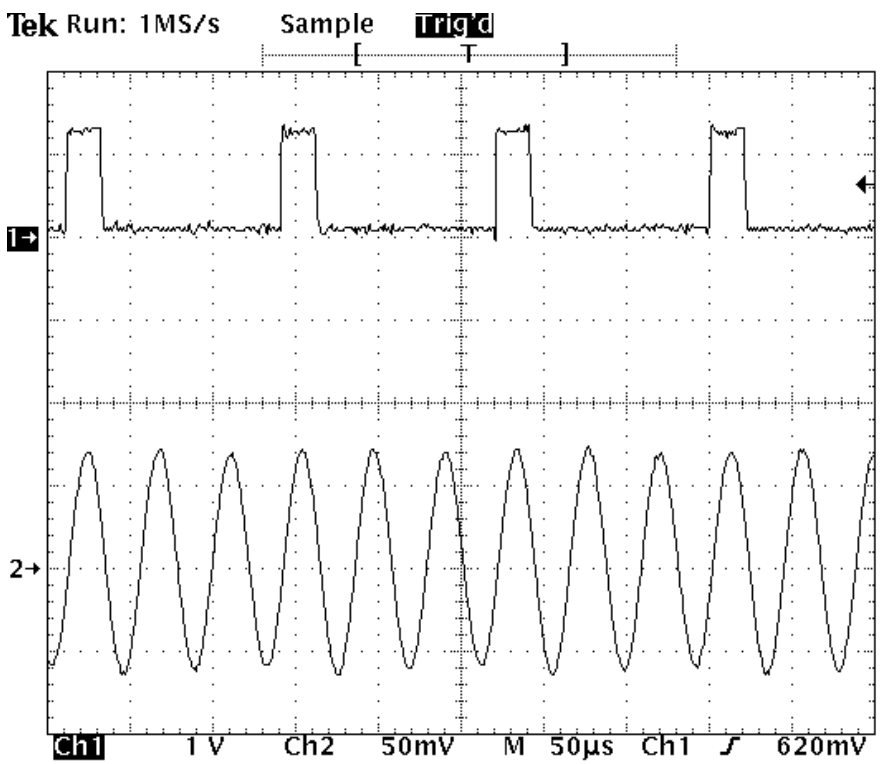


Experimental result (Ch1 → Gate drive voltage: 10V/div, Ch2 → Track inductor current: 2A/div)

**Fig. 7-3: Simulation and experimental results of a DC-AC converter based on energy injection control**



InductEV, Inc.
Exhibit 1020
Page 199

### 7.2.4 Investigation of a Direct AC-AC Converter

Apart from the simple example circuit shown in Fig. 7-1, other converters based on different circuit topologies and energy injection strategies may be constructed. A very important feature of this energy conversion technique that is worth special mention is that the energy (rather than the exact format of the driving source) is the primary concern in designing such converters. As such, it is not a critical requirement to minimise DC bus voltage variations. For a practical circuit powered by the mains supply, this means that a smaller DC filtering capacitance is acceptable. In some extreme situations, all the DC capacitors may be eliminated so that the cost and size of the converter can be significantly reduced.

Furthermore, even the rectifier for the DC supply can be eliminated so that the power input shown in Fig. 7-1 becomes an AC source, thus a very simple direct AC to AC converter as shown in Fig. 7-4 can be constructed. Fig. 7-5 shows a typical result of the injection current and resultant track current waveforms of such a converter. An ideal single-phase 50Hz/230V AC source has been used and shown in the same diagram for reference. Its voltage direction is detected, and the commutation of switches is controlled in such a way that the voltage and current of the AC source are in the same direction so that energy injection is ensured when necessary. Fig. 7-5 shows that the track current boosts up quickly to its reference peak value of 100A at an initial AC phase angle of $60^0$. This current is maintained approximately constant for the majority of the time. However, around the zero crossings of the AC source the voltage is too low to ensure sufficient energy injection to supply a 2.5 kW load. In consequence the current drops slightly. Obviously, for a given track circuit and current rating, this current sag will be related to the load level. A heavier load will cause larger current sag because even continuous energy injection around the zero voltage crossings (low voltage areas) of the mains power supply may be insufficient to compensate for the power losses in the track network.

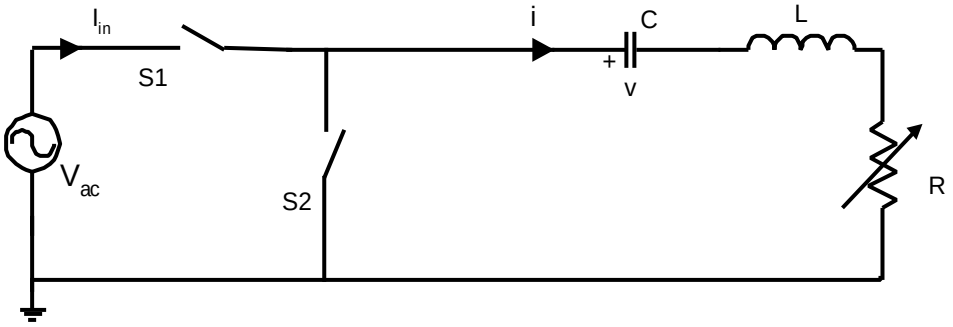


**Fig. 7-4: A direct AC-AC power converter**



InductEV, Inc.
Exhibit 1020
Page 200

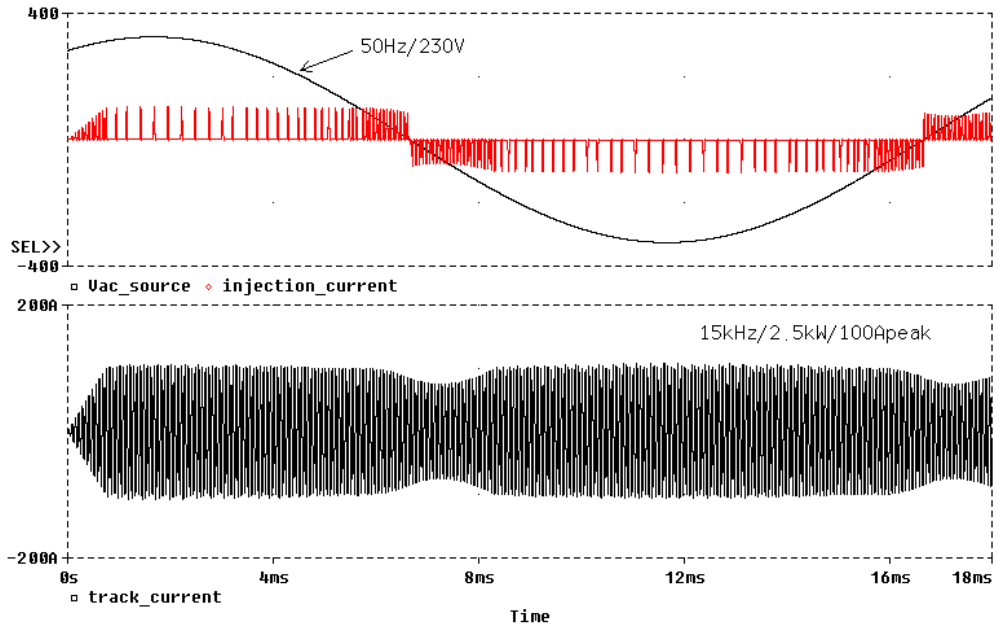


**Fig. 7-5: Injection and track current waveforms of the direct AC-AC converter**

The track current sag as shown in Fig. 7-5 is not ideal but a ripple of 100Hz, or 300Hz if a three phase supply were used for energy injection, may not be a severe problem for IPT power applications if appropriate power conditioners are designed on the secondary pick-ups. One very important concern of this AC-AC converter, however, is that it draws random high frequency current pulses from the mains power supply thereby introducing large harmonics and conducted EMI to the power utility. In a practical circuit the mains supply is not ideal but has an internal equivalent inductor comprising the leakage inductance of a power transformer and line inductance of the feeding cables. Additional capacitors may be added to filter the current pulses. Further studies are necessary to investigate the power quality issues involved in this type of matrix converter based on free ringing and energy injection control.

## 7.3 Self-sustained Operations without External Controllers

### *7.3.1 Structure of the Proposed Converter*

Various current-fed resonant converters with ZVS controllers have been developed and successfully put into practical IPT applications [1-3]. Although external controllers are used in these converters, a careful look into these systems reveals that there is in fact no direct control over the output voltage, current or frequency. The required track current is actually indirectly obtained via ZVS control. The track current output may have some slight variations in magnitude and frequency, but these variations are so small under normal working conditions that the converters are acceptable for



InductEV, Inc.
Exhibit 1020
Page 201

IPT applications [4]. In fact, the main function of the track power supply of an IPT system is to provide high frequency AC power in a form of magnetic field, thus a constant track current while desirable is not an absolute requirement. The secondary pick-ups normally have their own control units which can regulate power flow as required by the load.

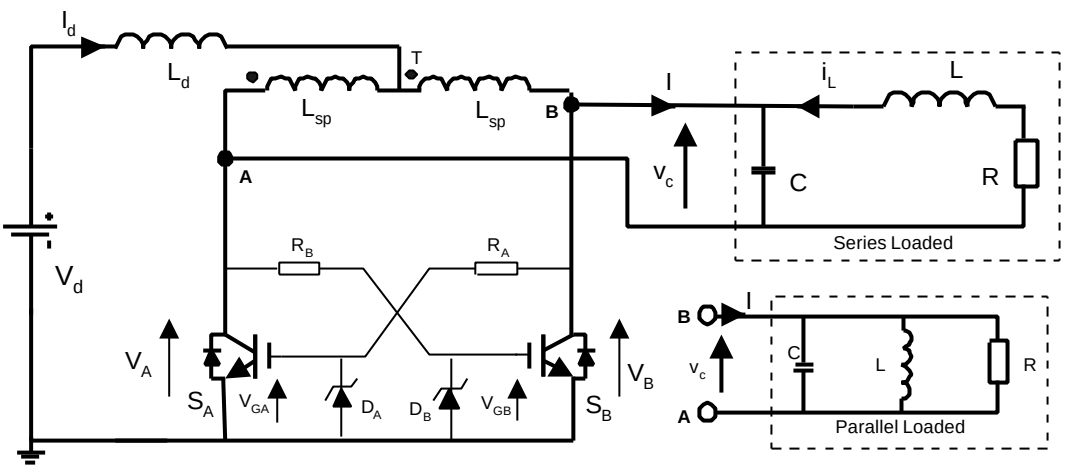


**Fig. 7-6: Proposed DC-AC converter without external controllers**

Based on the above concept and the particular application, a novel converter which can start up and keep sustained ZVS operation without any additional controllers is proposed. This converter is essentially an autonomous system which gives the same performance as the G1 power supply. As shown in Fig. 7-6, it comprises a DC inductor $L_d$, a phase splitting transformer $L_{sp}$, two switching devices $S_A$ and $S_B$, and a parallel resonant tank. The DC inductor forms an approximate current source from the DC voltage supply $V_d$ provided the inductance is large. The phase splitting transformer replaces the two top switches of a single phase full inverting network and essentially divides the DC current into two legs of the inverter network. As discussed in Chapter 3, compared to the full bridge topology, a push-pull configuration simplifies the gate drive design (as no isolation is required) and doubles the output resultant resonant voltage. The parallel resonant tank consists of an inductor L and a capacitor C, with an equivalent load resistor R that is series connected [5]. In other applications such as DC-DC converters [6-7], the load can also be connected in parallel as illustrated in the lower dotted block of Fig. 7-6.

For this current-fed converter (Fig. 7-6), ZVS not only minimises switching losses and EMI, but also is crucial for safe operation of the circuit [8]. If ZVS fails, then the resonant capacitor C will be shorted by the active switches and their body diodes, which may cause the switching devices to fail. In some topologies, additional diodes are placed in series with the active switches $S_A$ and $S_B$ to prevent the shorting and allow for non-ZVS operation, but these diodes cause voltage drops and power losses so they are not commonly used.



InductEV, Inc.
Exhibit 1020
Page 202

Unlike conventional converters with two function blocks comprising the main circuit and the controller, Fig. 7-6 shows a novel approach of driving the switching devices without any additional controllers. Both the power and signals needed for the gate drive are obtained directly from the voltages across the main switching devices. The circuit is so simple that only a resistor and a zener diode are used for each switch. The voltage rating of the zener diodes $D_A$ and $D_B$ are chosen according to the switching requirements of the devices, for example, 4.7-5.6V for most low voltage threshold MOSFETs and 12-15V for IGBTs. The current limiting resistors $R_A$ and $R_B$ are designed according to the resonant voltage level and the current rating of the zener diodes.

### *7.3.2 Self-sustained Operation Analysis*

In principle, autonomous operation of the converter shown in Fig. 7-6 is based on the oscillatory property of the proposed topology. The critical conditions of the series-loaded parallel-resonant tank have been investigated in Chapter 3. The minimum bounds on Q to ensure start-up and steady state ZVS operation of such series-load converters have been found to be 2.54 and 1.86 respectively [8-9]. Theoretically there is no limit on Q for a standard parallel-loaded tank (see Fig. 7-6) as no DC offset voltage exists across the load resistor.

An advantageous feature of the proposed resonant converter is that it can start up automatically. At turn-on, switches $S_A$ and $S_B$ are initially “off”. Once the DC source is switched on, a DC voltage will be exerted across the switches. In consequence both the switches are turned on and the current in the DC inductor increases, resulting in some energy storage in the DC inductor, which has been proven beneficial for boosting the circuit oscillation [8]. Due to the existence of parameter differences and external disturbances, the voltages across the active switches cannot be exactly the same in a practical circuit. The lower voltage, say $V_A$, will provide a lower gate drive voltage $V_{GB}$ in the other leg. Consequently, $S_B$ will turn off resulting in a higher voltage drop $V_B$ which will further increase the gate drive voltage $V_{GA}$ and decrease the voltage $V_A$. This positive feedback will quickly (typically within several ms) lead to complete resonant operation with ZVS.

Fig. 7-7 shows typical steady state voltage and current waveforms of the converter obtained from a PSpice simulation. It can be seen that the gate drive signal of one switch is in fact the capped voltage across the other switch. Switch transitions occur approximately at the zero voltage points with a maximum error of a zener diode voltage drop (4.7V). The resultant resonant voltage waveform is very good as shown.



InductEV, Inc.
Exhibit 1020
Page 203

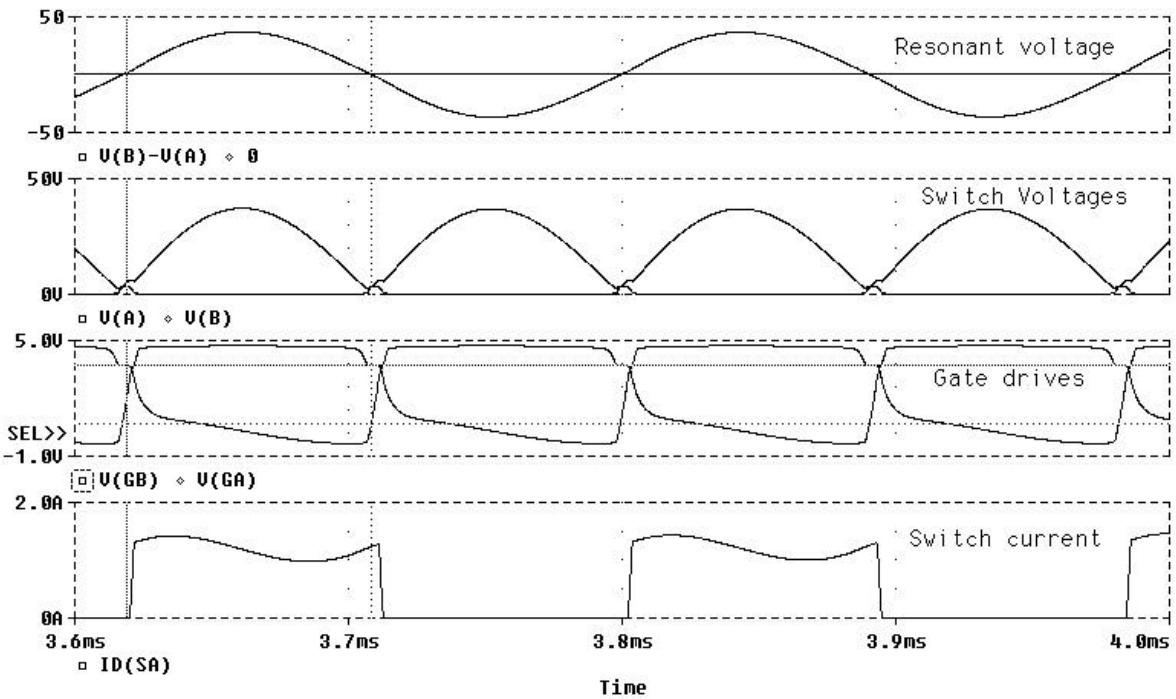


**Fig. 7-7: Typical simulated waveforms of the proposed converter**

If the resonant voltage is below the zener diode voltage level, the gate drive voltage becomes very small and both switches tend to switch off. This should be strictly prohibited for current-fed resonant converters, because the DC current has to continue to avoid the occurrence of dangerously high voltages. Fortunately, the proposed converter can protect the over voltage automatically. From Fig. 7-7 it can be seen that if the voltage $V_B$ is lower than the zener diode voltage 4.7V, the gate voltage $V_{GA}$ starts to drop. When $V_{GA}$ reaches the threshold voltage of about 3V, switch $S_A$ starts to turn off, causing a rapid voltage rise that turns the other switch $S_B$ on very quickly. As a result, the DC current follow continues and the occurrence of a high over voltage is avoided. Since in practice, switches turn on faster than they turn off, and no external control loop delay exists in this converter, it is impossible for the dynamic voltage to become too high although small glitches occur in the voltage waveforms of $V_A$ and $V_B$ during the switch transitions as shown in Fig. 7-7.

The gate drive waveforms shown in Fig. 7-7 have a reasonably good rising edge because they are directly driven by the large resonant voltages across the main switches which quickly rise above 5V. However the falling edge of the gate drive lasts longer due to the large resistance in the discharge path of the gate input capacitor and the miller effect. Theoretically a higher resonant voltage and higher frequency will make both the rising and falling edge of the gate drive signal sharper if only a simple resistor and zener diode circuit is considered, but practically the need for larger limiting resistances $R_A$ and $R_B$ and stronger miller effect at high voltages may prevent the devices from turning off. This problem is discussed further in the next section. At low voltages, all



InductEV, Inc.
Exhibit 1020
Page 204

these effects are small so that circuit oscillation can be sustained and the circuit functions well. An advantageous factor of this circuit is that the turn-on process is faster so that the current is quickly diverted away which helps the switch to turn off. Fig. 7-7 shows that the tail current of the switch ($I_D$) lasts a very short time. Also, the Miller effect is small during turn-on, but it helps to reduce the gate drive voltage during the fall period of the resonant voltage in the second half of the waveform. The gate voltage can become negative (as shown in Fig. 7-7) because the zener diode becomes forward biased as the Miller capacitor discharges. This ensures that the switch is turned off completely before it is turned on again in next switching cycle.

It should be noted that although some distortions exist over the switch voltages during circuit transitions, they hardly appear in the final resonant voltage waveforms as shown in Fig. 7-7. In consequence, the resultant resonant current in the track loop contains very low harmonic components and produces minimal EMI radiation.

### *7.3.3 Experimental Results and Discussion*

A prototype converter of the form of Fig. 7-6 with parameters of L=200μH, C=0.47μF, $L_d$=0.2mH, $L_{sp}$ =2mH, $R_A$=$R_B$=1kΩ, and a zener diode of 5.1V/1W, was built and tested in the laboratory using

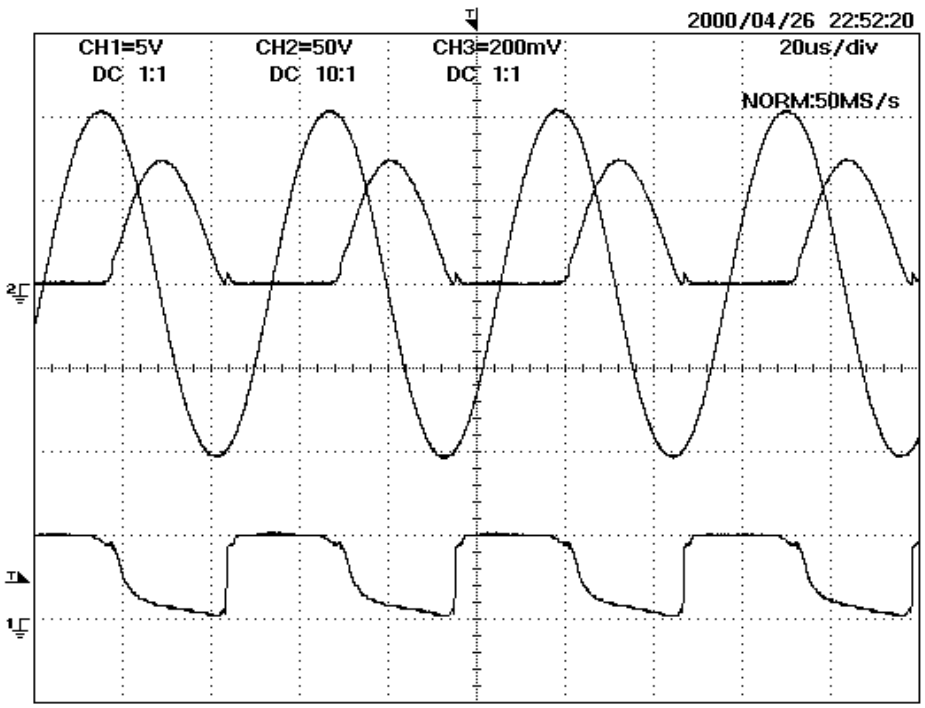


(Ch1 → Gate drive voltage: 5V/div, Ch2 → Switch voltage: 50V/div, Ch3 → track current: 2A/div)

**Fig. 7-8: Experimental result of the proposed converter**



InductEV, Inc.
Exhibit 1020
Page 205

100V/8A/0.4Ω MOSFETS. The converter can start up automatically by just turning on the main switch of a regulated DC power supply without employing any start-up equipment. Fig. 7-8 shows the measured waveforms of the switching voltage over switch $S_A$ (a half wave), the track current (a full wave), and the gate drive signal $V_{GA}$. The DC input voltage $V_d$ is 24V and the equivalent load resistance R on the track is 1Ω. It can be seen from this result that switching occurs approximately at the zero voltage crossing points as expected, and the sinusoidal waveform of the resonant current is perfectly acceptable.

The above test was based on a series-connected load (see Fig. 7-6). A parallel-connected load gave very similar results. In both the cases, the converter could start up automatically and keep self-sustained ZVS. The resonant voltage and current vary proportionally to the DC input voltage, and it has been observed that the gate drive waveforms improve with increasing the DC input voltage. Nevertheless, the increase is limited by the power ratings of the resistors and zener diodes of the gate drive circuit so that operating at high voltages is impractical as will be discussed later. Moreover, the operating frequency of the converter can be adjusted by simply varying the capacitor or inductor of the resonant circuit, and this can even be done during operation. Under such variations, the converter automatically adapts to the new operating conditions with dynamic ZVS operation. There is no danger of damaging the switching devices owing to the inherent over voltage protection property of the converter discussed earlier. Because of the elimination of any external controllers, the system delay and the total component count is greatly reduced. This helps to increase the maximum possible operating frequency and power density, as well as improve the power efficiency and reliability at reduced cost. However, as with the G1 and variable frequency power supplies based on free oscillation and energy injection control, the operational frequency of this converter is dependent on the load so that frequency stability problem can occur. As such the design of a complete IPT system using such converters requires care to achieve the required power transfer capacity.

Apart from the above example converter based on the current-fed parallel-resonant G1 supply, there are other options of achieving a self-sustained switch-mode operation that are worth further exploration in the future. One potential application of this type of converter is in the development of higher frequency converters (say 1-10MHz) aiming to significantly increase the power density. It is known that the design of gate drives becomes difficult at such high frequencies for normal low voltage drive circuits [10]. Surprisingly, it can be easier for the self-sustained converters to achieve desirable gate drive waveforms because the required signals and power are integrated and internally



InductEV, Inc.
Exhibit 1020
Page 206

supplied from the main circuit where high frequency voltages or currents are available. To overcome the shortcomings of this type of converter regarding the lack of control flexibility, other control mechanisms such as varying circuit parameters (rather than via gate drive control), may be used to regulate the final output as required.

## 7.4 Implementation of Self-sustained Converters for High Power Applications

### *7.4.1 Gate Drive Problems of the Self-sustained Converter at High Voltage levels*

The self-sustained converter is shown to be both simple and functional at low voltages up to a DC input of about 50V (157V peak for the resonant voltage). However, for practical high power industrial applications with a DC voltage of 200V to 300V or higher, the simple gate drive circuit used becomes impractical. This is because the resonant voltage, which functions as the input voltage of the gate drive can go as high as 1000V and this makes the design of the current limiting "dropper" resistors and zener diodes of the gate drive circuit impractical. At high voltage levels, the resistance of the "dropper" resistor has to be high to limit the current through the zener diode and reduce the power losses. However, this can result in several limitations on the gate drive. Firstly, the gate drive voltage will rise slowly due to the reduced charging current, which will affect the turn-on speed of the switching devices. This is particularly true in the initial period of zero voltage crossing when the resonant voltage is very low. Secondly and more importantly, the large resistance makes the discharge of the input capacitor very slow and this can cause turn-off failure. Moreover, during turn-off, the charging current of the Miller capacitor tends to increase the gate voltage and therefore further prevent the gate drive signal from falling down to zero. Since high VA rated MOSFETs and IGBTs have larger input and Miller capacitances, these problems become very challenging when designing high power converters.

A possible solution is to have a voltage-controlled non-linear resistor as shown in Fig. 7-9(a). If the resistance of this variable resistor decreases as the voltage across it decreases, then the problems discussed above can be solved automatically. In high voltage periods, the resistance is high so that the power losses are low. Conversely, during the low voltage transition periods, the resistance is low so that both the rising edge and falling edge of the gate drive signal can be improved. Unfortunately, no suitable resistor with such a nonlinear property has been found in the commercial market. Normal thermally variable resistors are far too slow for this application.



InductEV, Inc.
Exhibit 1020
Page 207

Alternatively, adding additional components, such as a speed-up capacitor in parallel with the current limiting resistor as shown in Fig. 7-9(b) can provide a phase advance and reduce the transition delay. However, the dilemma is that a small capacitance has little effect, but a large capacitance makes the gate drive voltage drop too early before the actual zero voltage crossing due to the fact that the resonant voltage starts to drop in the second half of the "off" period. As noted, turning the devices off too early interrupts the DC current flow and causes high over-voltages which may damage the switching devices. As a result, more sophisticated charging and discharging circuits are needed to achieve desirable gate drive waveforms for high voltage applications.

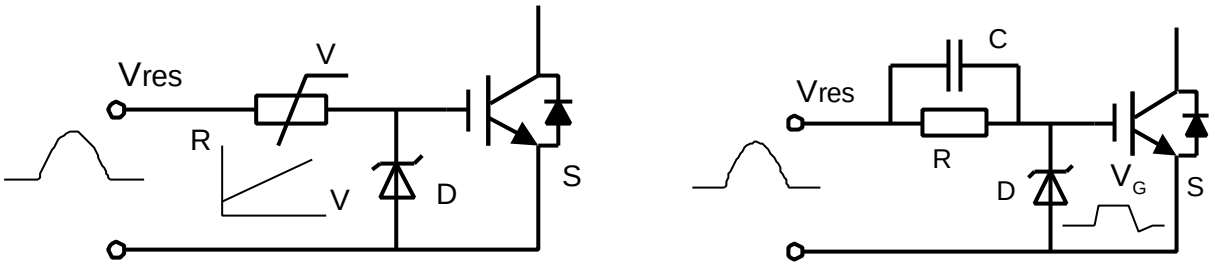


(a) Using a voltage-controlled variable resistor (b) Using a speed-up capacitor

**Fig. 7-9: Passive gate drive circuits for the self-sustained resonant converter**

## *7.4.2 Practical IPT Power Supplies Using PLL and ZVD Techniques*

A very appealing feature of the self-sustained converter proposed in Section 7.3 is that all the power and signals needed for driving the switching devices are supplied by the resonant voltages inside the circuit. This simplicity has many advantages as well as gate drive problems at high voltages as discussed earlier so the idea is worth following. Two novel gate drive schemes using PLL (Phase Locked Loop) and direct ZVD (Zero Voltage Detection) techniques were investigated to build IPT power supplies for practical high power applications.

Fig. 7-10 is a block diagram showing how the PLL technique can be used to control a resonant circuit. In this diagram the VCO (Voltage Controlled Oscillator) unit is set at a predetermined frequency by a resistor $R_T$ and a capacitor $C_T$, say 40 kHz, when its input voltage is set at half the DC supply voltage $V_{cc}$ by two equal resistors R. The output from the VCO is divided by 4 to obtain the system nominal frequency (eg. 10 kHz here) and a phase shift of 90 degrees using a normal D flip-flop circuit. Then the output signal is divided into two complementary signals and sent to an IGBT gate drive circuit (such as H7667) to drive the two main switches of the resonant circuit. From the ZVS frequency analysis of the current-fed resonant converter undertaken in Section 3.2 of



InductEV, Inc.
Exhibit 1020
Page 208

this thesis, it has been shown that the switching frequency has to be varied to achieve ZVS operation. For this reason, the resonant voltage ($v_{res}$) of the main circuit is detected and fed back to change the actual operating frequency which can be slightly higher or lower than the nominal frequency. The resonant voltage may be measured directly across the two main switching devices, however the voltage measured will be very high so a voltage divider with a very large turn down ratio has to be used and this is not desirable to cater for a wide range of operating voltages. Alternatively, a one-turn coil added to the phase-splitting transformer of the converter (see Fig. 7-6) can be employed as a very simple and reliable voltage sensor. The measured resonant voltage is converted to a square waveform using a high gain amplifier and is then compared with the output of the VCO (after the frequency divider) using a XOR logic circuit. These two signals should be equal in frequency but have a 90 degree phase shift as required for the XOR detection circuit. After a RC low pass filter, the output pulses from the XOR will control the input voltage of the VCO thus vary the actual gate driving frequency to the point where a stable ZVS frequency is obtained.

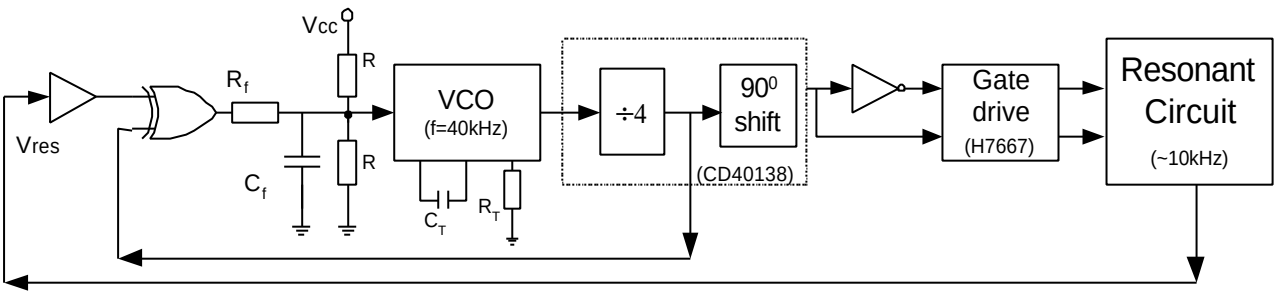


**Fig. 7-10: PLL gate drive technique**

Unlike PLL gate drive which is based on frequency shift control, Fig. 7-11 shows the block diagram of a direct ZVD technique. The advantage of this technique over PLL is that after the resonant voltage is measured, the zero crossings of the resonant voltage are detected instantly using a zero voltage detection circuit, and the output is used to control the gate drive directly. However, as discussed in Section 3.4 of this thesis, the current-fed resonant converter has start-up problem because the resonant voltage does not go to zero naturally in the beginning. A complete new technique is used to overcome this problem. On starting both switches are turned on at the same time so that the current in the DC inductor increases rapidly. When enough energy is stored in the inductor compared to the energy in the resonant circuit in normal operation, one switch is turned off and the circuit then completes a first half-cycle followed by normal operation with direct ZVS control [8]. To achieve this desirable condition, start-up timing logic is added as shown in Fig. 7-11. Also, to avoid an additional DC power supply for the gate control circuitry and form a completely self-sustained converter, a simple zener diode configuration is used although the initial power build-



InductEV, Inc.
Exhibit 1020
Page 209

up process has to be considered to make the circuit work properly. If the ramp up delay of a practical input DC supply is taken into account, an overshoot free soft start-up can be achieved. Consequently, the system can start up simply by turning on the main switch of the input power supply without employing any additional equipment.

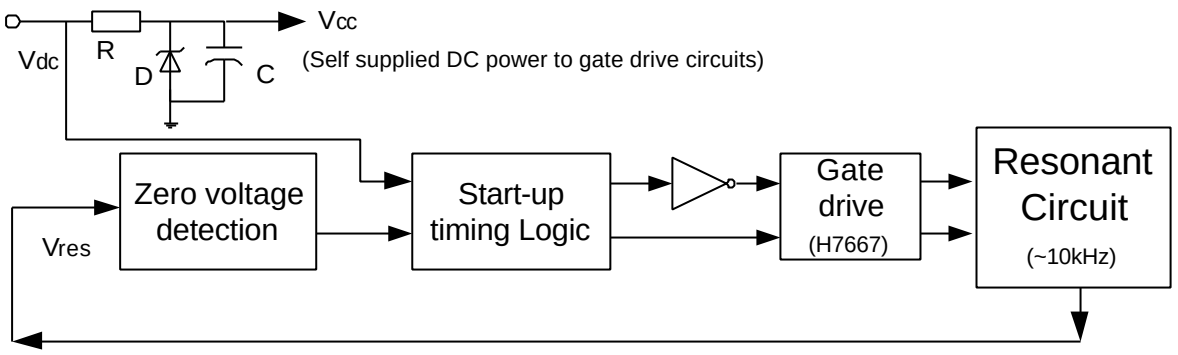


**Fig. 7-11: Direct ZVD gate drive technique**

Fig. 7-12 shows the measured steady state resonant voltage (across one of the main switches) and the gate signal waveforms of a practical 80A/10kHz current-fed parallel resonant IPT power supply using the direct ZVD technique. The DC input voltage is 240 V and the DC current can be up to 60 A corresponding to a maximum load of about 15 kW. The main circuit of the converter is the same as the self-sustained converter (essentially the G1 power supply) shown in Fig. 7-6. The track inductance is 125μH and its parallel tuning capacitance is about 2μF. It can be seen that ZVS operation is achieved and both the rising and falling edges of the gate drive waveform are significantly improved owing to the adoption of the specially designed MOS gate drive circuit (H7667).

A PLL circuit was also built to control a power converter with the same specifications as that of the direct ZVD. Because the same gate drive chip was used, very similar gate signal waveforms were obtained. To avoid repetition, Fig. 7-13 shows the resonant voltage and the resultant track current of this IPT power supply. In fact, it has been observed that the track current waveforms of the two supplies are basically the same because they achieve very similar steady state ZVS performance. However, a close look at the resonant voltage waveforms shows that the switching of the ZVD scheme is slightly slower due to the circuit delay (which is mainly caused by the practical comparator used). In comparison, the average ZVS error of the PLL circuit can be smaller under ideal steady state conditions because it has an integral control loop and can add in some phase advance to the gate drive signals. However, this is only true when the feedback loop of the PLL is tuned accurately. Practical circuit parameter and voltage variations can introduce errors in the PLL



InductEV, Inc.
Exhibit 1020
Page 210

circuit and as a result the actual difference between the steady state ZVS errors of the two IPT power supplies is barely perceptible.

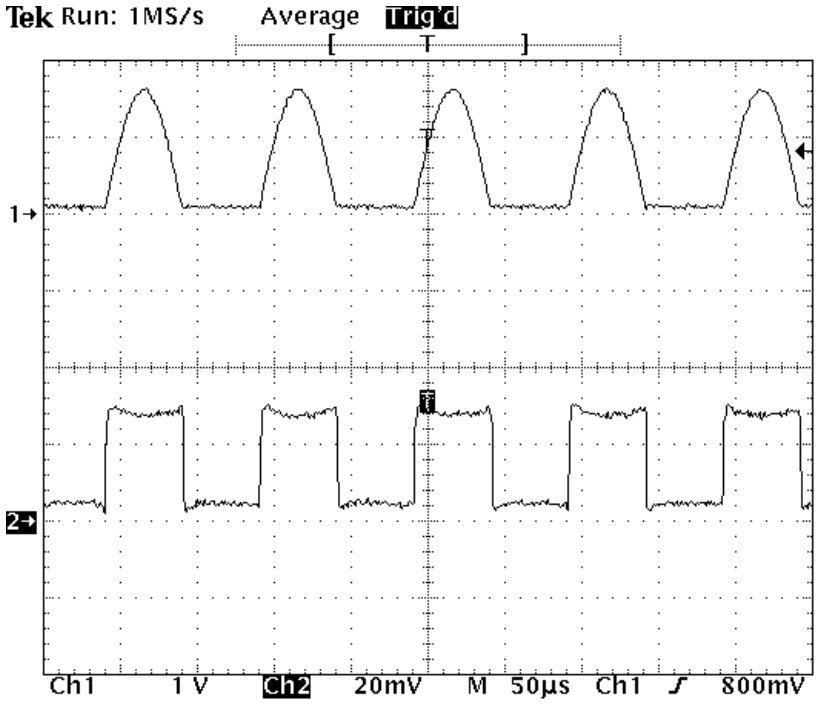


(Ch1 → Resonant voltage across the switch: 500V/div, Ch2 → Gate drive signal: 10V/div)

**Fig. 7-12: Steady state waveforms of an IPT power supply using direct ZVD**

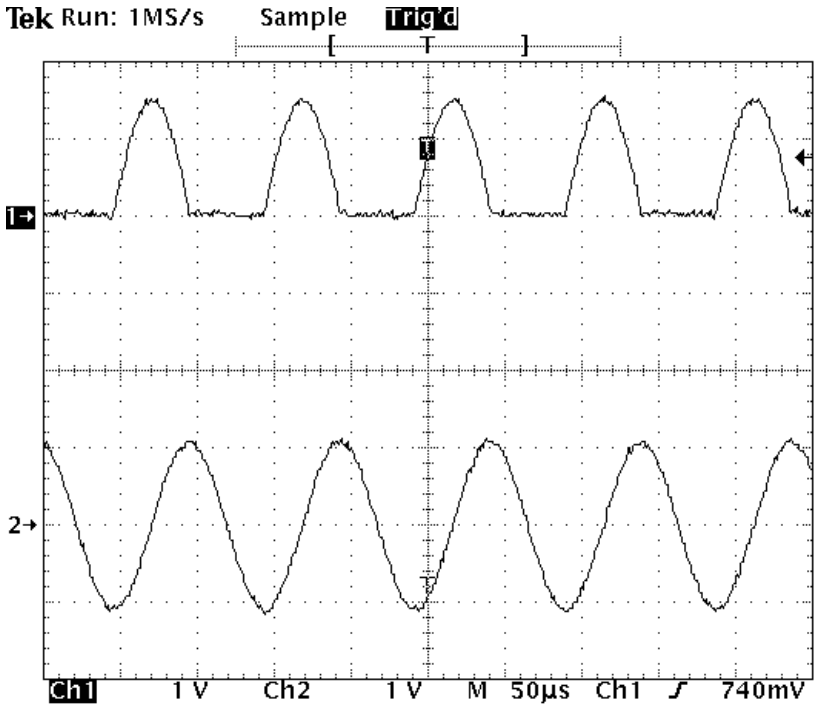


(Ch1 → Resonant voltage across the switch: 500V/div, Ch2 → Track current: 100A/div)

**Fig. 7-13: Steady state waveforms of an IPT power supply using PLL**



InductEV, Inc.
Exhibit 1020
Page 211

Apart from being simple and cost-effective, the most outstanding advantage of the direct ZVD circuit over the PLL is its dynamic performance. The PLL circuit has a predetermined frequency and its internal "integral" process causes relatively slow frequency response so that dynamic ZVS is impossible. As a result, additional blocking diodes have to be put in series with the main switches for safe operation and special care has to be taken in designing the PLL circuit to ensure the frequency can be captured by the PLL during start-up and load transients. Conversely, the ZVD circuit simply follows the zero voltage crossings with limited predictable errors during the whole process so that the series blocking diodes are optional. Although frequency stability problems may occur under some extreme conditions as discussed previously, during normal working conditions the circuit oscillation continues and the direct ZVD operation is very reliable. The actual operating frequency can be varied simply by changing the resonant inductor or the parallel tuning capacitor without any modification of the gate drive circuit. The basic concept employed here is essentially the same as the simple self-sustained converter proposed in Section 7-3, but the gate driving property is significantly improved making high power application possible.

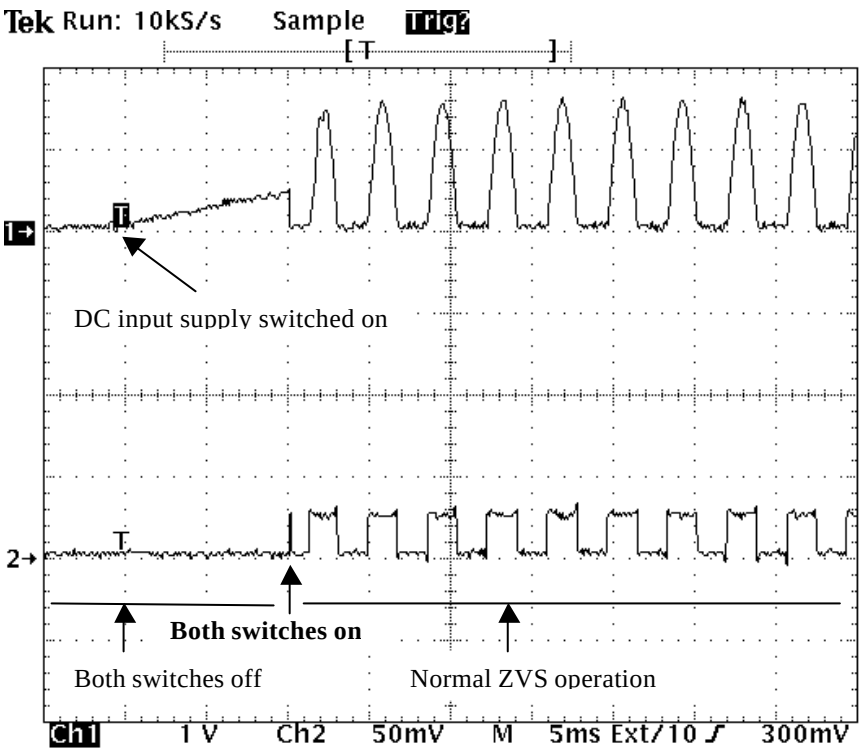


(Ch1 → Resonant switch voltage: 500V/div, Ch2 → Gate drive signal: 10V/div)

**Fig. 7-14: Start-up waveforms of a practical IPT power supply using direct ZVD**

Using the method discussed above, an 80A/10kHz IPT power supply based on direct ZVD has been built and overshoot-free dynamic ZVS start-up and steady state performance has been achieved. Fig. 7-14 shows a measured result of the resonant voltage across one of the two main switches and



InductEV, Inc.
Exhibit 1020
Page 212

the gate drive signal of the other switch. It can be seen that the voltage across the switch, which is equal to the DC input voltage, ramps up gradually in the beginning when both the switches are off. After a very short DC current build-up period (where both the switches are on, shown with the first short pulse of the gate drive signal in Fig. 7-14) before the DC voltage reaches its maximum value, the circuit goes into ZVS operation very quickly and smoothly without any overshoots. As a result, the stresses and losses of the switching devices are minimised. This feature is particularly useful for applications where frequent "on" and "off" control of the converter is required. An IPT pulse battery charging system controlled from the primary side is a good example of such an application.

## 7.5 Summary

Two novel resonant converters have been proposed in this chapter: the first one is based on free circuit oscillation and energy injection control, while the second one is concerned with self-sustained oscillation without using an external controller. Unlike conventional resonant converters, the switching frequency of the converter based on energy injection control can be much lower than the frequency of the track current, so that switching losses can be minimised. Moreover, its dynamic property is improved with very fast and smooth response.

From a system design and control point of view, the self-sustained converter has revealed an important fact: a well-constructed switch-mode nonlinear circuit can generate high frequency AC power without using an external controller. Because both the signals and power required for the gate drives are self-supplied, the circuit operation relies completely on switch-mode autonomous oscillation. As a result, the system component count, as well as the cost and size, can be significantly reduced.

Two practical example circuits have been analysed and implemented to verify the validity of the proposed converters. Both simulation and experimental results have shown that the innovative converters have many appealing features suitable for high frequency AC power generation. Practical aspects regarding their IPT applications were considered. A direct AC-AC converter has been proposed with its EMI concerns highlighted. After analysing the gate drive problems of the self-sustained converter at high voltage levels, two practical IPT power supplies using PLL (Phase Locked Loop) and direct ZVD (Zero Voltage Detection) techniques have been built and tested. It has been demonstrated that the latter has the preferable dynamic performance and is suitable for practical high power IPT applications.



InductEV, Inc.
Exhibit 1020
Page 213

## 7.6 References

[1] Boys, J. T. and Green, A. W.: "Inductively coupled power transmission – concept, design and application", *IPENZ Transactions*, No.22, (1) EMCH, pp.1-9, 1995.

[2] Knaup, P. and Hasse, K.: "Zero voltage switching converter for magnetic transfer of energy to movable systems", *European power Electronics Conference*, *EPE'97*, 2, pp.168-173, 1997.

[3] Hu, A. and Boys, J. T.: "Series-parallel resonant converters, Stage I: Current-fed, single ended, series-parallel converter simulation", *Research Report of Auckland Uniservices Ltd for Wampfler AG, Germany, and Daifuku Ltd, Japan*, 52 pages, June 1998.

[4] Green, A. W. and Boys, J. T.: "An inductively coupled high frequency power system for material handling applications", *International Power Electronics Conference*, IPEC'93, Singapore, (2), pp.821-826, 1993.

[5] Green, A. W. and Boys, J. T.: "10kHz Inductively coupled power transfer – concept and control", *IEE Power Electronics and Variable Speed Drives Conference*, PEVD, Pub.399, pp.694-699, 1994.

[6] Trzynadlowski, A. M.: *Introduction to modern power electronics*, John Wiley & Sons, Inc., 1998.

[7] Kazimierczuk, M. K. and Czarkowski, D.: *Resonant power converters*, John Wiley & Sons, Inc., 1995.

[8] Hu, A., Boys, J. T. and Covic, G.: "Dynamic ZVS direct on-line start-up of current-fed resonant converter using initially forced DC current", *Proceedings of 2000 IEEE International Industrial Symposium on Industrial Electronics*, Vol. 1, pp.312-317, Puebla, Mexico, December 2000.

[9] Boys, J. T., Hu, A. and Covic, G.: "Critical Q analysis of a current-fed resonant converter for ICPT applications", *IEE Electronics Letters*, Volume 36, Issue 17, ISSN 0013-5194, pp.1440-1442, August 2000.

[10] Ang, S. S.: *Power switching converters*, M. Dekker, New York, 1995.



InductEV, Inc.
Exhibit 1020
Page 214

## Chapter 8

# Conclusions and Suggestions for Future Work

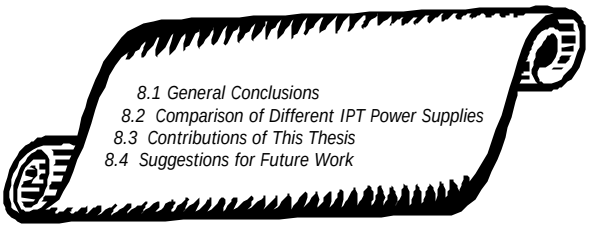


## 8.1 General Conclusions

A comprehensive study on selected resonant converters for IPT (Inductive Power Transfer) applications has been undertaken in this thesis. Attention has been paid to the following three main aspects:

The fundamental properties of basic current and voltage fed resonant converters;
Techniques for improving the performance of existing IPT power supplies;
New resonant converters and practical aspects of IPT power supply applications.

A general introduction to IPT and an overview of the technologies involved in the development of IPT power supplies has been presented in the first two chapters of this thesis. The major components of an IPT system have been systematically discussed in the overview which lays a basis for this thesis study and is also beneficial for future research in this area. It has been shown that high quality track current generation is one of the key issues affecting the overall performance of an IPT system. Therefore, high quality power converters are of primary importance. Resonant converters are most suitable for IPT power supplies as a result of minimised switching losses and electromagnetic interference. Since the inherent track inductor of an IPT system can be used as part of the resonant tank, load resonant converters are preferred to other resonant configurations. While the track current of an IPT supply can be directly controlled with closed-loop feedback, indirect control strategies such as ZVS control can be employed to reduce the system cost and simplify the controller design without compromising the overall performance of an IPT power supply.



InductEV, Inc.
Exhibit 1020
Page 215

Depending on the application, an IPT track can simply be a lumped coil, or an extended parallel set of cables (or partially parallel cables). The track can be series tuned, parallel tuned, or tuned in a composite form as long as the tuning does not conflict with the voltage-fed or current-fed network properties at its input port. A new parameter, termed the "coupling factor" has been introduced to describe the local coupling between the track and the power pick-ups more accurately.

Although the power flow from the track to the pick-up can be controlled in many ways, short circuiting the pick-up as discussed in section 2.4.3 is most suited to parallel tuned pick-up circuits whose output voltage can be boosted easily to meet the load requirement. Similar to the track tuning circuit, the pick-up circuit can be series, parallel, or compositely tuned in order to improve the power transfer ability. System frequency detuning and power blocking problems can occur because of the effect of the reflected impedance of the pick-up circuits which can be analysed using a pick-up load model.

Following the general review in Chapter 2, an extensive study has been undertaken in Chapter 3 into the current-fed parallel resonant converter power supplies (G1) that have been commonly used in IPT applications. The voltage balance between the DC and AC side of the inverter has been highlighted. In comparison to the full bridge topology, the push pull topology doubles the resonant voltage and does not need isolated gate drives. In consequence, it is widely used in applications needing a high AC drive voltage (compared to the DC input voltage) and simple control circuitry. For current-fed converters without series blocking diodes, ZVS is not only a control strategy but also a crucial requirement to prevent momentary short circuit. A variable frequency controller is normally needed to "track" the circuit oscillation so as to achieve ZVS.

For high Q circuits such as those used in radio systems, all the "resonant" frequencies are very close and converge to the undamped natural frequency of the system. However, in an IPT system, Q is normally designed as low as possible for economical and practical reasons. In this situation, the condition for the occurrence of different types of resonances and their corresponding "resonant" frequencies can be quite different. Based on a second-order parallel-resonant circuit used in the G1 power supplies, these various "resonant" frequencies, such as zero phase angle resonant frequency, maximum inductor current frequency, and maximum capacitor voltage frequency have been discussed and clarified. Moreover, the ZVS frequency which is normally the operating frequency of a current-fed resonant converter has been fully analysed using both analytical and numerical methods. A minimum bound for Q has been found to be 1.86 if steady state ZVS operation is to be



InductEV, Inc.
Exhibit 1020
Page 216

maintained. A full analysis of the results has also shown that the frequency at which ZVS occurs is lower than all other theoretical resonant frequency conclusions.

When the pick-up circuit is taken into account, the impedance of the track resonant tank becomes a high-order frequency and load dependent parameter. In consequence when determining the ZVS frequency, multiple solutions can exist which complicates any controller design and potentially causes system frequency detuning problems. For this reason the system operating frequency of an IPT power supply can jump between these solutions instead of shifting gradually around a predetermined nominal frequency. Such a frequency stability problem has been analysed for fully series-tuned tracks and pick-up circuits. Accurate and concise criteria that ensure the frequency stability of ZVS operation have been defined. Furthermore, closed form equations for determining the frequency shifts have been developed. Considering the dual circuit properties and approximations of high Q equivalent circuits, it has been found that the results obtained for the series tuned circuits are approximately valid for other tuning circuits as well. These results are of significant importance in designing a stable IPT system. Based on these results, several frequency stability enhancing methods, such as simply increasing the operating frequency of an IPT system with parallel tuned power pick-ups, increasing the track reactive power rating, and undertaking dynamic parameter tuning have been discussed.

In the final section of Chapter 3, significant improvements have been made to the start-up properties of the G1 power supplies. These power supplies used to be forced with an external oscillator during the first few switching cycles at start up and then switched to normal ZVS operation. A low voltage start-up process had to be employed to prevent failure of the devices. A dynamic analysis of a ramp-up current source model has been undertaken and it has been determined that no zero voltage crossing point exists during the first half switching cycle of a current-fed parallel resonant converter that employs normal oscillator control. As such ZVS is impossible and the resultant high shorting currents can damage the switching devices. A novel method has been proposed in this thesis to solve this problem using an initially forced DC current. All the switches of the inverter are controlled “on” for a short time so that the DC current increases and some energy is stored in the DC inductor. This stored energy can then be transferred to the resonant tank by turning one switch off. If enough energy can be transferred, then the resonant tank starts oscillating with the correct zero voltage crossings so that dynamic ZVS operation can be obtained easily. A critical condition ($Q>2.54$) has been derived for ZVS start-up. The validity of the method has been verified with PSpice simulations and experimental results. Considering the ramp up delay of a practical DC power supply, a complete overshoot-free start-up process has been achieved by timing the starting



InductEV, Inc.
Exhibit 1020
Page 217

point of the energy transition from the DC inductor to the resonant tank. Since a very simple controller can be used in a practical implementation and no additional starting equipment is required, this method has improved the system start-up performance as well as the reliability at reduced cost.

In Chapter 4, a new current-fed parallel-series CLC resonant converter power supply (the current-fed G3) which significantly improves the G1 supply has been proposed. The adoption of the trans-conductance CLC π network results in highly desirable track current properties as required by IPT power supplies. Specifically, it converts a voltage source into a constant track current source, presents a unity power factor load to the resonant converter by matching the impedance, and also filters the harmonics between the source and the load. The underlying properties of the tuned track network, such as the poles and zeroes of the trans-conductance transfer function have been analysed. Sensitivity studies, including worst case analysis and Monte Carlo analysis, have also been undertaken to identify the most sensitive components and predict the maximum system variations. Here the inductor of the CLC π network has been found to have the highest sensitivity affecting the track current magnitude, while the track inductor and its tuning capacitor are the most sensitive elements affecting the input phase angle and thus the ZVS frequency shift. A basic design methodology for this converter has been presented and the necessary design equations have been developed. With the pick-up circuit taken into account, the system dynamic properties have been studied using dynamic PSpice simulations under various track lengths and loading conditions. The validity of the proposed G3 power supplies and their design methods have been proven with the simulation results.

In Chapter 5, voltage-fed resonant converter power supplies have been studied and compared with series resonant converters. The basic properties of the voltage-fed G2 power supply have been analysed first. In particular, the phase shifted track current control and soft switching operation have been discussed in detail. In this converter, the energy stored in the net equivalent inductor of the series tuned track has to be sufficient to charge/discharge the soft switching capacitors, otherwise the shorting of the soft switching capacitors can damage the semiconductor devices. The voltage-fed G3, which is approximately the dual of the current-fed G3, has also been investigated. It is based on the adoption of an LCL trans-conductance T network which improves the track current quality in a similar manner to the CLC π network in the current-fed G3. However, the dynamic ZVS and phase-shift soft-switching operation of the voltage-fed G3 is very difficult to achieve due to the complexities involved in the high order transient process. It has been determined that the



InductEV, Inc.
Exhibit 1020
Page 218

system can operate at resonant modes that deviate from the nominal resonant frequency if only a simple ZVS control strategy is employed.

In Chapter 6, the current-fed G3 power supply has been mathematically modelled using GSSA (Generalised State Space Averaging) techniques. This has resulted in a dynamic linear model suitable for fast analysis of the complete IPT system including loosely coupled pick-ups. This model and its discrete equivalents have been used to undertake both steady state and dynamic analysis of the complete system. The results have shown fairly good agreement with the original system design and PSpice simulations.

A new concept for a resonant converter based on free oscillation and energy injection control has been proposed for IPT power supplies in Chapter 7. Unlike all other resonant converters, the uniqueness of this converter is that the switching frequency can be much lower than the circuit oscillation frequency. Switching transitions are only necessary when the resonant tank requires energy to maintain a defined oscillation level at the free ringing frequency. A simple example converter with only two switches, a series tuning capacitor, and a track inductor has been analysed, simulated, and experimentally verified. The results have shown that this converter possesses many appealing features suitable for high frequency AC power generation, particularly when a long track length, high track current, and high frequency are required. The proposed concept opens a new research area for the development of IPT power supplies and other power conversion applications. Many possibilities exist to design the circuit topology and control strategy. A direct AC-AC power converter has been investigated which looks very promising.

Another innovative concept has been proposed in Chapter 7 to utilise the switch mode non-linear autonomous oscillation without using an external controller. An example self-sustained converter has shown good simulation and experimental results at low input voltages. However, it has gate drive problems at high voltage levels in practical implementation. A simple cost-effective solution has been found and an IPT power supply suitable for practical high power applications has been built with excellent start-up and dynamic ZVS performance.

## 8.2 Comparison of Different IPT Power Supplies

Various IPT power supplies have been studied individually in this thesis. As part of the conclusion, the advantages and disadvantages of these power supplies are summarized in this section, and a table ranking their relative strengths and weaknesses is developed for comparison purposes.



InductEV, Inc.
Exhibit 1020
Page 219

***The generation one (G1) supply*** described in Chapter 3 is based on a current-fed parallel resonant converter. The track driving voltage is approximately constant at steady state provided ZVS is achieved. As the equivalent load is in series with the track impedance, the converter provides an approximate voltage-controlled current source in the track when the quality factor (Q) of the track is high.

*The main advantages of the G1 supply are:*

Low harmonics and EMI as a result of operating with full resonance in the track that produces good sine wave currents.

Low conduction loss and high power efficiency due to the parallel tuning that makes reactive power circulate inside the resonant tank and only the load current go through the main switches. For this reason, lower current rating devices can be used.

ZVS is easily achieved by allowing the frequency to follow the zero crossings of the resonant voltage. This essentially eliminates the switching losses so that the power efficiency is further improved.

There is no turn down ratio limit, which means that the DC input voltage can vary in a wide range to control the track current and regulate against mains voltage variations and other disturbances.

*The main disadvantages of the G1 supply are:*

Variable frequency ZVS operation may cause frequency stability problems at heavy loads where system detuning occurs.

The track length and current level are limited by the available voltage ratings of the semiconductor switches, typically being about 100m. The power level is thereby also limited.

The timing of the gate driving signal (of the converters without series blocking diodes) is critical to avoid momentary short circuiting of the tuning capacitor, or occurrence of an over voltage.

The circuit has no over-current or over-voltage protection capabilities via the main switches, therefore an additional circuit may be required for open circuit or short circuit protection.

***The generation two (G2) supply*** discussed in Chapter 5 is based on a voltage-fed phase shift soft-switching converter. The track circuit is series tuned above the resonant frequency for soft switching. In consequence, the circuit is not in full resonance. However, as the residual track inductor oscillates with the parasitic and/or additionally added soft switching capacitors in parallel



InductEV, Inc.
Exhibit 1020
Page 220

with the switches, soft switching operations can be obtained with zero voltage and/or zero current transitions.

*The main advantages of the G2 supply are:*

The frequency is stable owing to the phase shift PWM control.

The voltage rating of the switching devices is limited within the DC input voltage. Therefore, the voltage rating of the switching devices are lower than the G1supply.

Complete soft switching techniques can be utilised to eliminate the switching losses and alleviate the switch stresses and EMI.

The track length is easily extended using series compensation capacitors.

*The main disadvantages of the G2 supply are:*

The track current has more harmonics than the G1 supply so that EMI is relatively higher.

Conduction losses are high because the full (high) track current goes through the main switches and the DC source even under no load condition.

The turn down ratio for the DC input voltage is poor and the tolerance of the track impedance variation is small due to the critical soft switching conditions. If the soft switching fails, the soft switching capacitors will be repeatedly short circuited which will damage the devices.

The track length, current and power level are limited by the available voltage, track tuning and loading conditions.

***The newly developed generation three (G3) power supplies*** discussed in Chapter 4 and mathematically modelled in Chapter 6 are improved current-fed and voltage-fed power supplies. The current-fed G3 converter is a hybrid circuit combining the aspects of both the G1 and G2 supplies. The track is series tuned like the G2 except that it is fully tuned. The inverter side of the G3 is the same as the G1, therefore the track circuit needs to be parallel tuned at its input to meet the current source requirement. For this reason, the current-fed G3 converter is named a parallel-series resonant converter in this thesis to emphasise its hybrid and parallel tuning properties. The current-fed G3 involves the adoption of a trans-conductance CLC $\pi$ network which improves the system performance significantly. In the G1, the track current is controlled by the track inductance. Similarly, in the G2 power supply the track current is controlled by the net track impedance and an active closed loop control system. In the current-fed G3 however, the track current is controlled by the $\pi$ network and the track impedance has no effect. Impedance matching from the source to the track is achieved with a trans-conductance $\pi$ network. It is the development of this network that



InductEV, Inc.
Exhibit 1020
Page 221

makes the current-fed G3 supply possible as it converts a voltage to a current in exactly the form required for an IPT system.

*The current-fed G3 has almost all the good characteristics of the G1. In addition, it has the following improvements:*

The track current is independent of the track impedance and load. Therefore, a constant track current supply is obtained. Moreover, the track current is inherently short-circuit proof.

Theoretically there is no limit to the track length, current magnitude and power level as long as the track can be modelled with lumped parameters without considering the wave propagation problems.

The harmonics propagation between the source and the track is minimised due to the filtering of the CLC network which results in a high quality sine wave track current and reduced EMI.

Multiple $\pi$ networks and tracks can be connected to one converter so that multiple track power supplies at different current levels are possible. In addition, each individual track can be switched easily by just short circuiting it.

For variable frequency ZVS operation, the system frequency stability is enhanced due to the additional reactive power from the CLC network.

The voltage-fed G3 is essentially the dual of the current-fed G3, except that the track is kept series tuned to extend the track length. For similar reasons as mentioned in the current-fed G3, the converter used for the voltage-fed G3 is termed a series-parallel converter with series tuning at the input port of the track network. Its switching network topology is basically the same as the G2, and the impedance matching network is an LCL configuration that is the dual of the CLC used in the current-fed G3. The voltage-fed G3 has the basic properties of a G2 with improvements similar to that of a current-fed G3 as described above.

*The main disadvantages of the G3 power supplies are:*

The system can be bulky and expensive as a result the introduction of the CLC or LCL trans-conductance networks. This is particularly true when high power transfer is required which requires high voltage and current ratings for the reactive elements.

The system transient process may become very complex due to the increased system order. Dynamic controllers (such as ZVS controllers) designed for the G1 and soft switching controllers for the G2, may not work for the voltage and current fed G3 power supplies.



InductEV, Inc.
Exhibit 1020
Page 222

***The newly proposed converter based on the free oscillation and energy injection control*** is conceptually different from the conventional voltage-fed or current-fed converters. The emphasis is now on free oscillation with energy compensation rather than forced oscillation with driving sources.

*In comparison to the existing power supplies, notable advantages of power supplies based on this new converter include:*

The switching frequency is independent of the circuit oscillation frequency. A high frequency track current can be generated with a low switching frequency, therefore power efficiency can be significantly improved.

ZCS or ZVS operation can be easily achieved by selecting the energy injection instants so that the switching losses and stresses can be minimised.

The track length and current level are not limited by the available track driving voltages. High track voltages and currents can be boosted from a low voltage source.

Depending on the circuit topology, the maximum voltage and current stress of the switching device are contained. For the simple example DC-AC converter discussed in Section 7.2.2, the maximum voltage is limited to within the DC input voltage, while the maximum current is the peak track current.

The start-up and load transient response is both fast and smooth. There is almost no dynamic overshoot since the energy injection control is based completely on the dynamic system requirements. This is substantially different from direct source-driven converters such as normal voltage-fed and current-fed converters. In these converters, circuit operation completely relies on the steady state conditions and the transients may be very poor.

The converter is open-circuit and short-circuit proof because system protection can be simply undertaken by switching off the energy injection.

The converter is simple, cost effective, and robust.

*The disadvantages of power supplies based on the free ringing and energy injection control include:*

The magnitude of the track current has some fluctuation due to the discontinuous energy injection. This introduces random low frequency harmonics which are difficult to filter. Consequently, a large track inductance, high track current, high oscillation frequency, and a low input voltage are preferred in order to alleviate fluctuations and harmonics.



InductEV, Inc.
Exhibit 1020
Page 223

The free ringing frequency varies with the load, particularly when the quality factor Q of the track resonant circuit is low.

The output power capacity is determined by the energy injection ability which is related to the magnitudes of the source voltage and the injection current.

For the example DC-AC converter discussed in Section 7.2.2, the full track current has to flow through one of the switches which may result in high conduction losses.

***The converter based on self-sustained operation without an external controller*** originated from an insightful analysis of the current-fed parallel resonant converter (G1), which shows that the converter is virtually autonomous and ZVS can be regarded as an indirect control strategy. By reconstructing the circuit, an example converter without using any external controllers has been obtained in this chapter. The converter has achieved an overall performance that is better than or at least similar to the G1 but the circuitry is simplified significantly because all the power and signals required by the gate drives of ZVS are included inside the main circuit.

*The Main advantages of the self-sustained converter are:*

No external controller or other control circuitry is required, so that auxiliary power supplies, transducers, and gate drives are eliminated.

With decreased component count, lower cost, higher reliability, higher efficiency, and smaller size are expected.

*The main limitations of the self-sustained converter include:*

The converter, in its simple form, has gate drive problems at high voltage levels. Therefore, practical improvements are required for high power applications.

There is essentially no control ability via the gates of the switching devices as in the G1 power supply. Therefore, additional circuits are required if any protection or output regulations are required.

The system may lose its frequency stability under certain operating conditions such as heavy power pick-up loads due to the existence of multiple modes. The essence of the problem is the same as that of the G1 power supply.

*In summary*, table 8-1 compares general performance of IPT power supplies based on the various resonant converters covered in this thesis. Note that each performance rating is roughly graded using four levels for comparison purposes. The evaluation of the two newly proposed converters is



InductEV, Inc.
Exhibit 1020
Page 224

mainly based on the example converters with little consideration of their possible variations. It can be seen that the G3 power supply has the most ideal track current properties but it is also the most expensive and bulky. The G1 power supply and its self-sustained version are very efficient although their power rating and track length are limited. The G2 supply has the best frequency stability and a medium track length and power capacity. The power converter based on free ringing and energy injection control has the best dynamic response and very low switching losses. It can reach a long track length and high power level at a relatively low cost. However, its track current waveform is the poorest of all the converters.

**Table 8-1: Comparison of IPT power supplies based on different resonant converters**

| Supplies / Properties | Current-fed parallel (G1) | Voltage-fed series (G2) | Improved voltage or current-fed (G3) | Free oscillation & energy injection | Self-sustained without controllers |
|---|---|---|---|---|---|
| ***Track Length*** | Short | Long | Very long | Long | Short |
| ***Power Level*** | Low | Medium | Very high | High | Low |
| ***Current Waveform*** | Good | Medium | Very good | Poor | Good |
| ***Current level*** | Low | Medium | Very high | High | Low |
| ***Frequency Stability*** | Poor | Very good | Medium | Medium | Poor |
| ***Dynamic Response*** | Medium | Good | Medium | Very good | Medium |
| ***Switching Loss*** | Very low | Very low | Low | Very Low | Low |
| ***Conduction Loss*** | Very Low | Very high | high | Low | Very low |
| ***Cost*** | High | High | Very high | Low | Very low |
| ***Size*** | Small | Medium | Large | Small | Very small |

## 8.3 Contributions of This Thesis Work

The main contributions of this thesis work include:

The clarification of different “resonant” frequencies of a parallel resonant circuit used in current-fed IPT power supplies [1], as well as the analysis and computation of the ZVS frequency together with requirements for achieving ZVS [2].

A frequency stability analysis for tuned track and pick-up circuits, including the derivation of the stability criteria [3], and the determination of the frequency shift that could occur.



InductEV, Inc.
Exhibit 1020
Page 225

An investigation and development of a new ZVS start-up approach for the current-fed resonant converter. The proposed method can achieve overshoot-free dynamic ZVS start-up at reduced cost and simplified procedure [4].

The development of trans-conductance V/I converting networks for the current and voltage fed G3 power supplies. The proposed network significantly improves the track current performance, enabling higher power levels, longer distances, and less EMI than previously possible [5,6].

The analysis of the tuned track network of a current-fed G3 power supply, including the worst-case and Monte Carlo sensitivity analysis [7].

GSSA mathematical modelling and PSpice dynamic simulations of a practical current-fed G3 power supply system including up to16 power pick-ups [7].

The proposal and development of a new concept resonant converter based on free oscillation and energy injection control. A simple example converter has been simulated and verified with experimental results.

The proposal and implementation of a current-fed resonant converter without using an external controller. The converter operation is based solely on self-sustained non-linear oscillations, so that all the auxiliary power supplies, sensors and circuitry required by standard control techniques are eliminated. The validity of the converter has been proven by PSpice simulation and experimental results at low voltage levels, and practical solutions have been found for high power IPT applications.

Part of the above contributions have been published in one journal paper [3], four conference papers [1,2,4,5] and two research reports [6,7].

## 8.4 Suggestions for Future Work

The work conducted in this thesis has focused on the improvements of high performance resonant converters for IPT track power supplies. Various theoretical analyses, computer simulations, and experimental tests have been undertaken to achieve this goal. While some attempts have been highly successful leading to the useful results described in this thesis, more areas have been opened for further investigation. In concluding this thesis, the author has a strong belief in the usefulness of targeted research being investigated into several new research areas in the future. Some of the suggestions made in the following sections are open-ended, while others can be regarded as the extension of this thesis work.



InductEV, Inc.
Exhibit 1020
Page 226

**Fundamental Studies on Nonlinear Switch Mode Circuits**

Like most other power conversion and control applications using power electronic technologies, IPT is mainly concerned with the switch mode nonlinear circuits comprising semiconductor switches, passive RLC components, and loosely coupled "transformers" in particular. In general, switch mode nonlinear circuit theory substantially lags engineering practice in this area. As such the circuit design and implementation largely depends on experience, intuition, and trial & error approaches which are expensive in terms of both time and cost. Consequently, there is a need for further fundamental studies on this topic to help guide engineering design and promote practical applications in future.

There are three main aspects making the analysis, modelling and control of the switch mode circuits extremely difficult: nonlinearity, transient, and high order. A switch mode nonlinear circuit deals with abrupt state transitions caused by either forced or natural switch commutations. Strictly speaking, the circuit always varies and operates in dynamic modes. However, when the outputs of the next state identically repeat those of the previous ones, the circuit is said to have reached steady state. In many cases, the focus has been limited to only the steady state approximate analysis since the transients are too complicated. Analyses of resonant converters are more difficult since it is normally not easy to determine the exact natural commutation instants that correspond to zero voltage or zero current crossings. As revealed in the analyses of the current-fed resonant converters in this thesis work, sometimes it is even difficult to know whether these zero crossings exist so that the dynamic switch transitions can be assured. This is particularly true with high order systems as in the G3 power supplies, where dynamic analytical solutions are nearly impossible using current mathematical techniques.

With advances in numerical computation techniques, computer simulation has become the main means of analysing power electronic circuits. However, simulations only give limited insight into the essence of the circuit properties. Therefore, some in-depth studies on the system analysis, synthesis, modelling, and control remain invaluable. At present, even some basic concepts, such as reactive power, quality factor, resonant frequency, etc., need to be studied further for their proper use in nonlinear circuits. These concepts are directly borrowed from the linear circuit theories and are often applied vaguely to switch mode circuits. In this sense, some new concepts and approaches are required to help solve the switch mode dynamic problems.

For the resonant converter IPT power supplies studied in this thesis, approximate steady state AC analyses considering only the fundamental components have been employed to study the frequency



InductEV, Inc.
Exhibit 1020
Page 227

stability problems of current-fed resonant converters in Chapter 3. To undertake a more realistic analysis, the harmonics resulting from the switching process as well as the circuit transients need to be considered in the future. Moreover, chaos and bifurcation phenomena which arise in these systems [8] along with frequency detuning problems are worth further investigation with variable frequency IPT power supplies.

The GSSA mathematical model obtained in this thesis has a solution with complex coefficients. Although it has proven very useful for easy and fast analyses of an IPT system, little is known about the controller design based on this complex coefficient model. Consequently, more work is necessary to change it into a model with real coefficients so that standard control techniques can be applied. Alternatively, control methods must be developed for such models. A limitation of this modelling technique is that the resonant frequency needs to be known and should be approximately constant. For variable frequency converters with large frequency variations, more accurate modelling techniques are required.

Further work is also suggested into an investigation of the basic dynamic properties of resonant converters, particularly of those having high system orders. For example, the ZVS start-up method and the self sustained oscillation approach without external controllers proposed in this thesis are all based on the G1 power supply with a second order resonant tank. It has been observed that these methods do not work with the high order G3 power supplies. Further studies in this area may solve these problems and generate more useful results of theoretical and practical importance.

### A. Energy injection control and Combined Mode Operation

The investigation into the free oscillation and energy injection control method proposed in this thesis opens an important and interesting research area in the development of high frequency AC power generation. A simple example has been given in the thesis. However, this is not the only one belonging to this type of converter. Based on the concept proposed here, various free ringing circuits and energy injection control methods may be developed to construct new resonant converters. A further study could cover topics such as basic network oscillation properties, switching configurations, isolation and circuit protection, as well as different energy sources. As discussed in Chapter 7 of this thesis, a direct AC-AC converter is very promising if the problems related to the conducted EMI into the mains power supply could be properly solved.

Furthermore, converters based on energy injection control can be combined with conventional converters directly driven by voltage or current sources to form a composite IPT power supply



InductEV, Inc.
Exhibit 1020
Page 228

system. Traditional converters could be used to produce the basic track current operating at the correct frequency, while several energy injection circuits (possibly used as power pick-ups as well) could be placed at various locations along a track loop to compensate for any energy losses within the whole system. As such, the advantages of both types of the converters could be utilised so that a very large but flexible and efficient IPT system with a long track length and high power transfer ability could be built up.

### B. System Dynamic Tuning and Multiple Mode Tuning

Variable frequency operation is normally a more economical choice for achieving ZVS or ZCS operation as noted before. However, its frequency can vary slightly under normal working conditions and frequency stability problems may occur under various extreme operating conditions. To overcome this, a full resonant converter operating at a fixed frequency with system dynamic parameter tuning is suggested. An example of such a dynamic tuner is to use a phase-controlled inductor, which is controlled at different initial angles so that the equivalent current flowing through it varies, thus resulting in a “variable” inductor. Such an inductor can be used to keep the zero phase angle resonant frequency constant against load changes and other parameter variations so that a unity power factor input can be maintained. It addition, as discussed in section 3.3.4 of this thesis, the dynamic tuning method could also be used to improve the system frequency stability.

For high order resonant circuits such as those used for the G3 power supplies, normally all the reactive components are tuned at only one nominal frequency, while all the other zero phase angle resonant frequencies are to be avoided because of the frequency detuning problem. In fact, the multiple mode frequency property may be advantageously used in designing a tuning circuit to reduce the VAr rating of the reactive components so that the system cost and size could be reduced. This concept may also be applied to the G1 power supplies having tuned pick-up circuits.

### C. Track Loss Reduction

Most IPT power supplies require a large and constant track current to increase the power transfer capacity and frequency stability. In consequence the non-superconducting track consumes a large amount of power at all load conditions. This problem is particularly severe when the track length is very long where its ESR is high. Therefore, apart from the soft switching techniques that essentially eliminate the switching losses, further investigations as to how to minimise the power loss in the track are needed. For a single pick-up system, a possible solution is to change the basic design concept from a current-source to voltage-source track power supply whose track current is



InductEV, Inc.
Exhibit 1020
Page 229

controlled by the reflected pick-up impedance. For example, when a parallel tuned pick-up is not loaded, the reflected pick-up track impedance is nearly infinity so that the track current is zero. On the other hand, when the load is switched on, the track current increases since the reflected impedance reduces. This method improves the overall power efficiency, but is not suited to normal IPT systems with multiple pick-up loads because one power pick-up load can block the power flow to all others.

For a multiple pick-up IPT system, a more complicated control method is required. A possible approach is to reduce the track current to a low standby value at no load. With increasing load, the controller detects the change, eg. using variations in the DC input current, and boosts the track current appropriately for normal power transfer operation. If monitoring equipment is available at the pick-up load, then communication techniques could be employed to transmit the load information using either the track cable itself, or via an additional leaky feeder or a wireless radio link. The information transmitted between the track power converter and the pick-ups could be used for improving the control decisions of the power supply as well as other data acquisition purposes.

## 8.5 References

[1] Hu, A., Boys, J. T. and Covic, G.: "ZVS frequency analysis of a current-fed resonant converter", *Proceedings of the VII IEEE International Power Electronics Congress*, pp. 217-221, Acapulco, Mexico, October 2000.

[2] Hu, A., Boys, J. T. and Covic, G.: "Frequency analysis and computation of a current-fed resonant converter for IPT power supplies", *Proceedings of 2000 IEEE-PES/CSEE International Conference on Power System Technology*, Vol. 1, pp.327-332, Perth, Australia, December 2000.

[3] Boys, J. T., Hu, A. and Covic, G.: "Critical Q analysis of a current-fed resonant converter for ICPT applications", *IEE Electronics Letters*, Volume 36, Issue 17, ISSN 0013-5194, pp.1440-1442, August 2000.

[4] Hu, A., Boys, J. T. and Covic, G.: "Dynamic ZVS Direct on-line start-up of current-fed resonant converter using initially forced DC current", *Proceedings of 2000 IEEE International Industrial Symposium on Industrial Electronics*, Vol. 1, pp.312-317, Puebla, Mexico, December 2000.



InductEV, Inc.
Exhibit 1020
Page 230

[5] Hu, A.: "Theory and development of IPT power supplies", *Proceedings of the 5th Annual New Zealand Engineering and Technology Postgraduate Conference*, pp.246-251, Palmerston North, New Zealand, November 1998.

[6] Hu, A. and Boys, J. T.: "Series-parallel resonant converters, Stage I: Current-fed, single ended, series-parallel converter simulation", *Research Report of Auckland Uniservices Ltd for Wampfler AG, Germany, and Daifuku Ltd, Japan*, 52 pages, June 1998.

[7] Hu, A. and Boys, J. T.: "Current sourced CLC, G3 IPT track power supply, Stage II: Research and development investigation", *Research Report of Auckland Uniservices Ltd for Wampfler AG, Germany, Auckland University*, 78 pages, March 1999.

[8] Banerjee, S. and Verghese, G. C.: *Non-linear phenomena in power electronics - bifurcation, chaos, control and applications*, IEEE Press, NJ, 2001.



InductEV, Inc.
Exhibit 1020
Page 231

# Appendices

## Derivation of the Maximum Pick-up Loading Condition

For a series tuned pick-up circuit, its input impedance is:

$$Z_s = R + j(wL_s - \frac{1}{wC_s}) \tag{A-1}$$

where R is the pick-up load, $L_s$ is the inductance of the pick-up coil, and $C_s$ is the series tuning capacitor. This impedance can be referred back to the primary track circuit as:

$$Z_{sr} = \frac{w^2 M^2}{Z_s} \tag{A-2}$$

Denote $Z_{sr}$ with a complex number $R_{sr}+jX_{sr}$, then the total impedance of the a series tuned track can be expressed as:

$$\begin{aligned} Z_p &= R_{sr} + j(wL_p - \frac{1}{wC_p} + X_{sr}) \\ &= \frac{w^4 M^2 C_s^2 R}{(1-w^2 L_s C_s)^2 + w^2 C_s^2 R^2} + j\left[\frac{(w^2 L_p C_p - 1)}{wC_p} - \frac{w^3 M^2 C_s (w^2 L_s C_s - 1)}{(1-w^2 L_s C_s)^2 + w^2 C_s^2 R^2}\right] \end{aligned} \tag{A-3}$$

where $L_p$ and $C_p$ represent the inductance and capacitance of the track respectively, and M is the mutual inductance between the track and the pick-up coil.

The differential value of the input impedance $Z_p$ with respect of $\omega$ at the nominal frequency $\omega_0$ can be obtained as:

$$\frac{d}{dw} Z_p \Big|_{w=w_0} = \frac{2w_0 M^2}{R} + 2j(L_p - \frac{w_0^2 M^2 L_s}{R^2}) \tag{A-4}$$

Clearly, the polarity change of the phase angle of $Z_p$ is determined by the imaginary part of $Z_p$, therefore when

$$\mathrm{Im}(\frac{d}{dw} Z_p \Big|_{w=w_0}) > 0 \tag{A-5}$$



InductEV, Inc.
Exhibit 1020
Page 232

ie.,

$$L_p > \frac{w_0{}^2 M^2 L_s}{R^2} \qquad \text{(A-6)}$$

the phase angle of $Z_p$ at $\omega_0$ has a positive slope. Taking the definition of the pick-up quality factor $Q_s = w_0 L_s / R$ into consideration, equation (A-6) becomes:

$$L_p > \frac{M^2 Q_s{}^2}{L_s} \qquad \text{(A-7)}$$

As the coupling coefficient between the primary winding and the secondary winding is defined as k= $M / \sqrt{L_p L_s}$, the above condition can be further simplified as:

$$Q_s < 1/k \qquad \text{(A-8)}$$

This equation gives a concise maximum pick-up loading condition at which the slope of the impedance phase angle changes from positive to negative at the nominal resonant frequency.



InductEV, Inc.
Exhibit 1020
Page 233

# System Data of a Current-fed Full-bridge G3 IPT Power Supply

## ***Original Data***

| | |
|---|---|
| Inductance for a 400m track $L_s$ | =620μH |
| Track Current $I_t$ | =250A |
| Nominal Frequency $f_0$ | =15kHz |
| Nominal DC Bus voltage $V_d$ | =540V |
| Maximum pick-ups number n | =16 |
| Nominal power of each pick-ups | =10kW |
| Total output power of the pick-ups $P_0$ | =160kW |
| Pick-up efficiency $\eta_p$ | =95% |
| DC inductor $L_d$ | =100μH |
| Single Pick-up inductor $L_2$ | =120μH |
| Single Pick-up output DC inductor $L_d$ | =300μH |
| Single pick-up output DC voltage$V_0$ | =650V |
| Mutual inductor for a single track M | =7μH |
| Track (400m) series resistance $R_s$ | =0.3Ω (0.6Ω worst case) |
| ESR of the DC inductor $R_{dc}$ | =3mΩ |
| ESR of $C_p$ (π network) $R_{cp}$ | =0.6mΩ |
| ESR of $C_{p1}$ (π network) $R_{cp1}$ | =0.6mΩ |
| ESR of $L_{s1}$ (π network) $R_{Ls1}$ | =1mΩ |
| ESR of the $L_2$ (pick-up) $R_{dc}$ | =20mΩ |
| ESR of $C_2$ (pick-up) $R_{c2}$ | =2mΩ |
| ESR of $L_d$ (pick-up) $R_{dc}$ | =0.1Ω |
| ESR of capacitors (0.5μF/720V rms/30A) used | =0.002Ω each |

## ***Design Parameters***

| | |
|---|---|
| Nominal radium frequency $\omega_0$ | $=2\pi f_0$=94248 rad/s |
| Full-bridge resonant voltage $V_{ac}$ | $=\pi/2\times540/\sqrt{2}$ =600V rms, 848.2V peak |
| Track tuning capacitor $C_s$ | $=1/(\omega_0^2 L_s)$=0.18158μF |
| Maximum reflected load resistor $R_L$ | $=P_0/\eta_p/I_t^2$=2.7Ω |



InductEV, Inc.
Exhibit 1020
Page 234

| | |
|---|---|
| Total equivalent track resistor R | $=R_s+R_L=0.3\sim3\Omega$ |
| Track reactance $X_{Ls}=\omega_0 L_{s1}$ | $=94248\times620\times10^{-6}=58.4\Omega$ |
| Track series tuning quality factor $Q=X_{Ls}/R$ | =58.434/(0.3~3)=194.78~19.748 |
| Nominal Track tuning voltage $V_{Ls}=V_{cs}$ | =58.4×250=14.6kV rms |
| Net Track driving voltage $V_t$ | =250×(0.3~3)=75~750V |
| | |
| π network reactance $X_{ls1}=\omega_0 L_{s1}$ | =600V/250A=2.4Ω |
| π network inductance $L_{s1}$ | =2.4/94248=25.456μH |
| Coefficient $k=L_{s1}/L_s$ | =25.456/620=0.041 |
| π network Capacitors $C_p=C_{p1}$ | $=1/(\omega_0^2 L_{s1})=4.4225\mu F$ |
| Voltage $V_{Cp}=V_{ac}$ | =600V rms |
| Current $I_{Cp}=I_t$ | =250A rms |
| Voltage $V_{Cp1}=V_t$ | =75~750V rms |
| Current $I_{Cp1}$ | =(75~750)/2.4=31.25~312.5A rms |
| Voltage $V_{Ls1}$ | $=\sqrt{600^2+(75\sim750)^2}$ =604.6~960.5V rms |
| Current $I_{Ls1}$ | =(604.6~960.5)/2.4=251.9~400.2A rms |
| Total track power $P_t$ | $=250^2\times(0.3\sim3)=18.75\sim187.5kW$ |
| | |
| DC input current $I_d$ | $\cong(18.8\sim187.5)\times10^3/450=41.7\sim416.7A$ |
| Bias current $I_{Lb}=I_{Cb}$ | =250/2=125A rms (Bias factor=0.5) |
| Bias voltage=$V_{ac}$ | =600V rms |
| Bias inductance $L_b$ | =25.456/0.5=50.9mH |
| Bias capacitance $C_b$ | =4.4225×0.5=2.21μF |
| | |
| Open circuit voltage $V_{oc}$ | $=94247.7\times7\times10^{-6}\times250=164.93V$ |
| Pick-up coil reactance $X_{L2}$ | $=94247.7\times120\times10^{-6}=j11.3\Omega$ |
| Short circuit current $I_{sc}$ | =164.93/11.3Ω=14.6A |
| Output power $P_0$ | =650×14.583=9.48kW |
| Equivalent load resistor $R_2$ | =650/14.6=44.6Ω |
| Pick-up quality factor $Q_2$ | =44.6/11.3=3.94. |



InductEV, Inc.
Exhibit 1020
Page 235

# PSpice Schematic Set-up for System Dynamic Simulation

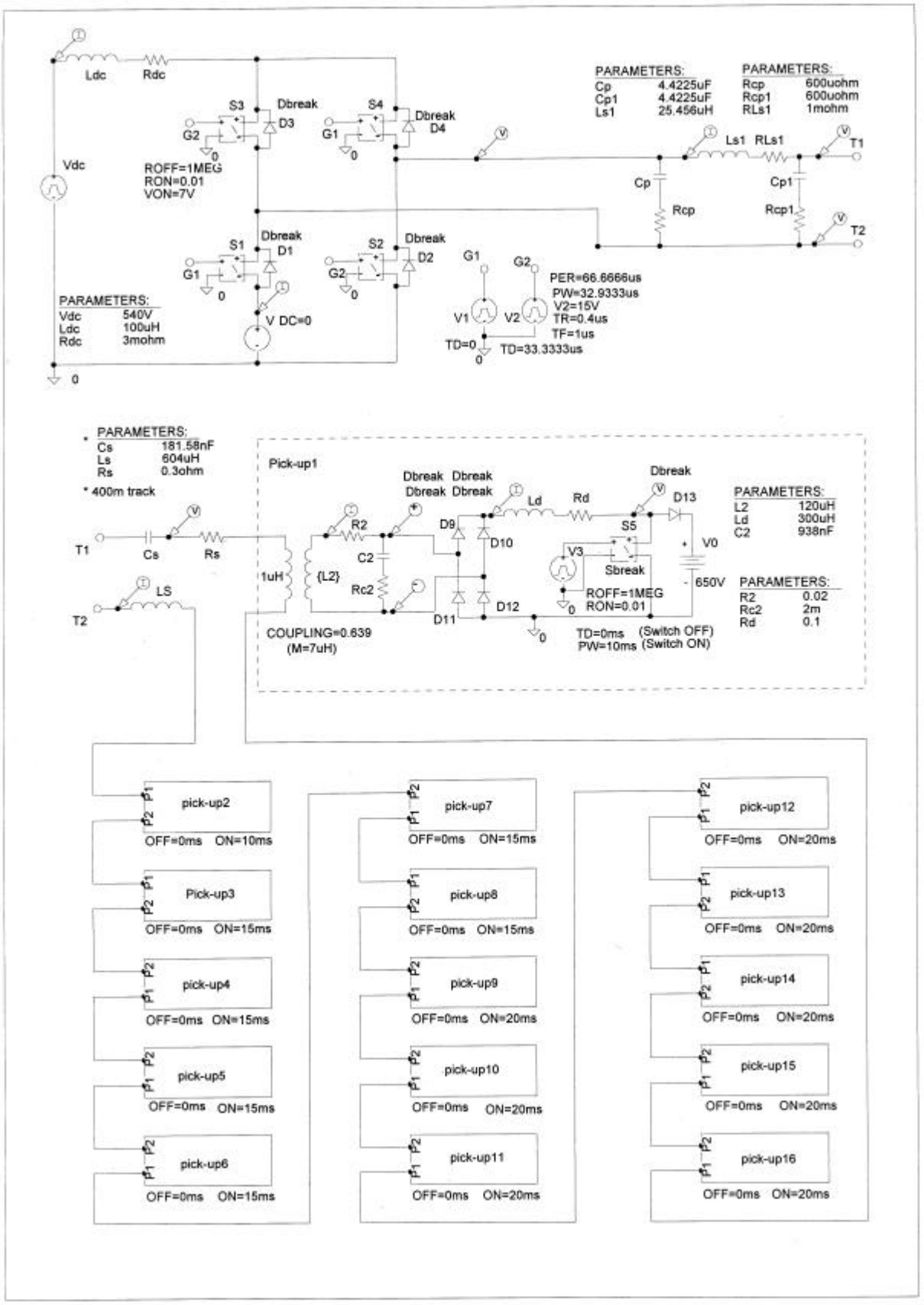


(400m Track with 16 Pick-ups, 200kW/15kHz Current-fed G3 IPT Power Supply)



InductEV, Inc.
Exhibit 1020
Page 236

# Bibliographies


[1] Ahmed, A.: *Power electronics for technology*, Prentice Hall, Upper Saddle River, NJ, 1999.

[2] Arrillaga, J. and Smith, B: *AC-DC power system analysis:* Institution of Electrical Engineers, 1998.

[3] Arrillaga, J.: *High voltage direct current transmission*, 2nd edition, London, Institution of Electrical Engineers, 1998.

[4] Barnard, J. M., Ferreira, J. A. and Van Wyk, J. D.: "Sliding transformers for linear contactless power delivery." *IEEE Transactions on Industrial Electronics*, Vol. 44, No.6, pp.774-779, December 1997.

[5] Barnard, J. M., Ferreira, J. A., and Van Wyk, J. D.: "Linear contactless power transmission systems for harsh environments", *Fourth Annual IEEE AFRICON*, Vol. 2, 1996.

[6] Barnard, J. M., Ferreira, J. A., and Van Wyk, J. D.: "Optimized linear contactless power transmission systems for different applications", *Proceedings of Twelfth Applied Power Electronics Conference and Exposition*, 1997.

[7] Barton, T. H.: *Rectifiers, cycloconverters, and AC controllers*, Calarendon Press, Oxford, 1994.

[8] Bollen, M. H. J.: *Understanding power quality problems: voltage sags and interruptions*, New York, IEEE Press, 2000.

[9] Bose, B. K.: Micro control of power electronics and drives, IEEE Press, New York, 1987.

[10] Bu, J., Sznaier, M., Wang, Z. Q. and Batarseh, I.: "Robust controller design for parallel resonant converter using μ-synthesis", *IEEE Transactions on Power Electronics*, Vol.12, No.5, September, 1997.

[11] Cogdell, J. R.: *Foundations of electric power*, Upper Saddle River, NJ, Prentice Hall, 1999.

[12] Covic, G. A.: *Third harmonic control of AC inverter drives*, Ph.D thesis, Electrical and Electronic department, University of Auckland, C83, February 1992.

[13] Debnath, L., Choudhury, S. R.: *Nonlinear instability analysis*, Computational Mechanics Publication, 1997.





InductEV, Inc.
Exhibit 1020
Page 237

[14] Esser, A. and Nagel, A.: "Contactless high speed signal transmission integrated in a compact rotatable power transformer", *Fifth European Conference on Power Electronics and Applications*, 1993.

[15] Fink, D. G. and Christiansen, D.: *Electronic Engineers' handbook*, McGraw Hill, Inc., 1989.

[16] Garrett, R. T.: "The EMC specifications of Australia, China, Japan and New Zealand", *IEEE 1996 International Symposium on Electromagnetic Compatibility,* Symposium Record, 1996.

[17] Geyger, W. A.: *Nonlinear-magnetic control devices - basic principles, characteristics, and applications*, McGraw-Hill, 1964.

[18] Ghahary, A. and Cho, B. H.: "Design of transcutaneous energy transmission system using a series resonant converter", *IEEE Transactions on, Power Electronics,* Vol.7, No.2, April 1992.

[19] Godyak, V. A., Piejak, R. B. and Alexandrovich, B. M.: "Electrical and light characteristics of RF-inductive fluorescent lamps", *Journals of Illuminating Engineering Society*, winter 1994.

[20] Hart, D. W.: *Introduction to power electronics*, Upper Saddle River, NJ, Prentice Hall, 1997.

[21] Hingorani, N. G., Gyugyi, L. and El-Hawary, M. E.: *Understanding FACTS : concepts and technology of flexible AC transmission systems*, , consulting editor, New York, IEEE Press, 2000.

[22] Isidori, A: *Nonlinear control systems: an introduction*, Springer-Verlag, 1989.

[23] Jackson, D. K., Leeb, S. B. and Shaw, S. R.: "Adaptive control of an inductive power transfer coupling for servomechanical systems", *Power Electronics Specialists Conference, PESC 99.* 30th Annual IEEE, Vol. 2, pp.1191-1198, 1999.

[24] Jiang, H. J.; Maggetto, G.: "Identification of steady-state operational modes of the series resonant DC-DC converter based on loosely coupled transformers in below-resonance operation", *IEEE Transactions on Power Electronics*, Vol. 14, No.2, March 1999.

[25] Jufer, M., Macabrey, N. and Perrottet, M.: "Modelling and test of contacatless inductive energy transmission", *Mathematics and Computers in Simulation*, No.46, pp.197-211, 1998.

[26] Kassakian, J. G., Schlecht, M. F. and Verghese, G. C.*: Principle of power electronics*, Addison-Wesley, 1991.

[27] Khan, I. Tapson, J. and Vries, D. I.: "Frequency control of a current-fed inverter for induction heating", *IEEE International Industrial Symposium on Industrial Electronics*, Vol. 1, pp.343-346, Puebla, Mexico, December 2000.

[28] Kraus, J. D.: Electromagnetics, McGraw Hill, International Student Edition, 1984.



InductEV, Inc.
Exhibit 1020
Page 238

[29] Krein, P. T.: *Elements of power electronics*, New York, Oxford University Press, 1998.

[30] Lee, F. C.: *Power electronics technology and applications*, IEEE Technical Activities Board, 1997.

[31] Liu, C: *Control of thyristor controlled series capacitor*, ME thesis, Electrical and Electronic Department, the University of Auckland, February 1999.

[32] Lukacs, J., Kiss, M., Nagy, I., Gonter, G., Hadik, R., Kaszap, K., and Tarsoly, A.: "Electric drives of vehicles with inductive feeding", *Proceedings of the Fourth Power Electronics Conference*, Budapest, 1981.

[33] Madawala, U. K.: *A brushless ironless DC machine - theory & practice*, Ph.D thesis, Electrical and Electronic Engineering, University of Auckland, 1992.

[34] Mohan, N., Undeland, T. M. and Robbins, W.P.: Power electronics: converters, applications, and design, John Wiley & Sons, New York, 2nd edition, 1995.

[35] Nagy, I. and Tarsoly, A.: "Transmission line operating at medium frequency", *Periodica Polytechnica*, Vol.30, No.1, Budapest, 1986.

[36] Ojo, O. and Bhat, I.: "Steady-state and dynamic analyses of high-order parallel resonant convertors", *Electric Power Applications, IEE Proceedings -B*, Vol. 140,No. 3, May 1993.

[37] Oruganti, R. and Lee, F. C.: "Resonant power processors – Part II: Method of control", *EEEE Industry Applications Society Annual Meeting*, pp.860-867, 1984.

[38] Paice, D. A.: *Power electronic converter harmonics: multipulse methods for clean power*, Piscataway, NJ, IEEE Press,1996.

[39] Pedder, D. A. G., Brown, A. D. and Skinner, J. A.: "A contactless electrical energy transmission system", *IEEE Transactions on Industrial Electronics*, Vol.46, No. 1, February 1999.

[40] Platts, J. and Aubyn, J. S.: *Uninterruptible power supplies*, P. Peregrinus on behalf of the Institution of Electrical Engineers, 1992.

[41] Pressman, A. I.: *Switching power supply design*, 2nd edition, New York, McGraw-Hill, 1998.

[42] Rashid, M. H.: *Spice for circuits and electronics using PSpice*, Englewood Cliffs, NJ, Prentice & Hall, Inc., 1995.

[43] Ross, H. R., Lechner, E. H. and Schweinberg, R. N.: "Plays Vista roadway powered electric vehicle project", *Proceedings of International Electric Vehicle Symposium*, Vol.10, Hong Kong, 1990.

[44] Ross, J. N.: *The essence of power electronics*, London, New York, Prentice Hall, 1997.



InductEV, Inc.
Exhibit 1020
Page 239

[45] Sachdev, P. L.: *Nonlinear ordinary differential equations and their applications*, M. Dekker, New York, 1991.

[46] Sakal, N. O.: "RF power amplifier, Class A through S, how they operate", *Professional Program Proceedings*, 1997.

[47] Sato, F., Murakami, J., Matsuki, H., Kikuchi, S., Harakawa, K. and Satoh, T.: "Stable energy transmission to moving loads utilising new CLPS", *IEEE Transactions on Magnetics*, Vol.32, No.5, Part 2, September 1996.

[48] Sato, F., Murakami, J., Suzuki, T., Matsuki, H., Kikuchi, S., Harakawa, K., Osada, H. and Seki, K.: "Contactless energy transmission to mobile loads by CLPS - test driving of an EV with starter batteries", *IEEE Transactions on Magnetics*, Vol.33, No. 2, September 1997.

[49] Scarpellini, B: *Stability, instability, and direct integrals*, Chapman & Hall/CRC, 1999.

[50] Skilling, H. H.: *Electrical engineering circuits*, New York, John Wiley & Sons, Inc., 1961.

[51] Soma, M.: "A package design technique for size reduction of implantable bioelectronic systems", *IEEE Transactions on Biomedical Engineering*, Vol. 37, No.5, 1990.

[52] Tarter, R. E.: *Solid-state power conversion handbook*, John Wiley & Sons, Inc., 1993.

[53] Thollot, Pierre, A.: *Power electronics technology and applications*, IEE Press, 1992.

[54] Thorpe, T. W.: Computerised circuit analysis with Spice – A complete guide to Spice with applications, John & Sons, Inc., 1992.

[55] Tihanyi, László: "Electromagnetic compatibility in power electronics", *Electronics Conference*, 1981, Budapest.

[56] Zierhofer, C. M. and Hochmair, E. S.: "High-efficiency coupling-insensitive transcutaneous power and data transmission via an inductive link", *IEEE Transactions on Biomedical Engineering*, Vol. 37, No.7, 1990.



InductEV, Inc.
Exhibit 1020
Page 240